Innovation for Sustainable Production

Proceedings of the first i-SUP conference

Conference 1: Smart materials for sustainable production

April 22-25, 2008
Bruges, Belgium

CONFERENCE OVERVIEW

Ctrl + Click on i-SUP logo of theme title page to return to overview

CONFERENCE 1: SMART MATERIALS FOR SUSTAINABLE PRODUCTION

Advanced materials technology is a key enabler for sustainable growth in our competitive economy. Strong porous and foam structures allow novel membrane and catalytic processing applications to reduce emissions and enhance industrial processes. Advanced surface treatments enable the environmentally friendly industrial production of ever more compact products, requiring less raw materials, and offering even more functionalities. Tribological improvements result in machinery that dissipate less frictional energy to produce commodities that last longer. Advances in biomaterials result in smarter, economically viable systems to enhance the quality of life.

Members of the Scientific Advisory Board

Theme 1: Production and application of nanomaterials

- Hans Vercammen, Sirris (BE)
- Chris Van Haesendonck, Catholic University of Leuven (BE)
- Klaus Rose, Fraunhofer-Institute for Silicate Research (DE)
- Jules Mullens, Hasselt University (BE)

Theme 2: Biomaterials for improved quality of life

- Jan Schrooten, Catholic University of Leuven (BE)
- Etienne Schacht, Ghent University (BE)
- Jean-Pierre Erauw, Belgian Ceramic Society (BE)
- Hans-Peter Buchkremer, Forschungszentrum Jülich (DE)

Theme 3: Porous materials for environmental protection

- Omer Van der Biest, Catholic University of Leuven (BE)
- Paolo Colombo, University of Padua (IT)
- Thierry Chartier, ENSCI (FR)
- Maiko Naito, Osaka University (JP)
- Rodrigo Moreno, C.S.I.C. (ES)

Theme 4: Advanced surface treatments: eliminating solvents by dry processing

- Chris Leys, Ghent University (BE)
- Annemie Bogaerts, University of Antwerp (BE)
- Richard van de Sanden, Eindhoven University of Technology (NL)

Theme 5: Controlling friction and preventing wear in industrial processing

- Patrick De Baets, Ghent University (BE)
- Jean-Pierre Celis, Catholic University of Leuven (BE)
- Kenneth Holmberg, Technical Research Centre of Finland (FI)

Theme 6: Looking at materials at the nano-scale

- Karel Van Acker, Catholic University of Leuven (BE)
- Stefan Kuypers, JEOL (Europe) B.V. (BE)

Partnerships

- Sirris
- Belgian Ceramic Society
- Belgian Polymer Group
- Leuven Materials Research Centre
- Bond voor Materialenkennis
- Flamac
- Agoria
- Koninklijke Vlaamse Chemische Vereniging
- Laser Centrum Vlaanderen
- SusChem
- Jeol
- Nanoforum
- ENIWEP
- VTI
- Falex Tribology

Invited presentation: Innovations in Materials Technology for a Sustainable World

Messing, G.L.

Department of Materials Science and Engineering and Materials Research Institute, Pennsylvania State University, 121 Steidle Bldg, University Park, PA 16802, USA, messing@matse.psu.edu, 814-865-2262

INTRODUCTION

The influence of materials technologists and scientists is ubiquitous in today's materials world. By their actions the materials community influences all of us from the production of simple eating utensils to sophisticated cell phones, computers, aircraft components and many more conveniences of life. The call for sustainability recognizes increasingly limited natural resources, and how current approaches impact the health and quality of life for current and future generations of the human race. Sustainable production is defined[1] here as "the creation of goods and services using processes and systems that are

- Non-polluting
- Conserving of energy and natural resources
- Economically efficient
- Safe and healthful for workers
- Socially and creatively rewarding for all working people"

The materials community through its collective expertise in the creation and production of goods has a profound position in creating a more sustainable world. Clearly, that role has two prongs (1) improving current manufacturing processes to become more energy efficient, non-polluting and resource efficient and (2) creation of alternative materials that enable more energy efficient operation, less dependence on petrochemicals, and less polluting products. In this presentation I will begin with some egregious examples of non-sustainable design of materials and the consequence on the current generation. Next, I will address how we can innovate current manufacturing of goods to be more sustainable with a special reference to the ceramics industry. Secondly, I will discuss a number of opportunities where innovative materials can play a major role in a more sustainable world. In all cases it is important to emphasize that innovation in materials technologies has to be a global effort to have the impact that is possible and required for future generations.

Invited presentation: Laser Surface Texturing

Etsion I.

Dept. of Mechanical Engineering, Technion, Haifa 32000, Israel
etsion@technion.ac.il, Telephone: 972 4 829 2096, Fax: 972 4 829 5711

ABSTRACT

Surface texturing has emerged in the last decade as a viable option of surface engineering resulting in significant improvement in load capacity, wear resistance, friction coefficient etc. of tribological mechanical components. Various techniques can be employed for surface texturing but Laser Surface Texturing (LST) is probably the most advanced so far. LST produces a very large number of micro-dimples on the surface and each of these micro-dimples can serve either as a micro-hydrodynamic bearing in cases of full or mixed lubrication, a micro-reservoir for lubricant in cases of starved lubrication conditions, or a micro-trap for wear debris in either lubricated or dry sliding. This presentation reviews the current effort being made world wide on laser surface texturing and the potential of this technology in various tribological applications.

INTRODUCTION

Surface texturing as a means for enhancing tribological properties of mechanical components is well known for many years. Perhaps the most familiar and earliest commercial application of surface texturing is that of cylinder liner honing. Today surfaces of modern magnetic storage devices are commonly textured and surface texturing is also considered as a means for overcoming adhesion and stiction in MEMS devices. Fundamental research work on various forms and shapes of surface texturing for tribological applications is carried out worldwide and various texturing techniques are employed in these studies including machining, ion beam texturing, etching techniques and laser texturing. Of all the practical micro-surface patterning methods it seems that laser surface texturing (LST) offers the most promising concept. This is because the laser is extremely fast and allows short processing times, it is clean to the environment and provides excellent control of the shape and size of the texture, which allows realization of optimum designs. By controlling energy density, the laser can safely process hardened steels, ceramics, and polymers as well as crystalline structures. Indeed, LST is starting to gain more and more attention in the Tribology community as is evident from the growing number of publications on this subject. LST produces a very large number of micro-dimples on the surface (see Fig. 1) and each of these micro-dimples can serve either as a micro-hydrodynamic bearing in cases of full or mixed lubrication, a micro-reservoir for lubricant in cases of starved lubrication conditions, or a micro-trap for wear debris in either lubricated or dry sliding.

The pioneering work on LST started at Technion in Israel as early as 1996 [1, 2]. At about the same time work on laser surface texturing was done in Germany but unfortunately, most of it is published in the German language and hence, is not even referenced in English archive journals. A few exceptions are papers coming from the group lead by Geiger at the University of Erlangen-Nuremberg e.g. [3, 4]. This group uses an eximer laser with a mask projection technique, a mask is illuminated with the laser beam and its geometrical information is projected onto the textured surface. This method was applied to a punch, used in a backward cup extrusion process for the production of rivets, and showed a substantial increase of up to 169% in cold forging tool life. These as well as many other papers on LST are described in a review of the state of the art of LST covering this subject until 2005 [5]. In the presentation the work that was done on LST prior to 2005 will be described briefly followed by the new developments since 2005. Laser surface texturing has been used in the magnetic storage industry [6, 7] mainly to prevent stiction during start up. This issue will not be dealt with in the present review. Instead, the potential of LST in enhancing Tribological performance during continuous operation will be described.

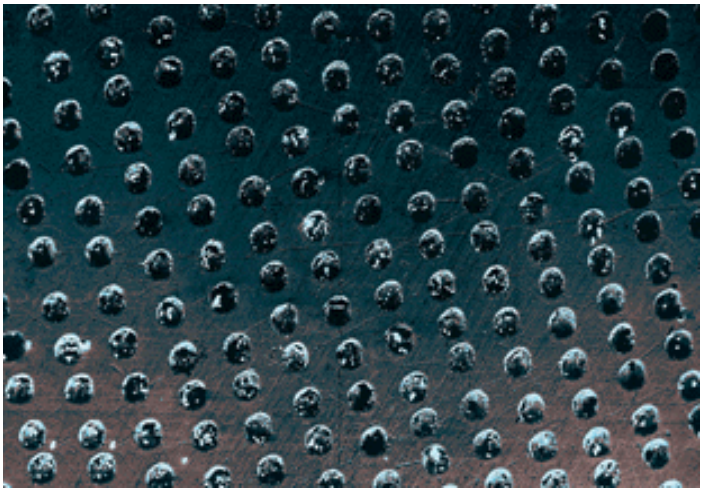

Figure 1. LST Regular Micro-Surface Structure in the Form of Micro-Dimples

REFERENCES

1. Etsion, I. Burstein, L. 1996. A Model for Mechanical Seals with Regular Microsurface Structure. Tribology Transactions, 39: 677-683.
2. Etsion, I., Halperin G., Greenberg, Y. 1997. Increasing Mechanical Seal Life with Laser-Textured Seal Faces. Proc. 15th Int. Conf. on Fluid Sealing, BHR Group, Maastricht, 3-11.
3. Geiger, M., Roth, S., Becker, W. 1998. Influence of Laser-Produced Microstructures on the Tribological Behavior of Ceramics. Surface and Coatings Technology, 100-101: 17-22.
4. Geiger, M., Popp, U., Engel, U. 2002. Eximer Laser Micro Texturing of Cold Forging Tool Surface- Influence on Tool Life. Annals of the CIRP, 51: 231-234.
5. Etsion, I. 2005. State of the Art in Laser Surface Texturing. J. of Tribology Trans. ASME, 127: 248-253.

Invited presentation: Nanomaterials for bottom-up manufacturing.

Huskens J.

University of Twente, MESA+ Institute for Nanotechnology
Molecular Nanofabrication group
P.O. Box 217, 7500 AE Enschede, The Netherlands
e-mail: j.huskens@utwente.nl, phone: +31-534892995, fax: +31-534894645

INTRODUCTION

Nanotechnology deals with enabling technologies for the fabrication and study of materials (atoms, molecules, particles, etc.) on the nanoscale. In order to study nanoobjects, the preparation of nanoobjects is not enough: careful study of their individual properties usually requires anchoring to a substrate, and preferably to targeted or prepatterned areas of a substrate.
Nanofabrication is the subdiscipline that deals with the development of general fabrication methodologies for the preparation of nanoobjects as well as of patterned substrates and of assembly methods for the anchoring of the objects to the patterned areas. In general, nanofabrication methods fall into two classes, which are called top-down and bottom-up. The integration of top-down and bottom-up nanofabrication schemes is considered a key issue for the advance of nanotechnology.
In this paper, we will show the integration of nanoimprint lithography (NIL) as the top-down technique [1] with layer-by-layer (LBL) assembly [2] as the bottom-up technique. The full integration of these methods is therefore envisaged to lead to the fabrication of 3D nanoobjects of arbitrary shapes on substrates, where the x,y dimensions are determined by NIL, while the materials versatility and the z dimension originates from the LBL assembly. For the LBL assembly, we have used a supramolecular approach [3], based on host-functionalized substrates ("molecular printboards" [4]) and nanoparticles (<5 nm) [5] in combination with guest-functionalized dendrimers. The whole procedure is shown to result in a multistep, high-fidelity process yielding 3D objects with all dimensions on the nanoscale.
After an introduction to the integration of NIL and LBL for 3D assembly, we will focus on the latest results, which cover (i) 3D assembly of larger (>50 nm) nanoparticles [6], (ii) the electrochemical reversibility of anchored nanostructures [7], (iii) the patterned layered assembly of biomaterials, including various proteins, antibodies, and light-harvesting proteins [8].

CONCLUSIONS

Bottom-up nanofabrication constitutes a powerful paradigm for nanomaterials assembly. It can be applied in the directions of photonic materials, energy materials, biochips, and many others. In particular the full integration with top-down methods will lead to exciting future developments.

ACKNOWLEDGEMENTS

The Council for Chemical Sciences of the Netherlands Organization for Scientific Research (NWO-CW) is acknowledged for financial support (Vidi Vemieuwingsimpuls grant 700.52.423 to J.H.), as well as the support from the European FP6 Integrated project NaPa (contract no. NMP4-CT-2003-500120).

REFERENCES

[1] P. Maury, M. Escalante, D. N. Reinhoudt, J. Huskens, *Adv. Mater.* **2005**, *17*, 2718.
[2] G. Decher, *Science* **1997**, *277*, 1232.
[3] O. Crespo-Biel, B. Dordi, D. N. Reinhoudt, J. Huskens, *J. Am. Chem. Soc.* **2005**, *127*, 7594.
[4] M. J. W. Ludden, D. N. Reinhoudt, J. Huskens, *Chem. Soc. Rev.* **2006**, *35*, 1122; J. Huskens, *Curr. Opin. Chem. Biol.* **2006**, *10*, 537; O. Crespo-Biel, B. J. Ravoo, D. N. Reinhoudt, J. Huskens, *J. Mater. Chem.* **2006**, *16*, 3997.
[5] O. Crespo-Biel, A. Juković, M. Karlsson, D. N. Reinhoudt, J. Huskens, *Isr. J. Chem.* **2005**, *45*,

353.
[6] P. Maury, M. Péter, O. Crespo-Biel, X. Y. Ling, D. N. Reinhoudt, J. Huskens, *Nanotechnology* **2007**, *18*, 044007.
[7] X. Y. Ling, D. N. Reinhoudt, J. Huskens, *submitted*.
[8] M. J. W. Ludden, A. Mulder, R. Tampé, D. N. Reinhoudt, J. Huskens, *Angew. Chem. Int. Ed.* 2007, *46*, 4104; M. J. W. Ludden, M. Péter, D. N. Reinhoudt, J. Huskens, *Small* 2006, *2*, 1192; M. Escalante-Marun, P. Maury, C. M. Bruinink, K. van der Werf, J. D. Olsen, J. A. Timney, J. Huskens, C. N. Hunter, V. Subramaniam, C. Otto, *Nanotechnology* 2008, *in press*.

Invited presentation: Materials Science, an Enabling Technology for Regenerative Medicine.

***Hendriks M.*[1]**

1 DSM Biomedical Materials BV, PO Box 18, 6160 MD Geleen, the Netherlands, marc.hendriks@dsm.com, Telephone: +31 (46) 4760330, Fax: +31 (46) 4763563

The ageing of the population is one of the biggest challenges facing the world in the coming decades. As the population grows older, age-related chronic diseases – neurodegenerative disorders such as Alzheimer's and Parkinson's; visual disorders such as glaucoma and age-related macular degeneration; cardiovascular disorders such as coronary heart disease, heart failure, and atrial fibrillation; nephropathy; osteoporosis, etc. - become increasingly apparent and will bring about a massive demand for new ways of treatment. There will be a growing need for curative or, better even, preventive, rather than the mostly palliative treatments of today.

The emergence of the biological sciences, particularly in the areas of cell and molecular biology (i.e., proteins, peptides and genes), has brought about hope of fulfilling said need. It has laid the fundament to a new and very active field that is generally referred to as Regenerative Medicine (RM). RM encompasses the convergence of a range of different technologies and can be defined as *"those technologies that provide substitute tissues (both synthetic and natural) and/or cells for implantation into the body, or promote tissue remodeling for the purpose of replacing, repairing, regenerating, reconstructing, or enhancing function."*

Today, RM is frequently positioned as the panacea to loss or degeneration of tissue from trauma and disease. In bringing about the realization of these promises, materials science is a great partner to stem cell biology, genomics, and proteomics in crafting the scaffolds that support regeneration of tissues lost to trauma, disease, or genetic defects. Notably, materials designed at (supra)molecular scales to interact with cells, biomolecules, and pharmaceuticals will have a profound impact. This article will review materials science's partnership role in general, and discuss some of the activities that DSM Biomedical pursues in this field in particular.

Theme 1: Production and application of nanomaterials

Nanotechnology is expected to evolve through overlapping stages of industrial prototyping and commercialization. A first route involves the development of passive nanostructures, mainly involving manufactured nanoparticles (metal oxides, quantum dots, carbon nanotubes, etc) serving as raw materials, ingredients or additives in existing products. A second route focuses on active nanostructures that change their size, shape, conductivity or other properties during use. For example, drug-delivery particles that release therapeutic molecules in the body when they target their diseased tissues. Papers are welcomed that describe the synthesis of nanostructured materials and addressing their potential applications and contribution towards sustainable economic development.

Microwave plasma enhanced chemical vapor deposition synthesis and applications of few layer graphene.

Malesevic A.[12], Vitchev R.[1], Vansweevelt R.[3], Ravelingien M.[1], Zhang L.[4], Kemps R.[1], Vanhulsel A.[1] and Van Haesendonck C.[2]

1 VITO Materials, Flemish Institute for Technological Research, Boeretang 200, 2400 Mol, Belgium, alexander.malesevic@vito.be , Telephone: (+32) 14-335687, Fax: (+32) 14-321186
2 Laboratory of Solid-State Physics and Magnetism, K.U.Leuven, Celestijnenlaan 200D, 3001 Leuven, Belgium
3 IMO, Instituut voor Materiaalonderzoek, Universiteit Hasselt, Wetenschapspark 1, 3590 Diepenbeek, Belgium
4 Electron Microscopy for Materials Science, University of Antwerp, Groenenborgerlaan 171, 2020, Antwerp, Belgium

ABSTRACT

A novel route for the synthesis of graphene by means of microwave plasma enhanced chemical vapor deposition is presented. This technique outclasses its competitors in many ways since it is less elaborate and better reproducible than micromechanical cleavage [1] of graphite and less expensive than thermal decomposition of silicon carbide wafers [2]. Methane diluted with hydrogen is decomposed in a high power microwave plasma and the resulting carbon radicals recombine on the surface of any substrate that withstands temperatures up to 700°C. A broad range of substrates were successfully tested including silicon, quartz, stainless steel and many metals. The resulting carbon nanostructures are freestanding graphene flakes as can be seen in Figure 1, only four to six atomic layers thick but up to several micrometers wide and high. The flakes are perpendicular aligned to the substrate surface. Thorough qualitative analysis with electron microscopy, scanning probe microscopy, X-ray diffraction and Raman spectroscopy lead to the conclusion that the flakes are highly crystalline sp^2 carbon nanostructures with few defects or impurities. A possible growth scheme is proposed, based on scanning electron microscopy at various stages in the growth process and X-ray photoelectron spectroscopy of the interface between the flakes and the substrate. Due to graphene's outstanding physical properties, hopes are nursed that several important graphene based applications will be developed over the coming years. We present efforts on the development of various prototype graphene applications. First, field emission measurements of as grown flakes reveal a low turn on voltage of only 3V/µm which is a promising value for possible future applications. Second, graphene coatings on titanium bone implants are suited nucleation sites for calcium phosphate which is a prerequisite for bone implants. Third, we show that graphene flakes are ideal DNA binding sites which is a first step into the development of a biosensor.

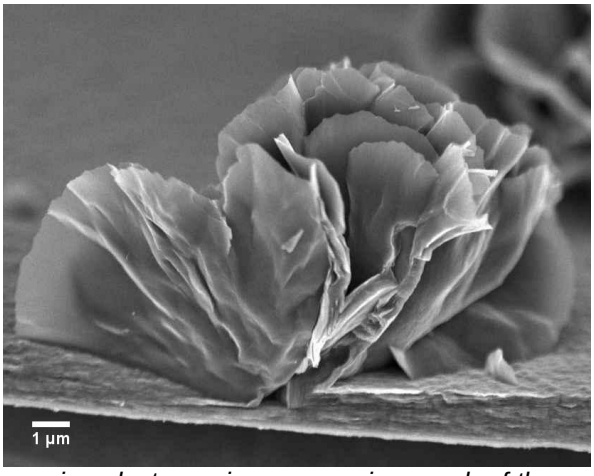

Figure 1. Cross-section scanning electron microscopy micrograph of the as grown graphene flakes.

ACKNOWLEDGEMENTS

A.M. thanks M. Mertens for XRD analysis. The authors gratefully acknowledge funding from the Flemish Institute for Technological Research, the Belgian Interuniversity Attraction Poles research program and from the Fund for Scientific Research – Flanders.

REFERENCES

[1] K. S. Novoselov et al., P. Natl. Acad. Sci. USA 102, 10451 (2005).
[2] I. Forbeaux et al., Phys. Rev. B 58, 16396 (1998).

A new generation of hierarchical structured materials with high adsorption capacities and shape selectivity

***Devriese L.I.*[1], *Martens J.A.*[2], *Aerts A.*[2], *Baron G.V.*[1], *Denayer J.F.M.*[1]**

1 Chemische Ingenieurstechniek en Industriële Scheikunde, Vrije Universiteit Brussel, Pleinlaan 2, 1050 Brussel, Belgium, lidevrie@vub.ac.be, Telephone: (+32)26293655, Fax: (+32)26293248
2 Centrum voor Oppervlaktechemie en Katalyse, KULeuven, Kasteelpark 200, 3001 Heverlee, Belgium

INTRODUCTION

For decades, zeolites have been used in catalysis and molecular separation. Zeolites are capable of discriminating among molecules with different size and shape as a result of the close matching between molecule and pore. This unique property is grasped by the term 'molecular shape selectivity'.

In past decades significant research efforts have been devoted to the synthesis of ordered mesoporous materials to overcome limitations such as the restricted access of larger molecules in the internal voids of zeolites and the inherently slow diffusion of molecules in the zeolite pores. While the hurdle of limited accessibility is overcome, the absence of the shape selective properties limits the application range.

Recently, two new types of hierarchical materials are developed by modifying the ordering of the building units through addition of surfactants and polymers: Zeogrids and Zeotiles [1]. Both types of materials are characterized by dual porosity and contain ultra-micropores of 0.55 nm. Zeogrids are obtained by interposed stacking of silicalite-1 nanoslabs and possess rectangular super-micropores of 3 nm. Zeotile-2, built from the assembly of half nanoslabs, contains cubic super-micropores of 2.7 nm. Zeotile-4 is obtained by the assembly of double nanoslabs and has hexagonal super-micropores of 7.3 nm. In the present work, adsorption properties of these new materials are evaluated.

RESULTS

Low coverage adsorption and separation

The adsorption properties of Zeogrid, Zeotile-4 and Zeotile-2 at low coverage were determined using the pulse chromatographic technique at temperatures between 50°C and 250°C. The adsorption properties (Henry constants, adsorption enthalpies and entropies) of alkanes, iso-alkanes, alkenes and aromatics were derived.

For all biporous materials the observed tendencies of zeolites are found: an exponential increase of the Henry constants of alkanes and iso-alkanes with carbon number, an exponential decrease of the pre-exponential factors and a linear increase of the adsorption enthalpy. Figure 1 shows the van 't Hoff plots of n-pentane and n-octane on the biporous materials Zeotile-2, Zeotile-4 and Zeogrid.
.

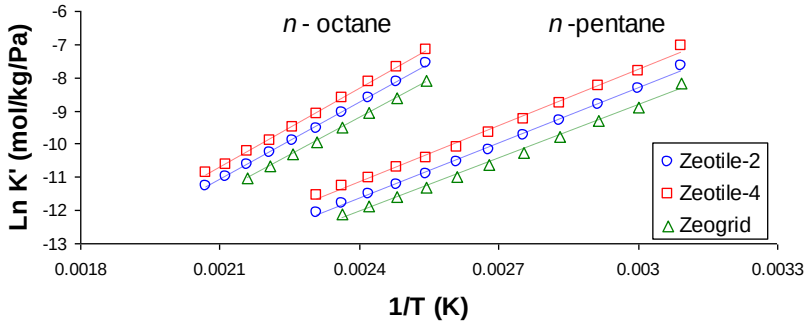

Figure 1. van 't Hoff plots of n-pentane and n-octane on Zeotile-2, Zeotile-4 and Zeogrid

Zeogrid and Zeotile-4 possess identical separation factors between linear and branched alkanes, while Zeotile-2 shows higher separation factors. Although all of these materials have lower separation factors compared to the highly selective ZSM-5 zeolite, they are still capable of separating linear from branched alkanes.

A simple method is proposed to identify shape selectivity in porous materials based on the use of the pulse chromatographic technique using linear and branched alkanes as probe molecules. A correlation between the retention volume (Vg) measured in pulse gas chromatography and the saturation pressure (ps) of the sorbate for homologous series can be used for this purpose [2, 3]: log Vg = a log ps + b. If the logarithmic of the retention volume of homologous series are plotted as a function of the logarithmic of the saturation pressure, a linear relationship is obtained [4]. The analysis is made of the shape selectivity properties of mesoporous solids (MCM-41, MCM-48, silica), classical zeolites (NaY, ZSM-5, Beta, MOR, SAPO-5) and new hierarchical structured biporous materials. Shape selectivity in the adsorption of n- and iso-alkanes was observed on Zeotile-2 at low coverage [5].

Adsorption isotherms

Vapour adsorption isotherms of n-octane, iso-octane, 1-octene, 2-octanol, m-xylene, p-xylene, o-xylene, ethyl benzene and water on Zeotile-2 were determined using the gravimetric technique at 70°C. A remarkably high adsorption capacity for organic vapours on Zeotile-2 (40-50 wt %) compared to zeolites (max. 35 wt %) was observed. 1-Octene and n-octane have similar adsorption capacities, but 1-octene is adsorbed more strongly at lower partial pressures. Figure 2 shows the adsorption isotherms of n- octane, 1-octene and o-xylene on Zeotile-2 at 70°C. o-Xylene is adsorbed stronger still at low partial pressure and possesses a higher adsorption capacity compared to 1-octene and n-octane. These observations are in conformity with the results of the pulse chromatographic experiments.

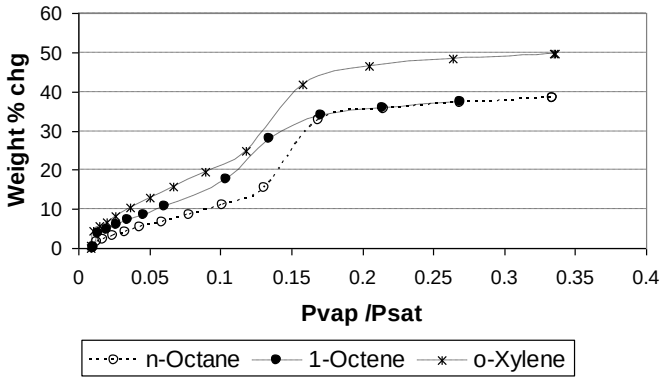

Figure 2. Adsorption isotherm of n-octane, 1-octene and o-xylene on Zeotile-2 at 70°C

CONCLUSIONS

Adsorption properties of the hierarchical structured materials Zeogrid, Zeotile-2 and Zeotile-4 are studied and evaluated in this work. These materials possess extremely large adsorption capacities. Zeotile-2 shows separation factors which are substantially larger than would be expected on basis of differences in interactions between molecules and a non-specific surface without shape selectivity.

ACKNOWLEDGEMENTS

J. Denayer is grateful to the F.W.O.-Vlaanderen, for a fellowship as postdoctoral researcher. The work was performed in a strategic basic research program sponsored by the Flemish government.

REFERENCES

1. Kirschhock C.E.A., Kremer S.P.B., Vermant J., Van Tendeloo G., Jacobs P.A. and Martens J.A. 2005. Design and Synthesis of Hierarchical Materials from Ordered Zeolitic Building Units. Chem.Eur. J. 11: 4307-4313.
2. Nabivach V.M.and Dmitrikov V.P. 1993. The use of correlation equations for the prediction of retention parameters in gas-liquid chromatography. Russian Chemical Reviews 62:23-33.
3. Herington E.F.G. 1957. Vapour phase chromatograpy. Desty D.H. (Ed.). The thermodynamics of gas-liquid chromatography.Butterworths scientific publications, London: 5-14.
4. Castello G. and D'Amato G. 1975. Influence of vapour pressure and activity coefficients on the retention volumes of branched-chain alkanes. Journal of Chromatography 107: 1-13.
5. Devriese L.I., Cools L., Aerts A., Martens J.A., Baron G.V., Denayer J.F.M. 2007. Shape Selectivity in Adsorption of n- and iso-alkanes on a Zeotile-2 Microporous/Mesoporous Hybrid and Mesoporous MCM-48. Adv. Funct. Mater. 17: 3911-3917.

Membrane emulsification for the micromanufacturing of micro-nano-particulates and their application

***Giorno L.*[1], *Piacentini E.*[1,2], *Bazzarelli F.*[1], *Mazzei R.*[1,3], *Drioli E.*[1,2]**

[1]Institute on Membrane Technology, National Research Council, ITM-CNR, At University of Calabria, Via P. Bucci 17/C, 87030, Rende (CS), Italy, l.giorno@itm.cnr.it

[2]Dept. of Chemical Engineering and Materials, University of Calabria, Via P. Bucci 42/A, 87030, Rende (CS), Italy

[3]Dept. of Ecology, University of Calabria, Via P. Bucci 6/B, 87030 Rende (CS), Italy

INTRODUCTION

Membrane emulsification is a relatively new technique able to produce microsized-to-nanosized droplets and particles functionalized with shear sensitive components [1-3]. Membrane wetting properties, pore size and shape, porosity, dispersed phase flux control particulate size and size distribution.
One of the most common membrane emulsification method involves an applied pressure to force a dispersed phase to permeate through a membrane into a continuous phase, while the continuous flows along membrane surface. The detachment of droplets on the membrane surface results in the production of emulsion/suspension with controlled droplet size distribution at mild conditions of shear stress and temperature. The distinguishing feature is that the resulting droplets size is controlled primarily by the choice of the membrane.
The viscosity of the dispersed phase also has an important effect on the performance of membrane emulsification. According to Darcy's law, the dispersed flux is inversely proportional to the dispersed phase viscosity. Thanks to thermal resistance of some membranes it is possible to carry out membrane emulsification using high viscose compounds at high temperature [4].
Since membrane emulsification allows production of emulsions with very narrow droplets size distributions at a low mechanical stress, it can be easily applied for manufacturing products that benefit from these properties [5]. In particular, membrane emulsification can be used formulate products and processes using labile bioactive molecules. For example, enzymatic reactions in which substrate and product have different solubility, can be carried out in heterogeneous systems, like emulsions, that permit the selective removal of products from the reaction site, thus increasing the conversion of product-inhibited or thermodynamically unfavourable reaction.
In general, membrane emulsification is very suitable for formulation of stable particles containing phase transfer catalysts.
It can be also used to prepare complex microstructures with interfaces functionalized able to respond at external stimuli, e.g. release of drugs activated by target molecules.
In this paper, case studies on the preparation of micro- nanosized functionalized particulates by membrane emulsification for phase transfer catalysis, reaction intermediate control and drug release will be discussed.

RESULTS

Lipase is an interfacial enzyme that catalyzes reactions of water insoluble substrates in presence of water/lipid interfaces [6]. Usually, lipase is distributed at oil-water interface by mechanical homogenization process. In this case, high-energy imputes are required and shear-sensitive ingredients, such as proteins, cannot be used without loss of their functional properties. In fact, it has been observed that various enzymes lose activity when a solution is maintained under a high shear stress for a long time. Furthermore, in mechanically homogenization processes droplets size distribution and interfacial area are constantly changing and it is observed phase separation when agitation is stopped. Therefore, it is necessary to add emulsifiers in order to stabilize emulsions.
Using membrane emulsification technique, lipase could be distributed at stable oil-water interface without addition of other surfactants.

Emulsion with narrow droplet size and size distribution was obtained. Droplets sizes ranged from 0.7 (±0.01) to 3.1 (±0.2) μm with a maximum at 1.6 μm (±0.4), representing more than 90 % of droplets emulsions. Activity and enantioselectivity of lipase distributed at the oil/water interface by membrane emulsification was evaluated by means of enantioselective hydrolysis of 5 mM racemic naproxen methyl ester present in organic droplets. The production of (S)-naproxen acid increased as a function of time and the enantiomeric excess of the (S)-naproxen acid was 100%. No enantiomeric excess decrease was observed as long as the conversion of the naproxen methyl ester did not exceed 45 % [7]. The control of droplets size favours the formation of stable and large interface through which conversion of hydrophobic substrates can be catalyzed. Increasing interfacial area increases the substrate availability for the reaction. Hydrophobic substrate dissolved in organic phase can be converted with high yields because removing the water-soluble product from the reaction microenvironment to the aqueous phase can shift the thermodynamic equilibrium of reactions. In this model the interface provides reaction site in stable conditions because the interfacial area of emulsion produced by membrane emulsification process does not change during the reaction course.
Membrane emulsification concept can be also applied to improve efficiency of reaction selectivity and product stability, e.g. in biomass processing. By properly designing the process, it is possible to integrate the reaction step (occurring in homogeneous phase) with the product separation step (occurring at heterogeneous interface) so that to separate the intermediate instable reaction products and protect them in stable droplets.

CONCLUSIONS

The suitability of membrane emulsification to optimise multiphase heterogeneous reactions by distributing phase transfer catalyst at the oil/water interface as well as to improve reaction selectivity and product stability in biomass processing has been investigated.

The mild operative conditions in terms of shear stress of this technique allowed obtaining emulsions with droplets stabilised by the lipase itself without the need of additional emulsifier.

Thanks to low shear stress and enzyme optimal spatial arrangement at the stable and constant oil/water interface, lipase showed very high enantioselectivity (100%), productivity and conversion degree (90% of the isomer of interest was converted in about 24 h).

REFERENCES

[1] A.J. Abrahamse, A. van der Padt, R.M. Boom, Status of cross-flow membrane emulsification and outlook for industrial application, J. Membr. Sci 230 (2004) 149-159
[2] C. Charcosset, I. Limayem and H. Fessi, The membrane emulsification process- a Review, J. Chem. Technol. Biotechnol., 79 (2004) 209-218.
[3] T. Nakashima, M. Shimizu and M. Kukizaki, Particle control of emulsion by membrane emulsification and its application, Advance Drug Delivery Reviews 45 (2000) 47-56.
[4] Marco A. Farah, Roberto C. Oliveira, Jorge Navaes Caldas, Krishnaswamy Rajagopal,Viscosity of water-in-oil emulsions: variation with temperature and water volume fraction, J. Petroleum Science & Engineering ,48 (2005) 169-184.
[5] L. Giorno, E. D'Amore, R. Mazzei, E. Piacentini, J. Zhang, E. Drioli, R. Cassano, N. Picci, An innovative approach to improve the performance of a two separate phase enzyme membrane reactor by immobilizing lipase in presence of emulsion, Journal of Membrane Science, 295 (2007) 95-101
[6] H. Stamatis, A. Xenakis, F. N. Kolisis, Bioorganic reactions in microemulsions: the case of lipases, Biotechnol. Adv. 17 (1999) 293-318.
[7] L. Giorno, E. Piacentini, R. Mazzei, E. Drioli, Membrane emulsification as a novel method to distribute phase-transfer biocatalysts at the oil/water interface in bioorganic reactions, J. Membr. Sci. (2007), doi:10.1016/j.memsci.2007.07.016

Development of a nano-sized abrasive for advanced polishing applications in IC manufacturing

Joke De Messemaeker, Stijn Put, Daniel Nelis, Dirk Van Genechten, Paul Lippens and Yves Van Rompaey

In the manufacturing of integrated circuit (IC) chips ever more and smaller transistors are placed on a single chip, leading to increasing chip capability and speed. This miniaturisation would not have been possible without chemical mechanical planarization (CMP), an IC process step invented by IBM in the 1980's. During this step deposited films of different materials are planarized and reduced to a precise target thickness by polishing with an abrasive particles containing slurry. In view of the extremely small dimensions of the integrated circuitry, CMP induced defects such as scratches and residual particles are able to destroy the functionality of the chip. Therefore specifically designed abrasives are required, allowing minimisation of the number and size of the defects. On top of these stringent defectivity requirements the abrasives – mostly SiO_2, CeO_2 and Al_2O_3 – should produce a sufficiently high material removal rate in order to comply with the high throughput demands of modern chip fabs.

Umicore developed a gas phase synthesis process producing nano-sized CeO_2 abrasive particles for CMP possessing the required narrow particle size distribution, very low trace metal contamination levels, and controlled morphology, with the possibility to vary the primary particle size in a wide range. The impact of different powder properties such as specific surface area, particle size distribution and particle morphology on CMP performance was investigated. To this end suitable, stable dispersions were developed. An excellent control of the coarse particle tail and the morphology of the particle turned out to be of particular importance.

Deposition of carbon nanotubes in microwave torch and their application

Buršíková V.[1], Buršík J.[2], David B.[2], Eliáš M.[1], Ficek R.[3], Franta D.[1], Jašek O.[1], Kadlečíková M.[4], Klapetek P.[5], Klementová M.[6], Kučerová Z.[1], Matějková J.[7], Nečas D.[1], Schneeweiss O.[2], Synek P.[1], Vondráček M.[8], Vrba R.[3] and Zajíčková L.[1]

1 Department of Physical Electronics, Masaryk University, Kotlářská 2, 611 37 Brno, Czech Republic, lenkaz@physics.muni.cz, Telephone: +420 54949 8217, Fax: +420 54121 1214
2 Institute of Physics of Materials, AS CR, Žižkova 22, 616 62 Brno Czech Republic
3 Department of Microelectronics, Faculty of Electrical Engineering and Communication, Brno University of Technology, Údolní 53, 602 00 Brno, Czech Republic
4 Department of Microelectronics, Faculty of Electrical Engineering and Information Technology, Slovak University of Technology, Ilkovičova 3, 812 19 Bratislava, Slovak Republic
5 Czech Metrology Institute, Okružní 31, 638 00 Brno, Czech Republic
6 Institute of Inorganic Chemistry, AS CR, 250 68 Husinec-Řež, Czech Republic
7 Institute of Scientific Instruments,AS CR, Královopolská 147, 612 64 Brno, Czech Republic
8 Institute of Physics, AS CR, Na Slovance 2, 182 21 Praha, Czech Republic

INTRODUCTION

Carbon nanotubes (CNTs) are extremely interesting materials with unique properties suggesting their future important role in nanotechnology engineering. The strength and flexibility of carbon nanotubes makes them of potential use in controlling other nanoscale structures. Carbon nanotubes have already been used as fillers in polymer composites to improve the mechanical, thermal and electrical properties of the bulk product. Because of their great mechanical properties, a variety of structures has been proposed ranging from everyday items like clothes and sports gear to combat jackets and space elevators. Their unique dimensions and unusual current conduction mechanism make them ideal components of electrical circuits. Nanotube based transistors have been made that operate at room temperature and that are capable of digital switching using a single electron. Carbon nanotubes have also been implemented in nanoelectromechanical systems, including mechanical memory elements and nanoscale electric motors. They can be used also in the applications requiring a cold emission of electrons.
In this paper we will give an overview on our present research of the CNT deposition using microwave torch at atmospheric pressure in plasma enhanced CVD technique. We also describe our efforts in application of carbon nanotubes either deposited directly on the substrates for pressure or sensor by above PECVD technique or purchased from Nanocyl and used as a filler in CNT/polyurethane nanocomposites.

CATALYSTS FOR CNT GROWTH

Carbon nanotubes were deposited either using the iron-based catalytical layer on the substrate or by the direct supply of iron catalyst into the plasma phase using iron pentacarbonyl $Fe(CO)_5$. The Fe layers (5 – 20 thick) were vacuum evaporated on the top of barier $SiO_xC_yH_z$ film prepared on silicon substrate. The $SiO_xC_yH_z$ coating was deposited by plasma enhanced CVD from hexamethyldisiloxane/O_2 gas mixture and annealed subsequently in vacuum at 700 ^oC. The iron phases present in the catalytical layers were determined by conversion electron Mössbauer spectroscopy (CEMS) of the layers prepared from ^{57}Fe isotope. The CEMS confirmed that the catalytic layers are composed of Fe^{3+} phase (Fe_2O_3). This phase was stable during UHV annealing according to CEMS but UV-photoelectron spectroscopy (UPS) with the sensing depth below 0.4 nm showed reduction of the surface and creation of island structure after annealing above 600 ^oC.
The catalytical layers were also studied by optical methods, ellipsometry and reflectometry, in UV/visible/NIR range. The aim was to determine their thickness and structure (nonhomogeneity, porosity). Fitting of the optical data represened a difficult task because of very low layer thickness. The measurement were intentionally performed on the sample with the $SiO_xC_yH_z$ coating. In other case, the presence of thin native oxide on the Si substrate with not well defined optical properties could not be neglected and it would complicate even more the data fitting. In order to decrease

parameter correlation the multisample method was applied in which the measurements on a bare $SiO_xC_yH_z/Si$ sample and two similar catalytical layers on $SiO_xC_yH_z$ of different thicknesses and optical properties were fitted together.

DEPOSITION OF NANOTUBES IN MICROWAVE TORCH

It was shown in our papers that the microwave torch can be succesfully applied to the fast deposition of multi-walled nanotubes (MWNTs) on the substrate without necessity of any vacuum or heating equipment. The torch apparatus was described in detail in Zajickova *et al.* 2005. It operated at the frequency of 2.45 GHz. MW power was transmitted by a waveguide through a coaxial line to a hollow nozzle electrode. The coaxial line and the electrode accommodated a dual gas flow. Argon passed through a central opening and the deposition mixture, H_2/CH_4, was added by a set of holes in the outer housing.
Nanotubes were usually prepared on $Fe_2O_3/SiO_xC_yH_z/Si$ substrates facing the torch. Their temperature was regulated by the distance from the nozzle and hydrogen flow rate, i.e. torch height, Zajickova *et al.* 2005. The substrate temperature used usually for the deposition was 700 ^oC. The catalytic layer treatment for the production of Fe nanoparticles was an integral part of the deposition. The deposition time of several micrometers long CNTs was below 1 min. The disadvantage of the torch deposition lay in its spatial non-uniformity given by the torch dimensions. It caused non-uniform substrate heating and consequently a non-uniform deposition of CNTs. This problem was overcome by substrate heating in Ar/H_2 discharge prior to the deposition, Jasek *et al.* 2007. The deposit was a continuous films of straight standing CNTs with an average diamater below 40 nm. HRTEM showed the presence of triple-walled nanotubes with outer diameter below 5 nm. Raman spectra in the low frequency region consisted in several weak peaks assigned to RBM of thin MWNTs whereas first-order Raman peaks in the high frequency region were attributed to D, G and D' bands, Zajickova *et al.* 2007.
For certain applications like emission-based pressure sensor (see below) it was not possible to deposited CNTs on insulating $SiO_xC_yH_z$ film that should serve as diffusion barrier preventing formation of iron silicides at the beginning of CNT deposition. Therefore, the deposition was tested also on Si substrate with only Fe-based catalytical layer. It was proved that, even in this case, similar CNTs films as above can be prepared (see Figure 1).

The CNT synthesis was preliminary tested using Fe catalyst in the gas phase instead of thin layer on the substrate. Vapors of $Fe(CO)_5$ were delivered to the plasma deposition zone by bubling argon

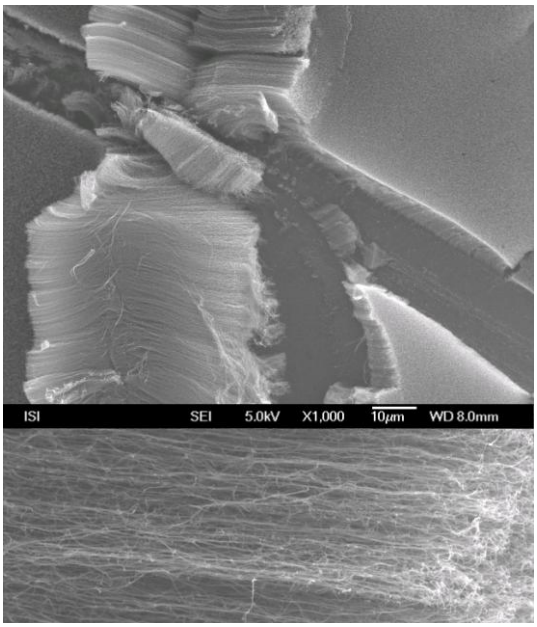

through the liquid $Fe(CO)_5$. For the characterization purposes the deposits were collected on the silicon substrate facing the torch as in the previous depositions. In certain range of deposition

conditions CNTs with quite low diameters were indeed observed by SEM (see Figure 2). It corresponded to Raman spectroscopy revealing a peak in the RBM region.

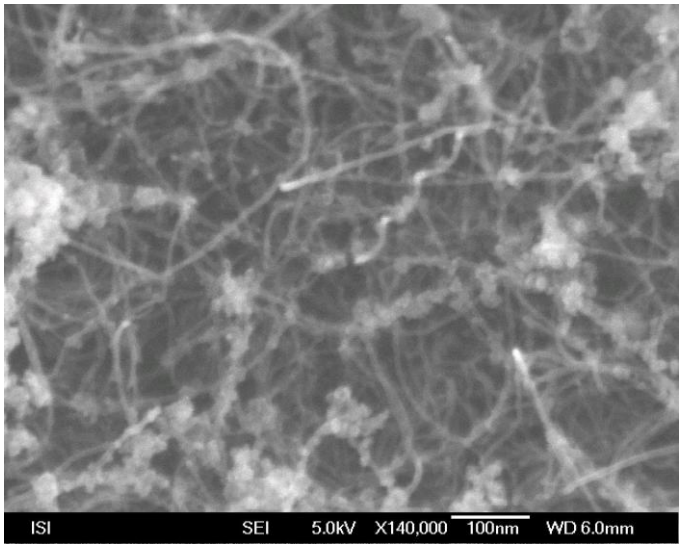

Figure 2. SEM micrograph of CNTs deposited using catalyst in the gas phase, i.e. using $Fe(CO)_5$ in the deposition mixture.

APPLICATIONS OF CARBON NANOTUBES

The CNTs prepared by the technique described above have been used in two novel sensors of pressure. The CNTs act either as an electron emission source or as an element increasing the capacitance due to an increase of the surface. Both sensors consisted of an elastic silicon membrane fabricated by wet anisotropic etching and a thicker counterpart electrode. The emission-based sensor was constructed with the elastic anode electrode and the cathode covered by MWNTs, Ficek *et al.* 2007. The capacitance sensor had both the electrodes covered by MWNTs. Additionally, the CNTs were tested in electrochemical detection of heavy metals.
Commertially purchased MWNTs were used as a filler in polyurethane composites. It was shown that 0.1 and 0.05 % of CNTs increases more than five times the plastic hardness of the composite when a good dispersion of CNTs in the polymer matrix was achieved. Further improvement of nanotube dispersion and mechanical properties was achieved when using commertially functionalized CNTs with COOH groups. The functionalization of CNTs was also performed in inductively coupled r.f. discharges in the gas feeds of Ar/H_2, Ar/H_2O and N_2/H_2. The functionalized CNTs were characterized by XPS, Raman spectroscopy and FTIR. XPS was not very sensitive technique to any kind of functionalization. It revealed about 1 % of oxygen present in the pristine commertial CNTs. This content did not changed with plasma functionalization in Ar/H_2O and N_2/H_2 but it increase to about 6 % for COOH-CNTs. FTIR showed presence of OH, COOH, NH_2 and NH_3 groups in CNTs functionalized with corresponding groups. The functionalization affected the ratio of D and G peaks in the Raman spectra.

ACKNOWLEDGEMENTS

This work was supported by the Czech Science Foundation under the contract GAČR 202/07/P523, by the Ministry of Education, Youth and Sports of the Czech Republic under the contract MSM0021622411and under the contract KAN311610701.

REFERENCES

Ficek R., Eliáš M., Zajíčková L., Jašek O, Vrba R. 2007. Gas pressure sensor based on pecvd grown carbon nanotubes. In Applications of Nanotubes and Nanowires MRS Proceedings, 1018E: 1018–EE14–05.

Jašek O., Eliáš M., Zajíčková L., Kučerová Z., Matějková J., Rek A., Buršík J. 2007. Discussion

of important factors in deposition of carbon nanotubes by atmospheric pressure microwave plasma torch. J. Phys. Chem. Solids, 68:738–743.

Zajíčková L., Eliáš M., Jašek O., Kučerová Z., Synek P., Matějková J., Kadlečíková M., Klementová M., Buršík J., Vojačková A. 2007. Characterization of Carbon Nanotubes Deposited in Microwave Torch at Atmospheric Pressure. Plasma Processes and Polymers, 4: S245–S249.

Zajíčková L., Eliáš M., Jašek O., Kudrle V., Frgala Z., Matějková J., Buršík J., Kadlečíková M. 2005. Atmospheric pressure microwave torch for synthesis of carbon nanotubes. Plasma Physics and Controlled Fusion, 47(12B): B655-B666.

Reduction of global warming potential of conductive nanocomposites using carbon nanotubes as filler

1.1 *LUIZI F.*[1], CLAES M.[1], FELLER J.-F.[2] and L. MAFFIA[3]

1 R&D Department, Nanocyl SA, Rue de l'Essor 4, 5060 Sambreville, Belgium, fluizi@nanocyl.com, Telephone: +32 71 750 383, Fax: +32 71 750 390
2 Université de Bretagne Sud, Laboratoire des Polymères, Propriétés aux Interfaces et Composites, rue de Saint-Maudé, BP 92 116, 56321 LORIENT Cédex, France
3 CDCMP - Centro di Cultura per l'Ingegneria delle Materie Plastiche, Politecnico di Torino Sede di Alessandria, Viale Teresa Michel 5, 15100 Alessandria, Italy

INTRODUCTION

Carbon nanotubes can be used, amongst other applications, as conductive filler for the manufacture of low resistivity thermoplastic materials. The added value of such nanocomposite compared to long existing solutions based on carbon black as the filler, lies mainly in the low addition of carbon nanotubes required for a given conductivity. The low filler content results in improved, or rather lesser degraded, mechanical properties of the composites.

Further to that mechanical interest of the substitution of carbon black by carbon nanotubes, the global environmental impact of the production of such materials is also largely in favor of the carbon nanotubes based composites. The research work presented in this paper was focuses on the quantification of such advantage as part of the determination of the Life Cylce Analysis of carbon nanotubes based nanocomposites.

RESULTS

Within the Life Cycle Analysis (LCA), two main parameters have been selected to reflect the impact of a material on the environment, the global energy requirement (GER) and the global warming potential (GWP). In view of minimizing such impact, two approaches have been followed. One consists in improving the dispersion of the filler in a nanocomposite, thereby reducing the loading of the filler for identical properties. The other consists in improving the production technology to reduce waste and energy consumption as well as to improve the yield. For this latter, two stages of improvement beyond the laboratory scale production have been developed and evaluated; an industrial production open line and one with recycling of gases. The various approaches have been quantified in the frame of the production of a reference conductive nanocomposite using carbon nanotubes as the conductive filler. Improvement of the production of the nanotubes reduced by 45% their GER and by 76% their GWP. Improved dispersion further reduced the GER of the nanocomposites. As a result the reference conductive composite material produced was impacting the environment as expressed by the Global Warming Potential significantly less than a referenced, commercially available, conductive composite.

ACKNOWLEDGEMENTS

Part of the work performed in this study was in the frame of EU-funded projects under the 6th FP, one being NANOFIRE and the other INTELTEX.

Totally water-based synthesis routes to nanostructured metal oxides with electronic applications

Van Bael M.K.[1,2], *Hardy A.*[1,3], Van den Rul H.[1,2], Mullens J.[1]

1 Hasselt University, Institute for Materials Research, Laboratory of Inorganic and Physical Chemistry, Agoralaan Building D, 3590 Diepenbeek, Belgium, marlies.vanbael@uhasselt.be, Telephone (0)11 268393, Fax: (0)11 268301
2 IMEC Division IMOMEC, Agoralaan Building D, 3590 Diepenbeek, Belgium
3 XIOS Hogeschool Limburg, Department Industrial Sciences and Technology, Agoralaan Building H, 3590 Diepenbeek, Belgium

INTRODUCTION

Metal oxides with different compositions have important applications in different devices, such as photovoltaic cells, based on nanocrystalline TiO_2 or ZnO, energy harvesting systems, containing e.g. piezoelectric $Pb(Zr,Ti)O_3$, or MOSFET high-*k* gate dielectrics, like ZrO_2 or HfO_2, for reduced power consumption, etc.

In our research group, a water based solution-gel route is being developed for the preparation of many different (multi)metal oxides. This route distinguishes itself from other sol-gel or metalorganic decomposition synthesis routes by the use of water as the solvent, having economic and ecologic advantages. To prevent hydrolysis and condensation of high-valent metal ions, water soluble coordination complexes, most often with citrato ligands, are synthesized. These are then used as the start materials in (multi)metal ion precursor solutions. It has been demonstrated that thus prepared water based-precursor solutions can be applied for chemical solution deposition (CSD) of thin films of e.g. ferroelectric multimetal oxides.

Currently, the use of water based precursor solutions is being evaluated for the preparation of more complex nanostructures such as ultrathin (< 10 nm) continuous layers and nano-islands.

Also, metal oxide nanoparticles are being synthesized by means of water-based chemical solution methods, and further implemented as the building blocks of nanostructured metal oxides or hybrid nanocomposite materials.

Water based chemical solution synthesis of (multi)metal oxides

In first instance, the aqueous solution-gel route is applied for the preparation of (multi)metal oxide (nano)powders, where the high degree of homogeneity in the precursor is maintained throughout the thermal decomposition and leads to low crystallization temperatures and phase purity. An in depth understanding of the precursor solution and gel chemistry and their decomposition mechanism is obtained [VdRul06, VBael05, Hardy03].
In a next step, the route has shown to be applicable for the deposition of thin metal oxide films (thickness > 100 nm) as well. The use of adequate substrate surface pretreatments hereby allows the preparation of uniform, dense or porous thin films [VBael02]. In this way, ferroelectric thin films were prepared as well as conducting and semiconducting oxides [Nelis04, Hardy05, Bretos06, VWerde07, Truijen07].

Up to date, materials research is progressing towards continued miniaturization into the nanoscale, combined with controlled nanostructure formation. Our most recent research is focused on advanced chemical preparation routes for these purposes. On the one hand, metal oxide or hybrid materials with a rather complex nanostructure are investigated for several different applications such as solar cells, while on the other hand applications requiring nanosized materials on substrates are envisaged, for instance in nanoelectronics.

The aqueous solution-gel route is now being investigated to achieve these goals, which implies stretching its limits beyond powder synthesis and thin films. The previous requirements still remain: phase purity, high degree of homogeneity, low crystallization temperature, economic and ecologic aspects, ... But, additional demands are made: control over shape, size, microstructure,....

Water based CSD: beyond the deposition of 'conventional' thin layers

The application of aqueous solution-gel synthesis to the preparation of continuous and uniform, ultrathin films as well as nanoislands on substrates, based on the microstructural instability phenomenon, will be discussed.

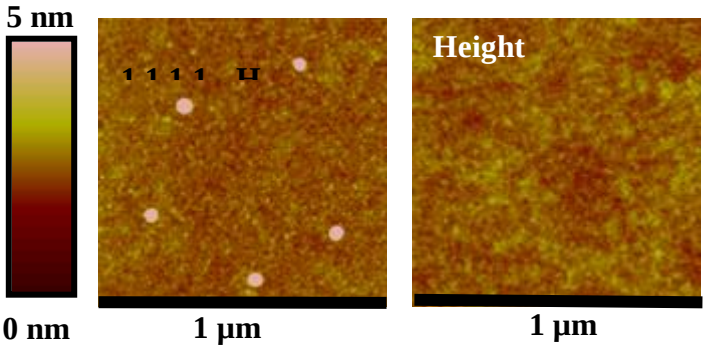

Figure 1: Upon CSD of a first precursor composition, separated, circular structures are observed (diameter ~ 50 nm), while the second precursor composition allows uniform substrate coverage.

The preparation of ultrathin films (<30 nm) by means of CSD has long been thought to be impossible, as partial substrate uncoverage was observed. However, recently, this has been shown to be possible by means of aqueous CSD. On the other hand, the rupture of the film into separate nanoislands can also be put to use, e.g. for the preparation of nanostructures on a substrate [Alexe06]. The factors that govern whether one or the other process occurs, are being studied studied.

Depending on the precursor composition or concentration and the thermal treatment, different results are obtained, as is illustrated for different metal oxide materials in figures 1 and 2.

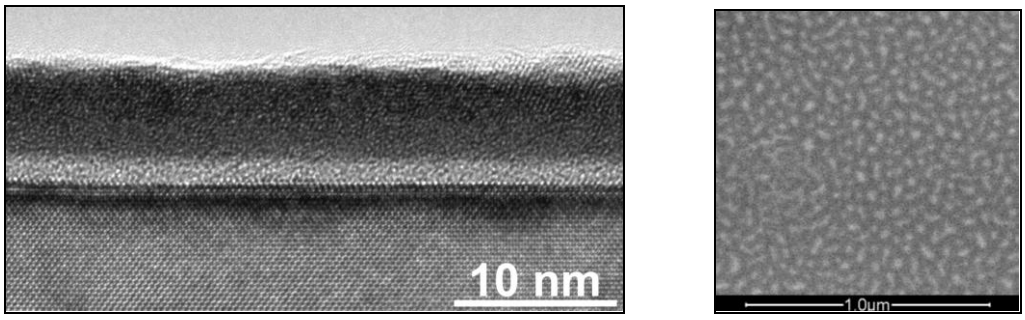

Figure 2: (left) A continuous metal oxide ultrathin film (5.7 nm), which possesses excellent thickness uniformity over a broad range, is obtained by means of CSD of a diluted water-based precursor solution.

(right) Individual nano-islands of a ferroelectric metal oxide are prepared by means of CSD of a water-based precursor solution.

This demonstrates the possibility of tailoring, on a nanosized scale, the metal oxide's microstructural properties and therefore its properties and applicability. The application of ultrathin film deposition by aqueous chemical solution routes in the search for alternative gate dielectric materials will be discussed in further detail [VElsh07, Hardy07] also considering their electrical performance.

Metal oxide nanoparticle based devices

The formation by water-based methods of nanoparticles of e.g. ZnO and TiO_2 with different morphologies is extensively reported on in international literature [VdRul2007]. However, still, no systematic and decisive information about the mechanisms, leading to either spherical or high-aspect ratio particles is known.
In the work presented here, ZnO and TiO_2 nanoparticles (figure 3) and nanorods are being synthesized by means of a hydrothermal method [Elen06, Lepot07]. The influence of different synthesis parameters on the particles' size and shape is investigated in a systematic way [Elen08].
The synthesized nanoparticles are used as building blocks for the mesoporous n-type electrode in Grätzel-type hybrid photovoltaic devices. A favourable effect on the properties of the photovoltaic cell is observed in the presence of a dense TiO_2 layer [Truij07] that reduces leakage current and shortcut between the transparent oxide electrode and the mesoporous n-type semiconducting layer.
Also, it has been demonstrated, that a water soluble organic hole conductor can be used in fully solid sate solar cells, and in combination with water processable TiO_2 layers, to develop 'green' solid state solar cells [Haeld07]. The presented water-based synthesis procedure for the photosensitizer, electron and hole conductor, demonstrates the possibility to develop fully 'green' solid-state solar cells. Further improvement of the solar cell properties, by optimizing the active layer's thickness, morphology and porosity are now in progress.

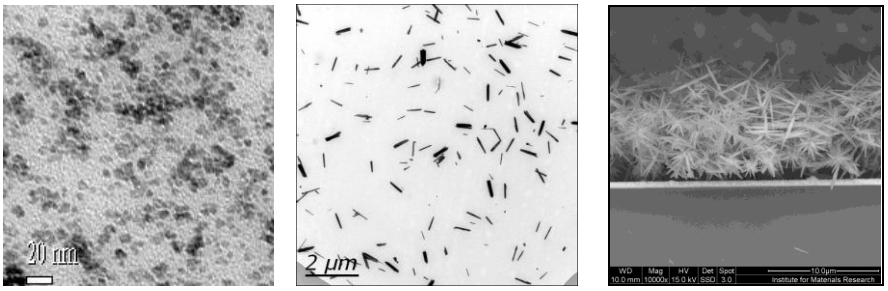

Figure 3. (Left) TiO_2 nanoparticles, (middle) ZnO nanoparticles and (right) ZnO based porous layer synthesized by a hydrothermal method.

CONCLUSIONS

It can be concluded that the aqueous solution-based synthesis method, and more specifically the water based solution-gel method, which has been developed intensively in our research group, is now a mature method. It shows a strong potential for the synthesis of highly complex, nanosized and nanostructured (multi)metal oxide systems. The presented water-based methods offer promising possibilities for the 'green' production of 'green' devices.

ACKNOWLEDGEMENTS

M. K. Van Bael and A. Hardy are postdoctoral research fellows of the Research Foundation Flanders (FWO-Vlaanderen). The research has been partly financially supported by the Fund for Scientific Research-Vlaanderen (FWO) under research project G.0273.05.

REFERENCES

Alexe, M., Hesse, D., 2006. Self-assembled nanoscale ferroelectrics, J. Mater. Sci., 41, 1.

Beusen, J., Van Bael, M.K., Van den Rul, H., D'Haen, J., Mullens, J. 2007. Preparation of a porous nanocrystalline TiO_2 layer by deposition of hydrothermally synthesized nanoparticles Journal of the European Ceramic Society, 27, 4529 - 4535.

Bretos, I., Jimenez, R., Calzada, M.L., Van Bael, M.K., Hardy, A., Van Genechten, D., Mullens, J., 2006. Low toxic processing of $(Pb_{1-x}Ca_x)TiO_3$ thin films by an aqueous solution-gel route, Chemistry of Materials, 18, 6448-6456.

Elen, K., Van Bael, M.K., Van den Rul, H., D'Haen, J., Mullens, 2006. J.Additive-free Hydrothermal Synthesis of High Aspect Ratio ZnO Particles from Aqueous Solution, Chemistry Letters 35, 12, 1420.

Elen, K., Van Bael, M.K., Peeters, R., Van den Rul, H., Hardy, A., Franco, D., D'Haen, J., Mullens, J., 2008. Hydrothermal synthesis of ZnO nanorods: a statistical determination of the significant parameters in view of reducing the diameter, submitted.

Haeldermans, I., Truijen, I., Vandewal, K. Moons, W., **Van Bael**, M.K., D'Haen, J., Manca, J., Mullens, J., 2007. Water based preparation method for 'green' solid-state polythiophene solar cells, Thin solid films, in press.

Hardy, A., Van Werde, K., Vanhoyland, G., Van Bael, L.K., Mullens, J., Van Poucke, L.C. 2003., Study of the decomposition of an aqueous metal-chelate gel precursor for $(Bi,La)_4Ti_3O_{12}$ by means of TGA-FTIR, TGA-MS and HT-DRIFT, Thermochim. Acta, 397, 143.

Hardy, A. Nelis, D., Vanhoyland, G., Van Bael, M.K., Van den Rul, H., Mullens, J., Van Poucke, L.C., D'Haen, J., Goux L., Wouters, D.J., 2005. , Effect of crystallization parameters on the properties of $Bi_{3.5}La_{0.5}Ti_3O_{12}$ thin films deposited by aqueous chemical solution deposition, Thin Solid Films, 492, 105.

Hardy, A., Van Bael, M.K., Van Elshocht, S., Adelmann, C., Conard, T., Franquet, A., Douhéret, O., Haeldermans, I., D'Haen, J., De Gendt, S., Caymax, M., Heyns, M., D'Olieslaeger, M., Van Bael, M.K., Mullens, J. 2007. Ultrathin functional metal oxide films from aqueous chemical solution deposition, submitted.

Lepot, N., Van Bael, M.K., Van den Rul, H., D'Haen, J., Peeters, R., Franco, D., Mullens, J., 2007. Synthesis of needle like ZnO nanoparticles from aqueous solution, Materials Letters 61, 13 (2007).

Nelis, D., Mondelaers, D., Vanhoyland, G., Van den Rul, H., Van Bael, M.K., Mullens, J., Van Poucke, L.C., D'Haen, J., Wouters, D.J. 2004. Influence of heat treatment on Sr0.9Bi2.2Ta2O9 thin films prepared by aqueous CSD, , Integr. Ferroelectr., 62, 177.

Truijen, I., Van Bael, M.K., Van den Rul, H., D'Haen, J., Mullens, J., 2007. Synthesis of thin dense titania films via an aqueous solution-gel method, J. Sol-Gel Sci. Technol, 41, 43.

Truijen, I., Van Bael, M.K., Van den Rul, H., D'Haen, J., Mullens, J. 2007. Preparation of nanocrystalline titania films with different porosity by water based chemical solution deposition. Journal of Sol-gel Science and Technology 43, 3, 291 - 297.

Van Bael, M.K., Nelis, D., Hardy, A., Mondelaers, D., Van Werde, K., D'Haen, J., Vanhoyland,G., Van den Rul, H., Mullens, J., Van Poucke, L.C., Frederix, F., Wouters, D.J. 2002 Aqueous chemical solution deposition of ferroelectric thin films Integr. Ferroelectr., 45, 113.

Van Bael, M.K., Arcon, I., Van Werde, K., Nelis, D., Mullens, J., Van Poucke., L.C., 2005. Structure determination by EXAFS of Nb-peroxo-citrato complexes in aqueous solution-gel systems Phys. Scripta, 415, T115.

Van den Rul, H., Van Bael, M.K., Hardy, A. Van Werde, K., Mullens, J., 2007. in Handbook of Nanoceramics and Their Based Nanodevices. edited by H. S. Nalwa & T.Y. Tseng, in press

Van den Rul, H., Mondelaers, D., Van Bael, M.K., Mullens, J. 2006. Water based wet chemical synthesis of (doped) ZnO nanostructures. Journal of sol-gel science and technology (special issue on ZnO) 39, 1, 41.

Van Elshocht, S., Hardy, *A., Witters, T., Adelmann, A., Caymax, M., Conard, T., De Gendt, S., Franquet, A, Heyns, M., Van Bael, M.K., Mullens, J.* 2007. Aqueous Chemical Solution Deposition - Fast Screening Method for Alternative High-k Materials Applied to Nd_2O_3, Solid State Lett. 10, G15.

Van Werde, K., Vanhoyland, G., Mondelaers, D., Van den Rul, H., Van Bael, M.K., Mullens, J., Van Poucke, L.C., 2007. The Aqueous Solution-Gel Synthesis of Perovskite $Pb(Zr_{1-x},Ti_x)O_3$ (PZT) Journal of Materials Science 42, 2, 624-632.

Production of high-strength aluminum alloys reinforced by nanosize quasicrystalline particles

Milman Yu.V., Sirko A.I., Neikov O.D.

Institute for Problems of Materials Science, 3, Krzhizhanovsky Str., 03680 Kiev-142, Ukraine, milman@ipms.kiev.ua, Telephone: 38(044) 424-3184, Fax: 38(044) 424-3061

Quasicrystals are a new class of materials with unusual atomic structure and mechanical properties. As distinct from the crystalline state, the translational long-range order is absent in quasicrystals, but there is a rotational symmetry with 5-, 8-, 10- or 12-fold axes, which is forbidden in crystalline materials. Absence of translational symmetry in all three orthogonal directions is characteristic of icosahedral quasicrystals. The special atomic structure of quasicrystals is responsible for a number of unique physical and chemical properties; in particular, a very high hardness (up to 10 GPa) with some microplasticity at room temperature indentation in nanosize volume.

Peculiarities of deformation processes in quasicrystals and composite alloy quasicrystal – Al matrix as well as very low diffusion rate in a complicated quasicrystalline lattice promised to achieve a higher level of elevated temperature strength combined with a sufficient ductility.

It has been shown [1, 2] that the creation of nanoscale quasicrystalline precipitates is possible in the Al-Fe-Cr system. The alloys indicated above can be produced only by using rapid solidification technique with semi-product manufacture by powder metallurgy (PM) methods.

Japanese scientists have published several patents about heat-resistant aluminum-base alloys, in which more than 200 compositions of high-strength elevated temperature aluminum alloys with quasicrystalline reinforcing phase are described. But the Japanese scientists used a very complicated and expensive technology of alloy manufacturing. In this technology the process of producing PM rod from argon-atomizing the melt to consolidation and extrusion is carried out in a hermetic chamber with high-purity argon without carry-over of powders and billets to air.

A water atomization technique [3] was used in the present work to produce powders of Al-Fe-Cr system with disperse quasicrystalline particles and was developed a technology of their consolidation (allowing one to conserve the quasicrystalline particles in a final product).

Water atomization gives a higher cooling rate in comparison to gas atomization as well an irregular shape of particles, which is more convenient for compaction.

For creating elevated temperature Al alloys the PM technology was used in the present work. Powders were produced by water-atomization technique (fig.1).

For protecting aluminum alloy powders against oxidation in water special methods were used (cooling water and application of inhibitors).

The process of powder consolidation (CD) was developed based on the experience of the granular technology. The CD process differs from traditional ones by the insertion into a capsule of powders in the form of briquettes initially pressed at room temperature. After that the briquettes are subjected to hot degassing and compacting in hermetic capsules.

The capsule with the briquette was extruded at 350-450 ^{0}C to a rod 7-9 mm in diameter (the reduction coefficient μ = 12.8-7.7).

The chemical composition of some investigated alloys are given in the table 1.

The shape and the structure of powders is shown in fig.2.

The rapid solidification technique, which is used for production of amorphous thin ribbons, was applied as well. In this case nanostructured Al matrix strengthened by nanosize quasicrystalline particles was obtained (fig.3).

It is clear from the results of X-ray diffraction analysis of the structure of rods that a small amount of crystalline intermetallics is formed at $T_{extrusion}$ = 400 ^{0}C. But no peaks of intermetallics were registered after the extrusion at 350 ^{0}C (fig.4). In this work it was shown that, according to X-ray diffraction analysis, only the quasicrystalline i-phase as a strengthening one is present in the structure of the rods of alloys manufactured by optimum regimes.

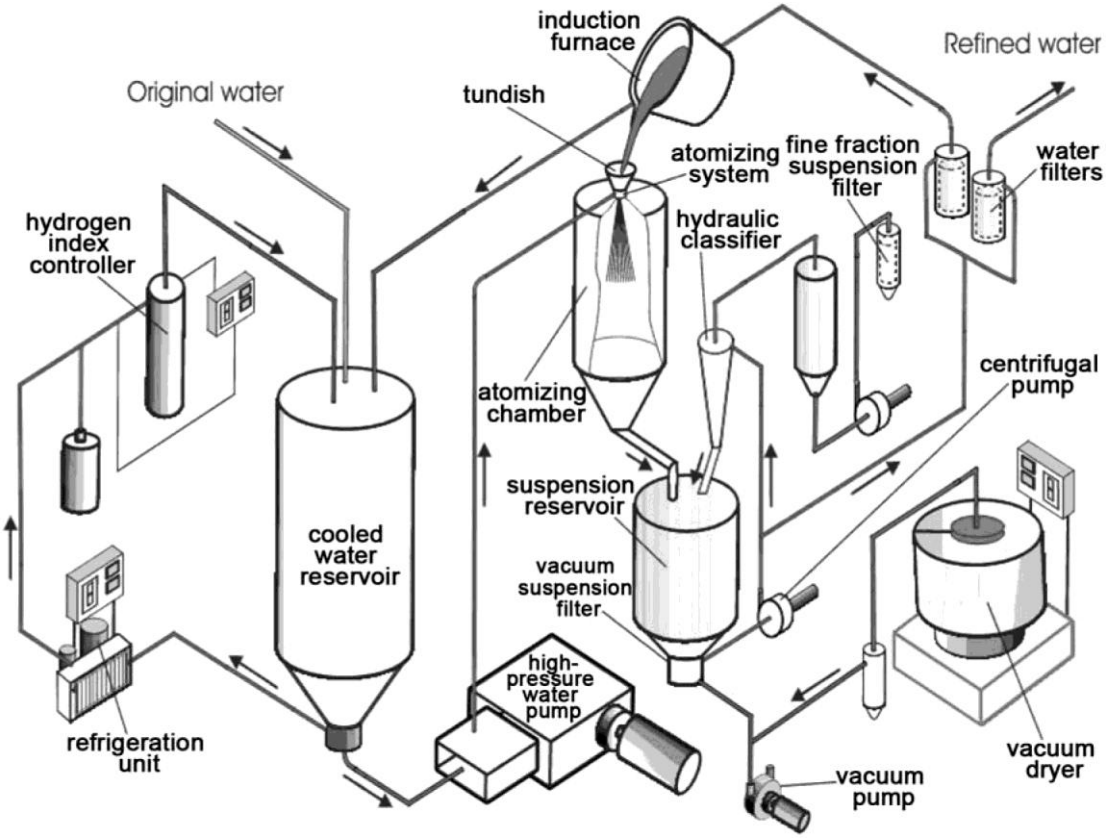

Figure1. Schematic representation of equipment for production of water atomized aluminum powders

Table 1. Composition of PM $Al_{94}Fe_xCr_yTi_zZr_{6-x-y-z}$ alloys chosen for the investigation

Alloy #	***Composition, at. %***	***Composition, wt. %***
1	$Al_{94}Fe_{3.5}Cr_{2.5}$	*Al-6.88Fe-4.54Cr*
2	$Al_{94}Fe_{2.5}Cr_{2.5}Ti_1$	*Al-4.89Fe-4.55Cr-1.68Ti*
3	$Al_{94}Fe_{2.5}Cr_{2.5}Ti_{0.5}Zr_{0.5}$	*Al-4.86Fe-4.52Cr-0.83Ti-1.59Zr*

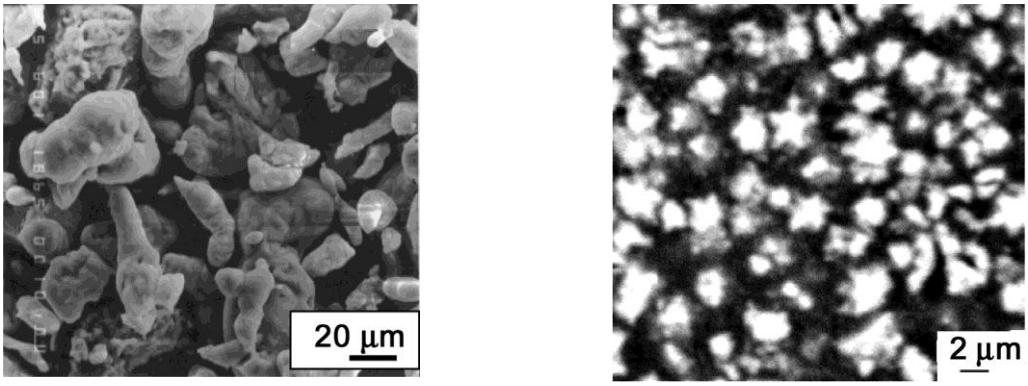

a *b*

Figure2. Characteristic particle shape in water atomized powders of Al-Fe-Cr-(Ti, Zr) alloys (a) and quasicrystalline participates in section of powder particles (SEM) (b)

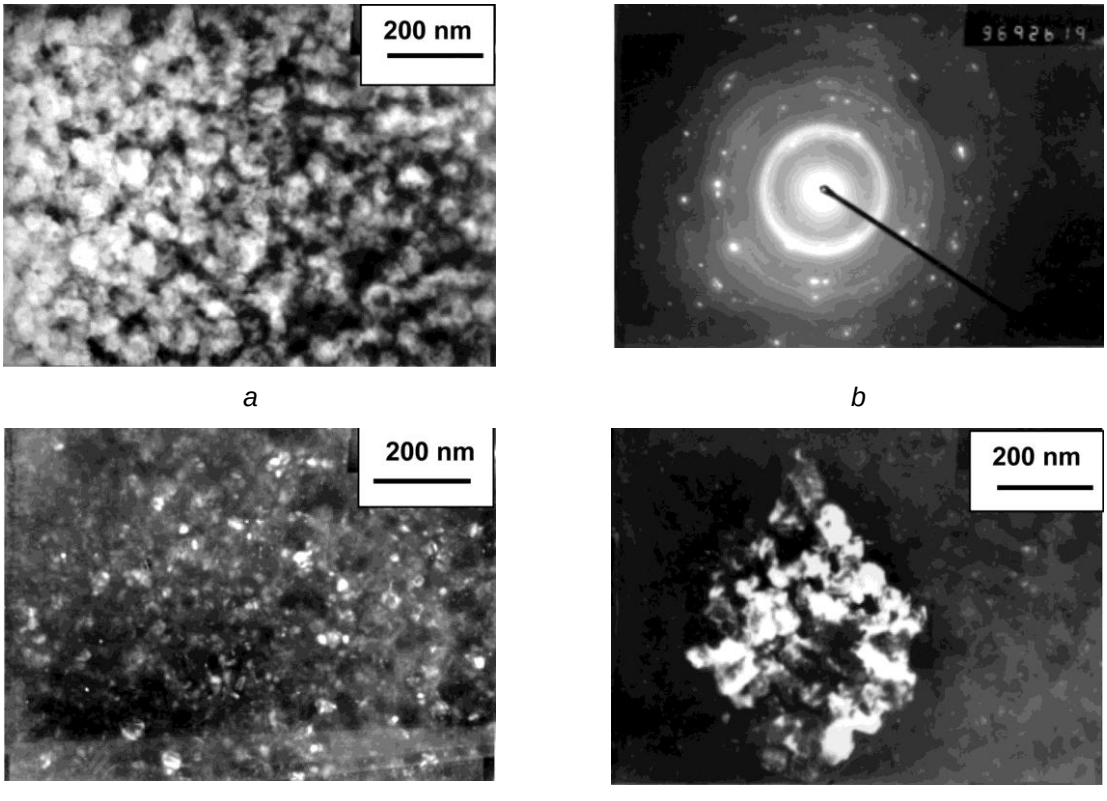

a *b*

c *d*

Figure 3. Nanocrystalline aluminum matrix reinforced by nanosize quasicrystalline particles: a) bright field image; b) electronic diffraction pattern; c) dark field image in a part of rings from quasicrystalline i-phase; c) dark field image in (220) reflection of Al

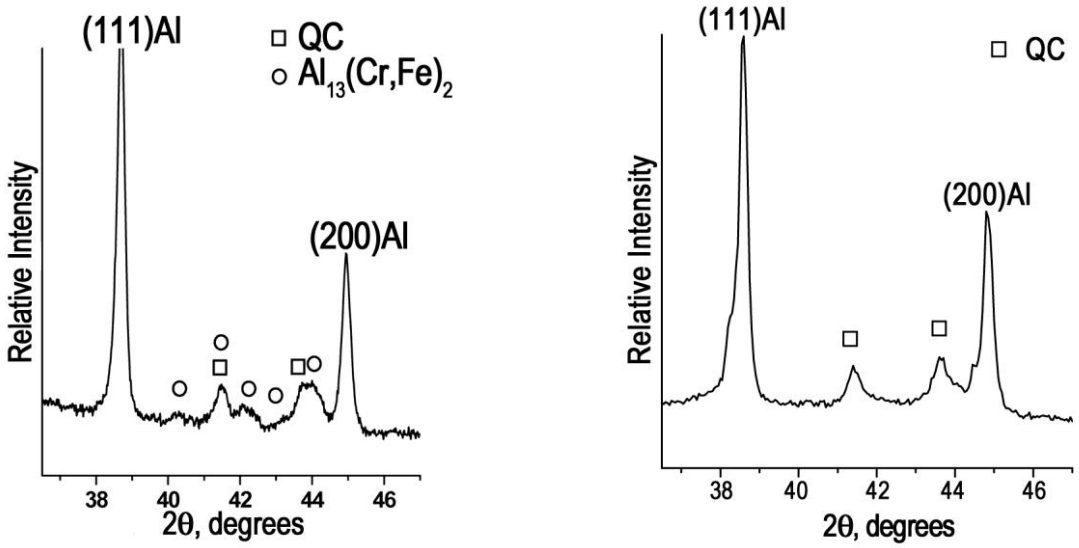

Figure 4. Sections of X-ray diffraction patterns of rods of alloys #1, λ = 12.8:
a) $T_{extrusion}$ =400 ^{0}C; b) $T_{extrusion}$ = 350 ^{0}C

Our estimation made from SEM images gives the volume part of reinforcing particles f in rods ≈ 30 % for alloys given in table 1.
The theory proposed by Gurland et al. [4] for the plasticity to fracture δ of plastic metals reinforced with particles of a rigid second phase has shown that δ is a function of the volume fraction f of the second phase only. This theory and many experimental results have shown that metal-matrix composites with f = 30 % must have very low plasticity to fracture δ, if reinforcing particles have usual crystalline structure. But there is the essential plasticity in alloys under investigation with high concentration of the second phase. We think that it is connected with unusual behavior of quasicrystals during deformation [5,6,7], namely with microplasticity of nano-quasicrystalline particles.
The values of Young's modulus in obtained alloys are 21-28 % higher than in unalloyed Al (table 2).
The produced rods have high mechanical properties both at room temperature and at the testing temperature equal to 190 and 300 ^{0}C (table 2).

Table 2. Mechanical properties of rods from Al-Fe-Cr alloys

Chemical composition	***Test temperature***									
	20 ℃				***190 ℃***			***300 ℃***		
	YS MPa	***UTS MPa***	***El %***	***E GPa***	***YS MPa***	***UTS MPa***	***El %***	***YS MPa***	***UTS MPa***	***El %***
Al-Fe-Cr	*485*	*542*	*7.0*	*87.7*	*388*	*413*	*3.44*	*283*	*297*	*3.5*
Al-Fe-Cr-Ti	*546*	*585*	*8.4*	*89.8*	*425*	*458*	*4.47*	*328*	*345*	*3.9*
Al-Fe-Cr-Ti -Zr	*648*	*677*	*7.0*	*90.0*	*464*	*511*	*2.63*	*331*	*351*	*1.8*

CONCLUSIONS

The process of water atomization may be used for producing powder of Al-Fe-Cr alloys containing i-phase. Compaction of these powders must be made by severe plastic deformation without sintering.
The elevated temperature aluminum alloys obtained by the optimum regimes had a nanostructural Al matrix (200-300 mm) and are reinforced by nanosize (50-100 nm) quasicrystalline particles.
The best compositions of Al-Fe-Cr-Ti and Al-Fe-Cr-Ti-Zr had tensile strength at 300 ^{0}C on the level of 300 MPa and higher together with the residual elongation at ambient temperature of about 8 % and Young modulus close to 89 GPa. The produced alloys had a good thermal stability of strength properties at 300 ^{0}C.
According to X-ray diffraction analysis, only the quasicrystalline i-phase as a strengthening one is present in the structure of the rods of alloys manufactured by optimum regimes.

REFERENCES

1. Inoue, A. 1998. Amorphous, nanoquasicrystalline and nanocrystalline alloys in Al-base systems. Progress in Mater.Sci., **43**, 365-520
2. Milman, Yu.V., Lotsko, D.V., Neikov, O.D. et al. 2002. Processing, structure and mechanical behavior of rapidly solidified aluminum alloys containing quasicrystalline particles. Mater.Sci.Forum, **396-403**, 723-728
3. Neikov, O.D. and Krajnikov, A.V. 1996. Water atomized powders of aluminum and its alloys. Mater.Sci.Forum, **217-222**, 1649-1653
4. Gurland, J. And Parih, N.M. 1972. in: Fracture Advanced Treatise, Academic Press, N.Y.-London, **7**, part 2, p.472
5. Milman, Yu.V., Ulshin, S.V., Iefimov, M.O. et al. 2007. Mechanical properties of submicron and nanosize quasicrystals. Abstracts of XVII Petersburg strength conference. S.-Petersburg, part 2, 9-10 (in Russian)
6. Milman Yu.V., Lotsko, D.V., Dub, S.N. et al. 2007. Mechanical properties of quasicrystalline Al-Cu-Fe coatings with submicron-sized grains. Surface & Coatings Technology, **201**, 5937-5943
7. Milman, Yu.V., Lotsko, D.V., Bilous, A.M. and Dub, S.M. 2001. Quasicrystalline materials. Structure and mechanical properties. Proc. Functional Gradient Materials and Surface Layers Prepared by Fine Particles Technology, Netherlands, 289-296

Hybrid and non siliceous ordered nanoporous materials: synthesis, applications and challenges[1]

Van Der Voort, Pascal[1]

1 University of Ghent, Dept. of Inorganic and Physical Chemistry, Centre for Ordered Materials, Organometallics and Catalysis (COMOC), Krijgslaan 281, Building S3, B-9000, Ghent. Tel: +32-9-264.44.42, email: pascal.vandervoort@ugent.be

In recent years, research efforts in the field of ordered mesoporous materials are shifting towards either hybrid materials, containing both inorganic (typically silica) and organic functionalities, or towards variants that do not contain silica at all. Promising examples of hybrid materials are periodic mesoporous organosilicas (PMOs); examples of non-siliceous mesoporous materials are carbons, polymers and metal oxides. They can be further tuned to obtain structures with a wide range of functional groups, and are candidates for applications in adsorption, catalysis, sensoring, environmental technology, microelectronics and several other applications.

INTRODUCTION

Porous materials were already known by the ancient Egyptians. The presence of voids of controllable dimensions at the atomic, molecular or nanometer scale makes them of high scientific and technological importance. A large diversity of materials with different properties is developed over the years, studied and evaluated by an interdisciplinary community ranging from chemists and physicists to medical doctors and mathematicians. The pores of the solids are classified by the IUPAC according to their size: pores with a diameter below 2 nm are called micropores, between 2 – 50 nm mesopores and above macropores.

The discovery that ordered mesoporous materials with a very narrow pore size distribution can be prepared by the hydrolysis and condensation of inorganic precursors (the sol gel process) in the presence of surfactant micelles (templates) represented a significant breakthrough in the porous materials synthesis. This discovery is generally attributed to the researchers of Mobil Oil Corporation in 1992[1]. Contrary to the microporous zeolites, ordered mesoporous materials are not necessarily ordered on an atomic level; most of the pure silica ordered mesoporous materials have amorphous silica walls. The term 'ordered' means in this context that the pores are ordered.

Pure silica based mesoporous materials have a number of intrinsic limitations. The mechanical and hydrothermal stability of the amorphous silica walls might cause problems in certain applications and the silica surface is a non ideal support material for many inorganic oxides and other catalytic active functions, which will form clusters on the silica surface (coalescence) or will dissolve in a liquid medium (leaching). Recent research efforts therefore focus on non-silica based or inorganic-organic hybrid materials.

PERIODIC MESOPOROUS ORGANOSILICAS: VERSATILE MATERIALS

The integration of organic functional groups into inorganic frameworks has led to the discovery of organic-inorganic hybrid materials with well-defined pore-structures and unique properties. These materials combine the structural characteristics of ordered mesoporous silica with the chemical functionality of organic groups. By fusing the properties of organic and inorganic building units within the same network an extremely versatile, robust and hydrothermally stable composite material is obtained.

Periodic mesoporous organosilicas (PMOs) are developed as an answer to the need for ordered mesoporous materials with high organic content in which organic and inorganic building units are

[1] For a more extensive discussion, the reader is referred to : Pascal Van Der Voort, Carl Vercaemst, David Schaubroeck and Francis Verpoort, "Ordered mesoporous materials at the beginning of the third millennium: new strategies to create hybrid and non-siliceous variants", Physical Chemistry and Chemical Physics (PCCP), (perspective article), 2008, in press (DOI : b707388g)

homogeneously dispersed throughout the network. These materials are synthesized via the direct condensation of bridged organosilanes $(R'O)_3Si\text{-}R\text{-}Si(OR')_3$ in the presence of a structure-directing agent (SDA).

The integration of organic bridges in the pore channel walls makes these organic-inorganic hybrid materials very unique. While having a high organic loading these materials can have very narrow pore size distributions, high specific surface areas, large pores, thick pore walls and large pore volumes. Furthermore, as the organic units are embedded in the channel walls, these functionalities

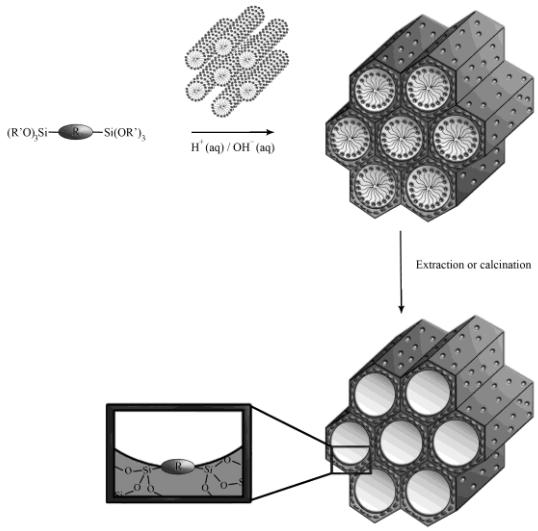

Figure 1. Synthesis procedure for PMOs.

are easily accessible for further modification.. By varying the reaction conditions, both the morphological and structural properties as the chemical and physical properties of these materials can be controlled. With these advantages and properties in mind, PMOs give way to a wide spectrum of applications in catalysis, adsorption chemistry, electronics, sensors and environmental technology.

PMOs: material challenges and progresses

The ability to control the chemistry within the channel walls as well as the typical material characteristics such as structure and morphology, offers scientists unlimited possibilities in developing materials with tailored properties. Dependent on the application, different demands will be made on PMOs. These can range from mechanical and hydrothermal stability to insulating properties.

Heterogeneous catalysts and support materials
PMOs are very promising materials for applications in catalysis, either directly as heterogeneous catalysts or indirectly as supports for homogeneous catalysts. Although the number of reports on catalytic applications is limited, these materials offer plenty of advantages over the common industrially applied microporous zeolites. The most obvious advantage is their pore sizes, which can be engineered from 2 - 30 nm, while retaining narrow pore size distributions. This broadens the applicability of PMOs as they can be employed both by petrochemical or refining companies as by pharmaceutical companies. Another important aspect in catalysis is the stability of the catalyst or the support. The hydrothermal stability of ordered mesoporous silica's, such as MCM-41 and MCM-48, is poor due to the hydrolysis of their thin pore walls (1 - 2 nm). Moreover, the hydrothermal stability of PMO materials is greatly enhanced due to the presence of organic units in the framework. Ethane-PMOs have been reported to withstand a 60-day boiling treatment, without any significant degradation[2].

Chromatography

The very surface area, the almost unlimited control over the surface functionalities and the polarity of the surface, combined with the very narrowly distributed pore channels, make PMO materials very important candidates for a next generation of chromatographic packings, either as a film in capillary columns or as a monolith. Theoretically, it can be expected that the performance and the number of theoretical plates for LC and HPLC can be augmented using these materials to values that are close to the performance of GC colums. For their use in chromatography however, it is highly desirable to obtain spherical particles with very narrow pore size distributions. In Figure 2 we show a SEM-picture of such spherical particles.

Adsorbents and environmental technology

The potential and applications of PMO's for environmental technology will be discussed in a separated paper at this conference (Els de Canck)

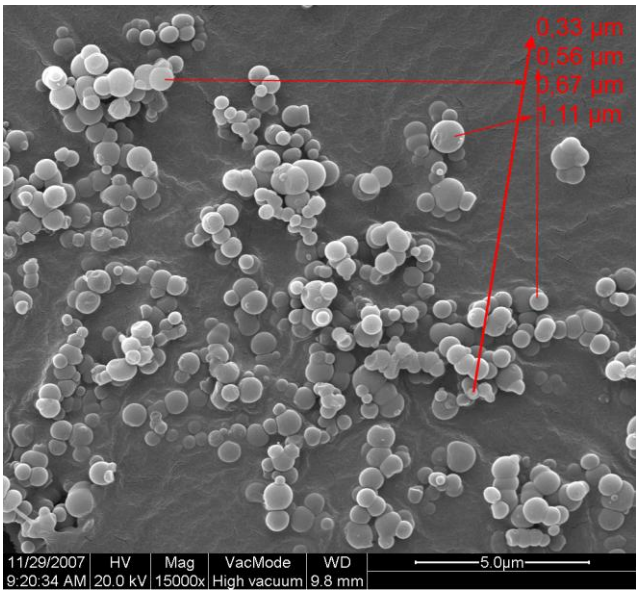

Fig. 2 SEM image of spherical particles to be used as chromatographic support material

Low-k materials

Due to their high organic content, easily controllable hydrophobicity and large pore volumes, PMO materials, under the form of thin films, are very suitable as low-k dielectrics. Besides the typical spin- and dip-coating methods, the EISA technique is especially suitable for the development of such PMO films.
Brinker et al.[3], the first group to apply the EISA approach, prepared ethane-PMO films, co-condensed with varying concentrations of TEOS and further hydrophobized with hexamethyldisilazane. Capacitance measurements indicated a decrease in dielectric values with increasing organic content, illustrating the potential of PMOs as low-k dielectrics.

ORDERED MESOPOROUS POLYMERS

Only a few studies have appeared so far on the direct templated synthesis of ordered mesoporous polymers[4]. The choice of the polymer precursor is the key to the successful organization of the organic-organic mesostructures. The polymer precursor needs (1) to dissolve in the same medium as the surfactants, (2) to interact with the template molecules (3) to organize itself neatly around the template; (4) to further polymerize, preferably forming a rigid

polymer structure, without losing the interaction with the template; and (5) the template then needs to be removed without destroying the polymer mesostructure.
The choice of resol as a precursor has been the reason for success, the resol has a large number of hydroxyl groups that strongly interact with the triblock copolymer through the formation of hydrogen bonds. Simple thermopolymerization of resol at low temperatures (<150°C) around the triblock copolymer can yield a rigid zeolite-like hydrocarbon network with tri-connected benzene rings through the formation of covalent bonds. This feature makes the polymer stable enough to withstand a thermal treatment in an inert atmosphere at 350°C, which is sufficient to decompose the surfactant. If desired, the mesoporous polymer can withstand a thermal treatment in inert atmosphere up to 900°C, converting the mesoporous polymer into a mesoporous carbon structure.
These mesoporous resol structures have, after a thermolysis process at 350°C, a specific surface area of app. 500-700 m²/g, a pore volume of 0.4 – 0.6 ml/g and a narrow mesopore distribution around a pore radius of 2.5 nm.
We believe that in the following decade, (a) a wide variety of ordered mesoporous polymer structures will be synthesized, containing all sorts of functional groups (resins containing e.g. styrene or amine functions fulfill the synthetic requirements) and (b) the range of applications of these polymers will expand towards support materials for heterogeneous catalysis and sensors. We are currently investigating these materials as a support material for VOx structures, and have solid proof that the leaching of the V-species in e.g. water is virtually zero, when anchored to the phenolic hydroxyl groups of the mesoporous resols.

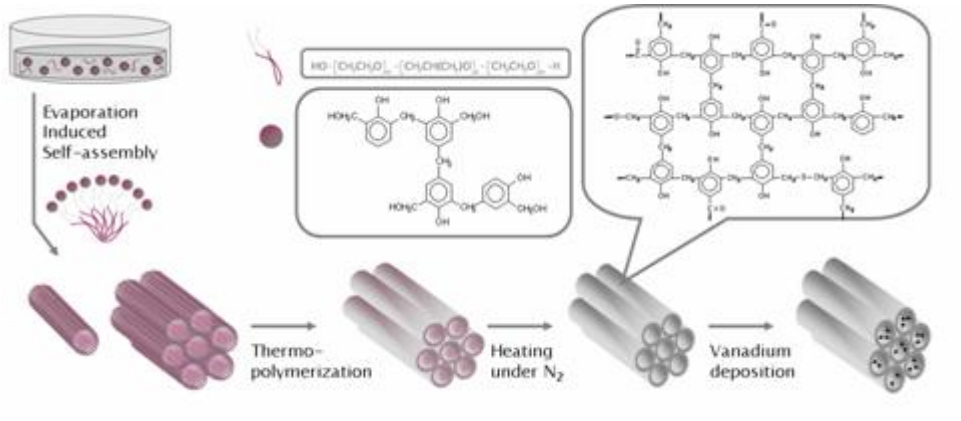

Figure 3: Overview of the synthesis of ordered mesoporous resol structures

On the other hand, the carbonized resols form mesoporous ordered carbon, which is a perfect mall to synthesis high surface area metal oxides. The general principle of this “exocasting” process is shown in Figure 4.

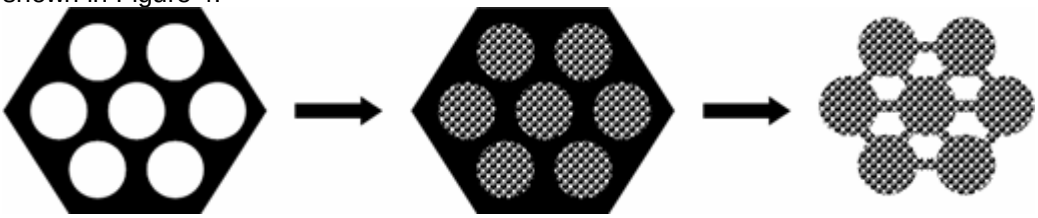

Figure 4: principles of exocasting

The use of carbon malls is a viable method for the synthesis of compositions that are difficult to prepare via direct surfactant templating. A range of porous metal oxides, including Al_2O_3, TiO_2, ZrO_2 and V_2O_5 has been prepared by this method[5] with high thermal stability and often a crystalline framework.

CONCLUSIONS

The research on the synthesis, characterization and applications of hybrid and non-siliceous ordered mesoporous materials is still in it's infancy. Yet, it is a rapidly expanding and interdisciplinary research area, not only because of the beauty of the science and the materials, but also because of the almost unlimited range of possible applications.
The preparation of ordered mesoporous materials is more laborous, more difficult and more expensive than preparing the non-ordered porous analogues; possible applications will therefore always reside in the high-tech area. Promising directions are heteregeneous (chiral) catalysis, high performance (enantioselective) chromatography and controlled drug delivery systems.
In the coming decade, an important criterion will be whether and to which extent the obtained knowledge on these materials will be converted into actual technical applications.

ACKNOWLEDGEMENTS

The author thanks his PhD-students, Els de Canck, Matthias Ide, Ilke Muylaert, David Schaubroeck and Carl Vercaemst and undergraduates Elke Roelandt and Marijke Borgers and technical staff Cindy Claeys and Danny Vandeput for obtaining most of the results shown. Financial support from the FWO-Flanders and the University of Ghent is gratefully acknowledged.

Nano-sized oxide powders for UV applications

Stijn Put, Daniel Nelis, Joke De Messemaeker, Dirk Van Genechten, Paul Lippens, Yves Van Rompaey

Inorganic ZnO, Rutile TiO_2 and CeO_2 powders are used as UV blocking compositions in paints, plastics, coatings, pigments and sunscreens. While these oxide powders absorb UV light efficiently, they also tend to catalyse the formation of super-oxide and hydroxyl radicals, which may initiate unwanted oxidation reactions. Such photo-oxidations may explain the ability of these oxides to degrade organic matter and, when present in sunscreens, cause DNA damage.

The above problem was addressed by the development of new UV screening compositions by incorporating manganese or chromium in the oxide host lattice. More specifically, a highly advanced nanosized manganese-doped titanium oxide powder having a rutile crystal phase has been developed for cosmetic sunscreen applications. This sunscreen has following advantages compared to organic based sunscreens on the market today: (i) increased UVA protection (50% increase to the best sunscreen on the market), (ii) up to 6 hours protection and (iii) high transparency and (iv) a sunscreen that can be easily spread out. Umicore developed a gas phase synthesis process for producing this highly advanced special version of nano TiO_2 with a particle size smaller than 100nm, a narrow particle size distribution and with very low trace metal contamination levels according to the pharmacopeia guidelines.

NANODISATION
A new process for sealing nanoporous anodic alumina

***Van Overmeere Q.*[1], Godeau N.[2], Langer L.[3] and Proost J.[1]**

1 Division of Materials and Process Engineering, Université catholique de Louvain, Place Sainte-Barbe 2, B-1348 Louvain-la-Neuve, Belgium; quentin.vanovermeere@uclouvain.be, Phone +32-10-47.94.08, Fax +32-10-47.40.28
2 Nanoxid sprl, B-1348 Louvain-la-Neuve, Belgium
3 Matrio-Group SA, B-4042 Liers, Belgium

INTRODUCTION

Pure aluminium is known, when exposed to air, to spontaneously develop a self-healing oxide layer that confers to the metal exceptional anti-corrosion properties. However, in some environments, or when aluminium alloys are used, the corrosion resistance may be decreased, for instance, because of the presence of second phase precipitates leading to localized corrosion or grain boundary corrosion. To avoid the corrosion of aluminium and its alloys, one strategy is to increase the thickness of the protecting oxide layer from a few nanometres to several microns. The most used process allowing such an increase in thickness is anodic oxidation, in which the aluminium part is used as the anode of an electrochemical cell. Upon application of current in a suitable, conductive electrolyte, an oxide layer starts to grow.
When an acidic electrolyte is used, anodic oxide growth proceeds in two steps : the formation of a thin but dense barrier layer, followed by the growth of an ordered, nanoporous film, with cylindrical pores aligned along the thickness direction. From a manufacturing point of view, such a porous layer has two advantages. The first one is that the voltage drop caused by the oxide is limited, allowing the total layer thickness to reach several microns while the voltage drop remains constant at about 20 V. The second advantage is that the anodic layer may be coloured by filling the pores with organic or inorganic dyes, or metallic salts. However, the disadvantage is that simply anodizing the aluminium does not result in a sufficient corrosion resistance, so that the pores also have to be sealed. Classically, this is done by immersing the anodized aluminium part in hot water, containing additives. On an industrial scale, this requires baths of hundreds of cubic meters of water, heated to about 95°C, which is both energy and water-consuming.
In this work, we propose a more environmentally-friendly route compared to the classical hot water sealing of the anodic layer. The new process, called "nanodisation", is based on a sol-gel filling of the pores after the high-speed anodising process. The resistance to corrosion, ultra-violet (UV) and heat of this new system was evaluated and compared to state-of-the art, hot water sealed anodic coatings. This already allowed to validate the new process on a lab-scale. Currently, the approach is also being tested on a continuous pilot-line with optimised current density distribution.

EXPERIMENTAL

A 5005 aluminium alloy plate was degreased and anodized in sulphuric acid to produce a 1 µm thick oxide. Half of the samples were sealed classically in hot water with nickel salt additives. The other half were pistol-sprayed with Nanoxid ALU, a commercially available Si-based sol-gel, and the three-dimensional network was formed at 150°C for 30 min. The total coating thickness was evaluated as 2.1 µm, including the porous layer. The adherence of the layers was excellent (ASTM 3359). A SEM cross section of the system is shown in Figure 1.

RESULTS

The corrosion resistance of the samples was evaluated in a salt spray chamber for 20 days. The corrosion resistance of the sol-gel sealed anodic oxide was better than the classically sealed one. UV-resistance tests were also conducted for 1000 h (ISO 11341). The measured colour (ISO 2813) of the surface changed negligibly, see Figure 2.

Heat resistance tests were conducted for 1000 h at 150°C (ECCA-T13). The measured colour of the surface is represented on Figure 3 (L*-a*-b* space). The gloss of the surface was also measured during the test (DIN 67530) and is represented on Figure 4. It can be seen that there is a slight change in the measured b-value of the colour, and in the gloss value.

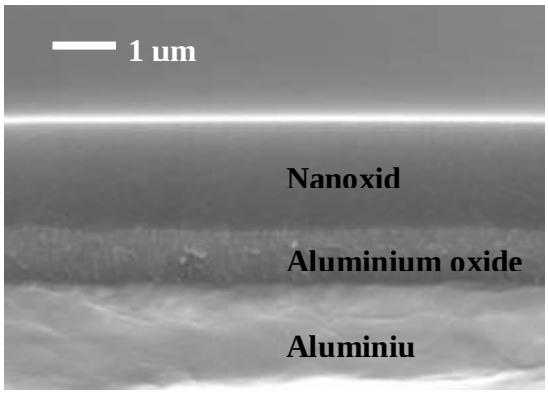

Figure 1 - SEM cross section of an aluminium anodized layer sealed by the Nanoxid ALU sol-gel

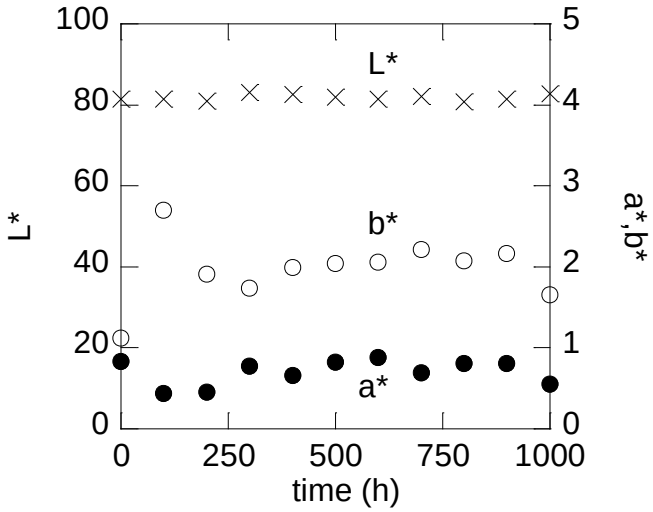

Figure 2 - colour measurements versus time when sample was submitted to UV light

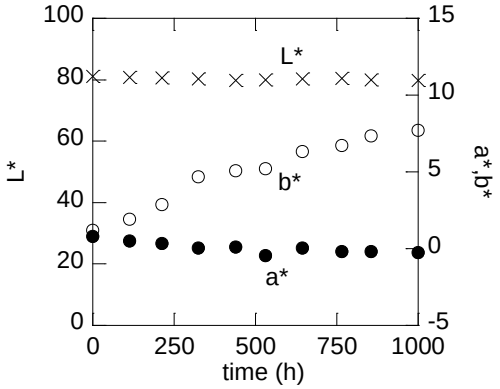

1.2

Figure 3 - colour measurements versus time when sample was heated at 150°C

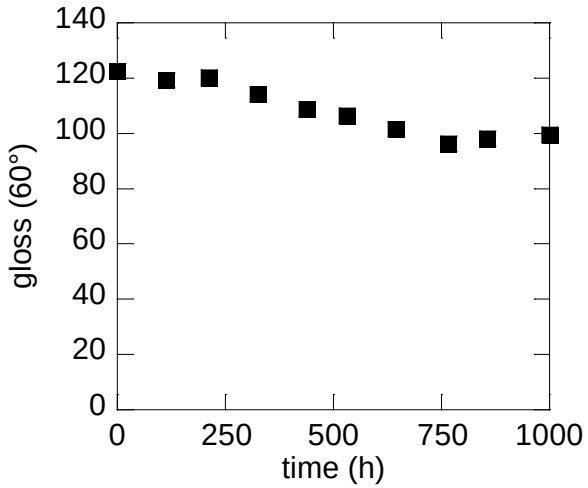

Figure 4 - gloss measurements versus time when sample was heated at 150°C

CONCLUSIONS

Anodized coatings sealed with a sol-gel technique have a level of performance similar to hot water sealed anodic coatings. On the other hand, energy and water consumption will be greatly reduced by the application of this new process on an industrial scale. Therefore, it seems to be a promising route for future anodizing processes.

ACKNOWLEDGEMENTS

Financial support from the Région Wallonne through contract number Cst-5303 is gratefully acknowledged.

REFERENCES

M. Zemanová and M. Chovancová, “New approaches for sealing anodic coatings”, *Metal Finishing* **103**, pp 33-34 (2005)

Theme 2: Biomaterials for improved quality of life

Material innovations have been at the origin of many important advances in implantable medical devices. Tissue engineering, drug /device combinations and surface modification are key issues in this medical field. The session will contain presentations on bioceramics, hybrid materials, improved porous orthopedic implants, bio-inspired ceramics, bio-nano coatings and more presentations on materials development for regenerative medicine.

Natural Fibre Composites; recent developments

***Van Vuure A.W.*[1,2] and Verpoest I.[2]**

1 Sirris[2], Celestijnenlaan 300C, bus 04026, B-3001 Heverlee, Belgium, aart.vanvuure@sirris.be, Telephone: +32-(498) 91-94-59, Fax: +32 (16) 32-1308
2 Katholieke Universiteit Leuven, Dept. MTM, Kasteelpark Arenberg 44, bus 2450, B-3001 Heverlee, Belgium

INTRODUCTION

Natural fibre composites, in which natural fibres such as flax, hemp, bamboo or kenaf are used to reinforce various polymer matrices, have drawn considerable attention in recent years. In developed markets this is mainly due to their favourable environmental characteristics. In developing markets natural fibres can often bring significant cost savings due to the utilisation of low cost fibres, which are available locally. Natural fibres are actually helping to open the market for composites in developing countries. An interesting variant, which has gained vast popularity recently is the use of so called Wood Polymer Composites, extruded profiles of short wood fibres and thermoplastic matrices, which are e.g. used for deckings and claddings. Wood-like appearance is combined with moisture resistance and durability, saving the use of tropical hardwoods.

Natural fibres can be considered as sustainable materials, because they can be grown naturally and during cultivation and harvesting typically a limited amount of energy is used. Energy required to obtain natural fibres is estimated at less than 10 MJ/kg. Data for e.g. glass fibre indicate energy utilisation up to 50 MJ/kg; for Carbon fibre this is 130 MJ/kg. Both 'renewability' and low energy consumption mean that natural fibres have a low carbon footprint. When a thermoplastic matrix is used, natural fibre composites are well suited for mechanical recycling. Wood polymer composites are typically recycled products themselves, where wood waste is combined with plastic waste. In case a biodegradable matrix is chosen, natural fibre composites can be fully biodegradable. In other cases, when thermal recycling would be the only waste handling option, at least the contribution of the natural fibre is largely carbon neutral. Recently, also renewable plastics are being developed, which can be combined with natural fibres into fully renewable or 'green' composites.

Natural fibres have other advantages: they are less abrasive than for instance glass fibres, leading to reduced machine wear. They are also more pleasant to handle and tend to fragment less easily into small particles, which should lead to health benefits. Natural fibres typically have material densities around 1.3, which is almost half the density of glass fibre. Because certain 'high performance' natural fibres like flax or bamboo have stiffness values which approach these of glass fibre, their specific stiffness is higher, which means that lighter designs are possible. Their specific strength is comparable to glass fibre. Other advantages include increased material and acoustic damping compared to glass fibre. Finally, a range of natural fibres delivers a scope of new design opportunities to the composite designer, accompanied by a natural image.

[2] Sirris houses a technological advisory service on composites and lightweight structures, in cooperation with KU Leuven and sponsored by IWT (Flemish agency for science and technology). Current advisors are Aart van Vuure and Dieter Decoster, dieter.decoster@sirris.be, tel: +32-(498) 91 94 80

This paper will highlight some recent developments in the research on natural fibre composites, zooming in on examples of work done at KU Leuven.

RESEARCH ON NATURAL FIBRE COMPOSITES

Natural fibre composites are still a relatively new member in the composites family. The current global market of fibre-reinforced plastics is about 1.5 million tons (to be compared with the total plastics market of about 120 million tons), which consists mainly of glass fibre reinforced plastics (about 600,000 tons of glass fibre). This excludes the wood-polymer extruded composites, which currently amount to roughly 0.5 million tons of composite. The annual production of natural (plant) fibres is about 27 million tons of which e.g. only about 40,000 tons currently go into composite materials for interior automotive applications in Europe (comparable to the global market of Carbon fibre which amounts up to 35,000 tons). This illustrates that the market in the developed world is still relatively small, but given the advantages listed above, there should be a good potential for further growth. The relative newness of the materials and specific issues regarding the physical and chemical composition of natural fibres, mean that there are still a few important problems which need to be addressed by research programs.

There are issues related to fibre properties, selection of matrices, control of fibre-matrix interface strength and processability.

With respect to fibre properties, major issues with natural fibres are their moisture sensitivity and limited temperature resistance. To improve moisture sensitivity, possible solutions are to hydrophobe the fibres, to coat them or to close some of their porosity (e.g. by a combined heat and pressure treatment), or to seal the fibres with the matrix material from outside moisture; in this case a good wetting and adhesion is paramount. Limited temperature resistance (about 200ºC) means that there are restrictions in the choice of matrix materials and processing conditions. Other fibre related issues are natural variability in properties and a lack of understanding of structure property relations. Natural variability could possibly be controlled by genetic selection, or controlled conditions of cultivation (e.g. reducing the impact of weather variability). Understanding structure-property relations, means producing more reliable material models.

Next to optimised natural fibres, there is a need for environmentally friendly matrices. Recently, many initiatives have started to develop both thermoplastic plastics and thermoset resins, which are either based on renewable resources or are biodegradable [Baillie, Wallenberger, Mohanty].

Crucial in making good composites is a good understanding and control of wetting and interfacial adhesion between matrices and fibres. Natural fibres and also the new environmentally friendly matrices are relatively new materials, so research is necessary to assure compatibility and control of adhesion. A complication is the relative complex geometry and composition of natural fibre surfaces. Research at KU Leuven focuses on understanding the physical-chemical aspects of wetting and adhesion (measuring surface tensions and contact angles), to allow selection of appropriate treatments or modifications of either resin or fibre surface, to control wetting and adhesion.

With respect to processability of natural fibres, important issues are development of improved extraction and separation processes to minimise damage to the technical fibres, methods to control fibre length and orientation in a composite part (many natural fibres are extracted as discontinuous fibres, which can not always easily be spun into yarns) and finally management of moisture, to prevent steam and foam formation during processing.

EXAMPLES OF RESEARCH RESULTS

In recent years research projects have been conducted and are still ongoing at KU Leuven, on flax fibres (focusing on improving the adhesion with particularly epoxy resin by various fibre surface treatments), on natural fibres for ballistic applications (panels for protection against landmines), on jute fibres (in cooperation with Bangladesh), on coir fibres (with Vietnam), on bamboo fibres (with Vietnam and Columbia, a novel process for technical bamboo fibre extraction was developed), on wood-PVC composites (with Deceuninck Plastics, focusing on further improving mechanical performance) and on silk fibres.

A first example is the use of silk fibres in biodegradable thermoplastic matrices, to make fully biodegradable and tough materials, which may be suitable for certain consumer goods. Silk fibres are exceptional, because they combine decent stiffness and strength with exceptionally high strain to failure (about 20% for cocoon silk, as compared to e.g. 1.5 – 4 % for most other fibres), which makes them very tough. By combining tough silk fibres with tough thermoplastic matrices, with a sufficiently high strain to failure, very tough composites can be produced. Figure 1 shows the absorbed impact energy as a function of the matrix strain to failure.

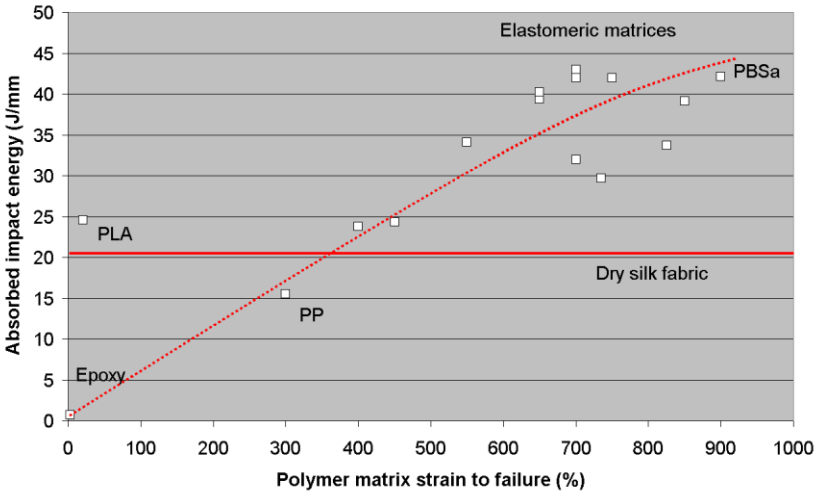

Figure 1. Absorbed impact energy normalised to panel thickness, for silk fibre composites, as a function of the matrix strain to failure.

The resulting composites are very tough compared to tough benchmark materials like 'Curv' and 'Twintex', which are currently available on the market, as demonstrated in figure 2.

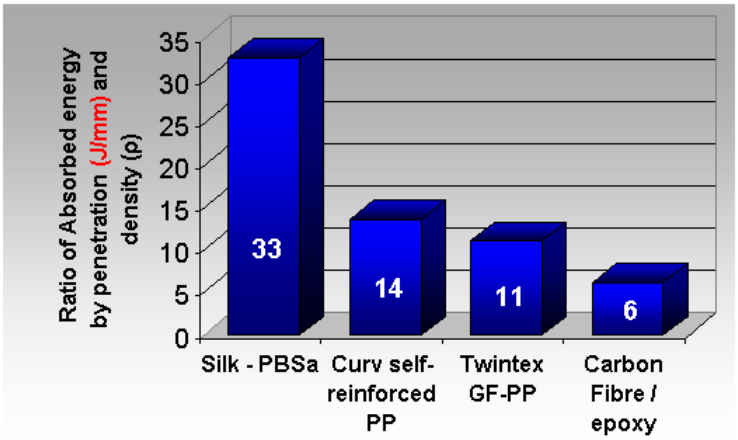

Figure 2. Impact energy normalised to plate thickness and material density for various materials; the biodegradable Silk-PBSa composite performs very well compared to various benchmark materials.

Next example is the research on fibre treatments of flax fibres to improve interfacial adhesion. Alkali treatment was shown to strongly improve the interface strength with epoxy resin, as measured by the transverse 3-point bending strength, see figure 3.

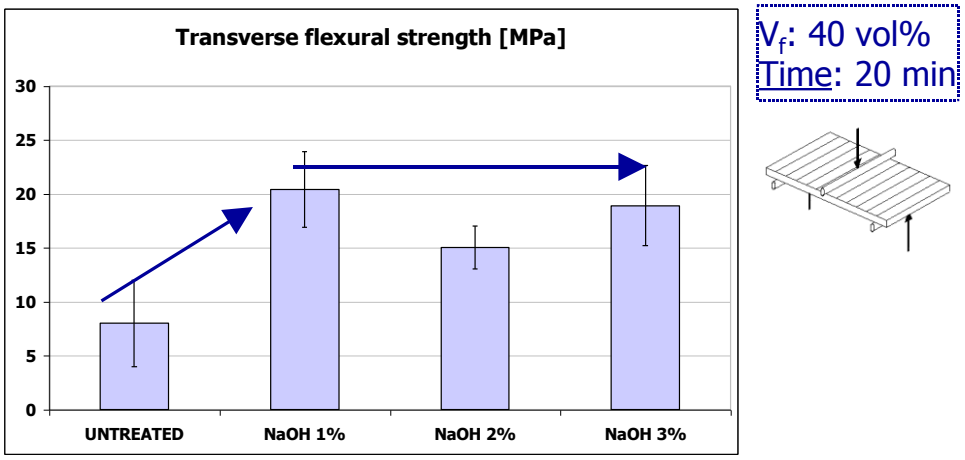

Figure 3. Transverse 3-point bending strength in flax-epoxy composites; alkali treatment strongly increases interfacial adhesion.

A third example is the development of a novel extraction process for technical bamboo fibre in a cooperation between KU Leuven and Columbian researchers. The process leads to much reduced fibre damage as compared to currently used processes like steam explosion and mechanical crushing. This is illustrated in figure 4.

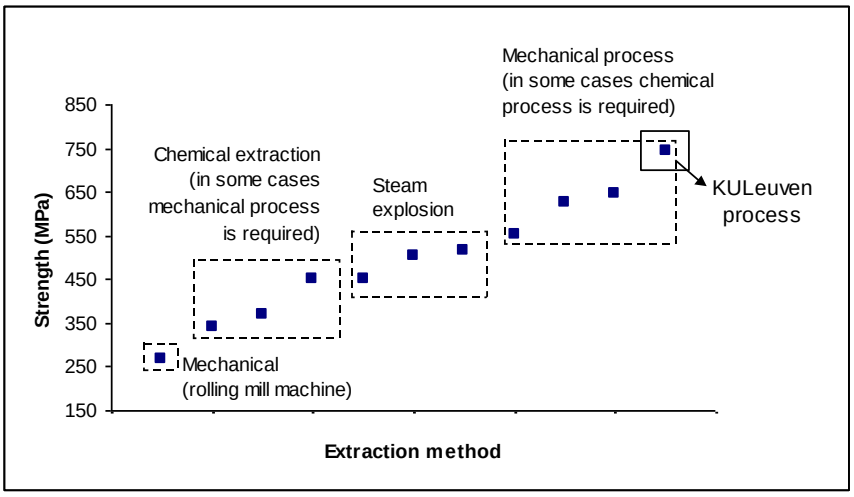

Figure 4. Comparison of various extraction processes for bamboo; the more gentle the process, the stronger the technical bamboo fibres which can be produced.

Bamboo fibre is very interesting, because bamboo is one of the fastest growing plants (grasses!) existing. Columbian bamboo can grow up to 20 m in 6 months, thus capturing large amounts of Carbon per hectare per unit of time. Interestingly, first results on bamboo fibre composites indicate a very good adhesion with epoxy resins (a transverse bending strength of 35 MPa, compare to results for flax in figure 3), without any additional surface treatment.

Finally, in figure 5 an example is given of a fully natural fibre honeycomb product: cardboard honeycomb with natural fibre composite skins, as marketed by the KU Leuven spin-off company Econcore. When a thermoplastic matrix is used, the panels can easily be shaped by thermoforming.

Figure 5. Example of 'Torhex' cardboard honeycombs with natural fibre composite skins, thus yielding a product fully made of natural fibres.

CONCLUSIONS

Natural fibre composites offer a range of favourable characteristics, of which environmental sustainability is an important one. Various case studies of recent research at KU Leuven were presented.

ACKNOWLEDGEMENTS

The research on bamboo and coir fibres is supported by BelSPO, the federal ministry of science in Belgium.

REFERENCES

Baillie, C. 2004. Green Composites, CRC Press.
Mohanty, A.K. et.al. 2005. Natural Fibres, Biopolymers and Biocomposites, CRC Press.
Wallenberger, F.T. & Weston, N. 2004. Natural Fibres, Plastics and Composites, Kluwer.

Novel development in electrospinning technology for biomedical applications: bringing a lab curiosity to a pre-pilot scale

***Ana dos Santos*, Marc Troch, Joris Dierck, Etienne Schacht**

Department of Organic Chemistry, Polymer Chemistry and Biomaterials Research Group, University of Gent,, Krijgslaan, 281-S4, 9000 Gent, Belgium

ABSTRACT

Electrospinning is a unique method capable of producing ultra thin fibres from melts or solutions of synthetic or natural polymers. The electrospinning technique involves the generation of a strong electric field between a polymer solution injected at constant flux rate though a charged needle and a grounded collector plate. When the charge overcomes the viscoelastic forces of the solution, a jet is formed and is accelerated toward the collector plate in complex pathway during which the fibres are subjected to stretching electrodynamic forces and extensive induced bending instability at the same time that the solvent evaporates. During this travel the fibres reduce their diameter till they finally randomly deposit on the collector plate [1, 2].

The morphology of electrospun fibres as well as those of the fibre mats can be by easy changed by simple control of solution parameters (e.g., molecular weight, solution viscosity, solution conductivity and dielectric effect) and processing condition parameters (e.g., applied voltage, distance, type of collector and surrounding atmospheric conditions) [3].

The versatility and potential applications of electrospinning leaded to the development of diverse electrospinning designs and a crescent interest and investment on this field with the objective different purposes as biomedical applications like scaffolds fabrication and wound healing, protective clothing, filtration improvement, controlled delivery systems like drug delivery, reinforced composites between many others [4]. How ever, limitations like small covered areas, low yield of the process and difficult up-scalling keep the concept of electrospinning at laboratory scale. To better understand its characteristics and potentialize the applications, research on the scaling up of this technology is fundamental for the growth and development of this field.

The present study intends to describe an improved design for continuous production of electrospun structures with a new way of fibres deposition. The designed prototype is based in a simple concept of “needle-printing” like production of unlimited areas of electrospun mats (Figure 1).

Due to the increase of bending instability and to the “needle printing” system the produced fibres are more regular in shape, longer and are deposited in a more stretched way (Figure 2). Unlike the traditional electrospinning process the fibres population is the same in all points of the mats imparting the same morphological and mechanical properties to each point of the produced structures. The new concept allows homogenous and limitless dimensions of electrospun mats to be produced.

Due to its simplicity and control an easy upscalling of this process can be anticipated.

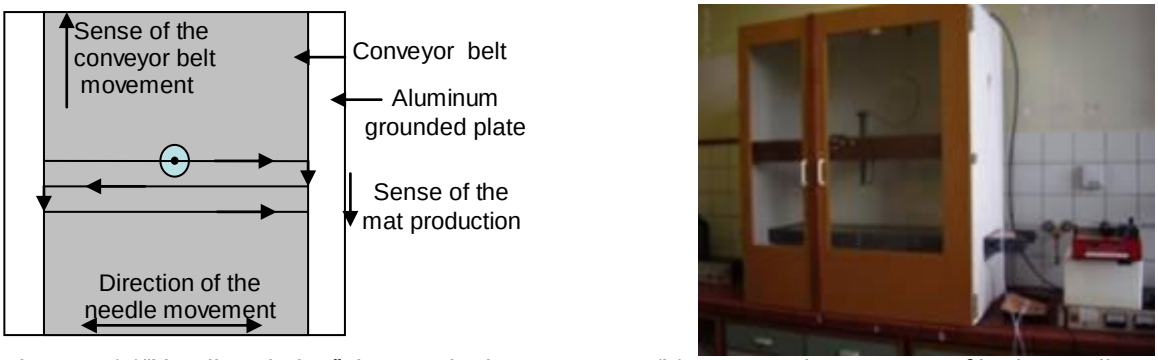

Figure1- (a)“Needle-printing”electrospinning prototype, (b) concerted movement of both, needle and conveyer belt.


a
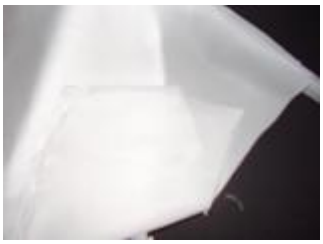
b

Figure 2- (a) Electrospun fibres and (b) mats.

References

1. Nanofiber technology: Designing the next generation of tissue engineering scaffolds, *Barnes, CP; Sell, SA; Boland, ED, et al.*, ADVANCED DRUG DELIVERY REVIEWS (2007)
2. Formation of fibers by electrospinning *Rutledge, GC; Fridrikh, SV*, ADVANCED DRUG DELIVERY REVIEWS (2007)
3. Electrospun nanofibers: solving global issues, *Ramakrishna, S; Fujihara, K; Teo, WE, et al.* MATERIALS TODAY(2006)
4. A review on electrospinning design and nanofibre assemblies, *Teo, WE; Ramakrishna, S,* NANOTECHNOLOGY (2006)

Biodegradable scaffolds for tissue engineering prepared from crosslinkable precursors.

***Etienne Schacht*[1], *Peter Dubruel*[1], *Thomasz Gorski*[1], *Ives Swennen*[1], *Sandra Van Vlierberghe*[1], *Maria Cornelissen*[2], *Evi Lippens*[2], *R. Unger*[3], *J. Kirckpatrick*[3]**

[1] *Polymer Chemistry & Biomaterials Research Group,Ghent University Krijgslaan 281, B-9000, Ghent, Belgium, etienne.schacht@ugent.be*
[2] *Laboratory of Cell Culture and Histology, Ghent University, Ghent, Belgium*
[3]*Department of Pathology, University of Mainz, Mainz, Germany*

Keywords : *biodegradable polymers, scaffolds, polyesters, hydrogels, gelatin*

Introduction

For soft and hard tissue engineering there is a need for materials adapted for a given application. We developed a series of crosslinkable prepolymers that provide either a more rigid porous structure or a soft hydrogel-type structure. All structures have in common that they are based on biodegradable polymers.

Results and discussion

Porous scaffolds based on biodegradable polyesters have been prepared by $ZnEt_2$ catalysed polymerization of lactones or trimethylene carbonates, initiated with polyols.
This results in linear or branched methacrylate-terminated polyesters/polycarbonates of reduced viscosity. The latter can be mixed with porogens or calcium phosphates. Upon photochemical curing and leaching of the porogens, scaffolds with interconnective pores can be obtained, as was evidenced by SEM and µ-CT (cfr Fig. 1).

The pore volume and pore morphology can be easily controlled by the selection of the porogen. It has been demonstrated that the pore structure influences the in vitro interaction with bone forming cells. Preliminary in vivo experiments on goats having thibia implants of the above materials showed absence of inflammation and an ingrowth of osteoblasts and bone formation starting from the periost site of the implantation.

Fig. 1 µ-CT of porous polyester

Cell seeded microcarriers based on porous gelatine matrices and osteoblast cells were immobilised into the above described crosslinkable polymers. In vitro experiments showed a significant cell viability. Such systems have been applied in vivo. Experiments are ongoing and results will be reported at the meeting.

Porous gelatine scaffolds with controlled pore morphology have been prepared by cryogenic treatment of crosslinked methacrylamide-derivatised gelatines.
The rate of cooling and the application of cooling gradients allows to control the pore morphology as illustrated by µ-CT and SEM analysis (Fig. 2). Hence, this technology has been exploited to develop porous gelatine scaffolds coated with a cell adhesive protein. Gelatine scaffolds exhibit a pronounced activity for fibronectin.

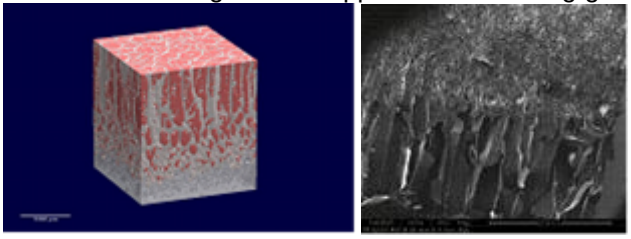

Fig. 2 µ-CT and SEM analysis of cryogenic hydrogel

In vitro studies with a series of endothelial cells and osteoblast cells have demonstrated that such carriers are good supports for cell ingrowth.

Biodegradable thermoresponsive hydrogels were prepared by modification of a PEO-PPO-PEO amphiphilic block copolymer (Lutrol) with methacrylamide end groups linked onto the polyether end groups via a biodegradable depsipeptide spacer. The latter is a combination of a selected amino acid residue and one glycolic acid or lactic acid moiety. These polymers are water soluble and photocrosslinkable ans suitable precursors for hydrogels. These gels form gels upon heating. The biodegradability can be controlled by the nature of the depsipeptide linker, leading to hydrogels with desintegration times ranging from weeks to months cfr. Fig 3).

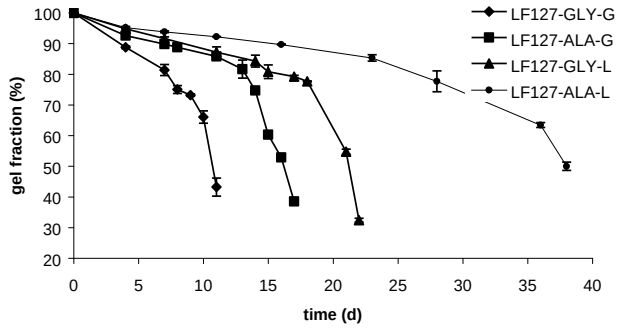

Fig. 3. In vitro degradation of hydrogels having different depsipeptide spacers

Such systems also allow the incorporation of drugs, proteins and cells into the hydrogels under very mild conditions.
In vitro biocompatibility studies indicate that these materials are well tolerated. Tests on mucosal irritations gave acceptable results.

Conclusions

Prepolymers or polymers carrying photopolymerisable end groups or side groups are attractive precursors for the fabrication of matrices for tissue repair. The versatility in the chemical design opens perspectives to tailor the systems for a given application.

Acknowledgements

The authors wish to acknowledge the financial support by the University of Ghent, the Foundation for Scientific Research Flandern and the Belgian Research Policy, IUAP-V-03

NEW MICROBIAL GALACTOSE-RICH POLYSACCHARIDE PRODUCED FROM GLYCEROL: PROPERTIES AND APPLICATIONS

Alves V. D.[1,3], Freitas F.[1,3], Hilliou L.[2], Pais J.[1], Costa N.[1], Carvalheira M.[1], Coelhoso I. M.[1], Oliveira R.[1], Reis M.A.M[1]

[1]REQUIMTE/CQFB, Departamento de Química, Faculdade de Ciências e Tecnologia - UNL, 2829-516 Caparica, Portugal. email: amr@dq.fct.unl.pt
[2]REQUIMTE/CEQUP, Faculdade de Engenharia, Universidade do Porto, 4200-465 Porto, Portugal
[3]IBET – Instituto de Biologia Experimental e Tecnológica, 2781-901 Oeiras, Portugal

INTRODUCTION

Microbial exopolysaccharides are biopolymers that represent alternatives to plant or algal polysaccharides, such as guar gum, arabic gum, carrageenan and alginate. These polymers are used in a variety of industrial applications as emulsifying, stabilizing or thickening agents. Currently, polysaccharides obtained from plants and algae still dominate the market, with microbial polysaccharides (ex: xanthan gum, gellan, pullulan and bacterial alginate) representing only a small fraction of the biopolymers market.

Nevertheless, during the last years, there has been an increasing interest in isolating and identifying new microbial polysaccharides that may compete with traditional polysaccharides due to their physical, chemical and rheological properties (Kumar et al., 2007). However, the high cost of the carbon sources used, mainly sugars such as glucose, sucrose and fructose, limits the market potential of these biopolymers. As a consequence, less expensive carbon sources must be searched in order to decrease the production costs. Glycerol is a good candidate, since it is generated in large quantities in many industrial processes, namely in biodiesel production, far beyond current consumption in traditional applications, making it a low cost substrate.

The objective of this work was the production of a new galactose-rich polysaccharide by a Pseudomonas strain using glycerol as carbon source. The polymer was isolated from the fermentation broth and characterised in terms of chemical composition, average molecular weight, rheology, flocculating and emulsifying activities, thermal properties and film forming capacity.

RESULTS AND DISCUSSION

The culture was grown on a 10 L bioreactor, under controlled temperature (30ºC) and pH (6.8 – 7.0). It was operated either in fed-batch or repeated fed-batch modes. The recovery of the EPS involved the dilution of the fermentation broth followed by centrifugation to remove the cells. After protein removal, the EPS was precipitated by adding cold ethanol to the supernatant (3:1). The polymer was then re-suspended in water and frieze dried. The operation in a repeated fed-batch mode resulted in higher exopolysaccharide production (12 g/l) and productivity (3.6 g/l day).

The exopolysaccharide has an average molecular weight of 2-5x10^6 and is composed by galactose (44 - 77%), glucose (2 - 34%), mannose (8 - 26%) and rhamnose (1 - 20%). Results have also shown that the purified exopolysaccharide contained non-saccharide components, namely, organic acid substituents, which accounted for 4.77% of the polymer's mass. Three different organic acids were identified in the acid hydrolysate: pyruvate (3.35%), succinate (1.04%) and acetate (0.38%).

Regarding its rheological properties, the polymer forms highly viscous aqueous solutions with pseudoplastic fluid behaviour. It shows a flow curve approaching the viscoelastic behavior of guar gum, with the same zero shear viscosity and similar shear thinning behaviour. The viscosity of exopolysaccharide solutions is stable under pH variations.

The exopolysaccharide revealed to have a high flocculating capacity of a kaolin suspensions (83%), similar to that of xanthan gum (65%), guar gum (76%) and carboxymethylcellulose (92%), and a significant emulsifying activity against n-hexadecane, with an emulsifying index of 38%, identical to the value observed for xanthan gum (41%).

The film forming capacity was studied by preparing aqueous solutions of the polymer, which were transferred to a casting container and left to dry at ambient temperature. Before tested, the films were equilibrated at a relative humidity of 58% resulting in a water content of about 14% (dry weight). The values of the stress at break, strain at break and Young modulus are presented in Table 1, as well as the values for the films from other polysaccharides referred in the literature.

Table 1 – Mechanical properties of the films prepared with the galactose-rich polysaccharide and with other polysaccharides referred in the literature.

Polymer	% water (dry basis)	Strain at break (%)	Stress at break (MPa)	Young modulus (MPa)
Galactose-rich polysaccharide	14	3	30	1200
Pectin (Alves et al, 2005)	10	0.9	39	51
Carrageenan (Alves et al, 2005)	20	2.3	44	28
Corn starch (Mali et al, 2006)	12	2.0	48	1229

The films show a higher strain at break and a lower stress at break when compared to the films prepared with pectin, carrageenan and corn starch. Exopolysaccharide films are as stiff as films from corn starch, as suggested by the roughly similar Young modulus measured at equivalent moisture content. Regarding the thermal properties, the galactose-rich polysaccharide films with a water content of 14% showed a glass transition temperature of 117ºC and a high melting point at 140-170ºC, revealing that the polymer is semicrystaline.

The water vapour permeability of the galactose-rich polysaccharide films (2.2×10^{-11} mol m^{-1} s^{-1} Pa^{-1}) is quite similar to that referred for pectin (3.0×10^{-11} mol m^{-1} s^{-1} Pa^{-1}, Alves et al, 2005) and corn starch (2.9×10^{-11} mol m^{-1} s^{-1} Pa^{-1}, Mali et al, 2006), but lower than that of carrageenan films (5.8×10^{-11} mol m^{-1} s^{-1} Pa^{-1}, Alves et al, 2005).

CONCLUSIONS AND PERSPECTIVES

A new galactose-rich exopolysaccharide was produced by fermentation using a *Pseudomonas* strain and glycerol as carbon source. The exopolysaccharide solutions revealed to have a viscoelastic behavior similar to that of guar gum and a stable viscosity value in a broad pH range. The polymer also possesses both flocculation and emulsifying activities. As such, these results suggest that this new exopolysaccharide may present a good alternative to natural carbohydrate polymers (for instance guar gum) currently used in applications ranging from oil recovery to food and pharmaceutical industries. The films prepared with the exopolysaccharide have shown better mechanical properties when compared to the films from corn starch. Their water vapour permeability is in the same range of that from corn starch and pectin, and much lower than that of carrageenan films. From these results, we believe that the exopolysaccharide produced is also a good agent for film formation. Moreover, the mechanical and thermal properties can be significantly improved with the addition of a plasticizer to the polymer matrix. Glycerol, used as substrate for the exopolysaccharide production, is also among the plasticizers most used in films from polysaccharides.

REFERENCES

Alves , V. D., Hilliou, L., Larotonda, F. D. S., Coelhoso, I. M., Gonçalves, M .P., Sereno, A. M. 2005. 9th International Chemical Engineering Conference (Chempor 2005), Coimbra, Portugal

Mali, S., Grossmann, M. V. E., García, M. A., Martino, M. N., Zaritzky N. E. 2006. Effects of controlled storage on thermal, mechanical and barrier properties of plasticized films from different starch sources. Journal of Food Engineering**,** 75, 453-460.

Kumar, A.S., Mody, K., Jha, B., 2007. Bacterial exopolysaccharides – a perception. J. Basic Microbiol., 47, 103-117.

ACKNOWLEDGMENTS

This project was financially supported by ENERSIS under the project “Production of biopolymers from glycerol”, 2005-2007. The financial support from Fundação para a Ciência e a Tecnologia, Pos-doc fellowship SFRH/BPD/26178/2005, is acknowledged.

Organic Coatings using Atmospheric Pressure Dielectric Barrier Discharge: En Route for a Straightforward Manufacture of Bioactive Films

***Heyse P.*[1,2], Roeffaers M.B.J.[2], Houthoofd K.[2], Hofkens J.[3], Paulussen S.[1], Jacobs P.A.[2] and Sels B.F. [2]**

1 VITO Materials Technology, Boeretang, 200, B-2400 Mol, Belgium
Pieter.heyse@vito.be , Telephone: (32) 14 335636, Fax: (32) 14 321186
2 Centre for Surface Chemistry and Catalysis, Katholieke Universiteit Leuven, Kasteelpark Arenberg 23, B-3001 Heverlee, Belgium
3 Department of Chemistry, Katholieke Universiteit Leuven, Celestijnenlaan 200f, B-3001 Heverlee, Belgium

INTRODUCTION

Material science and surface technology in particular, combined with biochemistry and molecular biology offer new and promising perspectives. A variety of applications can be though of like biosensors, implants, biocatalysis applications, among others, applicable in a vast body of industrial important sectors such as food processing, environmental technology, chemistry and medicine. The main requirement for the development of such applications is the careful and controlled synthesis of a bio-functional coating.
Plasma coating technologies are promising tools in for example the fabrication of bioactive and biocompatible materials.[1,2] Reported efforts however, are exclusively focused on two-step approaches in which the bioactive component is first immobilized on a substrate followed by a plasma polymerization treatment or vice versa.[3-5] We assert that upon minimizing the plasma energy numerous bioactive substances such as enzymes can be immobilized directly in plasmas via co-polymerization with organic precursors and entrapment in the organic polymer. [6]

Immobilization of biomolecules

A dielectric barrier discharge was employed at atmospheric pressure and ambient temperature to deposit organic coatings at reasonable growth rate containing immobilized enzymes. An enzyme solution (glucose oxidase, *Aspergillus niger*) and precursor gas (acetylene) were atomized into the plasma zone simultaneously. The enzyme activity of the obtained coating was monitored and the coatings were analyzed in depth by FT-IR, NMR, XPS, laser scanning confocal microscopy, single molecule wide field microscopy and GISAXS. These analysis provide a clear view on the activity of the immobilized enzymes, their distribution and the chemical composition of the organic matrix.

Conclusions

The mild atmospheric plasma immobilization process developed in this report may afford a sound basis for simple and straightforward plasma-assisted strategies for the immobilization of biomolecules such as enzymes in plasma-polymerized coatings. When combined with an intelligent selection of precursor and biomolecule with respect to the desired application, the ability to create plasma polymerized coatings at moderate power input and low frequency makes dielectric barrier discharges an interesting tool to develop new, single step immobilization strategies for biomolecules.

ACKNOWLEDGEMENTS

The European Commission is acknowledged for funding the presented work which was partly carried out in the framework of BIOPLASMA, a project funded by the EC under the Sixth Framework NEST program (Project no. 509012). This work was partly performed within the framework of IAP (K.U.Leuven). We also gratefully acknowledge support from the K. U. Leuven within the framework of the Centre of Excellence CECAT.

REFERENCES

[1] L. Detomaso, R. Gristina, G. S. Senesi, R. d'Agostino and P. Favia, 2005, Stable plasma-deposited acrylic acid surfaces for cell culture applications, Biomaterials, 26: 3831-3841.

[2] C. Geßner, V. Bartels, T. Betker, U. Matucha, C. Penache and C.-P. Klages, 2004, Surface modification for biomedical purposes utilizing dielectric barrier discharges at atmospheric pressure, Thin Solid Films, 459:118-121.

[3] B.J. Larson, J.M. Helgren, S.O. Manolache, A.Y. Lau, M.G. Lagally and F.S. Denes, 2005, Cold-plasma modification of oxide surfaces for covalent biomolecule attachment, Biosensors and Bioelectronics, 21: 796-801.

[4] L.C. Lopez, R. Gristina, G. Ceccone, F. Rossi, P. Favia and R. d'Agostino, 2005, Immobilization of RGD peptides on stable plasma-deposited acrylic acid coatings for biomedical devices ,Surface & Coatings Technology, 200: 1000-1004.

[5] H. Muguruma, A. Hiratsuka and I. Karube, 2000, Thin-film glucose biosensor based on plasma-polymerized film: Simple design for mass production, Analytical Chemistry, 72: 2671-2675.

[6] P. Heyse, R. Dams, S. Paulussen, K. Houthoofd, K. Janssen, P.A. Jacobs and B.F. Sels., 2007, Dielectric barrier discharge at atmospheric pressure as a tool to deposit versatile organic coatings at moderate power input, Plasma Processes and Polymers, 4: 145-157.

Scaffolds for bone tissue engineering: design, production and evaluation

***Schrooten J.*[1,2], Impens S.,[1,3] Chen Y.[4], Van Bael S.[5], Moesen M.[1] and Kerckhofs G.[1]**

1 Department of Metallurgy and Materials Engineering, Katholieke Universiteit Leuven, Kasteelpark Arenberg 44 - bus 2450, 3001 Leuven, Belgium, jan.schrooten@mtm.kuleuven.be, Telephone: +32 16 32 12 12, Fax: +32 16 32 19 92
2 Prometheus – Division of Skeletal Tissue Engineering, Katholieke Universiteit Leuven, O&N 1, Herestraat 49 – bus 813, 3000 Leuven, Belgium
3 Material Technology, Flemish Institute for Technological Research (Vito), Boeretang 200, 2400 Mol, Belgium
4 Laboratory for Skeletal Development and Joint Disorders, Katholieke Universiteit Leuven, O&N 1, bus 813, Herestraat 49, 3000 Leuven, Belgium
5 Division of Production Engineering, Machine Design and Automation (PMA), Katholieke Universiteit Leuven, Celestijnenlaan 300b - bus 2420, 3001 Leuven, Belgium

INTRODUCTION

Ageing, diseases and accidents are irrevocably related to the degeneration or malfunctioning of tissue and organs. Currently their replacement by implants, donor tissue or organs, holds very important restrictions. A new, more sophisticated biological approach seems to be the only long-term solution. An important contribution can be given by tissue engineering (TE). TE is an emerging multidisciplinary field involving biology, medicine, and engineering that is likely to revolutionize the ways we improve the health and quality of life by restoring, maintaining, or enhancing tissue and organ functions. In order to bring TE-concepts into clinical practice controllable, biocompatible, preferably biodegradable, porous materials (scaffolds) and a controllable 3D environment are required to aid in the 3D cell organisation and their development into functional tissue. The availability of consistent scaffolds will aid in the creation of a controllable 3D environment, together with the use of instrumented bioreactors.
More consistent and reproducible TE can be achieved, besides further progress in cell biology, by reducing the variability in TE-product outcome through high quality intelligent porous biomaterials together with quantitative scaffold screening techniques.

RESULTS & DISCUSSION

In this work a first step is taken towards a combined design, standardised production and quantitative in vitro and in vivo screening of both degradable and non-degradable scaffolds for skeletal tissue engineering, in order to have a motivated selection procedure prior to pre-clinical testing and secure a high quality product that will result in a guaranteed clinical improvement. Essential aspects concerning TE-scaffolds to create TE-concepts in a controllable and economically feasible manner are the following: (i) cell culturing in 3D bioreactors instead of 2D monolayer cultures because 3D cultured cells have a genetic behaviour that is more closely related to their in vivo behaviour, (ii) because cell behaviour is highly dependent on the substrate they are attached to, a thorough scaffold design, selection and consistency, based on biological requirements is needed and (iii) TE-constructs have to be produced in clinically relevant dimensions being >cm^3 instead of lab scale constructs of mm^3 and should guarantee controlled cell behaviour throughout the scaffold. Figure 1 gives a schematic representation of the different aspects mentioned above as part of an integrated approach.

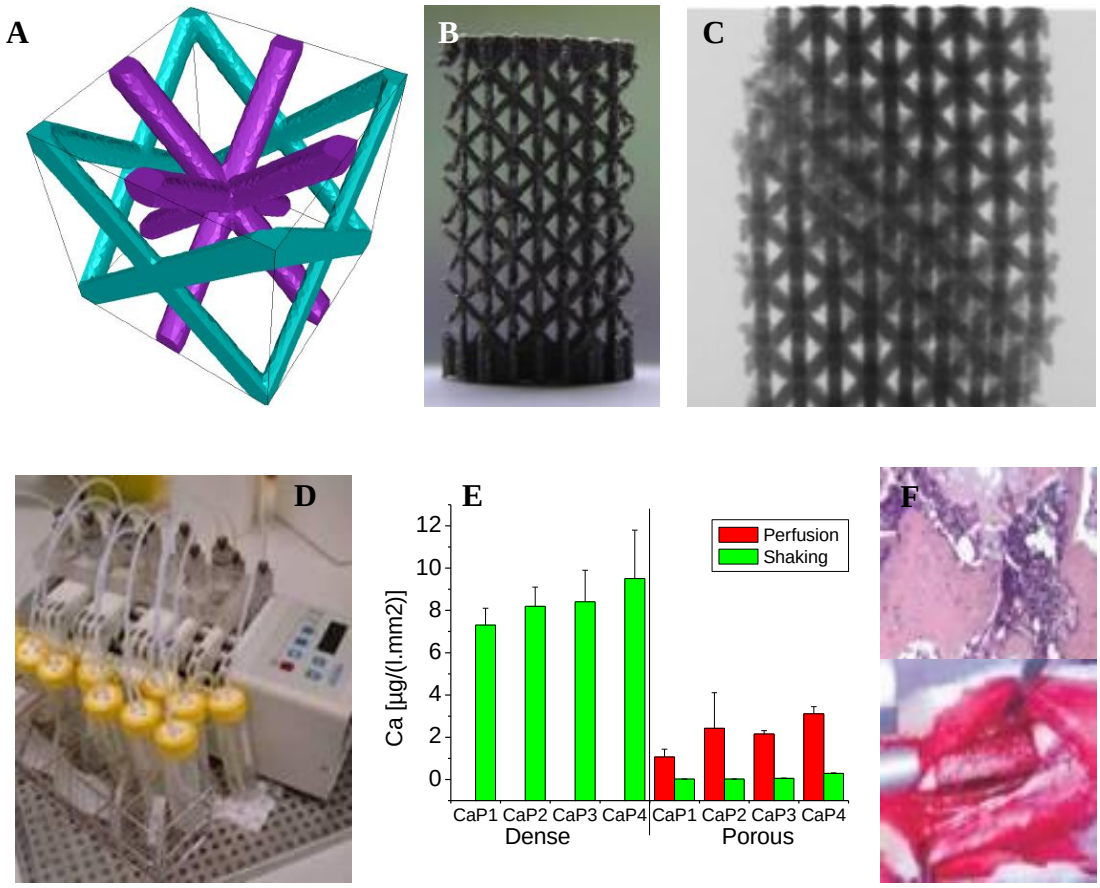

Figure 1. Schematic overview of scaffold design (A), production (B) and evaluation by in situ µCT loading(C), by perfusion bioreactor cell seeding and culturing (D), by dissolution testing (E) and in vivo implantation (F)

CONCLUSIONS

In a TE-therapy, where cells are combined with a scaffold material in order to result in a specific tissue, the scaffold needs to provide the cells with the proper signals to form the required tissue in a controlled way. In order to support this biological requirement, a proper scaffold design, production and evaluation, both in vitro and in vivo, are needed, providing quantitative data that can be correlated to the biological outcome and thus allowing controlled and more consistent cell behaviour. It is shown that an integrated approach will be required in order to evolve towards a controlled 3D cell-stimulating environment.

Validation of X-ray Micro-CT as Screening Tool for Bone Tissue Engineering Scaffolds.

***Kerckhofs G.*[1]**, **Schrooten J.**[1], **Van Cleynenbreugel T.**[2,3], **Lomov S.V.**[1] **and Wevers M.**[1]

1 Department of Metallurgy and Materials Engineering, Katholieke Universiteit Leuven, Kasteelpark Arenberg 44-bus 2450, B-3001 Leuven, Belgium, greet.kerckhofs@mtm.kuleuven.be, Telephone: 0032 (16) 321193, Fax: 0032 (16) 321990
2 Division of Biomechanics and Engineering Design, Katholieke Universiteit Leuven, Celestijnenlaan 300C, B-3001 Leuven, Belgium
3 Materialise Dental NV, Technologielaan 15, B-3001 Leuven, Belgium

INTRODUCTION

Bone scaffolds, based on biodegradable ceramics, polymers, composites of both or bio-inert metals, form an innovative solution for repairing large bone defects. To initiate the growth of bone tissue inside such structures, they need to meet certain demands, such as biocompatibility, favourable cell-material interactions, optimal pore structure and pore dimensions, mechanical properties equivalent to bone, etc. Thus, the success of bone scaffolds in bone tissue engineering largely depends on their design. Microfocus X-ray computed tomography (Feldkamp 1984; Ruegsegger 1996; Sasov 1987) (micro-CT) provides a means to acquire a complete 3D image of the structure, visualizing the internal architecture at the microscopic level in a non-destructive way. Therefore, it is a suitable tool for screening the structure of bone scaffolds. It is recently also put forward as a non-destructive, 3D imaging tool to quantify bone formation in and around scaffolds and implants.
However, since it is known that artefacts are inherently present in micro-CT images and since segmentation possibly causes errors in the structural analysis, the accuracy and reliability of the technique needs to be assessed. This study provides a protocol for 2D comparison between micro-CT and microscopy and assesses the effect of the sample material and threshold on the accuracy and reliability of the binarized micro-CT data.

MATERIALS AND METHODS

Materials

In this study, cylindrical porous titanium (Ti) structures with thin struts (figure 1) are selected as a first material to investigate the validation protocol. Two other types of scaffolds are at present still under investigation: biodegradable polyester-based scaffolds containing alpha-tricalcium-phosphate particles (PH-□TCP) and biodegradable hydroxyapatite (HA) scaffolds. The Ti cylinders have a mean radius of 3.00 ± 0.05 mm and a mean height of 10.0 ± 0.1 mm [supplied by VITO (Mol, Belgium)]. They are produced by gel casting (Impens 2005; Snijkers 2005), resulting in porous structures with struts ranging from 20 to 100 µm, pores ranging from 50 to 500 µm and a global porosity of about 80 %. The broad range in strut thickness and pore size is preferred to address structural elements much larger than the attainable spatial resolution together with the smallest possible structural elements to be visualized by our micro-CT device in the same sample.

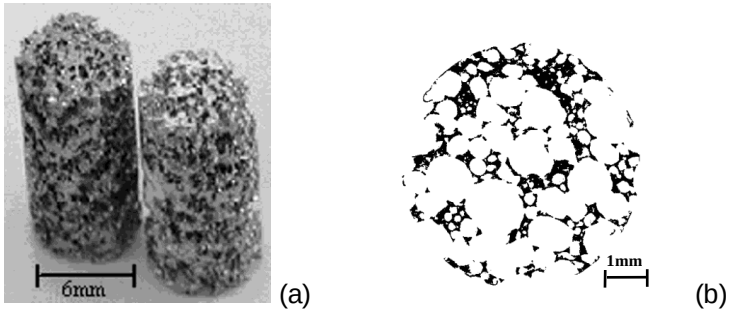

(a) (b)

Figure 1. a) A typical cylindrical porous titanium structure with a mean radius of 3.00 ± 0.05 mm, a mean height of 10.0 ± 0.1 mm and a global porosity of about 80 %, and b) an optical light microscopy image of a typical cross-section of such a sample.

Validation protocol

In 2D both the amount of material as well as its spatial distribution is verified by matching interpolated micro-CT images of the scaffolds to the corresponding microscopic sections. The validation protocol can be divided into six parts as shown in figure 2, namely (1) acquisition of a set of micro-CT images of the full sample, (2) metallographic preparation of the sample and digitizing by microscopy, (3) fitting a micro-CT image to the microscopic image, followed by the reconstruction of an interpolated micro-CT image when required, (4) registration of the microscopic to the interpolated micro-CT image, (5) binarization of the interpolated micro-CT image and (6) matching the interpolated micro-CT to the microscopic image. The visualization and binarization error in the micro-CT images is defined by the percentage overlap, overestimation and underestimation with respect to reality which are determined from the overlay images.

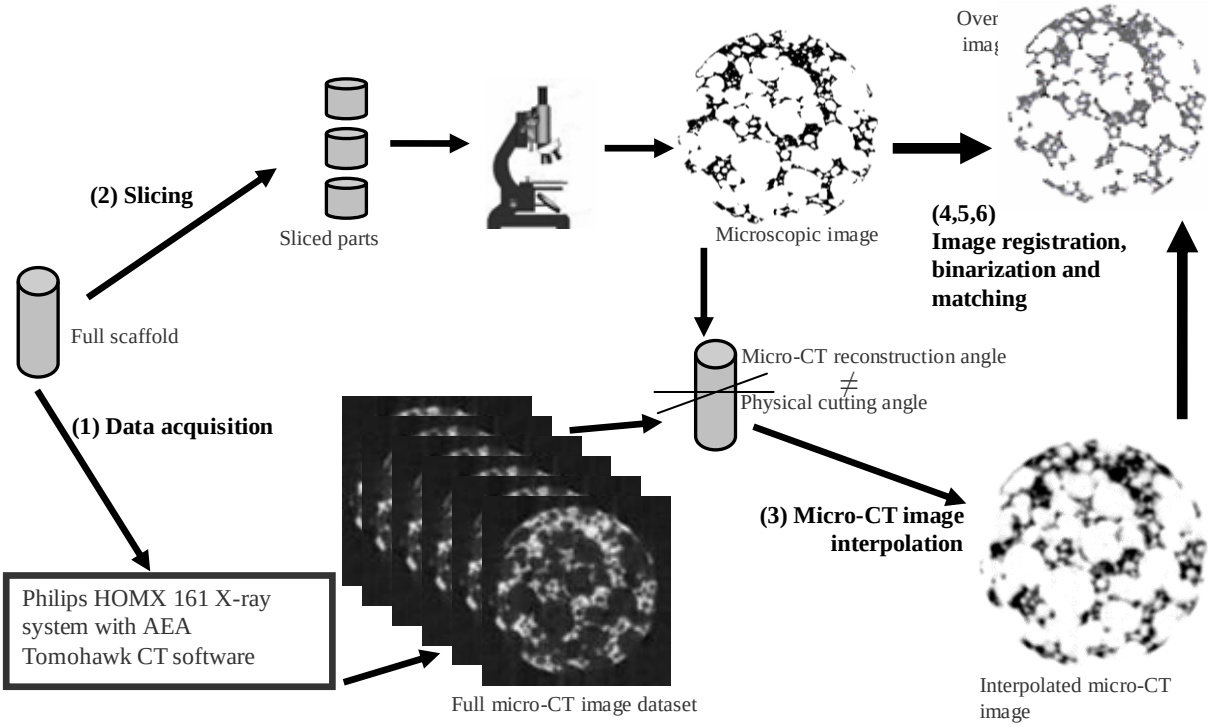

Figure 2. Schematic overview of the validation protocol consisting of six parts.

Thresholding method

In this study, a novel thresholding method is developed based on matching microscopic with their corresponding, interpolated micro-CT images. Microscopic images are 2D entities consisting of pixels (picture elements). Micro-CT images on the other hand are 3D entities expressed in voxels (volume elements) with a certain thickness. In this research the thickness of the micro-CT images is kept minimal which results in cubic voxels, thus no averaging is made over the thickness. To prevent confusion, from now on the pixels in the microscopic images and the voxels in the micro-CT images are referred to as ‘elements’.

When overlaying both the microscopic and their corresponding, interpolated micro-CT images, the optimum is represented by a maximum in coinciding and a minimum in non-coinciding solid elements. By altering the threshold value for the micro-CT images, this optimum can be approximated. Per set of microscopic and corresponding, interpolated micro-CT image (= image set), the threshold approximating the optimum the closest, named the ‘best’ threshold, is determined. By averaging the ‘best’ threshold values over a significant amount of image sets, the ‘optimal’ threshold is defined. This ‘optimal’ threshold is only valid for the selected material, micro-CT device and acquisition parameters. If one of these settings changes significantly, a new ‘optimal’ threshold needs to be determined.

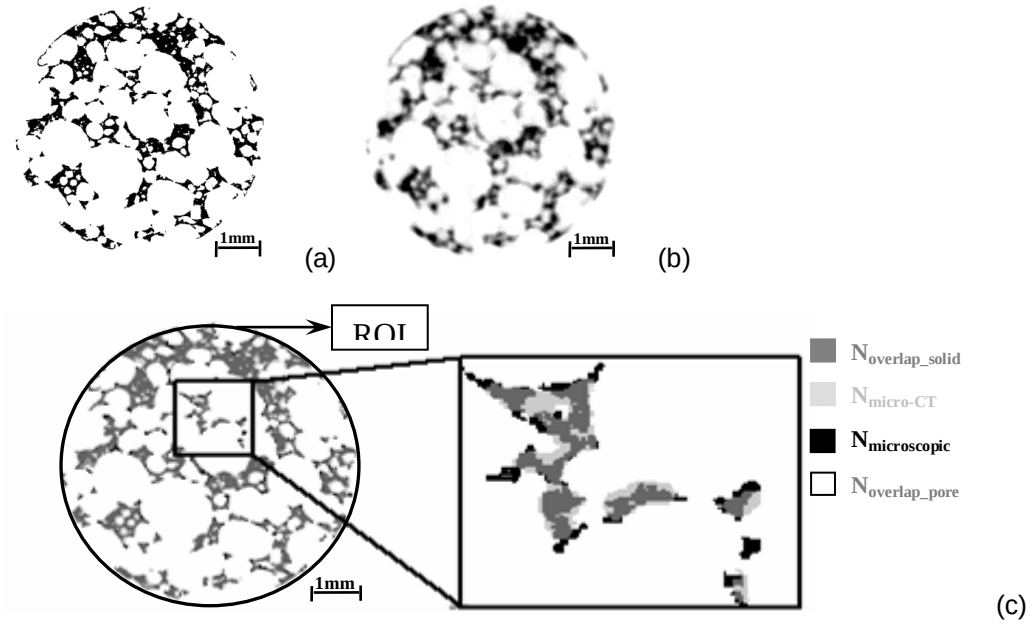

Figure 3. For a particular titanium porous sample (Φ 6mm): (a) the microscopic image of a metallographic slice, (b) the corresponding, interpolated micro-CT image and (c) the resulting match of both.

One of the major advantages of this novel thresholding method is that it accounts for closed pores, in contrast with the Archimedes method (Ding 1997, 1999). Also, since the physical visualization of the structure is taken as a reference, it results in binary images closely representing the real structure. It is a time consuming procedure, but once the 'optimal' threshold is determined for certain settings, it can be used for further research. Still, an important limitation of the method is that it is a global thresholding method and hence it does not locally account for the errors present in micro-CT images due to the limited spatial resolution, partial volume effect (PVE) etc. However, since this thresholding method is linked to the proposed validation protocol, this error can be quantified.

RESULTS AND DISCUSSION

In total 36 interpolated micro-CT images are matched to their corresponding microscopic images. Figure 3 shows an example of (a) a microscopic image of a metallographic section, (b) the corresponding, interpolated micro-CT image and (c) the resulting match of both where the overlapping pixels are displayed in dark grey, the non-coinciding microscopy image pixels in black and the non-coinciding micro-CT image pixels in light grey. White represents pore space. In this case, the ROI is defined as the circle with a radius of 3.00 mm surrounding the material present in both the microscopic and the corresponding, interpolated micro-CT image.

To get an overall view of the error made by micro-CT and binarization, all elements (solid and pore) within the ROI are accounted for. The 'optimal' threshold value is applied to binarize the 36 interpolated micro-CT images. For all 36 image sets the total overlap, overestimation, underestimation and total mismatch is determined and the results are summarized in table 1.

Table 1. Mean percentage in total overlap, total micro-CT mismatch, total microscopic mismatch and total mismatch.

Total overlap	89.1 ± 1.4 %
Overestimation micro-CT	7.8 ± 1.5 %
Underestimation micro-CT	2.8 ± 0.7 %
Total mismatch	10.9 ± 1.4 %

CONCLUSIONS

When using microscopy for characterizing porous structures, one is limited by its 2D character and a critical, time-consuming sample preparation. Therefore, micro-CT is put forward as the solution for 3D characterization of porous structures. However, to ensure and quantify the reliability and the accuracy of the micro-CT images, a validation protocol is developed by matching micro-CT tomograms to microscopic images. Microscopy is chosen as the 'golden standard' because of its physical character, its well-known procedure and its better resolution with respect to standard micro-CT. When high resolution micro-CT or nano-CT (standard or synchrotron) images are validated, SEM images can be applied to guarantee a superior resolution with respect to the CT images. The main advantages of the proposed validation protocol are first the opportunity to interpolate a micro-CT image under the same angle as the physical cutting angle of the microscopic sections, second the novel thresholding method and third the more precise and detailed quantification of the visualization and binarization error present in the micro-CT images.

In this study, as a proof of principle, the validation protocol is applied to porous titanium structures. Ceramic and polymeric scaffolds are at present under investigation. When scanning the samples on a Philips HOMX 161 X-ray system with AEA Tomohawk CT software and binarizing the micro-CT images with the determined 'optimal' threshold, a total overlap of about 89 % and a total mismatch of about 11 % are found. The total mismatch consists of about 8 % overestimation and about 3 % underestimation of the real structure. It has to be mentioned that, if only the solid fraction would be considered for validating micro-CT, one would conclude that micro-CT only overestimates the structure by about 5 %.

Thus, it is concluded that, despite the morphological complexity of the titanium samples and the variety in structural feature dimensions, a good match is found between microscopy and micro-CT. Additionally, the mismatch is quantified in a detailed manner providing the percentage of overestimation and of the structure not visualized by micro-CT. It is shown that metal porous structures can be analysed with sufficient accuracy by means of *standard* micro-CT. However, due to for example the limited spatial resolution and the high attenuating character of the metallic samples, a significant mismatch is found which needs to be accounted for when performing image-based structural analysis.

ACKNOWLEDGEMENTS

This work is done in collaboration with the Guided Bone Engineering project (www.tissue-engineering.be), an interdisciplinary research project funded by IWT-Flanders under the programme for strategic basic research (GBOU-020181). The research is funded by the Flemish Government through the Research Council of K.U.Leuven (OT-3E040097). The authors wish to thank VITO (Mol, Belgium) for supplying the materials.

REFERENCES

Feldkamp, L.A., Davis, L.C.and Kress, J.W. 1984. Practical Cone-Beam Algorithm. Journal of the Optical Society of America a-Optics Image Science and Vision, 1(6): 612-619

Ruegsegger, P., Koller, B.and Muller, R. 1996. A microtomographic system for the nondestructive evaluation of bone architecture. Calcified Tissue Int, 58(1): 24-29

Sasov, A.Y. 1987. Microtomography .1. Methods and Equipment. J Microsc-Oxford, 147: 169-178

Impens, S., Mullens, S., Luyten, J., Thijs, I., Van Humbeeck, J., Van Cleynenbreugel, T., Bakker, A., Luyten, F.P.and Schrooten, J. 2005. Production and characterization of CaP en Ti scaffolds for bone tissue engineering. 19th European Conference on Biomaterials, Sorrento, Italy,

Snijkers, F., Mullens, S., Luyten, J., Vandessel, W., Impens, S., Schrooten, J.and Van Humbeeck, J. 2005. Porous Materials as Scaffold for Bone Replacement. Acers-meeting, Cocoa Beach, Florida, USA,

Ding, M., Dalstra, M., Danielsen, C.C., Kabel, J., Hvid, I.and Linde, F. 1997. Age variations in the properties of human tibial trabecular bone. J Bone Joint Surg Br, 79B(6): 995-1002

Ding, M., Odgaard, A.and Hvid, I. 1999. Accuracy of cancellous bone volume fraction measured by micro-CT scanning. J Biomech, 32(3): 323-326

Gelatin and hydroxyapatite cell delivery systems in bone tissue engineering.

Lippens E[1], Vertenten G[2], Girones J[3], Luyten J[4], Gasthuys F[2], Schacht E[3] and Cornelissen R[1].

1 Department of Anatomy, Embryology, Histology and Medical physics. Ghent University, De Pintelaan 185, 6B3, B-9000 Ghent, Belgium. Evi.Lippens@Ugent.be, Telephone: (032) 09 332 51 35, Fax (032) 09 332 38 23.
2 Department of Surgery and anaesthesiology of domestic animals. Ghent University, Salisburylaan 133, B-9820 Merelbeke, Belgium.
3Department of Organic chemistry, Polymer Chemistry and Biomaterial Group. Ghent University, Krijgslaan 281, S4, B-9000 Ghent, Belgium.
4 Vito. Boeretang 200, B-2400 Mol, Belgium.

INTRODUCTION

To increase the healing efficiency of bone defects, it is important to "apply" an extra source of bone forming cells in combination with a filling material. *In situ* cross linkable biomaterials are preferable in irregular bone defects. Mixing of the cells in these polymeric biomaterials, and the process of cross linking/hardening can be harmful for the cells. For these reasons, we selected different cell microcarrier systems to obtain locally a sufficient cell amount and to protect the cells during their incorporation into the *in situ* polymerizable biomaterial.
Here we report the use of macroporous microcarriers Cultispher S and calcium phosphate as cell delivery systems for bone tissue engineering.

Gelatin cell delivery system

Cultispher S (Percell Biolytica) is a macroporous gelatin based microcarrier (Ø 130-380 µm) and commercially used as a cell culturing vehicle for adherent cells.
Different cell types were seeded onto the Cultisphers. In general, hydrated Cultisphers were spread in a suspension well plate and seeded with cells. Cells were allowed to attach/adhere in static culture conditions for 2 days. Afterwards the cell loaded carriers are cultured in a dynamic system for up to two weeks. We reported earlier, the good colonisation/proliferation of MC3T3-E1 and UMR-106 cells on and into the Cultispher.
Bone marrow cells (rat and goat origin) and mouse embryonic stem cells, predifferentiated into the osteogenic lineage in culture plates, retained their osteoblastic potential onto the microcarrier when cultured in osteoblastic differentiation medium, as shown immunohistochemically with cbfa-1 and osteocalcin antibody stainings.
The protection of the cells in the Cultisphers was evaluated by mixing the cell loaded carriers with an *in situ* photopolymerizable polymer (methacrylate-endcapped poly-D,L-lactide-co-caprolactone, with triacetin as solvent. The carrier-polymer solution was hardened by illumination with a dental lamp. Cell viability was assessed by MTT assay and light and electron microscopic sections. The *in vitro* tests showed promising results and were tested *in vivo* in the tibia of 8 goats. Four cylindrical defects (Ø 6mm) were drilled in the left and right back tibia. The four test conditions were i) untreated defect, ii) caprolactone polymer iii) caprolactone polymer with osteoblastic predifferentiated bone marrow cells loaded Cultisphers, iiii) caprolactone polymer with αTCP cement and osteoblastic predifferentiated bone marrow cells loaded Cultisphers.
Bone regeneration was evaluated with radiography and immunohistochemistry. After 12 weeks implantation it was noted that the polymer and the Cultispher did not degrade and that the absence of ingrowth of new bone cells or neo-vascularisation is probably due to the fact that the polymer is not so osteoinductive. The cells remained viable on the Cultispher, but showed little proliferation.

Hydroxyapatite cell delivery system

Recently we investigated the use of macroporous (30-150µm) hydroxyapatite macrocarriers (Ø 4mm) as a cell delivery system. MC3T3-E1 and UMR-106 cells were seeded onto these carriers, and cell viability and proliferation was evaluated at different time points with MTS assay and fluorescent labelling with calcein AM (viable cells) and propidium iodide (death cells). Already after 3 days in static culture conditions, high MTS absorbance values could be measured and fluorescent microscopy revealed an almost complete colonisation of the carriers with cells.

CONCLUSIONS

We are planning to investigate the use of the hydroxyapatite carriers seeded with predifferentiated goat bone marrow cells in tibia defects in 8 goats. Since hydroxyapatite is similar to the natural bone matrix, we expect a good repair of the bone defect with de novo bone matrix syntheses by the extra source of predifferentiated bone marrow cells onto the carriers. We will combine these cell loaded carriers with a *in situ* polymerizable hydrogel.

Dental Implants with biocompatible and bioactive coatings

Schiefer H.[1], T. Habijan[2], M. Bram[1], *H.P Buchkremer*[1], M. Köller[2] and D. Stöver[1]

1 Jülich Forschungszentrum GmbH, IEF-1: Institute of Energy Research, 52425 Jülich, Germany
h.schiefer@fz-juelich.de , Telephone: 02461 61 3520, Fax: 02461 61 2455
2 Universitätsklinik Bergmannsheil, Abteilung chirurgische Forschung, Bochum, Germany

INTRODUCTION

Because of its outstanding mechanical and biological properties, titanium is widely used in the implantology field [Thelen et al.]. Especially loaded implants like hip or dental implants are mainly made of titanium and its alloys. To improve the contact between implant and human tissue, various coating techniques can be applied. These are: keying of the surface [Triplett et al.], applying porous structures [Kutty et al.] and coating with biocompatible and bioactive materials, e.g. calcium phosphates (CAP) [Prado Da Silva et al]. This work shows the fabrication technique of dental implants with a porous coating using the powder metallurgical space holder method. Dental implants with a porous coating are necessary for patients with insufficient bone structure in the jaw. On these developed implants a fatigue test approaching to ISO 14801 was done. Two kinds of coatings were applied to test samples. A bioactive calcium phosphate coating was applied by an electrochemical process on the porous titanium sample. The aim is a faster and stronger bonding of bone tissue to the and inside the porous structure to get a durable connection between bone and implant. On the massive region on the head of the implant a dense contact of soft tissue of the gingiva is necessary. Thus, a thin zirconia coating was applied to dense titanium substrates by a PVD-technique, because there are some indications, that soft tissue gets a better connection to zirconia than to titanium. Both coatings were tested by cell culture experiments.

EXPERIMENTAL

Fabrication of dental implants

In this work the powder metallurgical space holder method was used for fabricating the porous layer of the dental implant. This method was described elsewhere [Laptev et al].

Figure 1 shows the schematic fabrication route of a dental implant with a porous coating. A mixture of titanium powder (30 Vol.%) and space holder (70 Vol.%) was cold isostatically pressed onto a titanium rod. The titanium powder, fabricated by the HDH-process has an irregular shape and a particle size smaller than 45 µm. The space holder was ammoniumbicarbonate (NH_4HCO_3) with a particle size distribution of 125-250 µm. After pressing, the coating is near-net-shape machined by turning in the unsintered state. After the spacer was removed at a temperature of 100 °C, the sintering-process was done at 1300 °C in argon-atmosphere. The sintered samples were machined by drilling and sawing to achieve a tube with a porous coating. Finally, a dense titanium core with an internal screw thread was pressed into the tube part and was additionally fixed by a screw on the tip of the implant. After joining, the screw was machined by turning to achieve a cone-like tip and roughened by sandblasting.

a)

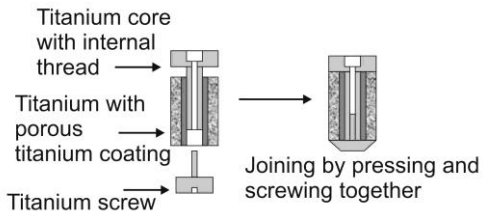

b)

Figure 1. a) Schematic processing of the dental implant with a porous coating, b) dental implant with porous coating.

Fatigue testing of dental implants

The dental implants underwent a fatigue test approaching to ISO 14801 (Figure 3). For this test, the porous dental implants were embedded in araldite under vacuum conditions to infiltrate the porous structure. To simulate an extreme loading condition, which may occur in cases of ongoing bone resorption, the porous coating hangs 3 mm over the edge of the polymer resin. The force was applied by a plunger directly to the head of the implant in an angle of 30° to the surface normal. The tests were performed at a temperature of T = 37 °C in a physiological 0.9 % NaCl solution. The implants were tested up to $2 \cdot 10^6$ cycles with a frequency of 2 Hz with different loading conditions of F = 200 und 300 N.

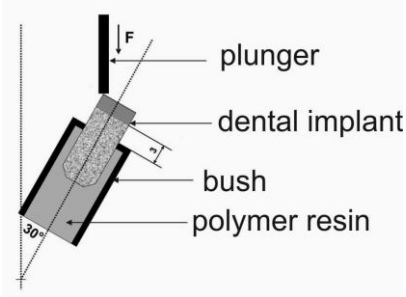

Figure 2. Loading conditions of the fatigue test of dental implant.

Coating of porous and dense titanium

a) Coating of porous titanium with calcium phosphate by an electrochemical process
The coating parameters were taken from [Prado Da Silva et al]. The experiments were done at test samples of porous titanium with a diameter of 11 mm and a height of 3 mm. A sample hung in an acidic electrolyte, consisting of 0.5M $Ca(OH)_2$, 0.3M H_3PO_4 and 1M lactic acid, heated on 80 °C. The sample was contacted as a cathode, the anode was a platinum foil. The coating time was 40 minutes. After the coating process the samples were washed in deionised water and dried at 50 °C in air. The coated samples were embedded in polymer resin and prepared by grinding and polishing.

b) Coating of dense titanium with zirconia (8YSZ) by EB-PVD
Polished titanium samples were coated with a thin zirconia layer by electron beam evaporation of 8YSZ (with 8 mol% yttria stabilized zirconia). The substrate temperature was 400 °C, the process time was 40 minutes. The coatings were analysed with SEM and XRD.

c) Cell culture experiments
To prove the influence of the coating to relevant cells, both coating systems were examinated by cell culture experiments at the Ruhr-University Bochum. The calcium phosphate coating was examinated with human mesenchymal stem cells. These cells are multipotent and self replicating. The zirconia coating was examinated with mouse fibroblasts, which are cells of soft tissue similar to the gingiva.

Results

Fatigue testing

Figure 3 shows the result of the fatigue test of the dental implants. The two lines are first prototypes with a persistent porosity. They do not fulfil the requirements for dental implants (striped area) and broke in the porous section of the implant body. The new developed dental implant reaches up to 2 million cycles without damage.

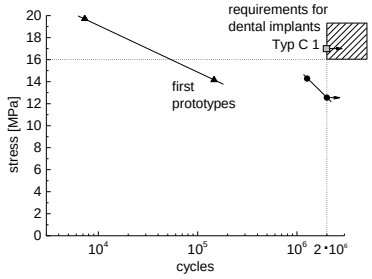

Figure 3. Wöhler-like diagram of fatigue testing of the developed dental implant with porous coating and other first prototypes.

Coatings on titanium

The calcium phosphate (CAP) coating on a porous titanium sample is shown in figure 4. XRD-analysis show, that the mean phase of the CAP-coating is brushite. Additionally hydroxyapatite and monetite was found in small amounts. Figure 4a shows that the brushite-crystals close nearly completely the open porous structure of the porous titanium substrate. The CAP-crystals stick closely together and have a size of 20 to 50 µm. Figure 4b shows, that the coating is about 100 µm thick and occurs only in the first two pore layers. The reason is probably the high gas evolution during the coating process. Therefore, CAP-crystals cannot adhere on the substrate. Additionally, gas bubbles press the electrolyte out of the porous structure.

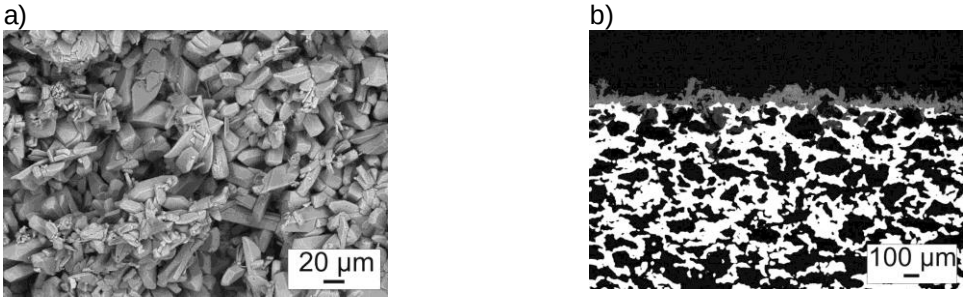

Figure 4. CAP-coating on a porous titanium sample with a pore size of 125-250 µm, a) Surface, b) preparated, grinded sample.

Figure 5a shows a SEM-picture of a human mesenchymal stem cell (hMSC) on a porous titanium surface. The cells show a good adherence on uncoated titanium and proliferate on the surface. On the CAP-coating, the cells proliferate, too, but in comparison to the result of the uncoated samples, the proliferation is much lower. The reason for this could be the irregular shape of the CAP-crystals and the decreased pH-value of the solution after an incubation time of 8 days. Figure 5b shows a cell on a CAP-surface and some CAP agglomerates (marked with an arrow).

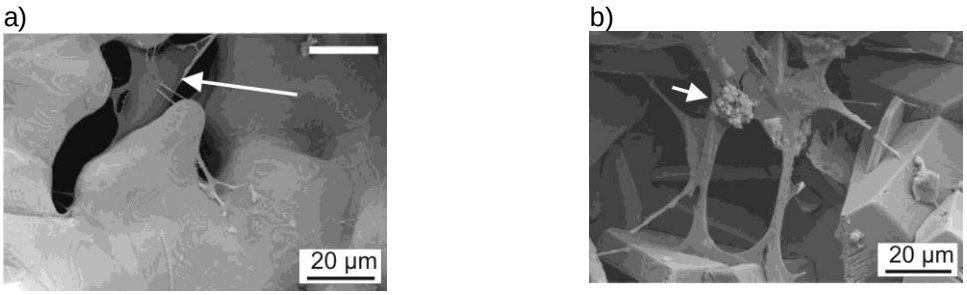

Figure 5. a) Human mesenchymal stem cell on a porous titanium surface, b) Human mesenchymal stem cell on brushite-crystals and CAP-agglomerates.

Figure 6a shows the surface of the zirconia coating, figure 6b the fracture surface. The coating morphology of the zirconia layer showed a strong dependence on the substrate temperature during the coating process. A substrate temperature of 400 °C was chosen, because of the consistent

topography of the zirconia layer (Figure 6). Higher temperatures lead to an oxidation of the substrate, which decreases the adherence of the coating layer.

a) b)

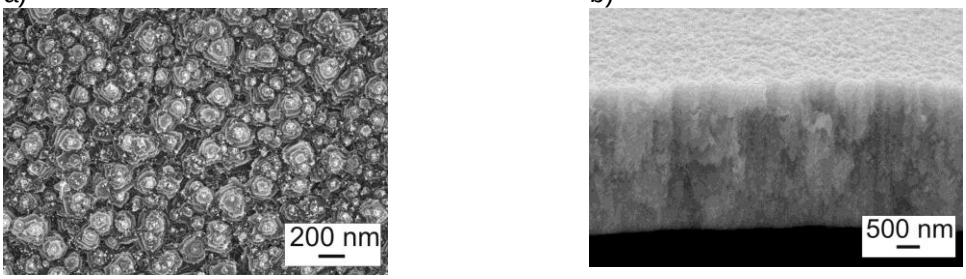

Figure 6. 8YSZ-coating on dense titanium sample, fabricated by EB-PVD coating, a) surface structure, b) fracture surface.

Cell culture experiments with mouse fibroblasts show dense contacts of the cells to the zirconia layer (Figure 7b) compared to the uncoated titanium (Fig. 7a). The surface material and its topography have a great influence to the adhesion of fibroblasts. For confirmation more experiments are necessary.

a) b)

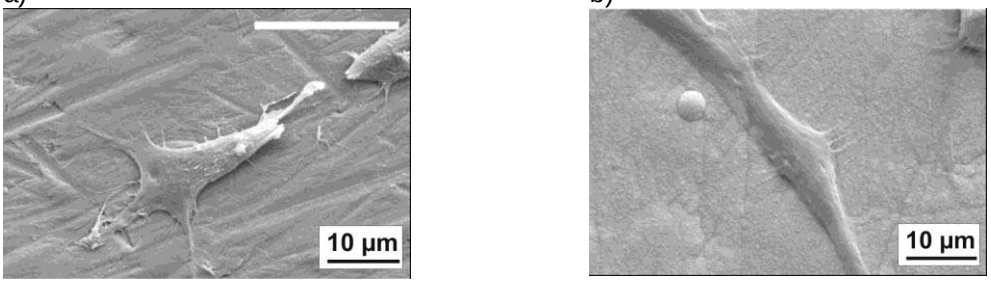

Figure 7. a) Fibroblast on a titanium surface, b) Fibroblast on a zirconia surface.

CONCLUSION

The great potential of the powder metallurgical space holder method was shown with the development of a dental implant with a porous coating. The fatigue tests of these implants show that they endure up to 2 million cycles without damage. To improve the in- and ongrowth of tissue into the dental implant, different coatings were applied to test samples. With an electrochemical coating process, a calcium phosphate layer (brushite) only occurred on the edge of the porous sample. A thin zirconia layer was applied to a dense titanium sample by a PVD-technique and shows a homogeneous topography. Cell culture experiments show disadvantageous behavior of cells on the calcium phosphate coating because of the irregular shape of the crystals and a lower pH-value of the solution. On the zirconia layer cells show a better adherence on the coated samples than on uncoated.

REFERENCES

Kutty M.G., Bhaduri S., Bhaduri S.B., 2004, Gradient surface porosity in titanium dental implants: relation between processing parameters and microstructure, J. Mat. Sci.: Mat Med., 15: 145-150.

Laptev, A., Bram M., Buchkremer H. P., Stöver D. 2004. Study of production route for titanium parts combining very high porosity and complex shape, *Powder Metallurgy*, 47 (1): 85-92.

Prado Da Silva M.H., Lima J.H.C, Soares, G.A., Elias C.N., de Andrade M.C., Best S.M., Gibson I.R., 2001, Transformation of monetite to hydroxyapatite in bioactiv coatings on titanium, Surf. Coat. Tech: 137: 270-276.

Thelen S., Barthelat F., Brinson C., 2004, Mechanics considerations for microporous titanium as an orthopedic implant material, J. Biomed. Mat. Res. A, 69 (4): 601-610.

Triplett R.G., Frohberg U., Sykaras N., Woody D.R., 2003, Implant Materials, Design, and Surface Topographies: Their Influence on Osseointegration of Dental Implants, J. Long-term Eff. Impl., 13(6): 485-501.

Local drug delivery from bone implants

***M. Ravelingien*[1,2], S. Mullens[1], J. Luyten[1], C. Vervaet[2], and J. P. Remon[2]**

1 Materials Technology, VITO (Flemish Institute for Technological Research), Boeretang 200, 2400 Mol, Belgium, matthieu.ravelingien@vito.be, Telephone: (32) 14-335675, Fax: (32) 14-321186
2 Laboratory of Pharmaceutical Technology, Ghent University, Harelbekestraat 72, B-9000 Ghent, Belgium

INTRODUCTION

Due to its biocompatibility and biodegradability [1], hydroxyapatite (HA) is a suitable matrix material for local drug delivery [2] from bone implants. The porous matrix could be loaded with the antibiotic gentamicin sulfate (GS) and coated with the biodegradable polymer poly(D,L-lactide) (PDLLA) to control the release of the antibiotic [3].

MATERIALS AND METHODS

Ceramic HA hollow fibres were spun while porosity was induced by phase inversion [4]. The structural properties of the sintered fibres were characterized by Hg-porosimetry and SEM. The porous matrices were loaded with GS, spray coated with PDLLA using an airbrush [5] and analyzed by SEM. The drug delivery systems were evaluated by an *in vitro* dissolution test in PBS at 37°C during 21 days.

RESULTS AND DISCUSSION

Prepared hollow fibres exhibited an outer diameter of 1.4mm and a wall thickness of 0.1mm with a porosity of 41v% and typical pore sizes of 2µm (Fig. 1a-b). This microporosity enabled a GS incorporation of 53mg/g. PDLLA coatings of approximately 1.5µm (Fig. 1c) and 4.3µm (Fig. 1d) were deposited after spray coating.

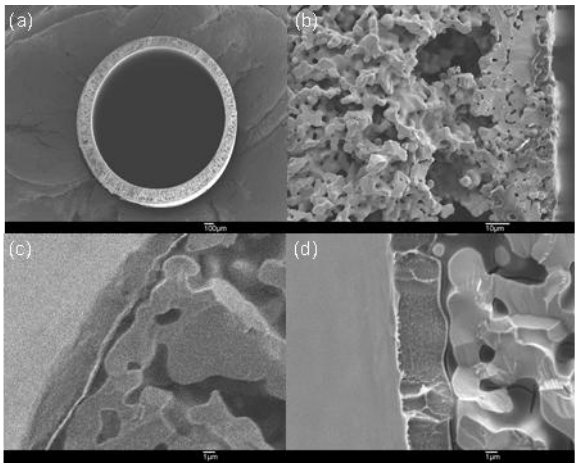

Figure 1. Micrographs of cross sections of HA hollow fibres without coating (a-b); with 1.5µm (c) and 4.3µm (d) coating.

The *in vitro* GS release profiles showed a complete release within the first day from fibres without coating and within 14 days from fibres with a 1.5µm coating. After 21 days only 70wt% was released from the drug delivery systems with 4.3µm coatings (Fig. 2). The release rate was significantly slowed down by PDLLA coating and depended on the coating thickness. The slower release rates from fibres with thicker coatings indicated that the antibiotic released from the matrix through the polymer coating via diffusion.

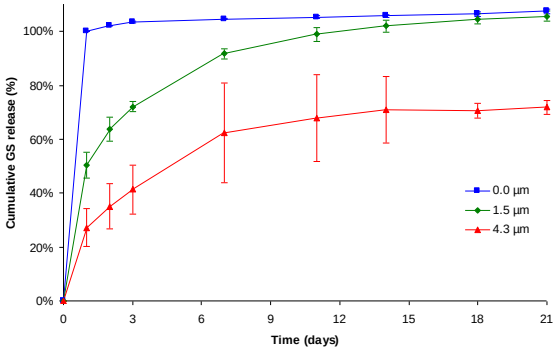

Figure 2. In vitro GS release profiles of drug delivery systems with and without PDLLA coating.

CONCLUSIONS

Porous ceramic HA hollow fibres spun by the phase inversion technique could be used as a matrix for a local drug delivery system to prevent bacterial infections associated to bone implants. They can easily be loaded with the antibiotic GS and a sustained release can be obtained by spray coating with the biodegradable polymer PDLLA. The drug release rate and duration can be controlled by adjusting the coating thickness. Release times of several weeks to months are desired to treat bacterial infections associated to bone implants. Therefore drug delivery systems with appropriate dissolution profiles will be optimized in future work.

ACKNOWLEDGEMENTS

This work was supported by VITO (Flemish Institute for Technological Research). The authors are grateful to the staff of Materials Technology.

REFERENCES

[1] R.Z. LeGeros, Properties of osteoconductive biomaterials: Calcium phosphates, Clin. Orthop. Relat. R. 395 (2002) 81-98.

[2]P.Wu, D.W. Grainger, Drug/device combinations for local drug therapies and infection prophylaxis, Biomaterials 27 (2006) 2450-2467.

[3] M. Lucke, B. Wildemann, S. Sadoni, C. Surke, R. Schiller, A. Stemberger, M. Raschke, N.P. Haas, G. Schmidmaier, Systemic versus local application of gentamicin in prophylaxis of implant-related osteomyelitis in a rat model, Bone 36 (2005) 770-778.

[4] J. Luyten, A. Buekenhoudt, W. Adriansens, J. Cooymans, H. Weyten, F. Servaes, R.Leysen, Preparation of $LaSrCoFeO_{3-x}$ membranes, Solid State Ionics 135 (2000) 637-642.

[5] T. Sharkawi, D. Leyni-Barbaz, N. Chikh, J.N. McMullen, Evaluation of the in vitro drug release from resorbable biocompatible coatings for vascular stents, J. Bioact. Compat. Pol. 20 (2005) 153-168.

A mathematical model for citric acid production from date pomad by *Aspergillus niger*

M. Sharifzadeh*
Islamic Azad university – Ayatollah Amoli Branch –Amol
maziarsharif@yahoo.com

Abstract
The fermentation kinetics of citric acid by *Aspergillus niger* were studied in a batch system. A simple model was proposed using the logistic equation for growth, the Luedeking–Piret equation for citric acid production and Luedeking–Piret-like equation for glucose consumption. The model appeared to provide a reasonable description for each parameter during the growth phase. The production of citric acid was growth-associated.

Key words: Kinetic model, citric acid, *Aspergillus niger,* Luedeking–Piret equation

1. Introduction
Citric acid, a tricarboxylic acid, is one of the world's largest tonnages of fermentation products. It is used in the food, and beverage industries as an acidifying and flavour-enhancing agent and also in other industries such as pharmaceutical. Considerable interest has been shown in using fruit pomace and other agricultural wastes for citric acid production. Date pomace consists of the press cake resulting from pressing dates for juice, as well as the press cake obtained in pressing peel and core wastes generated during the preparation of dates for canning, drying,
and freezing[1]. A model is that describes relationships between principal state variables and explains quantitatively the behavior of a system. The model can provide useful suggestions for
the analysis, design and operation of a fermenter. Fermentation models are normally divided into two classes: structured models where intracellular metabolic pathways are considered, and unstructured models where the biomass is described by one variable. Structured model seems complicated for normal use[2]. Unstructured models are much easier to use, and have proven to accurately describe many fermentations. Yet, to our knowledge, no investigations have been carried out on the unstructured model for citric acid production. In this study, experimental data from batch fermentations of citric acid by *A. niger* were examined in order to form the basis of kinetic model of the process.

2. Materials and methods

A. Preparation of date

Date refuse was obtained and was analyzed for determination of ash , moisture, reducing sugar, citric acid and etc…

B. Organism and inoculum

A. Niger PTCC 5010 was supplied by biotechnology department (Iran science and industrial research organ). The organism was maintained on potato dextrose agar (PDA) slants at 4 8C and renewed once at month intervals. A. Niger spores for inoculation were produced on PDA containing 50 ml in a 250 ml Erlenmeyer flask, incubated at 28. 8C for 5 days. A spore suspension was prepared by adding 50 ml distilled water containing Tween-80 (2%) and was stored at 4 8C for a maximum of 3 weeks. It contained 10^8 spores/ml.

C. Fermentation Process

Suspended fermentation

1. Prepreation of main media (batch cultures)

At first date refuse diluted with distillation water (14% concentrations).Then diluted date refuse treatment was carried out by centrifugation at 5000 rpm and 100 ml of the obtained solution transferred to 500 ml Erlenmeyer flask. Chemical treatments included potassium Ferro cyanide (El-Abyad et al., 1992), Sulfuric acid (Mayilvahanan et al., 1996), calcium phosphate (Mayilvahanan et al., 1996), Sodium phytate (Wang, 1998) and methanol (El-Abyadet al., 1992)[3].

2. Pre treatment

Pre treatment carried out by adding 0.1 gr/lit potassium Ferro cyanide, 1.5 percent (v/w) *Calcium Triphosphate,* 2.5 g/lit Ammonium sulfate and 3 volume percent of methanol. The PH regulation (at 4.5) carried out by HCL and normal NAOH before sterilization.

2.3. Analytical methods

Samples were withdrawn twice at defined time. Fermentations were performed in duplicate culture, and analyses were carried out in duplicate. The data given here are the average of the measurements. The dry weights of mycelium were obtained after filtration of broth samples through preweighed filter discs. The harvested biomass was then washed with deionized water, dried for 8 h at 105 ◦C, cooled in a desiccator and weighed.

Sugar was estimated by the phenol sulphuric acid method of Dubois et al. [4] and citric acid by the acetic anhydride and pyridine method of Marier and Boulet [5].

3. Kinetic model

The model employs rate equations for biomass (*X*), citric acid (*P*) and total sugar (*S*) to describe the fermentation process.

3.1. Microbial growth

The most widely used unstructured models for describing cell growth are the Monod kinetic model, the logistic equation and the haldane model. The logistic equation is a substrate independent model. It can finely describe the inhibition of biomass on growth, which exist in many batch fermentations [6,7]. The logistic equation can be described as follows:

$$\frac{dX}{dt} = \mu_m X\left(1 - \frac{X}{X_m}\right) \quad (1)$$

$$X = \frac{X_0 X_m e^{\mu_m t}}{X_m - X_0 + X_0 e^{\mu_m t}} \quad (2)$$

3.2. Product formation

The second-order rate of reaction with respect to citric acid production and sugar consumption for citric acid production is shown in Eq. 3[8]:

$$\frac{dP}{dt} = P_r P\left(1 - \frac{P}{P_m}\right) \quad (3)$$

The citric acid concentration profile is obtained by solving the differential equation in order to maximize citric acid production, as shown in Eq. 4:

$$P = \frac{P_0 e^{P_r t}}{1 - \left(\frac{P_0}{P_m}\right)\left(1 - e^{P_r t}\right)} \quad (4)$$

3.3. sugar uptake

carbon substrate is used to form cell material and metabolic products as well as the maintenance of cells. The sugar consumption equation given below is a Luedeking–Piret-like equation is following equation[9]:

$$S = S_0 - \left(\frac{1}{Y_{X/S}}\right)(X - X_0) - \left(\frac{1}{Y_{P/S}}\right)(P - P_0) \quad (5)$$

In this study, Eqs. (2), (4) and (5) are used to simulate the experimental results.

4. Results and discussion

4.1. Microbial growth

Citric acid fermentation by *A. niger* showed a classical growth trend. After a lag phase (about 5–10 h), the cells entered the exponential growth phase. The strain started to form citric acid when the cells entered the exponential phase and therefore cell growth and citric acid production took place simultaneously. Taking *X*m = 22 g l−1 from the experimental data, fitting the experimental data to Eq. (2) yields the values of parameters as follows: *X*0 and μm is 0.04 g l−1 and 0.015 h−1, respectively. A comparison of calculated value of Eq. (2) with the experimental data is given in Fig. 1. The fitting of results was satisfactory.

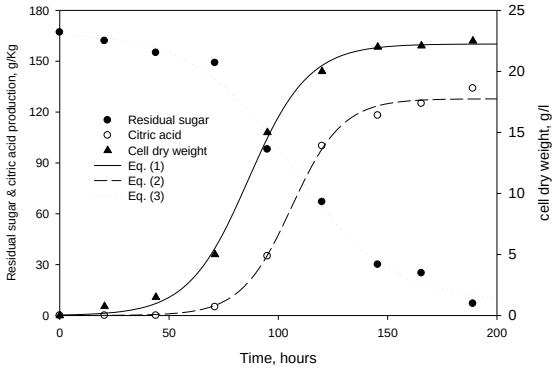

Fig. 2. The comparison of experimental data in this work and calculated values of biomass, sugar and concentration of citric acid fermentation: (▲) experimental data of biomass; (●) experimental data of sugar; (○) experimental data of citric acid.

.

4.2. Product formation

After fitting the experimental data to Eq. (4), the following equation was used to describe citric acid . From the result, it can be seen that citric acid formation is strongly linearly related to cell growth. The result shows that the biosynthesis of citric acid can be attributed to a growth-associated type. In the model, *Po* (0.652 g Kg−1) , Pm (120 g Kg−1) and Pr (0.044 g Kg−1) are the growth-associated product formation.

4.3. Substrate uptake

By fitting the experimental data to Eq. (5), the values of parameters of sugar uptake model were as follows: *YX/S , YP/S* and *S0* is 0.62 g g−1, 0.38 g g−1 and 170 g Kg−1, respectively.
The fitting of results was satisfactory (Fig. 1).

Acknowledgements

The authors wish to acknowledge the Islamic azad university-Ayatollah amoli branch for financial support to complete this research effort.

Reference:

1. Shojaosadati, S. A., & Babaeipour, V. (2002). Citric acid production from apple pomace in multi-layer packed solid-state bioreactor. Process Biochemistry, 37, 909–914.
2. Jian-Zhong Liu , Li-Ping Weng , Qian-Ling Zhang , Hong Xu, Liang-Nian Ji (2002).
A mathematical model for gluconic acid fermentation by *Aspergillus niger,* Biochemical Engineering , 3669 ,1–5.
3. Botella C, de Ory I, Webb C, Cantero D, Blandino A. Hydrolytic enzyme production by Aspergillus awamori on grape pomace. Biochem Eng J 2005;26:100–6.
[4] Dubois M, Gilles KA, Hamilton JK, Rebers PA, Smith F. Colorimetric method for determination of sugars and related substrates. Anal Chem 1956:28:350-6.
[5] Marier JR, Boulet M. Direct determination of citric acid in milk with an improved pyridine acetic anhydride method. J Dairy Sci 1958;41:1683-92.
[6] H. Gong, S. Lun, The kinetics of lysine batch fermentation, Chin. J. Biotechnol. 12 (Suppl.) (1996) 219–225.
[7] Habibollah Younesi, Ghasem Najafpour , Abdul Rahman Mohamed.(2006) Ethanol and acetate production from synthesis gas via fermentation processes using anaerobic bacterium, *Clostridium ljungdahlii.* Biochemical Engineering 27,110 -119.
[8] Najafpour, G,Younesi, H (2007) bioconversion of synthesis gas to hydrogen using a light – dependent photo synthesis bactium rhodospirillum rubrum. World journal of microbiology and biotechnology.23:275 -284.
[9] Panilaitis, B., Castro, G., Solaiman, D., Kaplan, D.L. 2007. Biosynthesis of emulsan biopolymers from agro-based feedstocks ,journal of applied microbiology 102 : 531 - 537

Near-net-shape fabrication of porous NiTi: Use as implant materials and energy-absorbers

Köhl M.[1], Bram M.[1], Buchkremer H.-P. [1], Stöver D. [1], Habijan T. [2], Köller M. [2]

1 Forschungszentrum Jülich, Leo-Brandt-Str., 52428 Jülich, Germany,
m.koehl@fz-juelich.de, Telephone: (0049) 2461 61 6712, Fax: (0049) 2461 61 2455
2 Bergmannsheilklinik Bochum, Bürkle de la Camp-Platz 1, 44879 Bochum, Germany

INTRODUCTION

Open porous metal foams are attractive materials for biomedical implants. Young's moduli of commonly used dense metals for bone replacement lie in the range of 100 to 200 GPa [Simske et al.], and are thus much higher than the modulus of human cancellous bone (< 3 GPa) or compact bone (12-17 GPa) [Gibson et al.]. This mismatch of stiffness between the implant material and the surrounding human bone may lead to stress-shielding, which can cause implant loosening.
An adjusted porosity allows the adaptation of the mechanical properties of the living human bone and reduces the risk of stress-shielding [Imwinkelried]. In addition, if appropriate pore structures are considered, bone ingrowth in the prosthetic material becomes possible, thus improving the strength of the implant/bone interconnection [Imwinkelried].
Due to the low stiffness of the bulk material and its proven biocompatibility [4], NiTi is a promising candidate for porous implant materials. Further, due to pseudoelasticity in Ni-rich NiTi, the material can recover up to 8% strain by a reversible stress-induced transformation [Yahia]. Since human bone also recovers strains up to 2% [Gibson et al.], porous NiTi is the most promising metal to match its mechanical properties. Several techniques of producing highly porous NiTi were investigated up to now. The disadvantages of these methods are the lack of controlling the pore size and pore volume fraction as well as chemical inhomogenities. Further, none of the methods is suitable for a near-net-shape production.
Recently, it was demonstrated that the metal injection molding (MIM) process enables the production of NiTi parts with comparable mechanical properties to melt metallurgy [Mentz et al.]. Based on this, the space holder method (SHM) combined with the MIM process broadens the range of applications of net-shaped NiTi alloys by introduction of well defined pore sizes and total porosities of up to 70% while keeping the content of impurity phases low.
The present work discusses the influence of the pore size and total porosity on the mechanical properties of NiTi. Furthermore, the different behavior due to variable Ni-contents of the starting materials is considered. To test the biocompatibility porous MIM samples were loaded with human mesenchymal stem cells (hMSCs). The cell reaction was analyzed in vitro.
Further, the present work shortly discusses the potential of porous, pseudoelastic NiTi as general energy-absorbers.

EXPERIMENTAL PROCEDURES

For the metal injection molding (MIM) process an Arburg 400-100 allrounder 270 CMD was used. For small feedstock amounts, axial warm pressing in a heated die (P/O/Weber, 10H, Ø12mm) was found to be suitable to approach the conditions of the MIM process. The MIM process consists of five steps summarized below:

a. Mixing and homogenization of pre-alloyed NiTi powder, NaCl and a binder system in a heated kneader (Haake HKD-T 0,6D)
b. Injection of the feedstock in a MIM machine (Arburg 400-100 allrounder 270 CMD)
c. Debinding of the first component at 150°C under air
d. Solution of the space holder NaCl in distilled water
e. Thermal debinding of second component under Argon at 480°C and sintering of the parts under vacuum (< 10^{-5} mbar) at 1250°C, 10 h

Figure 1 illustrates the different processing steps in SEM images (*Figure 1a.*) and for MIM19 cylinders (50% porous, 355-500 µm, *Figure 1b.*). *Figure 1c.* shows a picture of different MIM19 geometries in the green state (dark grey) and as-sintered (light grey).

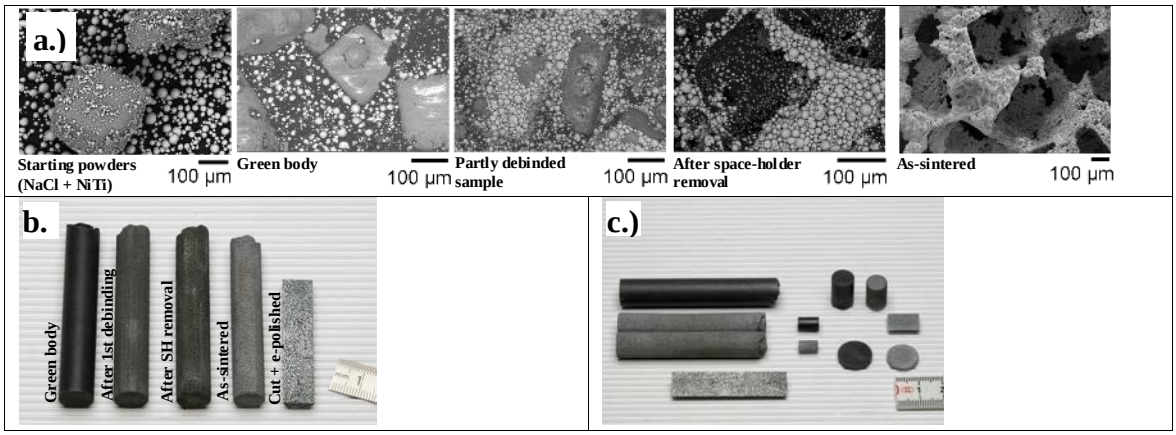

Figure 1. a.) SEM images of the different processing steps b.) Picture of MIM19 samples during the process. c.)Picture of different MIM19 geometries.

Table 1 summarizes the composition and particle size fraction of the starting powders mixture. All feedstocks had a binder content in the range of 20-25 vol.% depending on the tap density of the powder mixture. Variation of space holder size and content was mainly done on warm pressed samples (PHF1, PHF2, PHF6). The porosities analyzed by image analysis are also given in *Table 1*. Due to the oversized diameter of the warm pressed samples, the final geometry of the compression test samples (Ø = 4 mm, h = 5.7 mm) was achieved by electro discharge machining. The MIM experiments were conducted with space holder amounts of 50 vol.%. After sintering, the MIM samples had a size of Ø 5.44±0.02 mm x h 8.01±0.02 mm (for n = 6). Compression tests were performed in a Zwick/Roell Z100 electro-mechanical testing machine at a deformation rate of 0.5 mm/min and at constant temperature of 37°C in a climate chamber.

Table 1. Starting compositions of the tested samples.

Sample	NaCl	NiTi	Ni [at.%]	Porosity [%]	
				Micro	Macro
MIM19	50 vol.% (355-500 µm)	50 vol.% (25-45 µm)	50.6	1.5	47.5
PHF1	70 vol.% (125-250 µm)	30 vol.% (25-45 µm)	49.7	1.3	69.3
PHF2	70 vol.% (355-500 µm)	30 vol.% (25-45 µm)	49.7	1.8	70.1
PHF6	50 vol.% (355-500 µm)	50 vol.% (25-45 µm)	49.7	4.2	50.2

Chemical analyzing was performed to investigate the impurity content of oxygen and carbon. DSC measurements at the porous samples were performed with a 2920 CE machine from TA Instruments. HMSC (3rd-6th passage, Cambrex Bio Science) were cultured in RPMI1640 supplemented with 10% FCS using cell culture plates, 5% CO_2 and humidified atmosphere. Cells were seeded onto the samples, and after 24h, samples with adherent cells were transferred onto a new cell culture plate. Live/dead staining was performed using calcein-AM and propidium iodide.

RESULTS

Table 2 compares the impurity contents of carbon and oxygen for the starting NiTi material and the as-sintered samples. Acceptable oxygen and especially carbon impurity contents for the porous NiTi samples are remarkable.

Table 2. Impurities of the starting NiTi powders and the as-sintered NiTi samples.

	Impurity content [wt. %]	
	Carbon	Oxygen
NiTi-Powder, N557-45, 50,6	0.04	0.05

MIM19 (50%, 355-500 µm)	0.04	0.14
NiTi-Powder, H548-45, 49,7	0.03	0.06
PHF1 (70%, 125-250 µm)	0.08	0.17
PHF2 (70%, 355-500 µm)	0.07	0.21
PHF6 (50%, 355-500 µm)	0.06	0.15

The microstructures of the samples are shown in *Figure 2*. A homogenous distribution of the macro-porosity and the cubic pore shape resulting from the space holder NaCl are obvious.

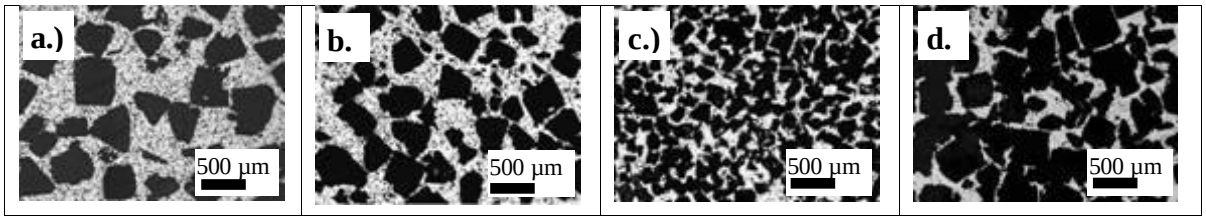

Figure 2. Microstructure of the porous samples. a.) PHF6, b.) MIM19, c.) PHF1, d.) PHF2.

The DSC measurements of the NiTi starting powders are shown in *Figure 3a.* For the as-sintered samples (*Figure 3b.*) the phase transformation changes slightly to lower temperatures due to the formation of Ti-rich phases like TiC and $Ti_4Ni_2O_x$. *Figure 3c.* compares the mechanical behavior of MIM19 and PHF6 samples in compression tests at 37°C. Both samples have approximately the same porosity and pore size (~50%, 355-500 µm). The as-sintered MIM19 sample recovers its shape nearly completely, up to compressions of 8%. By contrast, the PHF6 sample does not show a pseudoelastic behavior due to its higher Ni content. The lower yield stress plateau of PHF6 indicates the existence of the martensitic, shape-memory phase, while MIM19 is in the austenitic, pseudoelastic state at 37°C.

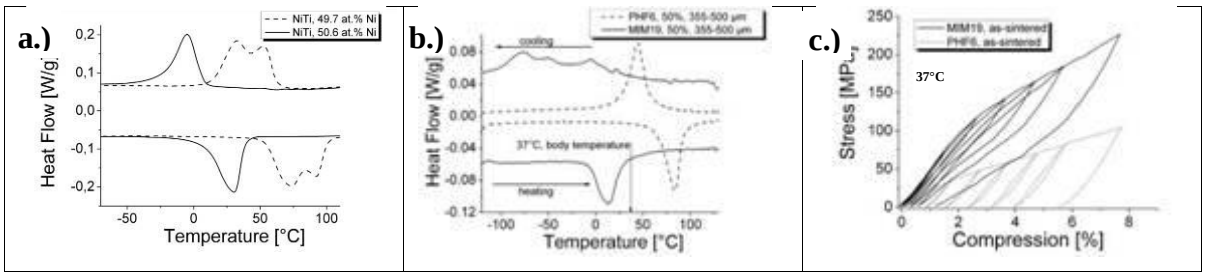

Figure 3. DSC-measurements of the starting NiTi powders (a.) and of as-sintered samples (b.). c.) *Compression cycles up to 8% of a MIM19 (Ni-rich) sample in comparison to PHF6 (Ti-rich)*

In *Figure 4a.* cyclic tests on PHF6 (50%, 355-500 µm) and PHF2 samples (70%, 355-500 µm) were performed up to deformations of 50%. Lower compression stresses and a decrease in the Young's modulus are significant increasing the total porosity. In *Figure 4b.*, PHF1 (70%, 125 250 µm) and PHF2 (70%, 355-500 µm) samples are compared. At a constant porosity, the influence of the pore-size on the Young's modulus and the compression strengths seem to be negligible.

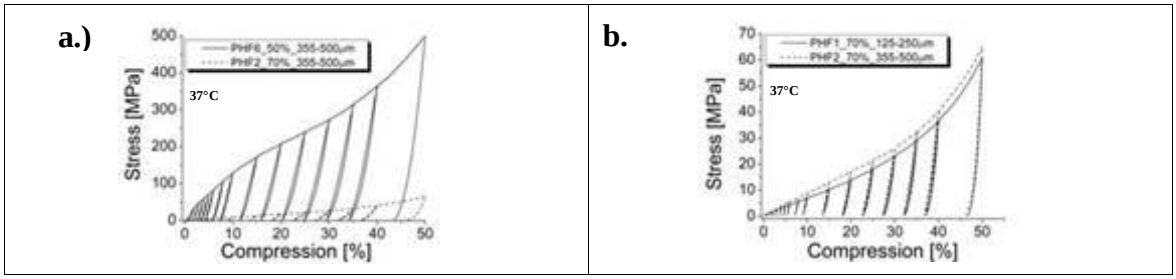

Figure 4. a.) Stress-compression cycles up to 50% compression of PHF6 in contrast to PHF2. b) Stress-compression cycles of PHF1 in contrast to PHF2.

The MIM19 samples were used for cell culture tests. To determine the biocompatibility of the samples produced by MIM combined with SHM, hMSCs were cultured onto those specimens for 48 hours (not shown) and 8 days. As shown in *Figure 5a.*, adhesion and proliferation of hMSCs on the porous test specimens are not affected by the production via MIM. Further, the fracture surface (*Figure 5b., c.*) shows in depth profiles that the pores are well populated by vital hMSCs.

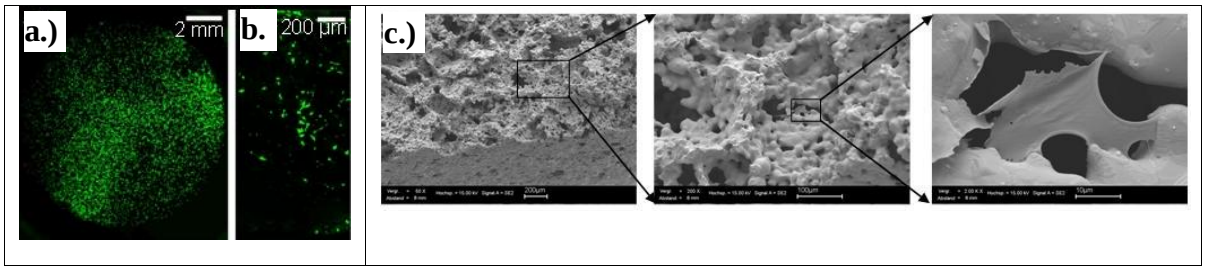

Figure 5. . Fluorescence microscopy of hMSCs cultured on a MIM19 sample for 8 days, stained with Calcein-AM. a.) Top view, b.) Fracture surface. c.) SEM images of fracture surface

CONCLUSIONS

The MIM process in combination with the space holder method enables the net-shape production of highly porous NiTi components with a well defined pore size. The Ni-content of the starting powder, the total porosity and the pore sizes can be varied to adjust the mechanical properties of the shape memory alloy. First compression tests showed promising results independent on the martensitic or austenitic phase.

Figures 6a,b demonstrate the bone like microstructure of porous NiTi achieved in this work (PHF2, 70% porous, 355-500 µm) in comparison to the human bone. The mechanical compression tests of the MIM19 (50%, 355-500 µm) samples are compared with the mechanical properties of the two main components of a living bone, the cortical and the trabecular bone [2], in *Figure 6c*. *Figure 6d* magnifies the important region of the stress-compression curve up to 2% compression, according to the natural elastic limit of a living bone.

It is obvious from *Figure 6d* that the mechanical properties of the porous NiTi produced by MIM with SHM fit very well with the mechanical properties of the trabecular bone at low compressions. The deformation behavior of the sample follows the trabecular bone up to 2% compression, adapting the damping properties of the trabecular bone structure which reduces the risk of stress shielding to a minimum. At higher deformations, enhanced loads are necessary for deformation of the porous NiTi which ensures the stability of the implant during handling and during long term operation after implantation.

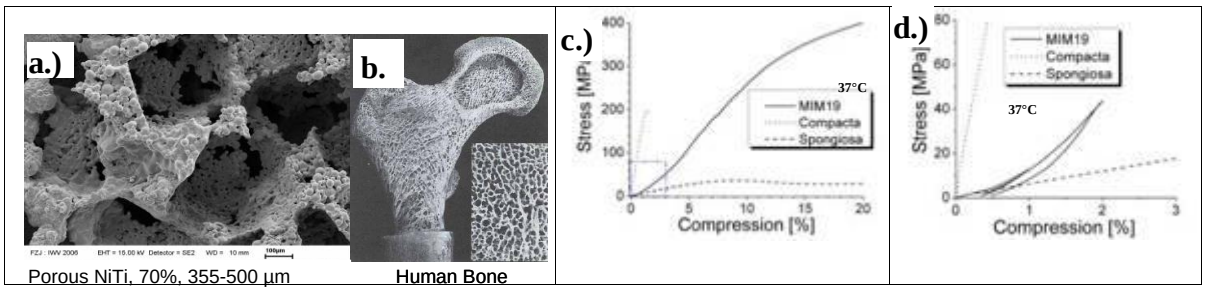

Figure 6. a.,b.) Comparison of the structure produced by powder metallurgy (PHF2) with the humane bone. c.,d.) Stress-Compression curve of MIM19 compared to bone material [2].

The cell culture tests indicate a proliferation of hMSCs on the analyzed specimens as well on the porous surface as in the fracture surface.

Additionally to the outstanding bone-like mechanical properties, the pseudoelasticity of Ni-rich NiTi combined with a defined porosity allows reversible and adjustable energy absorption. *Figure 7a.*

illustrates the amount of reversibly absorbed energy of MIM19 samples at RT in compression tests. Up to 8%, this energy can be used reversibly, after that the porous, metallic structure guarantees a damping buffer up to ~150 MJ/m^3 at stresses of 600 MPa (*Figure 7b.*). Porous NiTi produced by this method can with that be very attractive for damping specifically e.g. machine rooms or long projecting tools.

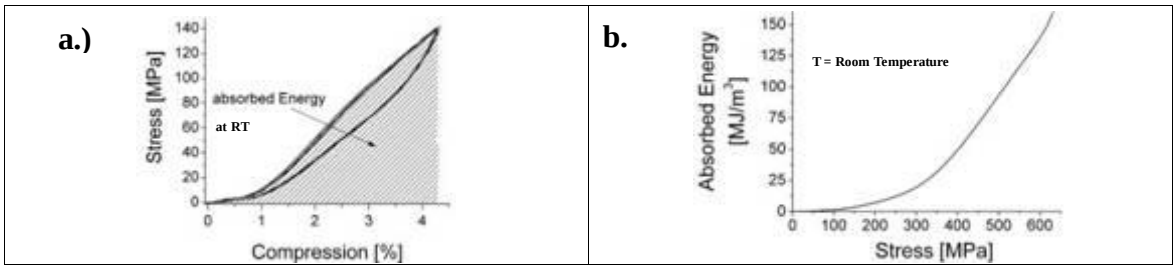

Figure 7. a.) Stress-compression cycles of MIM19 samples at RT up to ~4% compression. b) Absorbed energy in dependence of stress in compression tests of MIM19 at RT.

ACKNOWLEDGEMENTS

This work is funded by the Deutsche Forschungsgemeinschaft (DFG) as part of the SFB459.

REFERENCES

Gibson, L.J., et al., 1997. "Cellular Solids", Cambridge: Cambridge University Press.
Imwinkelried, T. 2007. "Mechanical Properties of Open-Porous Titanium Foams", 81A(4): 964-970
Mentz, J. 2006. "Improvement of Mechanical Properties Of Powder Metallurgical NiTi Shape Memory Alloys", Adv Eng. Mater, 8(4): 247-252
Simske, S.J., et al., 1997. "Porous materials for bone engineering". Mater Sci Forum, 250: 151-182
Yahia, D.L. 2000. "Shape Memory Implants", Berlin Heidelberg: Springer.

Porous titanium coatings through electrophoretic deposition of particle stabilized emulsions.

Mattheys T., *Braem A.*, Neirinck B., Van der Biest O. and Vleugels J.

Department of Metallurgy and Materials Engineering (MTM), Faculty of Engineering, K.U.Leuven, Kasteelpark Arenberg 44, B-3001 Heverlee, Belgium, annabel.braem@mtm.kuleuven.be, Telephone: +32 16 32 15 34, Fax: : +32 16 32 19 92

INTRODUCTION

Nowadays, porous materials are of great interest for a broad range of applications going from polymeric foams for packaging to ceramic soot filters in diesel engines. In the biomedical field, porous materials gain currency as scaffolds for guided bone growth and as coatings on prosthetic devices for an improved implant fixation. The latter being one of the major challenges in implant technology since loosening comprises the main reason for implant revision (65%). By tailoring the surface morphology and controlling the porosity and pore size of the coating, osteointegration can be promoted resulting in an optimal mechanical anchorage. Additional use of bioactive coating materials on the internal surface of this porous coating like bioactive glass (BAG) or hydroxyapatite (HA) can establish a firm chemical fixation between implant and tissue.
In this study, porous titanium coatings on Ti6Al4V substrates are obtained using titanium particle stabilized emulsions. After coating the substrate with the emulsion by means of electrophoretic deposition (EPD), the liquid phases are removed by evaporation and the porous coatings are sintered in a microwave furnace in helium.

OBJECTIVE

The goal of this study is to develop a macroporous Ti-coating with controlled porosity and pore size on a dense Ti6Al4V substrate (figure 1). The envisaged specifications of this macroporous Ti-coating are an overall open porosity of 15-40%, a thickness of 200-400 µm and a spherical macropore size that can be varied from 50 to 150 µm.
Later on, the surface of the macroporous structure will be covered with a second, multilayer coating. First, a TiO_2 -bond coating is created to improve the adhesion between the titanium and the second bioactive layer (BAG, HA,…). On top of this bioactive layer, a microporous amorphous silica layer containing biofilm inhibiting molecules can be applied. The ability of tuning the release of the molecules can reduce the risk of infections.

EXPERIMENTAL PROCEDURE

The development of the titanium coating is actually a three steps process.
In the first stage, an oil-in-water Pickering emulsion is prepared. 40 ml of absolute ethanol with 5 vol% demineralised water serves as the continuous phase and various amounts of paraffin oil (5 or 10 ml) are added. Magnetic stirring for 10 min gives rise to the dispersion of the oil phase into droplets. These droplets are stabilised by adding titanium powder particles.
For electrophoretic deposition the particles have to be properly charged. Since oxidation of the substrate should be avoided, the substrate is required to act as the cathode. This implies a positive charge on the dispersed droplets. 1,2 ml of a solution of polyethyleneimine (PEI, 50 wt% in water diluted with absolute ethanol to 0,01 g/ml) leads to an adequate positive charge at low pH. The desired pH is obtained by adding 0,3 ml of a phosphoric acid solution (85% diluted to 1 M in absolute ethanol) and 0,143 ml acetic acid. After some additional stirring the system is balanced.

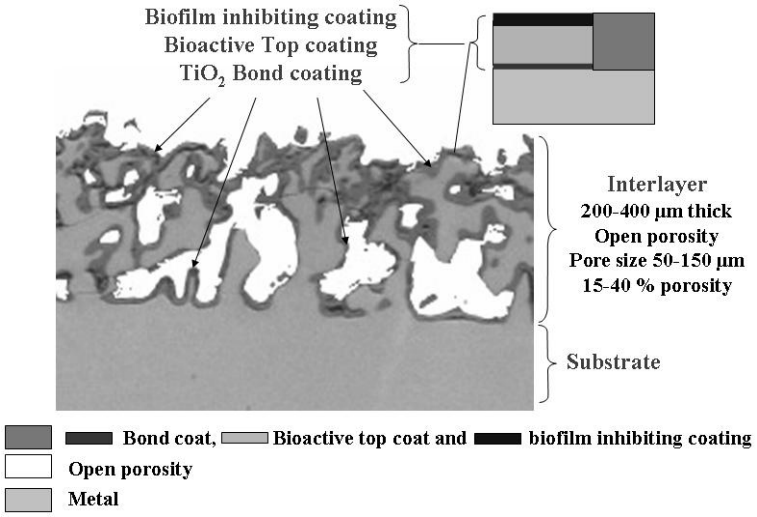

Figure 1. Schematic overview of the targeted coating.

The second step is the electrophoretic deposition of the emulsion on the Ti6Al4V substrates. In the deposition cell, the electrodes are placed vertically at a distance of 3,5 cm and the deposition electrode is coupled as the cathode. The electrical field is applied by means of a controlled voltage F.U.G. (type MCN 1400-50) power supply. Experiments are performed at 90 V and various times (150 s and 300 s).

In the final phase of the processing route, the obtained deposited substrate is dried for at least 24 hours and introduced in the microwave furnace. Since the dielectric loss factor of titanium is too low at room temperature, the principle of hybrid microwave heating is applied. The sample is hereby positioned in a SiC tube. At low temperature, the microwaves couple with the tube and the coating is heated by convection and radiation. At higher temperature, the titanium coating itself starts to couple with the microwaves. All samples are heated at 50°C/min to the sintering temperature. Various sintering temperatures (1000°C, 1050°C and 1100°C) and cooling speeds (2 and 120°C/min) are examined.

The EPD and sintering parameters are summarized in table 1. The surfaces of the coating, as well as the polished and etched cross-sections are analysed by means of scanning electron microscopy (SEM, XL 30 FEG, FEI).

Table 1. Experimental parameters used for the deposition and sintering of the coatings.

Experiment	m_{Ti} [g]	$V_{paraffin}$ [ml]	PEI [ml]	pH [-]	U_{EPD} [V]	t_{EPD} [s]	$T_{sintering}$ [°C]	t_{dwell} [min]	ΔT_{cool} [°C/min]
A	12	0	3,6	4,08	90	300	1100	10	120
B	6	5	1,8	3,97	90	150	1050	30	120
C	6	10	1,8	3,3	90	300	1000	15	120
D	6	5	1,8	3,97	90	300	1050	15	2

RESULTS AND DISCUSSION

The SEM micrograph of an untreated Ti6Al4V substrate is shown in figure 2. The original microstructure consists of an equi-axial α+β structure. To avoid a drastic reduction of the strength and fatigue resistance of the substrate material, this structure should be maintained after sintering. To do this, some characteristic temperatures of the alloy should be taken into account: the martensitic phase transformation starting temperature (800°C), the β-transition temperature (995°C) and the melting temperature (1660°C).

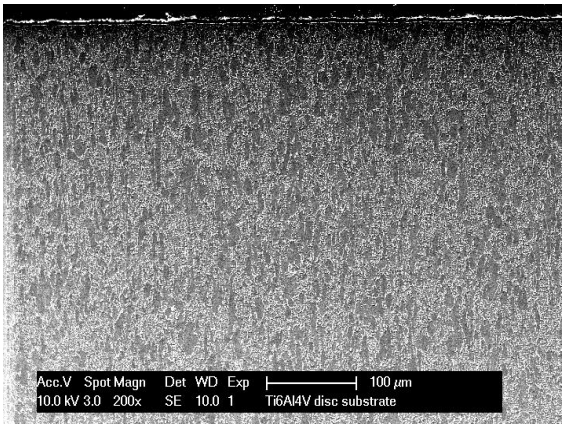

Figure 2. SEM micrograph of an untreated Ti6Al4V substrate: the microstructure consists of an equi-axial α+β structure (α is the dark phase, β is the light phase).

After microwave sintering, a spherical residual porosity is visible. Figures 3 and 4 demonstrate the difference in morphology between a suspension based coating; experiment A (figure 3) and an emulsion based coating; experiment B and C (figure 4a resp. 4b). The emulsion based coatings contain larger cavities, which can be attributed to the presence of the emulsion droplet templates. The coating thickness is about 200 µm and the pore network is mainly open with homogeneously distributed pores of an average pore size of 50 µm.

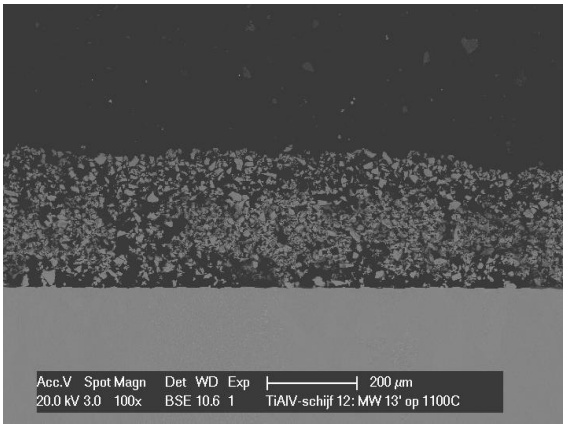

Figure 3. SEM micrograph of a cross section of a coating obtained from a Ti powder suspension; experiment A.

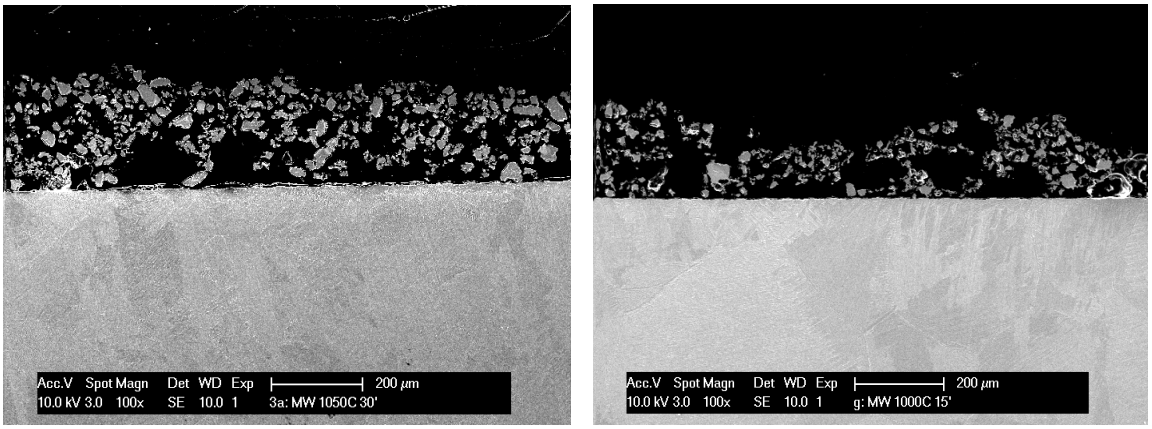

(a) (b)

Figure 4. SEM micrograph of a cross section of a coating obtained from a Ti particle stabilized emulsion; experiment B (a) and experiment C (b).

Since powder sintering is a diffusion driven process and the substrate material (Ti6Al4V) differs from the coating material (Ti), V and Al alloying elements diffuse from the substrate into the porous coating at the spots where neck formation occurs. This causes a change in the composition of the coating near the substrate surface (figure 5). Complete diffusion throughout the coating should be avoided to maintain the excellent biocompatibility of the pure titanium coating.

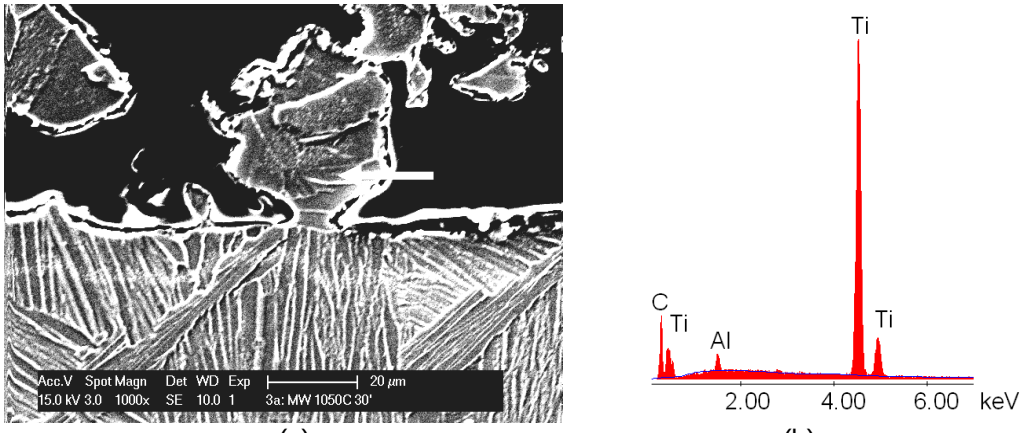

(a) (b)

Figure 5. SEM micrograph of a cross section of a coating after sintering for 30 min at 1050°C (a) and EDS point analysis (indicated by arrow) taken in one of the diffusion bonded particles (b).

In this study, the sintering temperature was raised above the β-transition temperature to establish particle bonding. This resulted in a modification of the original α+β structure (figure 2) after heat treatment. Figure 6 gives a schematic presentation of the final microstructure as a function of the cooling rate. In experiment A, the rapid cooling (120°C/min) during microwave sintering alters the microstructure into a Widmannstätten microstructure (figure 7a). Lowering the cooling rate (2°C/min) results in a more coarse Widmannstätten microstructure in experiment D (figure 7b). In order to preserve the better mechanical properties after sintering, the original α+β structure has to be maintained. Therefore, an even slower cooling rate or an additional heat treatment should be applied.

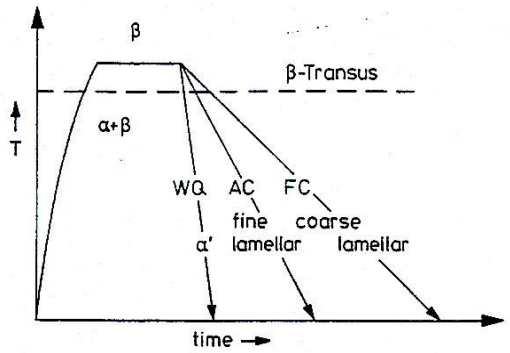

Figure 6. Schematic presentation of the microstructure in a Ti6Al4V alloy as function of the cooling rate.

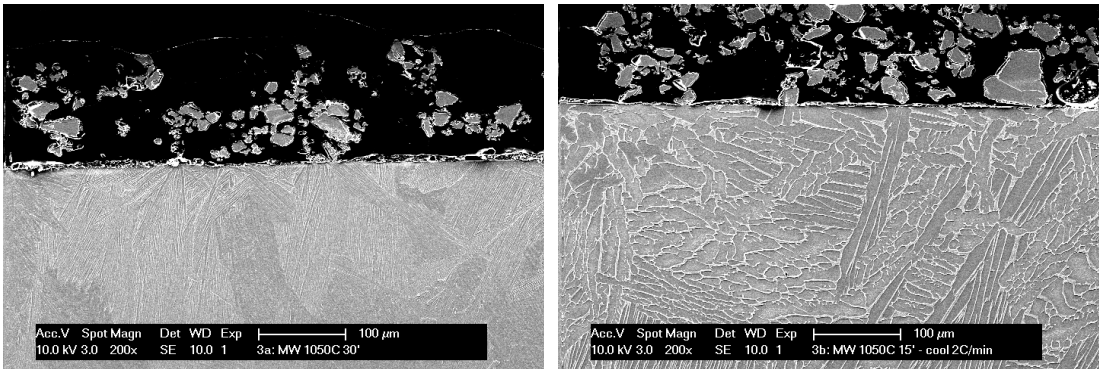

Figure 7. SEM micrograph of a cross section after cooling at (a) 120°C/min;experiment A and (b) 2°C/min, experiment D.

CONCLUSIONS

Macroporous Ti coatings on dense Ti6Al4V substrates were obtained by means of electrophoretic deposition of titanium particle stabilised emulsions followed by microwave sintering of the deposits in helium. The coatings had a final thickness of ± 200 µm with a prevalent open porosity and average pore size of 50 µm. Further work will focus on tailoring the pore volume and size by controlling the emulsion, the Ti particle size, the EPD and sintering parameters.

ACKNOWLEDGEMENTS

This work was supported by the 6 th Framework of the Commission of the European Communities under project contract No. NMP3-CT-2006-026501 (Meddelcoat), the Flemish Institute for the Promotion of Scientific and Technological Research in Industry (IWT) under grant SB/51092, and the Research Fund of K.U.Leuven under projects GOA/2005/08-TBA, IOF-HB/06/005 and IDO/06/013.

REFERENCES

Neirinck, B., Mattheys, T., Fransaer, J., Van der Biest, O. and Vleugels, J. Porous titanium coatings obtained by electrophoretic deposition (EPD) of Pickering emulsions and microwave sintering. Adv. Eng. Mater., in press.

Boyer, R., Welsch, G., Collings, E.W. 1994. Materials Properties handbook: titanium alloys.

Biofuel cells:
An alternative method for energy production?

Merle G.[1], Tingry S.[1], Rolland M.[1], Cretin M.[1] and Innocent C.[1]

1 Institut Européen des Membranes, UMR 5635, Place Eugène Bataillon, CC 047, 34293 Montpellier, cedex 5, France,
Geraldine.merle@iemm.univ-montp2.fr , Telephone: 0467149123, Fax: 0467149111

INTRODUCTION

The constant increase in energy consumption due to our modern society and the significant environmental impact involved in the use of non-renewable energy sources will shortly force us to find an alternative method of energy production. A fuel cell usually relies on hydrogen as carburant and oxygen as comburant to generate power through the electrochemical conversion of fuels directly into electricity. Because electrical energy is generated without combustion, fuel cells are an extremely attractive option from an environmental standpoint. The incurred redox reactions generate electrons at the electrodes and consequently a voltage, accompanied by the production of water and heat. Biofuel cells use biocatalysts (enzymes), to convert chemical energy into electrical energy with a low power output at room temperature and under physiological conditions (figure 1). The advantage of an enzymatic biofuel cell is to exploit the enzyme selectivity, thus eliminating the need for a membrane. Hence, miniaturisation can be achieved for various applications (for implantable devices, microdevices…)

Objectives and context

The concept of biochemical fuel cell appeared in 1964 with the works of YAHIRO *and all*[1], who described the elaboration of a methanol/ O_2 cell, methanol being oxidized by the enzyme methanol dehydrogenase, and with the works of YOUNG *and all*[2] in 1996.

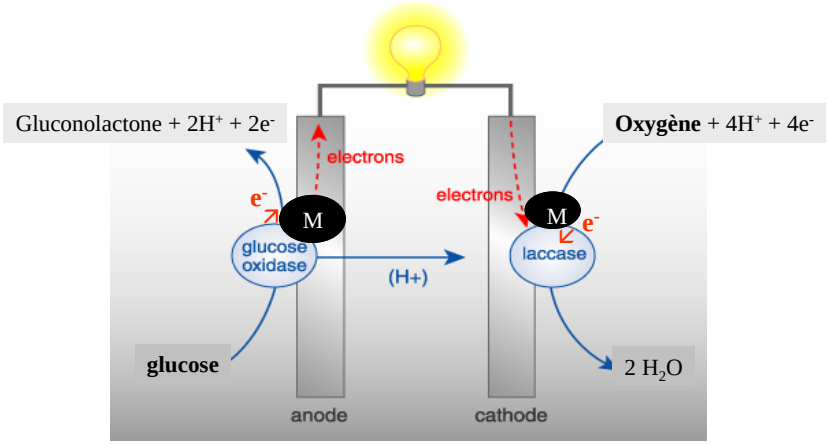

Figure 1: schematic configuration of a glucose/O_2 biofuel cell
M = redox mediators for electron transfer

In the nineties, biofuel cells have come in to prominence with the recent advancements in novel electrode chemistries developed by Katz and Willner, and in the miniature cells realised by Heller *et al*[3-4]. The development of these systems focuses on the different methods of enzyme immobilisation and the establishment of their electrical connection to the electrodes. Efficient connection is achieved by the use of appropriate redox mediators which can “shuttle” electrons between the active site of the enzymes and the electrode surfaces (figure 2).

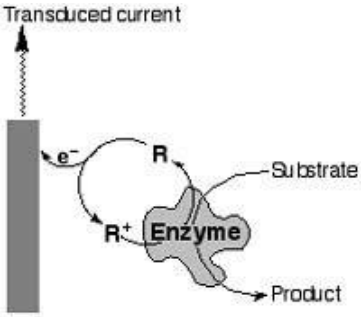

Figure 2: Electron transfer mechanism between the active site of the enzyme and the electrode surface via a redox mediator

Surface-immobilized mediators and enzymes are the key factors to improving electron transfer at the electrode interface. Some approaches have been devised to construct a glucose/O_2 biofuel cell by exploiting the oxidation of glucose coupled to the reduction of dissolved oxygen. Glucose is electrooxidized at the anode to □-gluconolactone by glucose oxidase (GOD) and dioxygen is reduced to water at the cathode by specific enzymes such as cytochromes oxydases [5] or bilirubin oxydase [6] or laccase [7].
The recent investigations in glucose/O_2 biofuel cells [8, **9** are devoted to] miniature and implantable cells that appear to be alternative methods of producing low power energy. This research field is currently under extensive development at an international level and a strong international competition exists
The objective is the construction of a glucose/O_2 micro biofuel cell, both efficient and stable. The application of this device is to generate electrical current to supply micro- machines (micro-pump, micro-distributor of active species) biosensors, or even implantable sources (pacemarker).

The originality of our work, compared to literature, concerns the structure and the porous nature of the electrodes. As O_2 is necessary only for bioelectrocatalysis at the biocathode, we developed a system of pseudo-compartmentalisation. The strategy consists of introduction by convection of an O_2 saturated liquid-phase through the porous carbon biocathode and an oxygen contactor (figure 3B). The inside of the cathode tube was continuously supplied by a saturated dioxygen solution that was likely to diffuse from the inner to the external surface of the porous tube. Oxygen diffusion in the electrolyte to the anode was limited. Various enzyme immobilisation techniques on porous supports have been developed [10]. On the other hand, the elaboration of a matrix polymer based on polypyrrole obtained by electrochemistry is a manufacturing technique, well mastered in the IEM [11, 12] to allow for producing stable conductive interfaces. The team has extensive experience in modified electrode construction and immobilisation and the use of enzymes on the conducting support.

At the cathode, oxygen is directly reduced to water by laccase or BOD and at the anode glucose is oxidised in gluconolactone by glucose oxidase, in the presence of their respective redox mediators ABTS (2,2'-azinobis(3-ethylbenzothiazoline-6-sulfonate)) and HQS (8-hydroxyquinoline-5-sulfonic acid). The enzyme/mediator couples were immobilized by covalent linkage via an N-substituted polypyrrole matrix beforehand electrodeposited on carbon porous electrodes (3cm, porosity 20%, figure 3A,B).

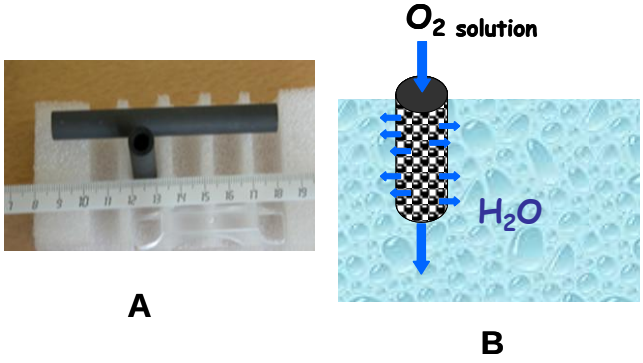

Figure 3: **A** – Carbon porous tube;
B – scheme of cylindrical biocathode. Dioxygen diffuses through the porosity of the carbon tube

Preliminary results:

This device delivers a maximum power density of 19 µW.cm^{-2} at 0.23 V, pH 7.0 with 10 mM glucose (figure 4, curve (■)). However, the power density was twice as low as that compared to the same system with oxygen bubbling directly in the cell (figure 3C, curve (□)).

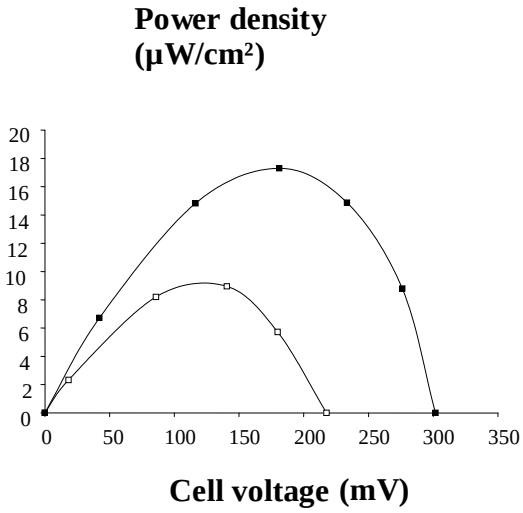

Figure 4:Power density versus cell voltage in phosphate buffer solution pH 7, glucose 10 mM, oxygen solution inside the tube (■), oxygen solution outside the tube (□).

The electrical performances of the biofuel cells (intensity-potential curves, power density versus cell voltage) will be determined according to the influence of parameters such as the pH and the temperature. These electrochemical studies will be carried out in model conditions [13, 14] in a pseudo physiological environment: pH 7.4, temperature 37°C, ionic conditions (0.15 M NaCl).

The advantage of an irreversible immobilisation of the biomolecules on the electrode is the longer stability of the biofuel cell. Our biofuel cells are less susceptible to poisoning and loss of activity under normal operating conditions.

CONCLUSIONS

In conclusion, the results obtained show the feasibility of glucose/O_2 biofuel cell prototypes as an electrical energy source. These studies bring have highlighted the following positive aspects:

* The advantage of the unique design of the device
* Stable immobilisation of enzymes and mediators
*An efficient electrical connection to the enzymes via redox mediators

At present, the delivered power values are of the order of around ten microwatt per cm^2. The objective is to increase the power values to the milliwatt per cm^2 magnitude. Studies on fuel cells have shown that the miniaturisation of the cell has led to a delivered power increase by ten fold. We plan to replicate such performances by combining the dimensions of the system with the improvements of the enzyme connection at the electrode surfaces.

ACKNOWLEDGEMENTS

We thank C. Jolivalt for the gift of laccase.

REFERENCES

[1] Yahiro, Lee, Kimble, Biochim. Biophys. Acta, 1964, 88, 375
[2] Young, Hadjipetrou, Lilly, Biotechnol. Bioeng. 1966, 8, 581
[3] Y. Degani, A. Heller, J. Phys. Chem. 1987, 91, 1285
[4] Bioelectrochemistry,G.S. Wilson, Encyclopedia of electrochemistry, vol 9, John Willey, 2002
[5] P.N. Bartlett, R.G. Whitaker, M.J. Green, J. Frew, J. Chem. Soc. Comm., 1987, 1603
[6] S. Tsujimura, H. Tatsumi, J. Ogawa, S. Shimizu, K. Kano, T. Ikeda, J. Electroanal. Chem. 2001, 496, 69
[7] G. Tayhas, R. Palmore, H.H. Kim, J. Electroanal. Chem. 1999, 464, 110
[8] R.F. Service, Science, vol. 296, 1222
[9] Kendall K., Nature Materials, 2002, 1, 211
[10] G. Merle, L. Brunel, S. Tingry, M. Cretin, M. Rolland, K. Servat, C. Jolivalt, C. Innocent, P. Seta, Mat. Sci. Eng C. (ss press)
[11] A.Naji, C. Marzin, G. Tarrago, M. Cretin, C. Innocent, M. Persin, J. Sarrazin, J. Applied Electrochem. 31, 2001, 547-557
[12] S. Gandasasmita, M. Persin, M. Cretin, J. Sarrazin, Desalination, 148 (2002) 5-9
[13] K. Servat, S. Tingry, L. Brunel, S. Querelle, M. Cretin, C. Innocent, C. Jolivalt and M. Rolland, J. Appl. Electrochem. 37, 23007, 121
[14] L. Brunel, J. Denele, K. Servat, K.B. Kokoh, C. Jolivalt, C.Innocent, M Cretin, M. Rolland and S. Tingry, Electrochem. Comm. 9, 2007, 331

Processing and characterization of porous scaffolds for bone regeneration.

S. Mullens, ***J. Luyten, I. Thijs, W. Bouwen***

Materials Technology, VITO, Boeretang 200, B-2400 Mol, Belgium

Large bone defects, caused by trauma or bone cancers, are a big challenge for surgeons. A biomimetic approach, in which a porous synthetic bone substitute with properties similar to these of trabecular bone is used, is a first step toward tissue engineering and might offer a solution for this clinical problem.

This work presents an overview on the different production methods of highly porous bioceramics and metals, which mimic the 3-dimensional architecture of trabecular bone with pore sizes between 50 and 800µm. Figure 1 presents the architecture of the titanium porous structures manufactured by (a) PU replica technology (b) gel casting and (c) 3D fiber deposition. Techniques which are used to characterize the porous architecture of the scaffold are discussed as well.

In order to stimulate the biological activity of the surface, bioceramics can be deposited onto the surface of the metallic porous scaffolds by several coating technologies. These composites combine the good mechanical properties of porous Ti (and some of its alloys) and the osteoinductive nature of the coating. The coating (figure 2) can also be used as a reservoir for drug delivery systems. These kind of materials are promising as bone scaffolds as they inhibit infection at the bone-implant interface, permit vascularization of the internal structure of the foam and the transport of other biological agents and nutrients to the newly formed bone.

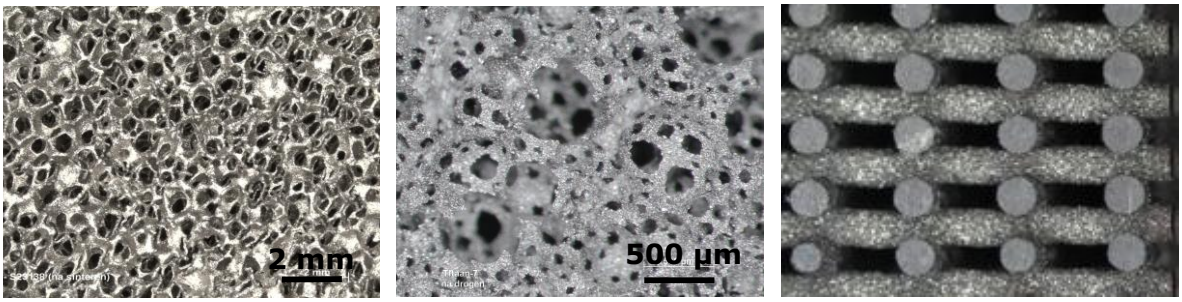

(a) (b) (c)

Figure 1. Porous titanium architecture made by (a) PU replica technology (B) gel casting and (c) 3D fiber deposition

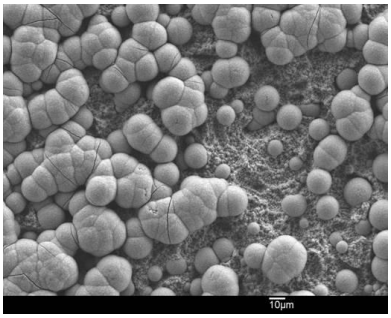

Figure 2. CaP nucleation on a Ti surface

Theme 3: Porous materials for environmental protection

Soot filters, catalytic supports, filters for molten metal, sensors and membranes are only a few examples of the widespread application of porous materials for innovative applications with a beneficial impact on our environment. Both basic research as well as technological development has resulted in novel porous structures through new synthesis routes, improved processing, better characterisation and modelling.

Development of multilayered ferrite-based ceramic membranes for partial oxidation of hydrocarbons.

***Kovalevsky A.V.*[1,2], *Kharton V.V.*[2], *Snijkers F.M.M.*[1], *Cooymans J.F.C.*[1], *Luyten J.J.*[1], *Frade J.R.*[2]**

1 Materials Department, Flemish Institute for Technological Research (VITO), 2400 Mol, Belgium, andrei.kavaleuski@vito.be , Telephone: (32) 474918506, Fax: (32) 14321186
2 Department of Ceramics and Glass Engineering, CICECO, University of Aveiro, 3810-193 Aveiro, Portugal

The key advantage of multilayered configuration includes the possibility to improve both oxygen permeation flux and thermodynamic stability of ceramic membranes for oxygen separation and partial oxidation of light hydrocarbons. Previous evaluations reveal an attractive combination of thermomechanical and oxygen transport properties for $(SrFe)_{0.7}(SrAl_2)_{0.3}O_{3.3-\delta}$ dual phase composite if compared to other ferrite-based mixed conductors. The present work was focused on assessment the impact of membrane architecture on oxygen permeation flux through planar ceramic membranes with dense layers made of this material. The asymmetric membranes with porous $La_{0.5}Sr_{0.5}FeO_{3-\delta}$ and $(SrFeO_{3-\delta})_{0.7}(SrAl_2O_4)_{0.3}$ supports were fabricated by a two-stage compaction procedure using various pore-forming additives and sintering at 1623-1723 K. The characterization of asymmetric membranes and, separately, the components of dense and porous support layers, was carried out using X-ray diffraction (XRD) analysis, scanning electron microscopy coupled with energy-dispersive spectroscopy (SEM/EDS), picnometry, gas-tightness control, mercury intrusion porosimetry, dilatometry and determination of steady-state oxygen permeation fluxes at 1073-1223 K under various oxygen partial pressures. Analysis of the oxygen permeation fluxes through model symmetric membranes showed significant limiting role of the composite surface oxygen exchange. At temperatures above 1173 K, a substantially improved and stable performance was observed for asymmetric self-supported composite membranes with the dense layer thickness of 0.12 mm, surface-modified with $(SrFeO_{3-\delta})_{0.7}(SrAl_2O_4)_{0.3}$ – Pt mixture. At 1023-1173 K, higher oxygen fluxes were achieved using perovskite-type $La_{0.5}Sr_{0.5}FeO_{3-\delta}$ as the porous support material.

Absortion of biolubricant oxidation products in nanoporous material

Coto B.[1], Marcaide A., [1]Aranzabe A[1]., and Zubizarreta C.[1]

1 Fundación Tekniker. Manufacturing Processes Dept. Otaola 20, Eibar 20600 Gipuzkoa. Spain, bcoto@tekniker.es, Telephone: +34 943-206744, Fax: +34-943-202757

In the framework of the Soilcy project, contract nº 515848, absortion of oxidation products from a biodegradable lubricant is examined by means of computational tools. Monte Carlo and Molecular Dynamics methods are used to study the absorption of different molecules in a nanoporous material proposed as absorbing media. Results of the ability of the proposed as absorbing media and preferred absorbing sites are obtained.

INTRODUCTION

The use of esters as base oil for biolubricants is nowadays highly extended, being the applications in which they are used, hydraulic and chainsaw oils, as well as metalworking fluids and concrete release agents. However, no bio-lubricants are known for compressor applications except for food industry. The most important restriction for biolubricants is that they are 1,5 to 5 times more expensive than the conventional ones. The development of a cost effective compressor bio-lubricant, using a renewable by-product its very interesting from an environmental and industrial point of view.

Besides the price, one of the major concerns about biolubricants is its performance, which is directly related to the use of additives. The advancement in mechanics and machine tools working under severe and stringent conditions leads to ask for improved lubricants. The use of additives allows to increase the overall performance of an oil and to improve its physical properties, but they also may raise the cost of lubricants and, in some cases, may even be harmful, as in the case of antioxidant lubricants commonly composed by phenolic and amine molecules.

Currently, the research in the field of additives is addressed to increase demands of the lubricants industry for higher performance and more cost effective systems with appropriate behaviour in increasingly stringent environmental requirements. The aim of this work is to propose a more environmentally friendly and cost effective alternative to antioxidant additives.

Usually, the oil in compressors is not filtered with and oil filter-removing particles in the sub-micron range because the particular contamination is very small. So this filtration device containing micro/nanoporous material is highly innovative.

Micro/nano-materials are promising materials to be used in compressor applications as selective absorbing sieves for oxidation molecules to replace harmful antioxidant additives and to lengthen the oil life making it more efficient.

A computational approach could help to design and select the absorbing sieve. In the present work Monte Carlo (MC) and Molecular Dynamics (MD) simulation methods are proposed as tools to examine the absorbing performance of micro/nanoporous materials as absorbing media for oxidation molecules.

In the present work a nanoporous material is studied as absorbing sieve for diferent oxidation product molecules using MC and MD methods. Accelrys© software Materials Studio 4.2 has been used to perform simulations.

COMPUTATIONAL APPROACH

Molecular Systems and Nanostructure Sizes

Molecules showed in Figure 1 have been proposed as oxidation products of a trimethylolpropane ester base oil. The proposed molecules have been modelled by means of an energy minimization.

COMPASS forcefield has been used to evaluate energy. Steepest Descent, Conjugated Gradient and Newton-Raphson methods of minimization have been consecutively used in order to minimize energy and lead to molecular configurations showed in Figure 1. The length of molecules, volume occupied and surface area have been measured and are represented in table 1. Volumes and surfaces have been calculated taking into account the Connolly surfaces for a Connolly radius of 1 Å.

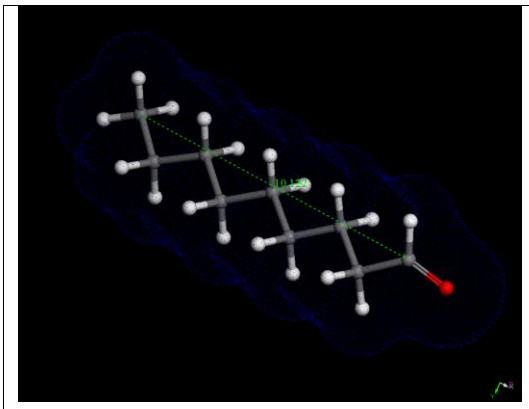

Nonanal

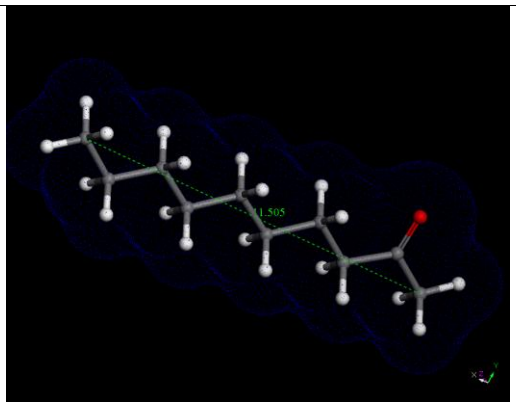

2-Decanone

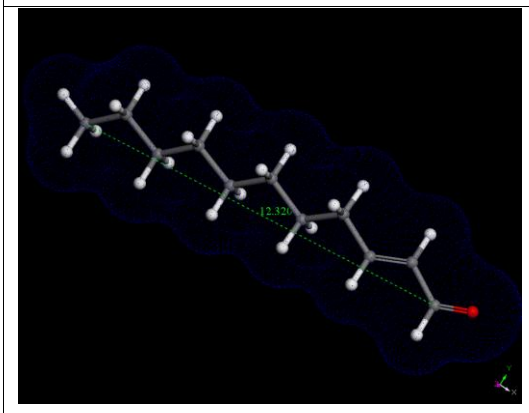

2-Undecenal

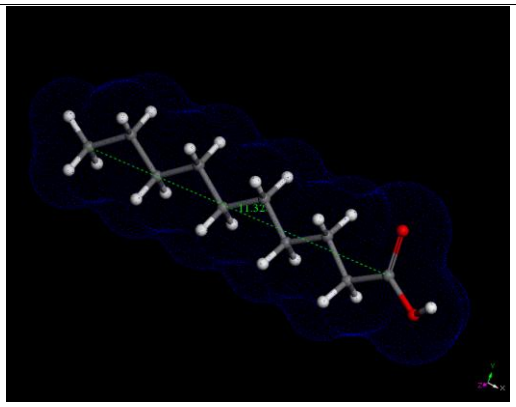

Decanoic Acid

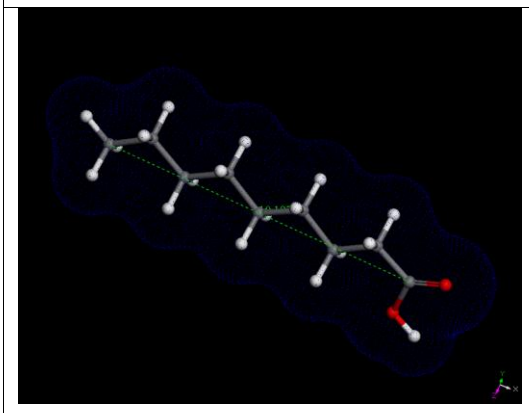

Nonanoic Acid

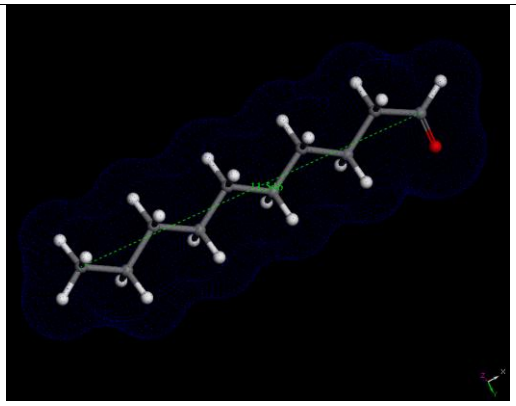

Hexadecanal

Figure 1. Oxidation products molecules

Table 1. Molecular Sizes

Molecule	Length (Å)	Occupied Volume (Å^3)	Surface Area (Å^2)
2-Undecenal	12,320	205,120	241,840
2-Decanona	11,505	193,500	226,800
Ácido Decanoico	11,510	209,810	242,810
Ácido nonanoico	10,197	183,470	215,570
Decanal	11,546	194,090	227,430
Nonanal	10,122	175,660	208,330

An micro/nanoporous material has been proposed as molecular sieve to trap the oxidation products. The surface has been obtained from this porous material with 3D boundary condition by cleaving along the (1 0 0) crystallographic direction and leaving a vacuum slab of 40 Å over the surface to keep 2D boundary conditions. Then a minimization process was performed in order to take into account surface effects in atomic positions. As in the case of the molecules molecules COMPASS forcefield was used to evalute energy and the minimization methods were Steepest Descent and Conjugate Gradient. Dimensions of the nanostructure unit cell obtained are a = 19.899 Å; b = 13.383 Å; c = 39.150 Å

Monte Carlo And MD Simulations

Fixed preassures simulations have been done. In this kind of simulations configurations are sampled from the Grand Canonical ensemble: the system can exchange energy and particles with a surrounding reservoir. In the Grand Canonical ensemble fugacities of all components as well as temperature are fixed as if the system was in open contact with a reservoir that contains an infinite amount of sorbate at a fixed temperature. Resorvoir is completely described by temperature and fugacities so it is not necessary to simulate it in a explicit way.

Fixed pressure simulations starts with an empty framework, the nanostructure selected and initial configuration is adjusted to the required temperature and fugacity.

A Monte Carlo configurational bias method was used. In this method trial configurations are generated with a probability. These trial configurations have an acceptance probability that depends on the energy of the system. In the configurational bias method torsional degrees of freedom are taken into account (see references for details).

Simulations were performed for T=298 K and fugacity f = 103.1 kPa.

Table 2 shows the results obtained for the molecules proposed.

Table 2. Results

Molecule	Maximun Load	Average Load	Average Energy (kcal/mol)	Maximun Density (molecules/nm^3)
2-Undecenal	14,000	13,048	-973,825	0,889
2-Decanona	16,000	14,527	-591,868	0,990
Ácido Decanoico	15,000	14,655	-988,189	0,998
Ácido nonanoico	17,000	15,641	-1005,992	1,066
Decanal	17,000	15,744	-545,818	1,073
Nonanal	18,000	17,215	-525,937	1,173

Density maps obtained show the zones where molecules prefer to be absorbed (Figure 2). Also minimun energy configurations are obtained for each molecule (Figure 3).

Once MC calculations are done MD simulations was performed in order to study stability of MC minimun energy configurations under dynamic conditions. 2 ns simulations were performed in the NPT ensamble for T = 298 K and P = 1 atm. Berendsen methods were used for the thermostat and the barostat. The evolution of the systems showed the stability of the configurations with time. No molecules are desorbed, moreover trajectories showed as some of the molecules adsorbed at the surface of the micro/nanoporous material moves inside the pore what may be desirable as allows more molecules to be absorbed at the surface.

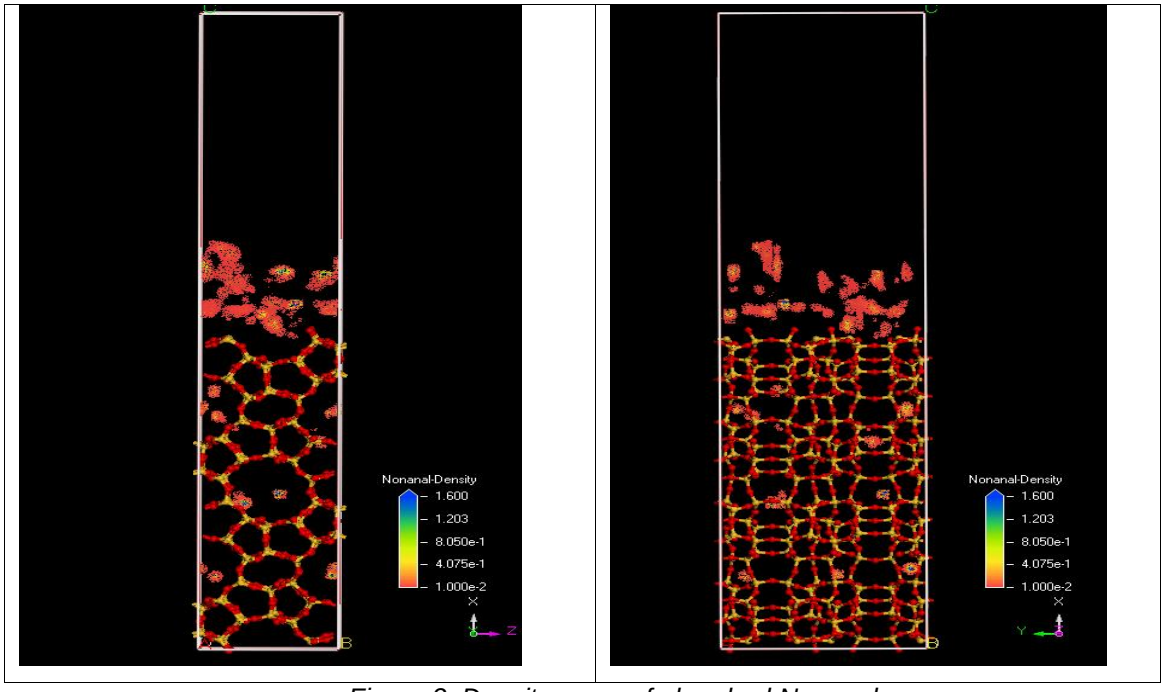

Figure 2. Density maps of absorbed Nonanal

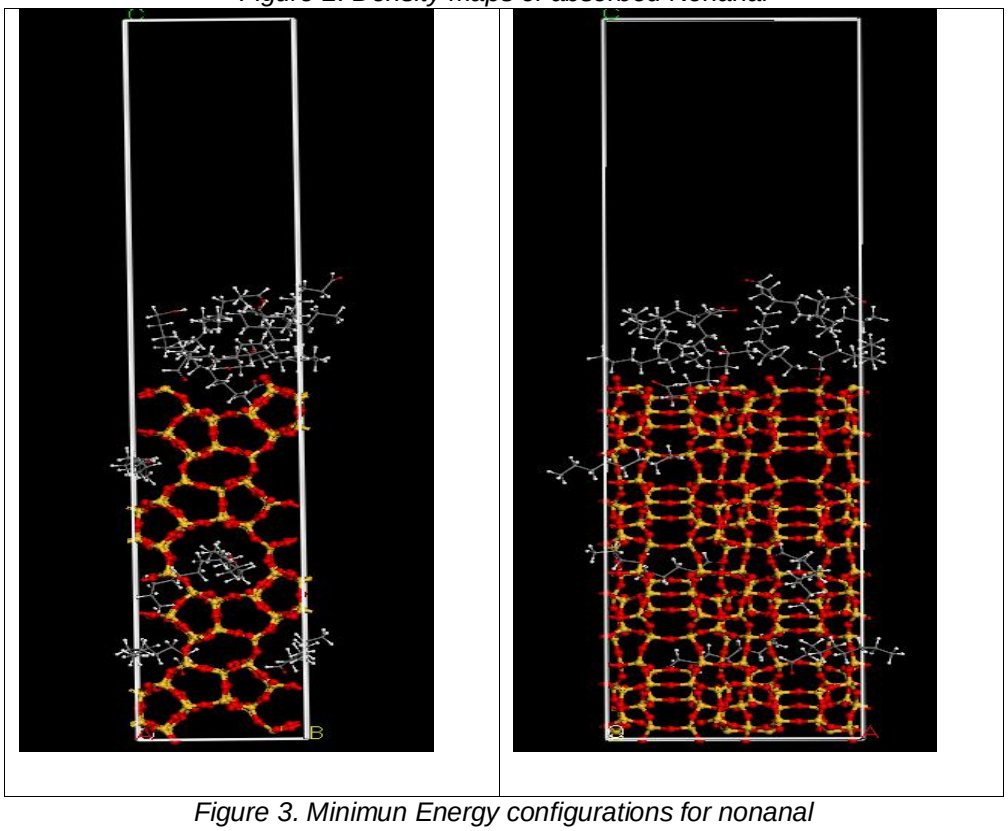

Figure 3. Minimun Energy configurations for nonanal

CONCLUSIONS

Absortion of each molecule has been simulated using a Monte Carlo method. Number of molecules absorbed per unit cell, density of molecules traped and the energies of the systems have been obtained. Preferred absortion sites can be deduced from density maps. Molecular dynamics simulations showed the stability of MC calculations under dynamic conditions.

Next steps involve simulations at different fugacities and temperatures in order to obtain absortion isotherms for each molecule. Also the same simulations will be done for systems containing a combination of molecules in order to know how molecular absortion behaves when we have a mixture of molecules.

REFERENCES

THEODORY, D. et als: “Development of criteria for the award of the European Eco-label to lubricants”, april 2004 (status:concept).
ADHVARYU, A.;ERHAN,S.; ZENGSHE, L. and PEREZ, J: Thermochimica Acta, 1999.
AMEYE, J. and KAUFFMAN, R.:“Antioxidant analysis for monitoring remaining useful life of turbine fluids”, Turbine lubrication in the 21st century ASTM STP 1407, 2001
“About Performance Additives and Fluids”, 2001 Great Lakes Chemical Corporation
LUNDBERG, M.; SKARMAN, B.; CESAR, F. and WALLENBERG, L.R.: Microporous and Mesoporous Materials, 54, 2002
Scientific Program of “Fluid Transport in Nanoporous Materials”, France 2003
MS Modelling 4.2 Accelrys Inc., San Diego, CA, 2003.

Environmental applications of low-cost porous electrodes : electro-recovery, electro-destruction and electro-catalysis

***de Radiguès Q.*, Santoro R. and Proost J.**

Division of Materials and Process Engineering, Université catholique de Louvain, Place Sainte-Barbe 2, B-1348 Louvain-la-Neuve, Belgium, quentin.deradigues@uclouvain.be, Phone +32-10-47.24.90, Fax +32-10-47.40.28

INTRODUCTION

Electrochemical reactors based on porous, three-dimensional electrodes are nowadays contributing substantially to effluent traitement [1]. Such electrodes can have a very high surface area, and can lead to more efficient mass transport conditions close to the electrode surface. This combination of properties leads to a much enhanced rate of electrochemical reactions, which in turn gives the possibility of a high conversion rate of reactant to product either in a short time or during a single pass of the effluent through the cell, even when the reactant is present in very low concentration. Three-dimensional electrodes are therefore ideally suited for the removal of low concentrations of metal ions (electro-recovery) or environmentally harmful substances (electro-destruction) from industrial elluents prior to discharge.
The approach taken in this work is to combine the electro-recovery and electro-destruction capabilities of the same, low cost reticulated vitrous carbon (RVC) porous electrode. In a first stage, the electrode is used as a three-dimensional matrix for dispersing application-tailored electrocatalysts with electrochemically-controlled morphologies and compositions. In a second stage, the thus electrochemically modified RVC support is used in the same electrochemical cell for the selective electrocatalytic destruction of specific toxic substances. This abstract discusses in detail the feasibility of this combined approach for the electrocatalytic destruction of nitrate and nitrite ions on porous, Cu-coated RVC cathodes, providing a viable alternative to state-of-the art biological or chemical technologies currently used during wastewater treatment of powerplants [2]. The very same approach can be easily extended to a wide range of other catalyst-support material combinations. For instance, it is expected to hold much promise as well for the fabrication of monolithic fuel cell electrodes aiming at an improved catalyst mass specific power output [3].

EXPERIMENTAL

The electrochemical process parameters for both process steps were optimised using a lab-scale hydrodynamic circuit based on a commercially available filter-press cell with continuous flow (Figure 1).

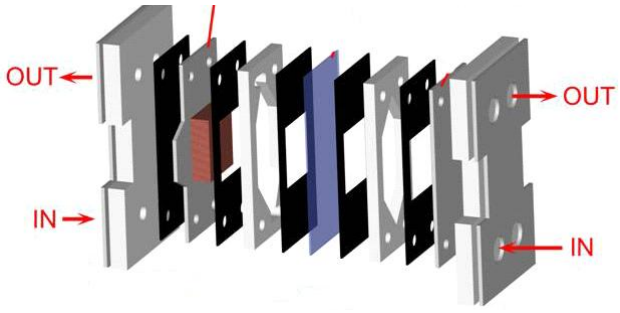

Figure 1. Schematic of a filter-press type electrochemical cel with a porous, three-dimensional cathode, operating in flow-by configuration.

As cathode material, a 100 ppi porous RVC electrode was used with a specific surface area of 66 cm^2/cm^3, a flow-through surface of 1.40 cm^2 and a total volume of 4.90 cm^3. For the catalyst deposition and dispersion during the first step, 1 L of a Cu-containing solution (Cu^{2+}: 0,35 g/L, H_2SO_4: 160 g/L) was circulated through the cell in a flow-by configuration at constant flow rates of

0.47 L/min and 0.73 L/min for the cathodic and anodic compartment, respectively. The kinetics of the Cu electrorecovery process was monitored as a fonction of applied current both by a continuous monitoring of the cell voltage, as well as by the evolution of the residual Cu-concentration in solution, measured ex-situ with ICP on periodically sampled solution fractions. For the second, electro-destruction process, an optimised Cu-coated RVC electrode was then used in the same filter-press cell for the electrocatalytic destruction of nitrate and nitrite ions, present in a simulated aqueous industrial effluent at an initial concentration of 330 mg/L.

RESULTS AND DISCUSSION

Electro-recovery of Cu on a porous RVC electrode

In order to optimise the morphological and the energetic performance of the Cu electro-recovery process, a number of experiments was performed to unravel its underlying kinetics by following the evolution of the Cu-concentration in solution as a function of current density. Figure 2 shows a typical evolution of the Cu-concentration with time for an imposed current of 0.27 A, superimposed on the cell voltage evolution. From the slope of the concentration evolution, which represents the characteristic underlying rate constant *k*, two separate kinetic regimes can be identified. Strikingly, the cell voltage evolution shows a transition as well which moreover occurs around the same time, allowing for reliable in-situ process monitoring. The first region is believed to be indicative for a reaction-controlled regime, followed by a mass transport controlled electro-recovery process. This was explicitly verified by studying the current density dependence of the rate constant, as shown in Figure 3. It is seen that the initial rate constant first increases with current, indicative for a reaction-controlled regime, and then reaches a constant value, as suggested by the horizontal dotted line in Fig. 3, and characteristic for a transport controlled regime. Moreover, the 2nd rate constant in Fig. 2 (open circle) is found to be similar in magnitude to this transport controlled value as well. The transition between reaction to transport control is believed to be indicative for the condition where Cu recovery starts to take place on an already exisiting Cu-layer, rather than on virgin RVC electrode material. A typical morphology of a Cu-coated RVC electrode in the mass transport regime at 5 A is shown in Figure 4.

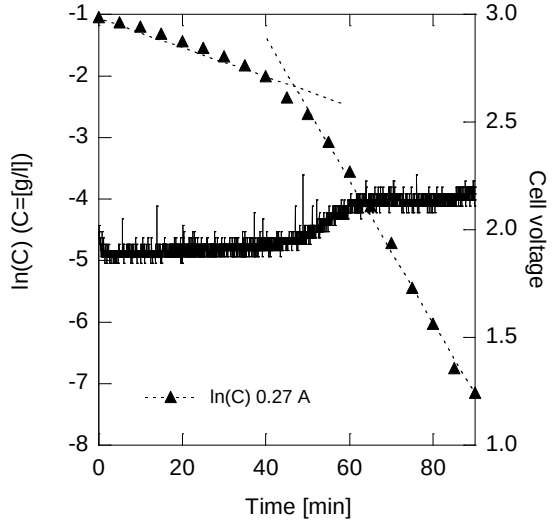

Figure 2. Evolution of the Cu concentration and cell voltage with time during electro-recovery at 0.27 A on a porous RVC electrode.

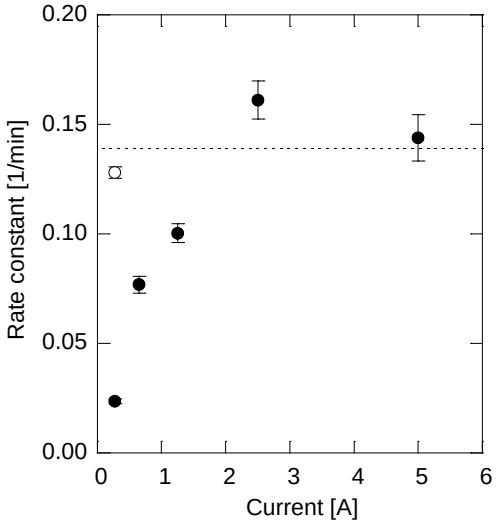

Figure 3. Dependence of the initial rate constant on imposed current. The open symbol represents the 2nd regime in Fig. 2.

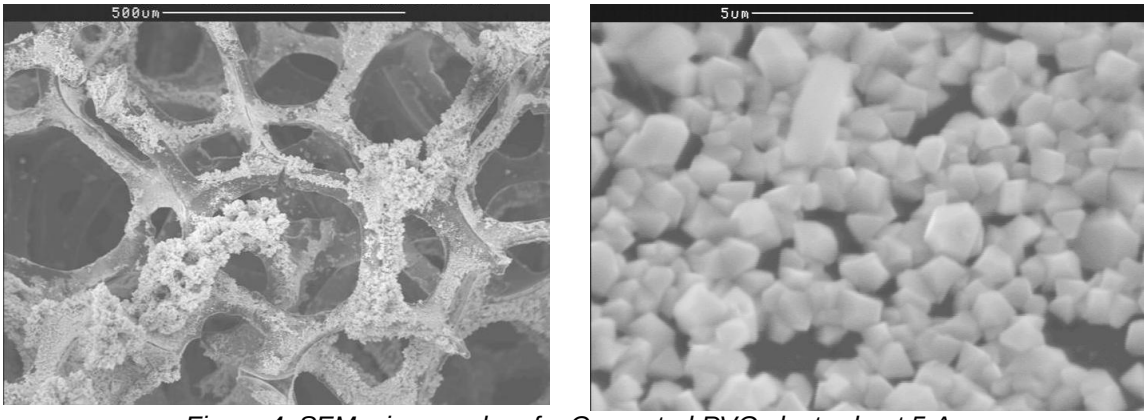

Figure 4. SEM micrographs of a Cu-coated RVC electrode at 5 A.

Electro-destruction of nitrate and nitrite ions on a Cu-coated RVC electrode

In a second stage, the Cu-coated RVC electrodes were then used in the same filter-press electrochemical cell for the electro-destruction of nitrate and nitrite ions in a simulated industrial wastewater. In order to determine the optimal morphology of Cu-dispersion on the RVC supporting electrode for the reduction of nitrate and nitrite, a series of electroanalytical experiments were conducted first using cyclic voltammetry. The results, shown in Figure 5 for nitrate (left) and nitrite (right) reduction, show a significant electrocatalytic effect of Cu in the case were the effluent is being exposed to both a RVC and a Cu surface. Therefore, the for this application optimal Cu-coated RVC morphology should still present some uncoated carbon surfaces. Based on the results of the previous section, such an electrode can be obtained by a reaction-controlled Cu electro-recovery process. A SEM-micrograph of an optimally Cu-coated porous RVC electrode is shown in Figure 6. Its final electro-catalytic performance for combined nitrate and nitrite desctruction is demonstrated in Figure 7. The latter clearly illustrates the significantly improved electro-destruction rate as compared to commercially available, uncoated material.

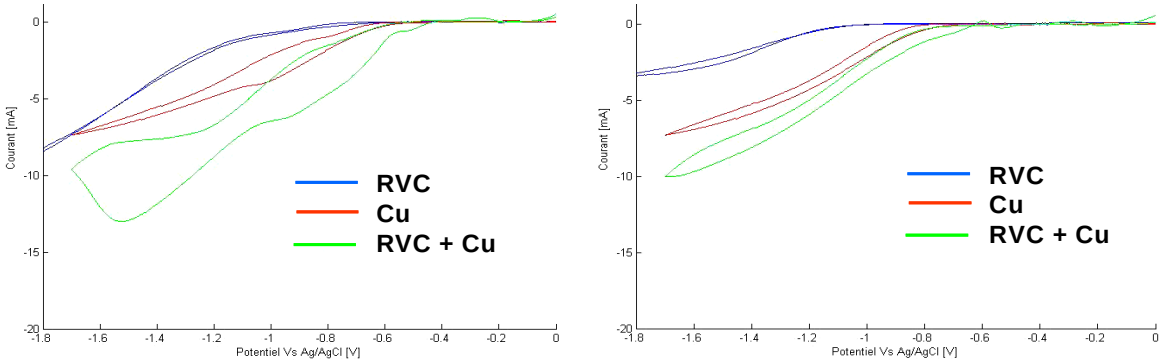

Figure 5. Cyclic voltammograms for nitrate (left) and nitrite (right) reduction on Cu-coated RVC, as compared to commercially available, uncoated electrodes of, respectively, RVC and Cu.

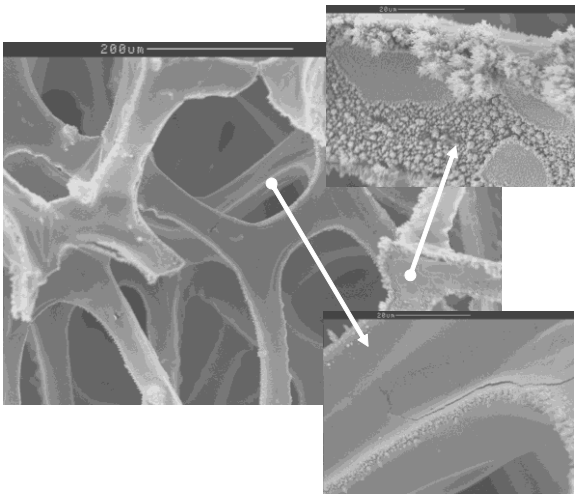

Figure 6. SEM micrograph of a Cu-coated RVC electrode, optimised for the electro-catalytic destruction of nitrate and nitrite ions.

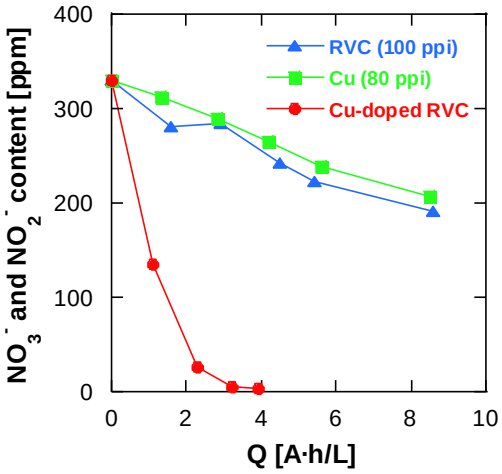

Figure 7. Evolution of the combined nitrate and nitrite concentration during reduction on the same electrodes discussed in Figure 5.

CONCLUSIONS

In this work, we have demonstrated the environmental interest of using of a low cost RVC porous electrode in a sequential electro-recovery and electro-catalytic destruction process. In a first stage, the RVC electrode has been used as a three-dimensional support for the electrorecovery of Cu with well-controlled morphologies. In a second stage, the Cu-coated RVC support was then used in the same filter-press type electrochemical cell for the selective electrocatalytic destruction of nitrate and nitrite ions. The latter was shown to proceed at a significantly increased rate as compared to state-of-the art, commercially avaible monolithic electrodes.

REFERENCES

[1] Pletcher D., Walsh F.C. 2001. Electrochemistry: now and the future. Chemistry & Industry, 18:564-566.
[2] Vanlangendonck Y., Corbisier D., Van Lierde A. 2005. Influence of operating condictions on the ammonia electro-oxidation rate in wastewaters from power plants (ELONITA™ technique). Water Research, 39:3028-3034.
[3] Cheng T.T., Gyenge E.L. 2008. Direct methanol fuel cells with reticulated vitreous carbon, uncompressed graphite felt and Ti mesh anodes. J. Appl. Electrochem., 38:51-62.

Manufacture of porous cordierite samples using gelcasting of polysaccharides

I. Santacruz[1], J. B. Rodrigues Neto[2], R. Moreno[1]

1 Instituto de Cerámica y Vidrio, CSIC, c/ Kelsen n° 5, Cantoblanco, 28049 Madrid, Spain, cruz@icv.csic.es, Telephone: (+34) 917355840, Fax: (+34) 917355843.
2 Sociedade Educacional de Santa Catarina, Albano Schmidt, 3333, 89227-700 Joinville, Brazil.

Stoichiometric cordierite samples with tailored open macroporosity were prepared by a gelcasting route through the rheological characterisation of agar and foaming surfactant-containing slips. Their solids loading, and thus, their rheological properties have resulted to be key parameters for the design of materials with different average cell sizes. In this work, samples with open-porosities from < 2 to 74 vol% have been obtained by varying the solids loading of the slip from 45 to 20 vol%, containing gelling and foaming agents, and casting them into non porous moulds at 45ºC.

INTRODUCTION

Porous ceramics have received increased attention because their potential use in applications that require high permeability, high surface area, and good insulating characteristics (Colombo P., 2002). Ceramics with controlled porosity can be prepared by different methods (Scheffler M. 2005, Luyten J., 2003), including freeze drying (Tallón C., 2003) or direct foaming methods, the latter consists in the incorporation of air or gas into a slip which is able to retain the structure of the air bubbles during the polymerization of monomers (Fuji M. 2007), or by gelcasting of polysaccharides (Santacruz I., 2005); in most cases, surfactants are usually added to the slip for reducing the surface tension of the gas-liquid interface and hence to stabilize the liquid foams for a limited period of time. These consolidated foams are normally sintered at high temperatures.

Cordierite, $2MgO{\cdot}2Al_2O_3{\cdot}5SiO_2$, is a ceramic material that displays low coefficient of thermal expansion (Camerucci M.A., 2001), low dielectric constant, good chemical durability, excellent refractoriness, and good mechanical strength (Song I.H., 2008). These properties make it suitable for many industrial applications (Velasco J.R., 1999) as honeycomb-shaped catalyst supports in automobiles, as substrate material in integrated circuit boards, and as refractory material. Many of these applications require a porous microstructure.
Previous works (Rodrigues Neto J.B., 2007 and 2008) studied the rheological behaviour of concentrated slips of kaolin/talc/alumina mixtures up to 45 vol% for manufacturing both cordierite dense bulks and foams; the latter being prepared by impregnation of polyurethane foam into the optimized slip. Cordierite samples were obtained after optimizing the sintering cycle. This manuscript deals with the rheological characterization of aqueous slips of those natural raw materials for obtaining cordierite materials with tailored macroporosity using a gelcasting process with agar and a foaming surfactant. The influence of processing parameters such as solids loading (20, 30 and 45 vol%), viscosity and addition of the surfactant on the slip on the microstructure and porosity of the obtained bodies is discussed.

EXPERIMENTAL

The composition of the stoichiometric cordierite consists of SiO_2, Al_2O_3 and MgO in molar ratios 55.6/22.2/22.2 (weight ratios being 51.4/34.9/13.8). As raw materials the following powders were used: kaolin and talc (both provided by Colorminas S.A., Criciúma, Brazil) and a 85/15 wt/wt mixture of fine and coarse Al_2O_3 powders (1000SG and CL3000FG, both supplied by Alcoa, USA) with average particle sizes of 0.6 and 5.7 µm, and surface areas of 10.2 and 0.72 m^2/g, respectively, was used. These powders were mixed in relative weight contents of 40.0 wt% kaolin, 43.8 wt% talc and 16.2 wt% alumina, according to previous works (Rodrigues Neto J.B., 2007 and 2008). The slips were prepared to a solids loading of 45 vol% by mechanical agitation using a helices mixer for 15 min with the addition of 1.5 wt% (on a dry solids basis) of a polyacrylic-based deflocculant, Dolapix PCN (supplied by Zschimmer-Schwarz, Germany) and adjusting the pH to 11.0±0.1 with KOH. The so-prepared slips were milled using a high-speed planetary mill with porcelain jar and alumina balls for 45 min, and the pH was readjusted to 11.0±0.1 (Rodrigues Neto J.B., 2007 and 2008). More

diluted slips, 20 and 30 vol% solids, were prepared by dilution of the optimised 45 vol% slips maintaining a constant pH 11.0±0.1 in all cases.

As gelling agent, a concentrated agar solution (6 wt%) (Santacruz I., 2003) maintained at 65ºC was used and added to the slip after preheating it at 65ºC. The amount of added solution was that required to introduce 1.0 wt% of agar powder with regard to the total water content. Once the gelcasting slips were ready, at 65ºC, a surface active agent was incorporated into the hot slips, viz. an anionic surfactant namely ammonium dodecylbenzene (DDB). The amount of solution added was that required to introduce 1.0 wt% of DDB referred to the total weight of the slip. This surfactant was prepared by mixing 20 g of dodecylbenzenic acid and 20 ml of ammonia in 80 ml of water. The slips were subsequently subjected to strong mechanical stirring with a high shear mixer (Silverson L2R, UK) for shearing times of 3 min (Santacruz I., 2005) in order to promote bubbles formation.

The rheological behaviour was studied using a rotational rheometer (RS50, Haake, Thermo Electron Co., USA) with a double-cone/plate sensor configuration (DC60/2º, Haake). Flow curves were obtained at controlled rate conditions (CR) with a three-stage measuring program with a linear increase of shear rate from 0 to 1000 s^{-1} in 180 s, a plateau at 1000 s^{-1} for 60 s, and a further decrease to zero shear rate in 180 s. Slips with solids loading of 20, 30 and 45 vol% were prepared in this way and maintained at 45ºC at which they were poured into open stainless steal moulds. They were further cooled in a freezer at -7.0±0.1ºC for two minutes in order to allow the consolidation of the bodies while impeding the water freezing.

Cast bodies were left in air for 24 h to dry and further sintered at 1280ºC/1h where the cordierite phase appears as the main phase in the XRD pattern (Rodrigues Neto J.B., 2008), with a thermal treatment at 550ºC/0.5h to burn out the organic matter. Microstructures of the sintered samples were observed by SEM (Zeiss DSM400, Germany). The density and open porosity of sintered bodies were measured by immersion in water (UNE 61033 and 61035, respectively).

RESULTS

Figure 1 shows the flow curve of the slips with 20, 30 and 45 vol% solids at room temperature without any gelling or foaming agents. The viscosity and also the shear thickening behaviour of the slips increase with the solid loading, so that the torque was exceeded for the most concentrated slip.

Since slips need to be heated at 65ºC before the polysaccharide addition, the effect of heating on the rheological behaviour of the slips was first studied. Figure 2 shows the variation of viscosity with temperature of 45 vol% slip on heating, measured at shear rates of 5 and 100 s^{-1}. The heating viscosity of the additives-free slip seems to decrease at the beginning and then maintains nearly constant up to 70ºC for 100 s^{-1}; in the case of 5 s^{-1}, the viscosity maintains nearly constant up to 50ºC and slightly increases from that temperature. Although stability maintains at any temperature as demonstrated by the constant viscosity measured at 100 s^{-1}, the different behaviour found at the low shear region suggests that some structure starts to develop above 50-60ºC.

Once the gelling agent was added to the slip at 65ºC a sharp increase of viscosity was observed on cooling at the gelling temperature, below 40ºC, at any solid loading content because of the agar gelation, as shown in figure 3. In order to promote the bubbles formation and to reduce the surface tension of the gas-liquid phases, a surfactant, DDB, was added, and its influence on the rheological behaviour was also studied (fig. 3). The viscosity on cooling for the slip with agar and the foaming agent (DDB) shows much lower viscosity at any temperature as compared with the slip without DDB, and the increase of viscosity at the gelling temperature is also lower. This fact is believed to be due to the effect of DDB on the gelling properties of agar, and the higher pH value of the final slip which changes from 9.5±0.1 to 10.6±0.1. Although the gels obtained with the agar/DDB mixtures slips are less stiff, they are strong enough to maintain a rigid structure with open cells as desired.

The slips with different solids loading, gelling and foaming agents were maintained at 45ºC (marked with an arrow in the figure) and a strong mechanical shearing was applied to promote foaming, before casting on metallic moulds cooled at the same temperature. Different porous microstructures were obtained depending on the solids loading: slips with lower solids loading presented higher volume of bubbles after high shearing, related with the lower viscosity.

Figure 4 shows the cross-sectional fracture surface microstructure of sintered samples obtained from slips with solids loadings of 20, 30 and 45 vol% (figure 4 (a), (b) and (c), respectively) cast at 45ºC. All pictures were taken at the same magnification, and the bottom of each micrograph corresponds to the bottom of the obtained sample (that in contact with the mould). As it can be observed, cell sizes and distribution are strongly related with the solids loading of the slips. Samples prepared from the lowest solids loading, 20 vol%, fig. 4 (a), show "medium" size cells distributed around all the samples. In the case of 30 and 45 vol%, fig. 4 (b) and (c), respectively, "medium" and "large" cells are present in a matrix of "small" cells; in the case of 45 vol%, the presence of "small" cells is more dominant than in the former. All these observations were quantified by image analysis where "small", "medium" and "large" cell sizes correspond to < 10 □m, < 50 □m and up to 100 □m, respectively. Such differences in the microstructure of the samples are believed to be due to the slips viscosity, which changes from 13, 162 and 221 mPa.s as solids loading increases from 20, 30 and 45 vol%, respectively. The apparent density values increase from 0.6 to 1.9 g/cc when the solids loading increases from 20 to 45 vol%. In addition, the distance among particles increases as solids loading decreases, thus leading to larger volume of cells. Samples with open porosities ranging from < 2 to 74 vol% have been obtained.

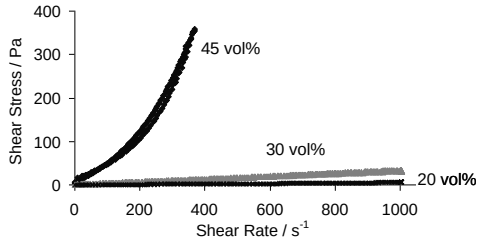

Figure 1. Flow curves of the slips without gelling or foaming agents.

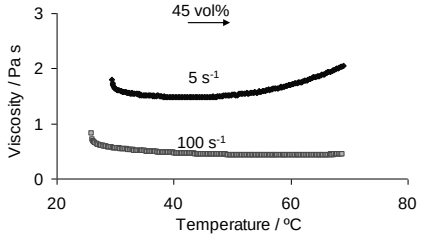

Figure 2. Viscosity vs. temperature curves during heating for the 45 vol% slip without gelling or foaming agents measured at two shear rates.

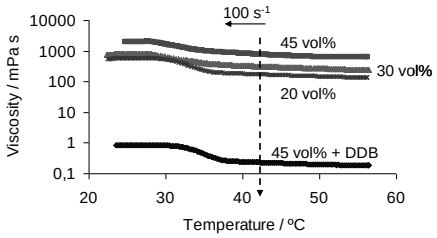

Figure 3. Viscosity vs. temperature curves during cooling for the slips with 1 wt% agar at different solids loading, and 45 vol% slip with gelling and foaming agents.

CONCLUSIONS

Porous cordierite materials with tailored porosity have been obtained using the gelcasting of polysaccharides in combination with a foaming agent. A rheological characterisation of the slips was a key parameter for the design of these samples. The obtained bodies were characterized through density and microstructure studies. The influence of the solid loading of the precursor slip has been

shown to be critical parameters to design samples with tailored porosity. Samples with different cell distributions, apparent density and percentage of open porosity have been obtained changing the solid loading from 20 to 45 vol%. These differences in the microstructure of the samples are related to the slips viscosity, which changes from 13 to 221 mPa s as the solids loading increases from 20 to 45 vol%, respectively.

ACKNOWLEDGEMENTS

This work has been supported by Spanish Ministry of Education and Science (MAT2006-13480 and MAT2006-01038 projects), by CNPq (Conselho Nacional de Desenvolvimento Científico e Tecnológico, Brazil) and by ESF and CSIC under postdoctoral contract I3P-PC2005L. Authors thank Dr. M. I. Nieto (Instituto de Cerámica y Vidrio, CSIC) for useful discussions.

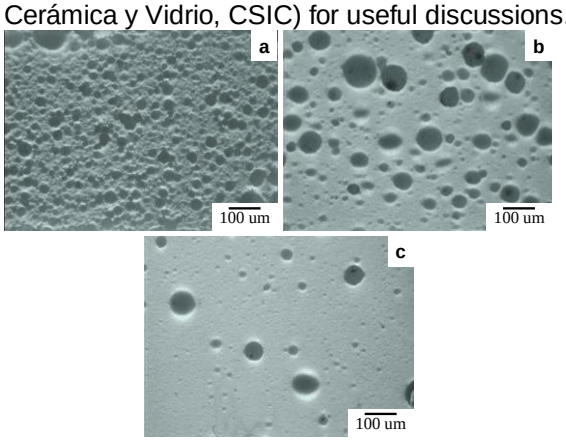

Figure 4. Microstructures of the fracture surface of sintered samples prepared from 20 vol% (a), 30 vol% (b), and 45 vol% (c). Slips cast at 45ºC.

REFERENCES

Camerucci M.A., Urretavizcaya G., Castro M.S., Cavalieri A.L. Electrical properties and thermal expansion of cordierite and cordierite-mullite materials. 2001. J. Eur. Ceram. Soc. 21: 2917–2923.

Colombo P., Hellmann J.R. 2002. Ceramic foams from preceramic polymers. Mater. Res. Innovat., 6: 260–272.

Fuji M., Shiroki Y., Menchavez R.L., Takegami H., Takahashi M., Suzuki H., Izuhara S., Yokoyama T. 2007. Fabrication of cordierite filter by in-situ solidification for high temperature dust collection. Powder Tech. 172: 57–62.

Luyten J., Mullens S., Cooymans J., De Wilde A. M., Thijs I., 2003, New processing techniques of ceramic foams. Adv. Eng. Mater., 5: 715-718.

Rodrigues Neto J.B., Moreno. 2007. Rheological behaviour of kaolin/talc/alumina suspensions for manufacturing cordierite foams," Appl. Clay Science. 37: 157-166.

Rodrigues Neto J.B., Moreno R. 2008. Effect of mechanical activation on the rheology and casting performance of kaolin/talc/alumina suspensions for manufacturing dense cordierite bodies. Appl. Clay Sci. 38: 209-218.

Santacruz I., Nieto M.I., Moreno R., Faraldos M., Sastre E. 2005. A novel method to prepare zeolites with hierarchical porosity. Adv. Eng. Mater. 7: 858-861.

Santacruz I., Nieto M.I., Moreno R., Ferrandino P., Salomoni A., Stamenkovic I. 2003. Aqueous Injection Moulding of Porcelains. J. Eur. Ceram. Soc. 23: 2053-2060.

Scheffler M., Colombo P. 2005. Cellular Ceramics. Structure, manufacturing, properties and applications, WILEY-VCH Verlag GmbH & Co. KGaA, Weinheim, Germany.

Song I.H., Kim M.J., Kim H.D, Kim Y.W. 2006. Processing of microcellular cordierite ceramics from a preceramic polymer. Scripta Materialia. 54: 1521–1525.

Tallón C., Yates M., Moreno R., Nieto M.I. 2007. Porosity of freeze-dried □-Al_2O_3 powders. Ceram. Intern. 33: 1165–1169.

Velasco J.R., Gutiérrez-Ortiz M.A., Ferret R., Aranzabal A., Botas J.A. 1999. Synthesis of cordierite monolithic honeycomb by solid state reaction of precursor oxides. J. Mater. Sci. 34: 1999–2002.

Porosity as a contributor to solutions for sustainable production

***J. Luyten*, S. Mullens, F. Snijkers, A. Buekenhoudt**

Materials Technology, VITO, Boeretang 200 , B-2400 Mol, Belgium

In order to not jeopardize the health and quality of life of future human generations, a sustainable manufacturing of goods is needed. For reaching this, material processing should become more efficient, less energy demanding, non or less-polluting and resource efficient. As such, the design of materials and the controlled introduction of porosity plays an important role and offers unique opportunities. On one hand, introduction of porosity will result in weight reduction and less material consumption, but controlled porosity in materials can offer much more. In this contribution several examples will be presented that illustrates this for a variety of application areas.
First we discuss the synthesis and characterization of multilayer ceramic membranes for gas and solvent separation. The processing of different membranes types, e.g. nanofiltration membranes, zeolite membranes and dense ceramic membranes produced from mixed ion electronic conductors are explained.
Further, in order to improve the quality of life of elder people, new medical approaches like bone replacement using scaffolds, tissue engineering and drug delivery are needed.
Thirdly, it is shown how ceramic foams can be used as filter for cleaning Al-alloys for recycling purposes, as filter for removing soot from diesel exhaust, and as support for catalysts in chemical industry. Routes for the fabrication of materials with controlled porosity are discussed and attention is paid to specific characterization methods.

Design of alumina bodies with directional porosity by a freeze-casting method

C. Tallón, R. Moreno and M. I. Nieto

Instituto de Cerámica y Vidrio, CSIC, Kelsen 5, 28049, Madrid, Spain, Telephone: (0034)917355840, Fax: (0034)917355843, rmoreno@icv.csic.es.

Porous ceramics materials have been manufactured by different shaping techniques due to their wide range of applications. Among these methods, freeze-casting has received great attention since it allows the manufacture of near-net-shaped bodies with controlled porosity. The present work deals with the preparation of alumina bodies with directional porosity by using the freeze-casting technique. The effect of one of the process parameters, such as concentration of the suspension, has led to the preparation of bodies with aligned porosity and different pore sizes distribution.

INTRODUCTION

The great number of applications of porous ceramic materials in different areas has received great attention. The evolution of the porous ceramic materials has lead to more specific applications and requirements, so the traditional processing techniques are continuously under study, optmization and development. This is the case of preparation of porous piezoelectrics materials by dry and wet methods (Galassi, 2006), highly porous ceramics from blowing agents, sacrificial fillers that decompose during pyrolisis or mixing preceramics polymers (Colombo, 2008) or the preparation of multilayers membranes for nanofiltration by reaction bonded alumina manufacturing process (Gestel et al., 2002). The use of freeze casting allows overcoming the problems of the traditional porous materials processing methods by controlling easily a few parameters. Moreover, freezing techniques allow obtaining near-net-shaping bodies (Jones, 2000) and challenging the specifications of these new applications.

The freeze casting method consists of freezing a suspension and the further sublimation of the ice, leading to a porous microstructure. The parameters involved in this technique are the solid content of the suspension, the freezing temperature, the features related to the freezing device and the addition of cryoprotectors. The solid content of the suspension determines the total volume of pores of the sample, since the lower concentration, the higher amount of water and the higher porosity in the sample. The freezing temperature has a strong influence on the solute rejection during the freezing and therefore on the microstructure (Tallon et al., 2006). The freezing device is related to the distribution of the total porosity. If the sample is frozen as a bulk body, a homogeneous, porous microstructure is obtained (Sofie et al., 2001; Lu et al. 2006; Cho et al. 2007). However, this distribution can be orientated in specific paths by means of directional freezing, having in contact one part of the suspension with the freezing agent (Fukasawa et al. 2001; Statham et al.1998). Finally, some authors have pointed out the needing of the addition of cryoprotectors in order to control the ice formation, being glycerol the most used compound for this purpose, especially for homogeneous freezing. The freeze-casting route can also be carried out by adding some compound that sublimates at room temperature after heating, such as camphene, as it has been thoroughly reported by Araki and Halloran (Araki et Halloran, 2004).

In the present work, the preparation of alumina bodies with aligned porosity by freeze-casting is reported. The influence of the solid content of the starting suspension on the final microstructure is studied considering the addition of glycerol as cryoprotector.

EXPERIMENTAL PROCEDURE

Concentrated suspensions of alumina (Condea HPA05, USA) were prepared to solid contents of 50 and 80 wt% in deionized water using a poly(acrylic acid) based polyelectrolyte (Duramax D3005, Rohm and Haas, USA) as dispersant (Gutierrez et al. 2000). Glycerol (>99.5%ACS reagent, Sigma-Aldrich, Germany) was added as a cryoprotector in a concentration of 20 wt% with respect to the water content of the suspension. The mixing was performed by mechanical stirring and further ball-

milling for 6 hours to achieve homogenization. The rheological behaviour of the suspensions was studied using a rheometer (RS50, Haake, Germany) with a double cone/plate sensor configuration (DC60/2º). Flow behavior was obtained with a three-stage measuring program with a linear increase of shear rate from 0 to 1000 s^{-1} in 300 s, a plateau at 1000 s^{-1} for 120 s, and a further decrease to zero shear rate in 300 s.

The directional freeze-casting of the sample was performed using a plastic mould with metallic base, according to the flow-chart of Figure 1. The freezing of the sample took place gradually from the bottom to the top as a consequence of the contact of the mould with a metallic piece that is surrounded by liquid nitrogen. Once the sample was frozen, it was demoulded and inmersed for a few minutes in liquid nitrogen for ensuring its total freezing. The samples were then introduced in the freeze-dryer (CRYODOS-50, Telstar, Spain) for 24 hours. The condensator temperature was –50ºC, and the conditions of the storage camera were 20 ºC and 0.050 mbar. After 24 hours in the freeze-dryer, the samples were sintered at 1500 ºC for two hours, at a heating rate of 2 ºC/min up to 250ºC for 30 min for removing the organic compounds (according to DTA-TG measurement) and then at 5ºC/min up to 1500ºC. The cooling down was carried out in two steps, with a cooling rate of 10 ºC/min up to 1200 ºC and 2ºC/min up to room temperature.

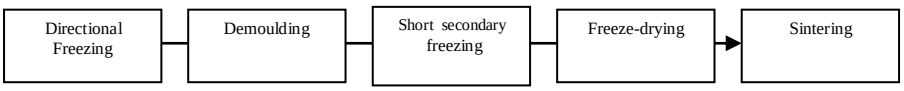

Figure 1. Flow chart of the Directional Freeze-Casting method.

The green and sintered densities were determined by Archimedes' method in mercury and water, respectively. From the sintered values, open and total porosity percentages were calculated. The microstructure was observed by field emission microscopy, FEM, (Hitachi S-4700 type I, Japan) on fracture surfaces of sintered samples. The porosity was measured by mercury intrusion porosimetry (Pore Master PM-33-8, Quantachrome Instruments, USA).

RESULTS

The freeze casting method consists of the creation of pores due to the sublimation of the ice present in frozen suspensions. The higher water content, the higher porosity achieved. However, there is a limitation associated to the handling of the sample in the green state, since the high porosity could produce the collapse of the structure. For this reason, the concentration of the suspensions is one of the most important parameters of this method. The flow behaviour of the suspensions is plotted in Figure 2. Both suspensions show shear-thinning behaviour and the absence of thixotropy indicates that the components are well-mixed and the suspension is stable against time. The role of the glycerol has been reported by Sofie (Sofie et al., 2001), including the control of the ice growth, the inhibition of solute rejection and the reduction of the volume expansion of the water.

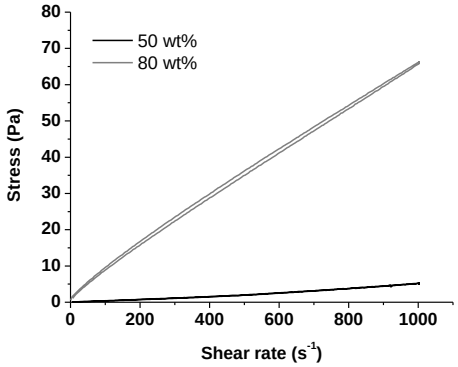

Figure 2. Flow curves corresponding to the suspensions with glycerol (20wt% with respect to the total water content) prepared to solid contents of 50 and 80 wt%.

After freeze-drying, the samples had a good consistency, keeping the same shape as the mould. Only in the case of 50wt% sample, some pores could be observed at first sight, which remains after

sintering. Table I shows the values of green and sintered relative densities of the samples. In the green state, no significant differences were found, being the green density around 50% of the theoretical value. As expected, the higher concentration of suspension, the higher sintered density values. The total porosity after sintering reaches values above 50% of the total volume in the case of 50wt% sample and the density does not change during the sintering step (green density value is a little higher due to the presence of water associated and the glycerol). This is very noticeable since the sintering step usually implies a decreasing of the number of pores in order to close the structure and grain growth.

Table 1. Densities and porosity values of both samples.

Muestra	□ green	□ sintered	***Open porosity* (%)***	***Total Porosity* (%)***	***Intrusion Volume* (cm^3/g)***
50wt%	51.9	47.2	29.2	52.8	0.12
80wt%	50.6	78.4	10.4	21.6	0.06

*for sintered samples

The mercury intrusion porosimetry performed on sintered porous bodies reveals very different curves for the samples, Figure 3. In both cases, there is a single pore size distribution, being the maximum intrusion mercury volume corresponding to pore sizes between 10-100 □m for 50wt% sample and 0.1-1 □m for the 80wt% sample. This difference is clearly associated to the higher amount of water in the first case. The uniformity observed in the pore size distribution is due to the presence of glycerol, since it controls the ice growth process.

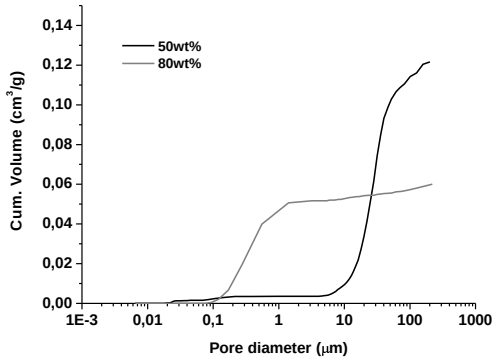

Figure 3. Cumulative pore volume curves for both sintered samples

a b

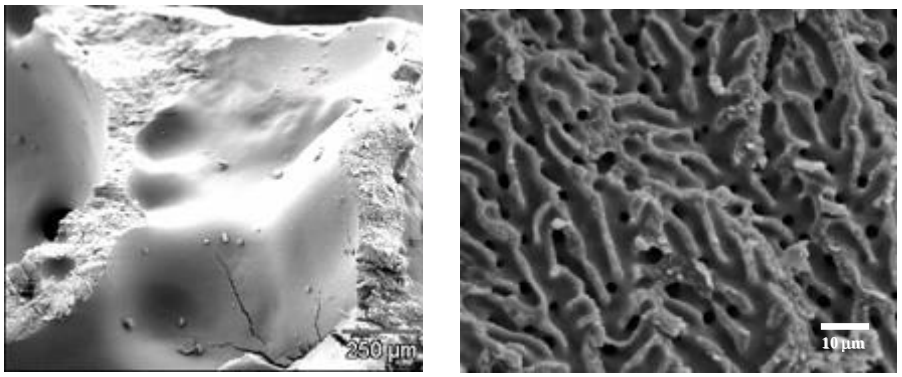

c d

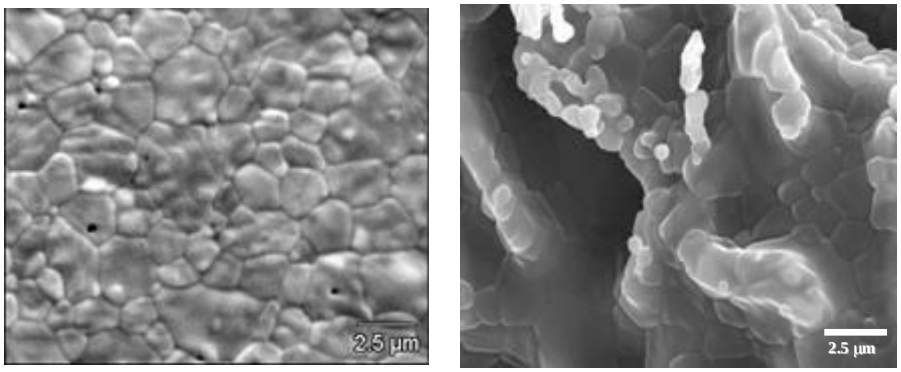

Figure 4. FESEM micrographs of sintered samples: (a) 50/20DIR, (b) 80/20DIR, (c) channel surface for 50/20DIR and (d) channel surface for 80/20DIR.

The microstructure of the sintered samples was observed by FESEM, Figure 4. In the case of 50wt% sample, larger channels were observed all over the samples as a consequence of the ice sublimation, but without any directional trend. The surface of these channels show a well sintered microstructure, with homogeneous grain size (Fig. 4c). However, the inner walls of the channels present an open structure, where the particles are loose, forming agglomerates with pores between them and between the particles (Fig. 4a). These pores are the corresponding to the mercury intrusion porosimetry graph (Fig. 3). The 80wt% sample shows a totally different aspect. Directional channels appear all over the sample, being positioned in the ice growth direction. The channels show a dendritic aspect as reported by other authors (Fukasawa et al. 2001; Araki et Halloran, 2004). The surface of the channels are totally sintered, with some cylindrical pores in the perpendicular direction (Fig. 4d), being in good agreement with the mercury intrusion porosimetry values (Fig. 3). The micrographs indicate the need of using concentrated suspensions for preparing directional bodies. Further studies will be carried out to determine the influence of the rest of the freeze-casting parameters.

CONCLUSIONS

Freeze-casting method has been successfully used to shape porous bodies of alumina with aligned porosity in the direction of the ice growth. The effect of the concentration of the starting alumina suspension has been checked. Sintered samples presented total porosities values between 20-60% and densities around 50-80%. Both samples showed monomodal pore size distribution, although different order of magnitude for pore diameter, being 0.1-1□m for the 80/20DIR. The microstructure shows channels in the ice direction with well sintered walls.

ACKNOWLEDGEMENTS

This work has been supported by CICYT (Spain, contract Nº MAT2006-01038 and MAT2006-13480). C. Tallón acknowledges CSIC and ESF for the concession of an I3P-BPD2004 grant.

REFERENCES

Araki, K. Halloran, J. W. 2004. New freeze-casting technique for ceramics with sublimable vehicles. J. Am. Ceram. Soc. 87, 10:1859-1863

Cho, Y.K., Yang, T.Y., Lee, J.M., Yoon, S.Y., Stevens, R., Park, H.C. 2007. Freeze cast symmetric three-layer alumina-matrix composites with improved damage resistance. J. Phys. Chem. Sol. In press

Colombo, P. 2008. Engineering porosity in polymer-derived ceramics. J. Eur. Ceram. Soc. In press.

Fukasawa, T., Ando, M., Ohji, T., Kanzaki, S. 2001. Synthesis of porous ceramics with complex pore structute by freeze-dry process. J. Am. Ceram. Soc. 84: 230-232

Galassi, C. 2006. Processing of porous ceramics: Piezoelectric materials. J. Eur. Ceram. Soc. 26:2951-2958

Gutiérrez, C. A., Moreno, R. 2000. Preventing aging on alumina casting slips dispersed with polyelectrolytes. J. Mater. Sci., 35:5867-5872.

Jones, R.W. 2000. Near net shape ceramics by freeze casting. Ind. Ceram., 20, 2.
Lu, K., Kessler, C. S., Davis, R. M. 2006. Optimization of a nanoparticle suspension for freeze casting. J. Am. Ceram. Soc., 89, 8: 2459-2465.
Sofie, S.W., Dogan, F. 2001. Freeze casting of aqueous alumina slurries with glycerol. J. Am. Ceram. Soc., 84, 7:1459-1464.
Statham, M.J., Hammet, F., Harris, B., Cooke, R.G., Jordan, R.M., Roche, A. 1998. Net-shape manufacture of low-cost ceramic shapes by freeze-gelation. J. Sol-gel Sci. Technol. 13:171-175.
Tallón, C., Moreno, R., Nieto,M.I. 2006. Synthesis of □-Al_2O_3 by freeze-drying. Mat. Res. Bull. 41:1520-1529.
Van Gestel, T., Vandecasteele. C., Buekenhoudt, A., Dotremont, C., Luyten, J., Leysen, R., Van der Bruggen, B., Maes, G. 2002. Alumina and titania multilayer membranes for nanofiltration: preparation, characterization and chemical stability. J. Memb. Sci. 207:73-89.

MANUFACTURING OF MICROPOROUS CERAMIC MEMBRANES FOR ENVIRONMENTAL APPLICATIONS

***Tim Van Gestel*, Wilhelm A. Meulenberg, Hans-Peter Buchkremer**

Forschungszentrum Jülich GmbH, Institute of Energy Research, IEF-1: Materials Synthesis and Processing
Leo-Brandt-Strasse, D-52425 Jülich, Germany

INTRODUCTION

A microporous ceramic separation membrane can be considered as a graded multilayer porous ceramic material, in which the last membrane layer shows a pore size < 2 nm. The number of potential applications of such a material which looks very simple at first sight is immense. Microporous membranes can be used for separation of all types of liquid – solid, liquid – liquid or gas – gas mixtures through effective exclusion mechanisms such as molecular sieving. The application field of the material is mainly determined by the pore size of the functional microporous layer, which implies that this layer must contain a minimal amount of defects and for certain applications the functional layer should be completely defect-free (e.g. gas separation). Possible application fields of a microporous ceramic membrane in environmental related separation problems are given in Table 1.

Table 1. Application fields of microporous ceramic membranes in different membrane processes

Appication field	**Membrane process**	**Pore size functional layer**	**Complexity of preparation process**
Separation Liquid – Dissolved Macromolecules	Nanofiltration	1 – 2 nm	Few larger defects are tolerated
Separation Liquid – Liquid	Pervaporation	< 1 nm	Few smaller defects or larger pores are tolerated
Separation Gas – Gas	Gas separation	< 0.6 nm	Defect-free membrane required

Nanofiltration (NF), pervaporation (PV) and gas separation (GS) membranes can be classified into two major groups according to their material properties: organic polymeric membranes and inorganic microporous ceramic membranes. Organic polymeric membranes constitute the most important group and have been commercially available for many years. They are relatively easy to prepare and can be produced cheaply at large scale. However, their application is limited to moderate temperatures and to feed streams which are not too corrosive. The goal of our current work is to prepare novel ceramic membranes with a higher thermal and chemical stability than polymeric membranes and an improved pore size and quality in comparison with the microporous ceramic membranes described in literature.

Substantial progress has already been made toward development of NF membranes comprising a functional TiO_2 toplayer, for application in corrosive media. For the best membranes, a pore size of ~ 1 nm has been reported and these membranes can separate effectively small molecules from water or an organic solvent, based on a molecular sieving mechanism [1]. For the separation of mixtures of gases, which show a significantly smaller diameter than the molecules involved in a molecular nanofiltration process, membranes with a smaller pore size in the range of ~ 0.4 - 0.6 nm are required (e.g. kinetic diameter CO_2 0.33 nm, H_2 0,29 nm, N_2 0.36 nm). Membranes with a toplayer made of microporous SiO_2 have been frequently considered for this application, because the material can be rather easily synthesized with the desired pore size, leading to a high selectivity in combination with a relatively high flux. Another important advantage includes the possibility to apply a relatively simple coating method based on common sol-gel technology for the deposition of ultra-thin layers, which is also applicable for the development of membranes at large-scale [2,3].

A significant drawback of current microporous GS membranes, which have been introduced as competitors for polymeric membranes, is, however, the limited chemical stability of the applied membrane materials towards water (vapour), acids and bases. In order to improve the stability towards water, SiO_2 membranes with ZrO_2 or TiO_2 added as a second component have already been developed [4]. In our work, membranes made from Y_2O_3-doped ZrO_2 are proposed for NF as well as PV and GS. Membrane materials based on zirconia are generally recognized for their excellent chemical stability and – with the addition of a doping compound – also a high thermal stability can be obtained for such materials [5].

EXPERIMENTAL

1. Preparation of membrane substrate

The substrate consists of a porous $8Y_2O_3$-ZrO_2 plate with an average pore size of ~ 1 µm and a macroporous $8Y_2O_3$-ZrO_2 layer with an average pore size of ~ 100 nm. The substrate plates were prepared according to a large-scale procedure, which is applied in our institute for the manufacturing of solid oxide fuel cells. The first step in the preparation procedure includes the formation of a plate with a size of 25 x 25 cm² and a thickness of ~ 1 mm by a warm-pressing procedure. In order to reduce the roughness and the pore size for further modification with very thin mesoporous and microporous membrane layers, an intermediate macroporous $8Y_2O_3$-ZrO_2 layer is deposited. In this work, the intermediate layer is made by means of vacuum slip-casting or by screen-printing, starting from a well-known commercially available $8Y_2O_3$-ZrO_2 powder (Tosoh corporation, TZ-8Y).

2. Preparation of mesoporous intermediate membrane layer

Mesoporous membrane layers were made by a 'so-called' colloidal sol-gel coating procedure. In our standard coating procedure, a zirconia sol with a particle size of ~ 50 – 100 nm was prepared by hydrolysis of $Zr(OC_3H_7)_4$ (Sigma-Aldrich). Yttria-doped zirconia sols (8 mol% yttria) were prepared by adding the proper amount of $Y(NO_3)_3.6H_2O$ to the zirconia sol. Small-scale membranes are made by dip-coating, using an automatic dip-coating device, equipped with a holder for 4 x 4 cm^2 substrates. The substrates were cut from the porous $8Y_2O_3$-ZrO_2 plate, made by the standard production process. In order to obtain the mesoporous $8Y_2O_3$-ZrO_2 membrane interlayer, firing (calcination) was performed in air at 500°C for 2 h and the entire dip-coating – drying – firing cycle was carried out twice.

3. Preparation of microporous membrane toplayer

For the manufacturing of an ultra-thin microporous toplayer with a pore size of 1 nm or smaller, a 'so-called' polymeric type of sol-gel method was considered. In a preferred preparation procedure, a solution of a modified precursor was made by adding a common chelating agent such as acetyl acetone (AcAc) or an alcohol amine (diethanol amine (DEA) to a solution of a zirconia precursor ($Zr(OC_3H_7)_4$), an yttrium precursor ($Y(OC_4H_9)_3$) and n-propanol (n-C_3H_7OH). A stable yttria-doped zirconia sol containing nano-particles could be obtained by hydrolysing these modified precursors with 5 mole of H_2O, in the presence of HNO_3. Then, a mesoporous $8Y_2O_3$-ZrO_2 membrane was dipped into the diluted sol during 15 s. Subsequently, the coating was allowed to dry for a few minutes in ambient air and fired at 400 – 500°C, to give a supported membrane layer on the mesoporous carrier membrane. In the preparation procedure, each dip-coating – drying – firing cycle was carried out twice.

RESULTS AND DISCUSSION

1-2. Preparation of membrane substrate and mesoporous intermediate membrane layer

Figure 1 shows overview and detail cross-section micrographs of a mesoporous $8Y_2O_3$-ZrO_2 membrane layer, prepared by dip-coating with a sol containing colloidal particles with a size of ~ 65 nm. From these micrographs, the graded structure of the obtained mesoporous membrane can be observed, with successively the substrate material, a macroporous $8Y_2O_3$-ZrO_2 layer with a thickness of ~ 25 µm made from a suspension and a mesoporous $8Y_2O_3$-ZrO_2 membrane layer with a thickness of ~ 1 µm made from the described colloidal sol (Figure 1c). The pore size of the different layers measures 1 µm (substrate), 100 nm (macroporous layer) and 6 nm (mesoporous layer). The phase composition of the sol-gel derived material was characterized as single-phase cubic-ZrO_2, in accordance with data given in literature for yttria-doped zirconia powders with a similar percentage of doping. By looking at the detail image of this membrane given in Figure 1d, the separation line between the successive membrane layers is also clearly visible and it is confirmed that the thickness of a single layer measures ~ 0.5 µm.

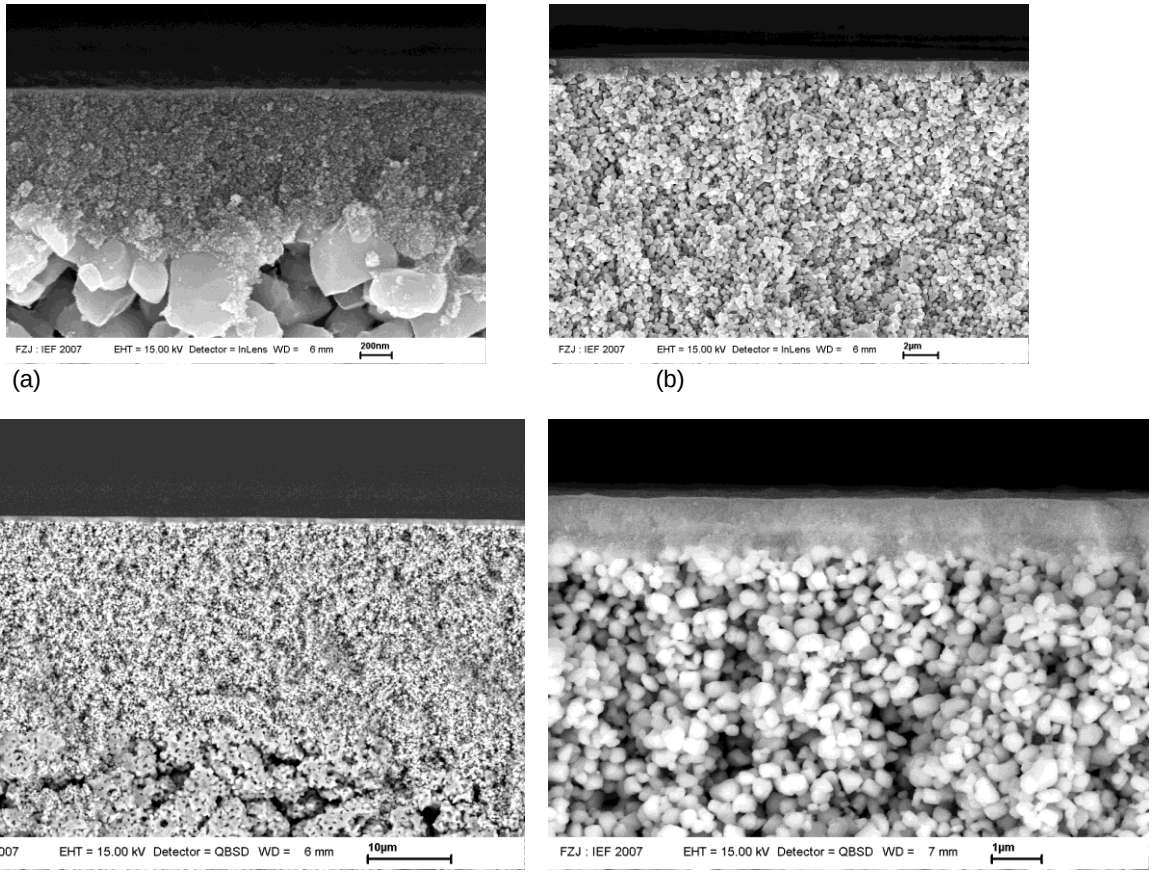

Fig. 1. Micrographs of a mesoporous $8Y_2O_3$-ZrO_2 membrane, dip-coated on a macroporous $8Y_2O_3$-ZrO_2 membrane layer made by screen-printing (particle size in sol ~ 65 nm)
((a) detail cross-section micrograph of mono-layer membrane (bar = 200 nm); (b) cross-section micrograph of double-layer membrane (bar = 2 µm); (c) overview cross-section micrograph of double-layer membrane in back-scattering mode (bar = 10 µm); (d) detail cross-section micrograph of double-layer membrane in back-scattering mode (bar = 1 µm))

3. Preparation of microporous membrane toplayers

All of the prepared nano-particle sols were stable, precipitate-free and showed an average particle size in the range 5 – 10 nm and a narrow particle size distribution (Figure 2a). Figure 3 shows micrographs of a $8Y_2O_3$-ZrO_2 toplayer, made by dip-coating an ultra-thin layer of nano-particles on a mesoporous $8Y_2O_3$-ZrO_2 membrane layer. From the detail micrograph in Figure 3a, an average thickness of ~ 50 - 100 nm can be estimated for the nano-structured Y_2O_3-ZrO_2 toplayer. In Figure 3b, an overview image is given in which the following layers are present: a macroporous layer made from a suspension, two mesporous layers made from a colloidal sol and two nano-structured $8Y_2O_3$-ZrO_2 membrane layers made from a sol with nano-particles. Pore analysis of the toplayer material indicated a microporous structure (type I isotherm), with an average pore size of ~ 1 nm (Figure 2b).

The formation of continuous membrane layers is evident from surface micrographs made after the respective coating procedures (Figures 4a-c). Figure 4a shows the surface of the first macroporous layer, which functions as a substrate for the sol-gel membrane layers. Figure 4b shows a micrograph of the surface of the mesoporous $8Y_2O_3$-ZrO_2 intermediate membrane layer. Figure 4c shows the surface after dip-coating with a nano-particle sol. By comparing these pictures, it appears clearly that in each coating step a membrane layer with a finer pore structure is formed leading to a graded multilayer structure. In addition, the overview micrograph shown in Figure 4d indicates that a crack-free membrane was obtained after the last coating step with the nano-particle sol.

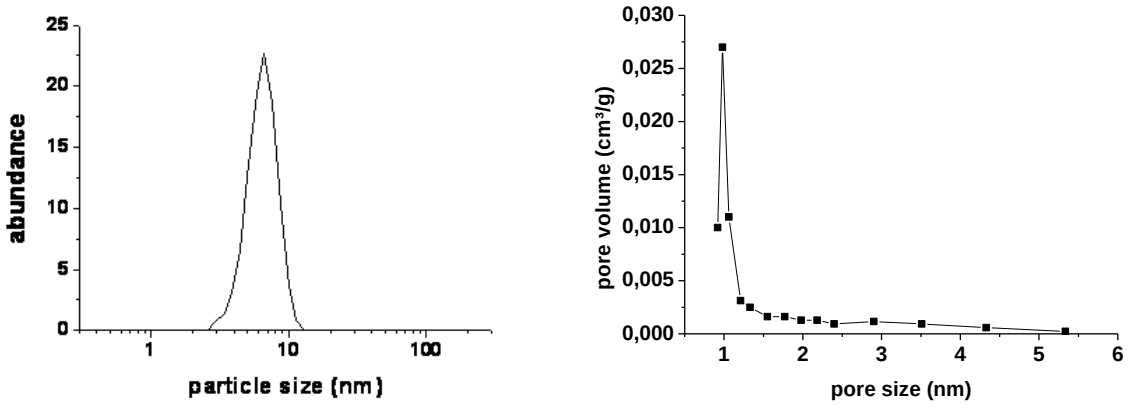

(a) (b)

Fig. 2a. Particle size distribution of yttria-zirconia sol used for the formation of the microporous $8Y_2O_3$-ZrO_2 membrane layer; Fig. 2b. Pore size distribution of $8Y_2O_3$-ZrO_2 microporous membrane material (firing 450°C)

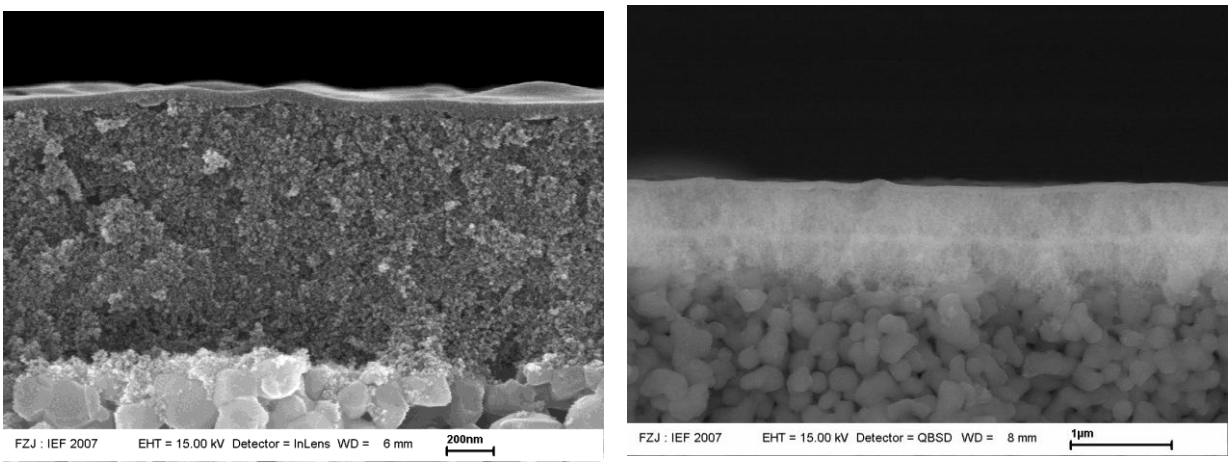

(a) (b)

Fig. 3. Micrographs of a microporous $8Y_2O_3$-ZrO_2 membrane, dip-coated on a mesoporous $8Y_2O_3$-ZrO_2 membrane (particle size in sol ~ 6 nm)((a) cross-section micrograph (bar = 200 nm); (b) cross-section micrograph in back-scattering mode (bar = 1 µm))

CONCLUSION

In the present work, a novel porous ceramic membranes with a functional toplayer made of Y_2O_3-doped ZrO_2 has been obtained, using classical ceramic membrane processing procedures (suspension coating, sol-gel). This membrane shows a typical graded membrane structure in anology with current microporous separation membranes and the application of zirconia based materials represents a significant improvement in terms of chemical and thermal stability over current silica based materials.

For applications requiring a fine microporous structure, ultra-thin nano-structured $8Y_2O_3$-ZrO_2 membrane layers with a thickness of ~ 50 - 100 nm were made from sols containing particles with a size of ~ 6 nm. The average pore size of the nano-structured membrane material measured ~ 1 nm, which approaches the pore size of current gas selective membranes (~ 0.4 nm). Further studies are currently devoted to tune the pore size of the novel membranes to the aimed ultra-microporous region (pore size < 0.5 nm), in order to obtain a functional separation membrane with an optimal pore size, an excellent thermal and chemical stability.

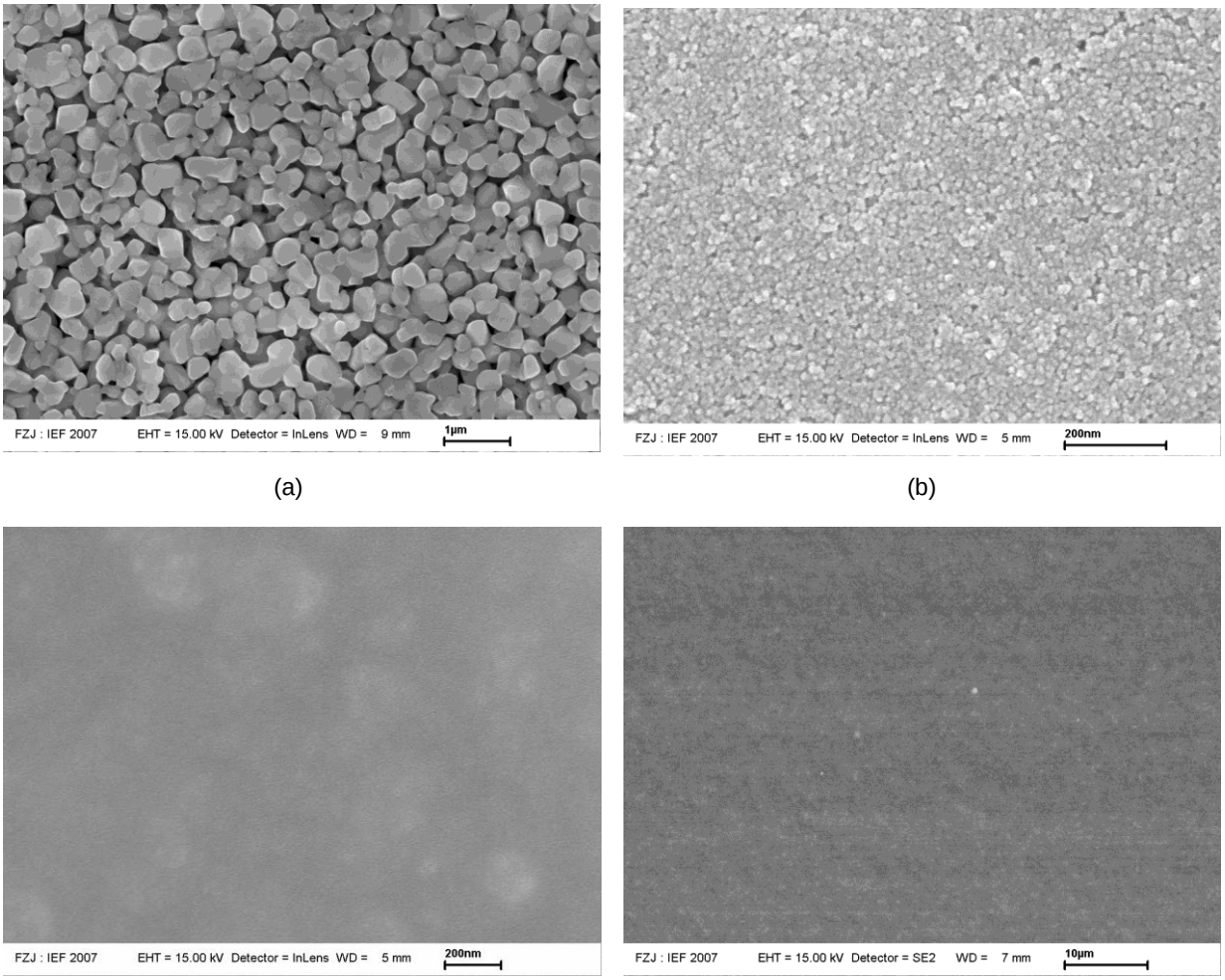

Fig. 4. Micrographs of the membrane surface taken after the respective coating and firing steps ((a) detail surface micrograph of $8Y_2O_3$-ZrO_2 macroporous membrane (bar = 1 µm); (b) detail surface micrograph of $8Y_2O_3$-ZrO_2 mesoporous membrane (bar = 200 nm); (c) detail surface micrograph of $8Y_2O_3$-ZrO_2 microporous membrane (bar = 200 nm); (d) overview surface micrograph of $8Y_2O_3$-ZrO_2 microporous membrane (bar = 10 µm))

REFERENCES

[1] P. Puhlfürß, A. Voigt, R. Weber and M. Morbé, Microporous TiO_2 membranes with a cut-off <500 Da, J. Membr. Sci. 174 (2000) 123-133

[2] H.M. van Veen, Y.C. van Delft, C.W.R. Engelen and P.P.A.C. Pex, Dewatering of organics by pervaporation with silica membranes, Sep. Pur. Techn. 22-23 (2001) 361-366

[3] T.A. Peters, J. Fontalvo, M.A.G. Vorstman, N.E. Benes, R.A. van Dam, Z.A.E.P. Vroon, E.L.J. van Soest-Vercammen and J.T.F. Keurentjes Hollow fibre microporous silica membranes for gas separation and pervaporation: Synthesis, performance and stability, J. Membr. Sci. 248 (2005) 73-80

[4] M. Asaeda, J. Yang and Y. Sakou, Porous Silica-Zirconia (50%) Membranes for Pervaporation of iso-Propyl Alcohol (IPA)/Water Mixtures, J. Chem. Eng. Japan 35 (2002) 365-371

[5] R. Vacassy, C. Guizard, V. Thoraval and L. Cot, Synthesis and characterisation of microporous zirconia powders. Application in nanofiltration characteristics, J. Membrane Sci. 132 (1997) 109-118

[6] T. Van Gestel, D. Sebold, W.A. Meulenberg, H.-P. Buchkremer, Development of thin-film nanostructured electrolyte layers for application in anode-supported solid oxide fuel cells, Solid State Ionics, in press

Theme 4: Advanced surface treatments: eliminating solvents by dry processing

Surface treatments are often used to improve the performance of products or components, their useful working lifetimes, aesthetic appearance or economics of production. Typical surface treatment processes are cleaning, etching, sterilisation, chemical activation and coating deposition. The purpose of coating deposition may be to control adhesion and release properties, minimise corrosion, reduce friction and wear, act as a diffusion barrier, provide thermal or electrical insulation, enhance biocompatibility, control optical properties or simply improve the aesthetic appearance for the surface. Papers are invited on developments and applications of innovative solvent free surface treatments using low, intermediate or atmospheric pressure processing technologies. Special attention will go out to plasma assisted chemical vapour deposition processes.

SiO_2 dry etching with the Expanding Thermal Plasma Technique

***A.S. Kagilik*, W.M.M. Kessels, and M.C.M. van de Sanden**

Department of Applied Physics, Eindhoven University of Technology, P.O. Box 513, 5600 MB Eindhoven, The Netherlands, phone: +31 40 247 2116, fax: +31 40 245 6442 ,e-mail: a.kagilik@tue.nl

INTRODUCTION:

Wet chemical processing of high efficiency silicon solar cells are still applied for many fabrication steps like, wafer surface texturing and cleaning, saw damage etching, Phosphorous silicate glass (PSG), and edge isolation by single side emitter etching etc. Due to increasing water costs and using harmful acids like hydrofluoric acid replacement by dry processing technique, which is characterized by low costs of water consumption and chemical waste disposal, is mandatory. On the other hand, full control of all process parameters attracts considerable interest in the PV industry [1].
PSG etching represents one of the most applications of dry plasma etching than can substitute the wet chemical etching. During the PSG etching, high selectivity of PSG to silicon should be achieved to prevent the emitter from back etching, and it has to ensure that the surface damaging is extremely low, because it is not followed by another high temperature step. On the other hand, residue free surface must be obtained for good adhesion of metallization and ARC. It was demonstrated that dry PSG etching for mc-Si solar cells achieve nearly efficiencies comparable to the wet chemically etched references using several types of plasma sources [2, 3].
In this work, we have investigated the plasma etching of the silicon oxide film, which served as a substitute for PSG layer due to the very similar etching properties, by using the expanding thermal Plasma (ETP) technique. This technique is characterized by high density remote plasma source and is successfully used in industrial high rate deposition of a-SiN_x:H passivated layer on silicon solar cells. On the other hand, many different materials such as: a-Si:H, a-C:H, etc. with high deposition rates and deep anisotropic silicon etching are obtained through this technology [4, 5].

EXPERIMENTAL RESULTS:

In this study, we used both p- and n-types single sided polished silicon wafers that were thermally grown with 400 and 500 nm SiO_2 respectively. Etching experiments were performed using CHF_3/SF_6 gas mixture gases. In order to evaluate the SiO_2 etching behaviour, the dependence of the etch rate on plasma operating conditions is demonstrated.
SiO_2 etch rate as a function of the percentage increase of SF_6 and the flow rate of the Ar gas is shown in Fig 1. As can be seen, the increasing in the etch rate by increasing the SF_6 gas is due to

the increase of the active F containing species. Etch rate increases by increasing of the Ar flow. This is due to the increasing of the plasma source efficiency.

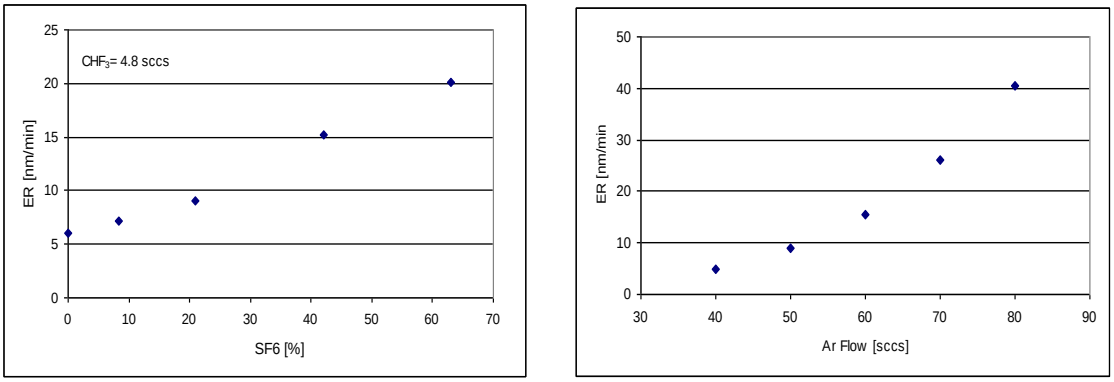

Fig. 1 SiO_2 etch rate as a function of increase in flow rate of SF_6 and Ar gases.

The dependence of etch rate on some plasma conditions (pressure and temperature) is illustrated in Fig. 2. The increase of pressure leads to an increasing of the etching particle flux flowing to the substrate (decrease of the beam diameter at high pressure), then the etch rate will be enhanced. The substrate temperature has a significant impact on the etch rate, at high temperature carbon-rich reaction layer is performed which causes a decrease in the etch rate.

Fig. 2 Effect of pressure and temperature on SiO2 etch rate

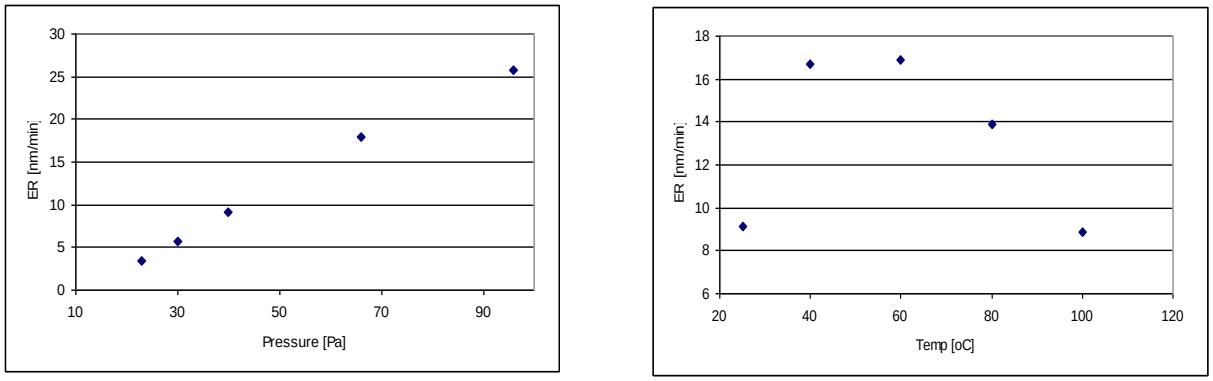

Fig. 3 shows the etch rate as a function of the RF bias. The oxide etch rate is strongly depending on the etchant flux and ion energy. It is observed that the increase of the negative DC bias voltage enhancing the oxide etch rate. This is due to the ion bombardment energy which is determined by the DC bias voltage.

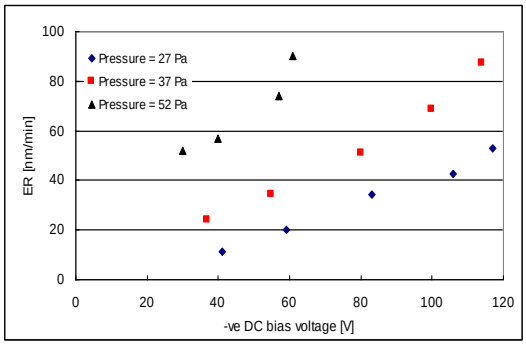

Fig. 3 The dependence of oxide etch rate on the RF biasing condition at different pressure values.

Etch rate values at different wafer positions and different pressure conditions using the Expanding Thermal Plasma system are shown in Fig. 4. Best wafer surface homogeneity is obtained at low pressure (larger plasma beam diameter) after etching.

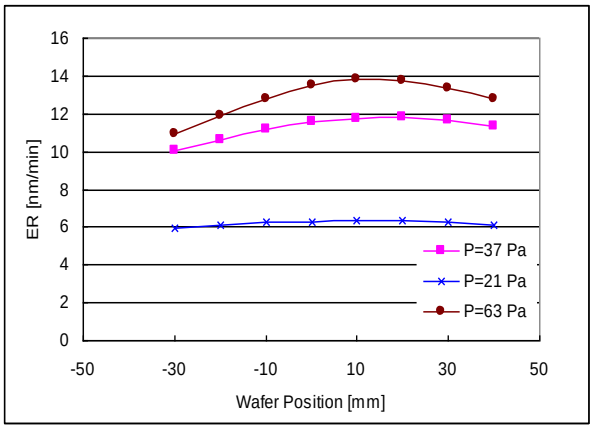

Fig. 4 Homogeneity of the etch rate on the whole wafer surface at different pressures

CONCLUSIONS:

A dry plasma etching is implemented as an alternative to the wet chemical etching. By using CHF_3/SF_6 mixture gases in expanded thermal plasma, the thermal silicon oxide is etched. The etching behaviour is characterized by measuring the oxide etch rate at different plasma operating conditions and its dependence is investigated. It was found that the plasma parameters have a significant impact on the etching process and high etch rate and high etch uniformity have been obtained. On the other hand, high SiO_2 to Si selectivity (> 10) can be estimated by using this technology. Moreover, dry plasma etching can substitute the conventional wet chemical etching process for PSG etching during solar cell processing. In this direction, further work will be conducted

REFERENCES:

[1] R. Lüdemann et. al., Proceedings 2nd World Conference and Exhibition on Photovoltaic Solar Energy Conversion, Vienna, Austria, Vol. II (1998) 1499.
[2] W. A. Nositschka et al., Progress in Photovoltaics: Research and Applications, 11, 7 (2003) 445.
[3] J. Rentsch et al., Proceedings 22th European Photovoltaic Solar Energy Conference, (2007).
[4] B. Hoex, A.J.M. van Erven, R.C.M. Bosch, W.T.M. Stals, M.D. Bijker, P.J. van den Oever, W.M.M. Kessels, and M.C.M. van de Sanden, *Prog. Photovolt: Res. Appl.*, 13, 705 (2005).

Fast plasma surface processing of powders

***A. Sonnenfeld*[1], *A. Spillmann*[1], *C. Arpagaus*[1,2], *Ph. Rudolf von Rohr*[1]**

1 Institute of Process Engineering, ETH, 8092 Zurich, Switzerland, Telephone: +41 44 632 79 41, Fax: +41 44 632 13 25
2 BÜCHI Labortechnik AG, Meierseggstrasse 40, 9230 Flawil, Switzerland

INTRODUCTION

Motivation

Today, the plasma treatment of polymers is commonly regarded to improve adhesion of subsequently attached materials. Furthermore, plasma cleaning, i.e. oxygen based treatment of metal or ceramic surfaces prior bonding, is already a common processing step in many production lines, e.g. of semiconductor industries (Thornton et al. 1994).
Commercially available reactors are usually suitable to treat (preferably flat) objects with macroscopic surface dimensions. However, they are not for microscopic particulate materials, i.e. powders. This becomes most obvious when considering the insufficiencies in homogeneity and thus efficiency of the desired treatment of a compact powder bulk in such batch reactors.
Agitating the powder bulk, while processing, has shown to improve the desired processing. Here, two designs are to be mentioned: the drum-reactor using baffles, mostly applied in industries, and the fluidized bed reactor often used to conduct fundamental studies (Arpagaus et al. 2005-1).Thus, agitation of the powder bulk is a key factor in determining the residence time distribution the micro-particles. In 1996, Wei and Zhu have already shown that so-called down-stream reactors are superior to other designs in terms of an extremely narrow residence time distribution and of a small mean residence time at all. These parameters, however, exert tremendous influence in view of the aspired homogeneity of the plasma-chemical treatment and its time and energy efficiency, see e.g. Yasuda's parameter. Nevertheless, the beneficial symbiosis of carefully designed reactors, in order to optimize the treatment conditions of particulates (Arpagaus et al. 2005-1), and the benefits of non-thermal plasma-chemistry was rarely achieved.
Powders of the hot-melt adhesives high density polyethylene (HDPE) and Co-polyamide (CoPA) are inherently non-dispersible in water. Required aqueous dispersions or pastes of them, today, are obtained by admixing considerable amount of tensides (Urban and Takamura 2002).
At the example of such powders treated in a plasma down-stream reactor (PDR) for the purpose of improving their wettability, and by an outlook on the treatment of lactose powder, in the same set-up, in order to increase its flowability, the benefits of this approach will be shown.

Precis

This study, partially financed by generous contributions of the Claude & Giuliana Foundation and Novartis Pharma AG, describes plasma assisted improvement of wettability and flowability of different powders, showing the possibility of efficient treatment by choosing a reactor design being adequate in terms of homogenous powder dispersion in the plasma. The time savings possible (tenth of second instead of hours) due to a PDR must be emphasized.

EXPERIMENTAL

The PDR applied (Fig. 1) consist mainly of a cylindrical glass tube (1) of ∅ 4 cm × 50 cm, where at medium height, a low pressure capacitively coupled radio frequency (RF) discharge (13.56 MHz) is ignited. By means of a nozzle in the upper end of the tube, the particulate material supplied by the metering screw (4) is evenly dispersed in the gas stream to the entire cross section of the tube (Arpagaus et al. 2005-1). Optimal exposure of the particulate surfaces to the plasma is achieved. Varying the rotation of the metering screw enables to set the mass of powder dm/dt (Table 1) conveyed from the storage container (3) to the collecting vessels (6).
In the experiments on rendering powders of HDPE and CoPA wettable, mixtures of O_2 and Ar were fed at the top end of the glass tube (1), while in study of improving the flowability of lactose powder, hexamethyldisiloxane (HMDSO) was additionally admixed by means of the evaporation mixer (8).

Here, Ar served to supply the mixer with HMDSO from the tank (7) and further to replenish the gas mixture as to keep the mixing ratio q and the total gas flow Q_{tot} (Table 1) constant for all parameter sets. Experiments have been conducted for 1 to 3 min in order to obtain an adequate amount of powder treated for the analytical methods to be applied afterwards.

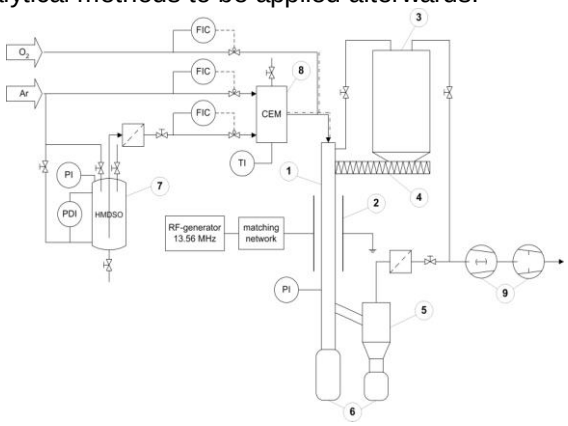

Figure 1. Schematic of the PDR: Descriptive of parts enumerated see in the text.

All powders have been characterized by means of a Krüss tensiometer K100 in order to determine the water contact angle (WCA). To derive the contact angle θ of a test liquid at the surface of particulate material, the capillary penetration method (Buckton 1993) and based on Washburn's theory (1921) was applied. The capillarity constant of the solid powder bulk was determined by the test liquid n-hexane. Water and diiodomethane were used to subsequently determine the surface energy of the powders of HDPE and CoPA. Therefore, Young's equation for the total surface energy at the solid

$$\sigma_s = \sigma_{sl} + \sigma_l \cos(\theta) \tag{1}$$

is combined with the approximation of the solid-liquid tension

$$\sigma_{sl} = \sigma_s + \sigma_l - 2\sqrt{\sigma_s^d \sigma_l^d} - 2\sqrt{\sigma_s^p \sigma_l^p} \tag{2}$$

by Owens and Wendt (1969). Accordingly, the polar part and the disperse part of the total surface energy of the particulate material measured were derived.

Table 1. Properties of the HDPE, CoPA and two qualities of lactose. Plasma treatment conditions.

	HDP	CoPA	Lactose	
particle size, x_{50} [µm]	55.6	48.5	6.7	71
specific density	950	1100	1525	
powder flow, $\dot{m}$ [kg/h]	5.0	5.0	1.3	2.4
discharge power, *P*	100	100	100	
Gas pressure, *p*	1.7	1.7	2.0	
total gas flow, Q_{tot}	500	500	1183	
$N^*_{HMDSO}/N^*_{O2} = 1/q$	0	0	0.1	
Gas velocity, v_G [m/s]	4.3	4.3	8.7	

In the case of lactose, the contact angle measurements were more complicated than for HDPE and CoPA, because the solubility of the lactose in the test liquids mentioned cannot be neglected. Therefore, measurements had to be conducted with lactose-saturated test liquids. However, the saturated solutions revealed different surface tensions than the pure liquids and especially the saturated diiodomethane no longer penetrated the solid lactose bulk, indicating a contact angle θ > 90°. Therefore, diiodomethane was substituted by propanol as a test liquid. Furthermore, an experimental procedure for reproducible measurement of the capillarity constant of the lactose powder with a mean particle size of x_{50} = 6.7 µm could not be established. Finally, lactose with x_{50} = 71 µm was chosen as an adequate substitute, assuming though that the tendencies observed are also valid for lactose of a different particle size. Additionally, the plasma effect on the flowability of powder was mainly studied for lactose when admixing HMDSO to the gas (Tab. 1).
The flow behavior is described by the flow factor

$$ff_c = \sigma_1 / \sigma_c \quad (3)$$

Here, σ_1 is the consolidating pressure and σ_c the unconfined yield strength. The higher ff_c, the better a powder flows. Based on ff_c, Schulze (1996) coined the following classification: $ff_c < 1$: not flowing, $1 < ff_c < 2$: very cohesive, $2 < ff_c < 4$: cohesive, $4 < ff_c < 10$: easy flowing, $ff_c > 10$: free flowing. The flow factors reported were determined by a ring shear tester (Schulze Schüttgutmesstechnik, Germany, RST-XS) at a pre-shear stress of 5000 Pa. The powders were antecedently tested by a laser diffraction system (Sympatec, Helos) concerning the cumulative and the differential particle size distributions as to determine the particle size x_{50} (Tab. 1).

RESULTS

Wettability of the HDPE and CoPA powders

The WCA is an adequate quantity to study the wettability. Tests on different external plasma parameters as RF power, gas flow, etc. showed that the most affecting tool is the ratio $[O_2]/[Ar]$.
In Fig. 2, the respective influence of the O_2 content on the WCA for both HDPE and CoPA is shown. Evaluating WCA values of exactly 90° appears questionable since the process of liquid penetrating the powder, on which the analytical method used (Sect. 2) is based, is obviously limited to the very same angle. Thus it belongs to speculations, whether the pure Ar treatment is as well effective or not. Nevertheless, for 10% of O_2, a strong reduction of the WCA is already evident compared to untreated powders. Wettability further improves with increasing O_2 content.

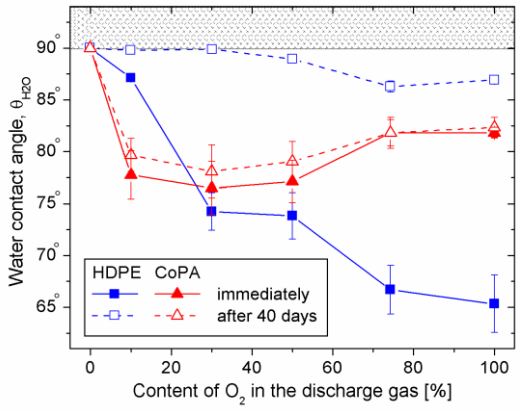

Figure 2. WCA for HDPE and CoPA powders immediately after being treated in the PDR at different O_2 contents (solid symbols) and 40 days after treatment (open symbols)

This behavior is stronger for HDPE, which is free of O (Arpagaus et al. 2005-2). Here, the production of O containing structures at the surface as C-O-C, C=O and O-C=O (evidenced by XPS) appears to be more effective than for CoPA, although the increase in the [O]/[C] ratio is approx. the same. Treated in equal conditions, spectra showed an increase by $\Delta([O]/[C]) \approx 0.16$, adding up to [O]/[C] = 0.27 for CoPA since its innate ratio is ~0.11 (Arpagaus et al. 2005-3). At first sight, these promising results are deteriorated by some kind of hydrophobic recovery of the powders after treatment (Fig. 2) Especially over 7 days after treatment of HDPE, the [O]/[C] ratio was found to decay by approx. 0.05 for O_2 contents of the plasma higher 10% (Arpagaus et al. 2005-2). But, 40 days after treatment, the decay in [O]/[C], i.e. aging, seemed to have stopped. For CoPA, the decay in [O]/[C] is less pronounced (Arpagaus et al. 2005-3). Consequently, almost the same WCAs were obtained when analyzing the powder samples after 40 days (Fig. 2).
The decrease in [O]/[C] witnessed by XPS due to the aging of HDPE could be attributed to the diffusion of oxygen containing groups from the surface of an HDPE particulate into its bulk [10]. Obviously this process would be less important for CoPA since the material itself contains oxygen as mentioned before. Thus, the gradient in concentration would be smaller. Nevertheless, also aged powders were found to be dispersible in water if being plasma-treated at O_2 contents > 30% for HDPE and > 10% for CoPA. The aqueous pastes produced are still (2 years later) fully intact. Finally, it must be emphasized that assuming the mean particles velocity being equal to the gas velocity (Table 1), the mean residence time, i.e. the mean treatment time of the particulates is τ =

0.12 s. This is especially noteworthy, since the wettability improvement, obtained by the PDR, is comparable to long-term achievements (1 h) by other workers (Jung et al. 2001).

Wettability of the HDPE and CoPA powders

The idea of flowability enhancement by PECVD in the PDR is illustrated in more detail in (Spillmann et al. 2007). By admixing HMDSO to the plasma in O_2 and Ar at relatively high pressure compared to thin-film PECVD, the creation of agglomerates in the range of a few nanometers (below 3 nm) is favored.

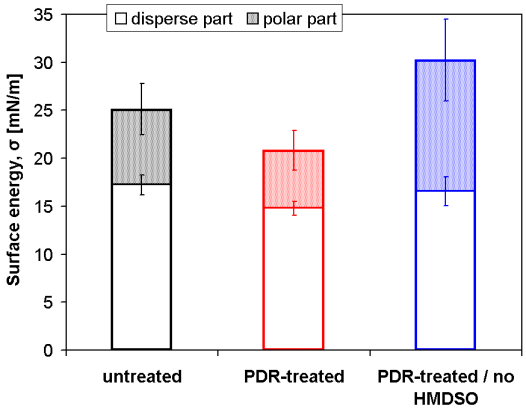

Figure 3. Comparison of surface energies and their disperse and polar parts for lactose (x_{50} = 71 µm) analysed before treatment, after PDR treatment with HMDSO admixed and in O_2/Ar only.

In the same time, the nanoparticles attach to the surface of the particles, here, evoking a decrease of the Van der Waals forces (VdW) between the particles.
Considering the inter-particulate forces acting, we have found the VdW to dominate (Spillmann et al. 2007). According to Hamaker (1937), the VdW between two sphere-like particles is the higher, the larger their radius is. Moreover, it is the smaller, the larger the inter-particulate distance is. Furthermore, it is proportional to the material specific Hamaker constant. The attachment of SiO_x nanoparticles was found to slightly decrease the surface energy of lactose treated (Fig. 3), while lactose treated without HMDSO in the PDR revealed the opposite behavior.
Hamaker's constant is likely to decrease if the disperse part of σ decreases. Being the case for HMDSO treated lactose, the VdW would decrease as well. However, the expected positive effect is much inferior the actual increase in ff_c for lactose treated by HMDSO containing gas mixtures (Fig. 4).

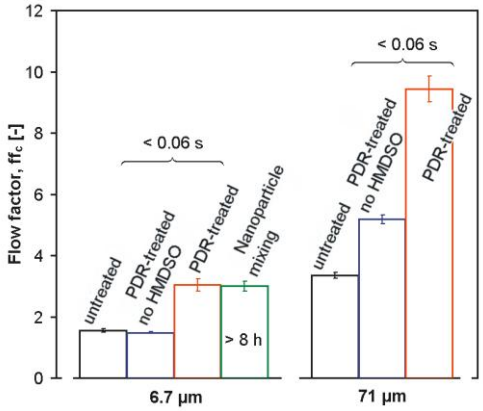

Figure 4. Flow factors of lactose (6.7 µm) and lactose (71 µm) analyzed before treatment, after PDR treatment with HMDSO admixed and treated in O_2/Ar only: Comparison to conventional mixing with silicate nanoparticles for more than 8 h.

Surprisingly, lactose of particle size of 71 µm showed as well a significant increase in its ff_c when being treated without HMDSO admixed. It is speculated that this finding is due to a lasting attachment of charges. The resulting electrostatic repulsion would also enhance flowablity.

REFERENCES

Arpagaus, C., Sonnenfeld, A., Rudolf von Rohr, Ph. 2005. A Downer Reactor for Short-time Plasma Surface Modification of Polymer Powders. Chem. Eng. Technol. 28(1): 87.

Thornton, J. A., Greene, J. E., 1994. in: Handbook of Deposition Technologies for Films and Coatings, ed. R. F. Bunshah, Noyes, Park Ridge: 55.

Wei, F., Zhu, J. X. 1996. Journal of Chemical Engineering 64, 345: 186-190.

Urban, D., Takamura, K. 2002. Polymer Dispersions and Their Industrial Applications. Wiley-VCH, Weinheim.

Buckton, G. 1993. Assessment of the wettability of pharmaceutical powders. J. Adhes. Sci. Technol. 7(3): 205.

Washburn, E. W. 1921. The dynamics of capillary flow. Phys. Rev. 17(3): 273.

Owens, D. K., Wendt, R. C. 1969. Estimation of the surface free energy of polymers. J. Appl. Polym. Sci. 13: 1714.

Schulze, D. 1996. Flowability of Bulk Solids - Definition and Measuring Techniques, Powder and Bulk Engineering 10 (6): 17.

Arpagaus, C., Rossi, A., Rudolf von Rohr, Ph. 2005. Short-time plasma surface modification of HDPE powder in a Plasma Downer Reactor, Appl. Surf. Sci. 252: 1581.

Functionalising textiles using environmental friendly techniques

Buyle G.[1], De Meyere T.[1] and Van de Vyver D.[1]

1 CENTEXBEL, Technologiepark 7, 9052 Zwijnaarde, Belgium, Telephone: +32 9 220 41 51, Fax: +32 9 220 49 55

INTRODUCTION

Coating is an ideal technology to realize innovation and differentiation. Through the application of one or more polymer layers with specific functions, high performance materials can be developed:

- modification of the textile surface;
- optimization of different mechanical properties;
- addition of specialty additives.

Here, we consider the use of hot melt, UV curing and plasma as eco-friendly methods for obtaining high performance textile materials, which form the basis for the production of innovative products.

HOTMELT

General: definition of a hot melt

Hot melts are 100% polymers which do not contain any water or organic solvent. According to their chemistry they are available in different forms as powder, granules, blocks, drums… These hot melts can be melted and subsequently be applied as a melt to a substrate. To melt the polymers a conventional fuser/melter, a drum melter (= an airtight melter used specifically to melt reactive polymers) or even an extruder can be used.

Being 100% products, the main advantages of using hot melts, are to be found in economical and ecological savings. Traditionally used water based products have a solid content in the region of 40-60%, while for solvent based this is even less and is situated between 20 and 50%. All solvent (or water) that is present in the formulation needs to be evaporated. In addition to the need of quite large and expensive ovens to dry off the solvent, there are explosion, fire and toxic hazards when using solvent based products. When working with solvent based products a lot of attention (and accordingly a lot of money) needs to be paid to “safety” and “environmental” issues. Legislation foresees the need of installing expensive equipment to recover, incinerate or oxidate the evaporated solvents. Although water based systems are safer and less polluting, they require even more energy to evaporate the water, which means the ovens have to be more powerful and accordingly are more expensive.

The currently commercially available hot melt polymers can be divided into two main classes: thermoplastic hot melts (e.g. polyolefines, polyester, ethylenevinylacetate …) and reactive hot melts (e.g. moisture curing polyurethanes or APAO’s[3], UV-curing acrylics …).

The big difference between thermoplastic and reactive polymers concerns their method for curing. Thermoplastic polymers are cured by cooling, while for reactive polymers reaction with moisture or UV is necessary to complete the curing of the polymer. Thermoplastic polymers become liquid (= melted state) when in contact with heat (depending on the chemical nature of the polymer temperatures can vary from 80 to 220°C) and solidify (= solid state) when cooled down. This is a reversible process that can be repeated. This is not the case with reactive polymers. Once cured (= solid state) it is impossible to melt them again since reaction with moisture or UV established a permanent solidification. This makes the reactive systems the most interesting ones for application where resistance to elevated temperatures is required.
Next to “standard” (= unmodified) polymeric hot melts, more recently some functionalised (mostly FR or antimicrobial modified) hot melts entered the market.

[3] APAO = amorphous poly-α-olefines

To apply the melted polymers (= hot melts) to a substrate a lot of different techniques are available. Available application units are e.g. gravure roller, multiroller system, slot-die applicator, spray-system …

The difference in the application machinery is mostly situated in the type of coating, i.e. a discontinuous (= patterned) or continuous (="full") coating. Another parameter is whether the coating is applied to the substrate in a contact less way or not. An example of a contact less method is applying a hot melt by a spray-system.

Opportunities of hot melts for different textile treatments

Hot melt polymers are not a new type of polymers. In fact, they are used since a long time in different sectors (e.g. non-woven, paper, film, foil,…) mainly for gluing purposes. Regarding the textile industry, hot melts are up to now almost exclusively used for lamination purposes. Typical examples are the production of articles like lingerie, work wear, sportswear, outerwear, protective clothing,… More recently, hot melts are also gaining interest in the automotive industry as an ecological replacement for the flame lamination technique. Flame lamination is traditionally used to laminate a textile to a PU[4]-foam, but this technique is currently dealing with a lot of environmental pressure and might be phased out soon. Flame lamination causes a reduction reaction in the PU-foam liberating a range of volatile materials including isocyanates, hydrogen cyanide and others. Several producers already replaced this technique by hot melt lamination.

The potential of using hot melts for different textile applications is however much wider. Hot melts can potentially be used for all kind of finishing or coating treatments. The potential of applying hot melts to mattress ticking fabrics to improve the seam slippage was emphasized. Trials of applying hot melts to carpets have shown a potential as well. Up till now, good results have been obtained on both "pile anchorage" and "adhesion of the backing", however further optimisation of the fibre bonding is still required.

Our current efforts regard the further optimisation of the already elaborated processes. Next to this, the possibilities of inducing specific properties (e.g. FR[5], antimicrobial, or antistatic properties) to standard hot melt polymers will be investigated. Knowledge in this topic is a requirement for hot melts to enter the textile industry more globally. The reason is that the process for applying hot melts to a textile substrate is completely different in comparison with the traditionally used water or solvent based textile finishing processes. Textile companies lack know-how and practical experience to be able to replace their traditional processes with these new ones. Nowadays there are a lot of different textile materials on the market and they all require different end properties. To be able to fulfil all these kinds of properties, the standard hot melt polymers will need to be functionalised with different types of additives.

UV TECHNOLOGY

General: UV treatment in textile industry

The UV coating technology is state of the art in a lot of industries. This radiation curing technology covers the graphics industry, as well as applications in the automotive industry. Because of the growing international competition and new environmental regulations the textile industry looks for new technologies which can match efficiency and innovation.

In textile industry the UV technology still represents a relatively small part of the coating market, although there are a lot of interesting applications in which the UV curable coating technology will be the major reason for success due to its potential advantages (energy efficiency, economics and ecology) compared to conventional solvent- or waterborne coating systems. This new, eco-friendly technology opens new opportunities for existing or new textile markets.

[4] PU = polyurethane
[5] FR = Flame Retardant (or Fire Retardant)

The use of the UV-technology can reinforce the possibilities for textile coating, because the application on thermal sensitive textile materials becomes available. UV-coating is a relative dry process, which implies certain economical and ecological advantages. The use of traditional processes requires a high water and energy consumption and represents a certain degree of pollution. The evaporation of water and other solvents require a lot of energy and high water consumption. UV-technology, as a dry process, offers a reliable alternative and diminishes the high water amount. Because the curing is very fast with this technique the energy cost decreases spectacularly. This results in an increase in production efficiency.

Research has been done to introduce the UV-technology in the textile industry. Different formulations were adapted and used on several textile materials. Important properties such as abrasion resistance, tactile properties, and durability were tested and evaluated.

The specific research was focused on three main topics:
- the development of 100 % or waterborne UV-systems;
- the optimization of UV process parameters;
- environmental effect and impact of the UV technology.

The emphasis in this research was focused on the free radical curing systems with special attention to system stability, adhesion strength and flexibility of the coating layer.

The UV technology offers a lot of advantages for the textile industry. The main reason for the implementation of the technology is economical, because of the reduced curing times, low temperature curing, higher production speed and low energy cost. Because of the low VOC emission the radiation curing also contributes to a cleaner environment which makes this technique a green, eco-friendly technology.

PLASMA TECHNOLOGY

General: plasma treatment of textiles

Plasma treatment of textiles can be done in different ways. Plasma activation is the (temporarily) lowering of the surface energy of the substrate. Plasma functionalisation comprises the grafting of chemical elements on the surface, resulting in tailored chemical properties. One can also cover the whole substrate surface, i.e. deposit a coating by means of plasma. Typically, this is done by vaporising a liquid precursor and adding it to the plasma discharge. The main advantage of this method is that the deposited agent interacts with the plasma, which leads to a unique chemistry and coating properties.

It is important to realise that this kind of coating is different from standard textile coating techniques. Typically, a textile coating means an add-on of several tens of grams per square meter. This way a relatively thick coating is formed on top of the substrate surface. However, for plasma coating the deposit layers are much thinner (order of nanometres). The reason is that only a limited amount of product can be added to the plasma. Otherwise, the typical interaction between the plasma and the added agent would be lost. As a result, the typical add-on in a plasma process is of the order of tenths of a gram per square meter.

Clearly, for applications requiring a lot of active agent, plasma coating will not be feasible. However, some applications can do with only a (very) small amount of active agent, e.g. for obtaining an antimicrobial effect. Indeed, also in a conventional coating, the active agent comprises only a small fraction of the applied coating. The other components of the coating formulation are intended mainly to provide the protective and binding matrix. This example of antibacterial finishing will be discussed in more detail.

Anti-bacterial coating on textile fabric via continuous atmospheric pressure plasma deposition

We investigated the deposition of a commercially available ammonium chloride-based antimicrobial agent via an in-line atmospheric pressure plasma system. The plasma system used is the

commercially available Coating Star (Ahlbrandt Systems, D). This system combines the addition of a liquid precursor with an atmospheric plasma treatment. The line speed was varied up to a maximum of 5 m/min.

Experiments were done to characterise the deposition process. This involved finding the optimised parameters (temperature, concentration, gas pressure) for nebulising the liquid agent. Further investigated topics were the influence of the line speed, the influence of the time lag between the plasma pre-treatment and subsequent deposition. This time lag seemed to have a very strong influence on the amount of antibacterial agent that could be fixed to the textile substrate. The best results were obtained by performing both treatments simultaneously.

Surface analysis was performed on the samples using XPS and ToFSIMS. One of the main outcomes of these measurements was that a uniform layer of about 1-2 nm could be deposited on the fabrics. No covalent bonding between the fabric and agent was found.

Functional analysis of the deposited layers was done by performing the standard antibacterial test described in [ISO20743] on the fabrics. The results indicate that after an incubation of 24 hours at a temperature of 37°C a log reduction of up to four orders could be obtained using Staphylococcus Aureus.

Also the abrasion resistance of the coatings was investigated using the Martindale test. The very good abrasion resistance obtained can be explained by the distribution of the deposited agent within the fabric. Indeed, because of the vaporisation, the agent is presented to the substrate in the form of very small droplets (order of micrometer). These droplets can penetrate in the substrate. As a result, a plasma coated substrate does not show the typical layer “on top” (as shown in the left part of the figure below) but the coating is rather “within” the substrate (as shown in the right part of the figure below), which ensures a good abrasion resistance. Of course, the penetration of the deposited agent is also strongly dependent on the substrate characteristics.

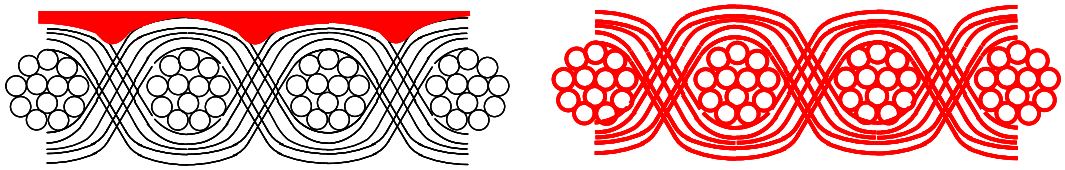

Figure 1. Different types of coating: deposition “on top” (left), typically obtained with conventional coating methods, or “within” the substrate (right), which can be obtained via plasma coating.

CONCLUSIONS

The use of hot melt, UV curing and plasma for the functionalisation and coating of textile materials is increasing. Main reason is that compared to current traditional finishing processes, these techniques have crucial advantages like a reduced usage of process water, energy and solvents. In this paper, the application of these three techniques for textile processes is illustrated.

ACKNOWLEDGEMENTS

IWT Flanders supported the hot melt (50742) and UV coating (050110 and 060875) related parts. The plasma related part of the work is supported by the EC Project # 515859 – Acteco.

REFERENCES

Fung W. 2002. Coated and laminated textiles
Kemper P. 2005. Griltex hotmelt adhesives – the alternative to flame bonding. International Dyer.
Kemper P. 2002. Copolyester und copolyamid-Schmelzklebstoffe für technische Anwendungen. Allgemeiner Vliesstoff Report 4.

Reuscher R. 2002. Modern hotmelt applications for the growing market for laminates. Technical Textiles, 45: E148-E149.
Halbmaier J. 1992. Overview of hot melt adhesives application equipment for coating and laminating full-width fabrics. Journal of Coated Fabrics, 21: p 301-310.
Petrie E M. 2002. Reactive hot melt adhesives. Adhesives & Sealants.
Petrie E.M. 2004. Fire retardant adhesives. Adhesives & Sealants.
Schnerring K. 2002. Moderne Schmelzklebesysteme. Allgemeiner Vliesstoff-Report 4, 36-38.
Barton J. 2005. Growth market continues to attract innovation. International Dyer, 28-34.
Welter C. 1998. Mashinen zur Herstellung textiler Verbundwerkstoffe mittels Hotmeltklebern. Technical Textiles, 41.
Schnerring K. 2002. Multi-roller hotmelt technique, Unitex nr. 2.
HIP-MITSU's equipment and Lines for advanced web-coating and laminating. Unitex nr. 3, 2006
Hotmelt-Auftragsverfahren, Allgemeiner Vliesstoff-Report 4, 2003, p 42
Weiss E. 2005. Application of hotmelt technology in the textile field. Unitex, 6.
Grillo-bontemps C. 2004. Reactive hot-melt adhesives close the performance gap. Technical Textiles International; 33-34.
Gillessen G. 2000. Flame, dry or hot-melt. Internation Dyer.
Albers K., de Jong H., Katzenmayer S. 2003. Advanced reactive polyurethane hot melt adhesives for high - performance textile laminates and industrial composites. Technical Textiles, 46: 32-33.
Krijnen E. 1994. UV-Curing Coatings for Textiles: Coatings with a Future. Journal of Industrial Textiles, 24: 152-161.
Decker, C. 1998. The use of UV irradiation in polymerization. Polymer International (UK), 45: 133-141.
Decker C., Nguyen Thi Viet T., Decker D., Weber-Koehl E. 2001. UV-radiation curing of acrylate/epoxide systems. Polymer, 42: 5531-5541.
Morent R., De Geyter N., Verschuren J., De Clerck K., Kiekens P., Leys C. 2008. Non-thermal plasma treatment of textiles. Surface & Coatings Technology, doi:10.1016/j.surfcoat.2007.12.027.
Shishoo R. 2007. Plasma technologies for textiles. Woodhead publishing, ISBN-13:978-1-84569-073-1.
Paul A., Bretagnol F., Buyle G., Colin C., Lefranc O., Rauscher H. 2007. Evaluation of plasma-deposited anti-adhesive and anti-bacterial coatings on medical textiles by surface analysis techniques. contribution to MEDTEX07.

Release / adhesion enhancement of polymeric substrates using Atmospheric Plasma Technology

Dubreuil M.F.*, *Bongaers E. M. and Vangeneugden D.

VITO (Flemish Institute for Technological Research), Materials Technology, Boeretang 200, 2400 Mol, Belgium
Marjorie.dubreuil@vito.be, Tel+32.14.33.56.86, Fax+32.14.32.11.86

The present work describes the synthesis of nano-scale coatings by atmospheric plasma technology to modify the surface properties of different types. The presentation will be divided in two sections, while the first part will be dedicated to the enhancement of the adhesion properties of plastic foils, the second part will be focused on the deposition of release coatings to prevent adhesion. Parallel plates dielectric barrier discharge (DBD) at atmospheric pressure has been investigated to modify and functionalize the surface of different polymer substrates, e.g. polyolefins, poly(ethylene terephtalate), poly(vinyl chloride), polyamide,… According to the targeted application, different functionalities have been introduced to tailor the final surface properties. The obtained coating have been characterized in term of wettability measurements, IR-spectroscopy, XPS labelling, and adhesion tests.

INTRODUCTION

From an industrial point of view, there is an increasing interest to control the surface functionality and the surface properties. More and more demands arise to control adhesion and release properties of different substrates, more specifically of polymer substrates. Recent developments in the field of atmospheric plasma technology are creating new perspectives beyond current state-of-the art in corona pre-treatment of materials. By controlling the gas atmosphere and electrical conditions, one can increase the efficiency of the plasma surface treatment significantly. Furthermore, by adding reactive chemical precursors to the plasma discharge, the surface chemistry can be controlled and thin functional coatings can be deposited.

EXPERIMENTAL SET-UP

Atmospheric plasma technology has been used to deposit very thin organic coatings on polymer foils to modify[1,2] their adhesion properties. Parallel plates dielectric barrier discharge (DBD) at atmospheric pressure has been investigated (scheme 1).
The DBD was produced between two parallel stainless steel electrodes, both covered with an insulating glass plate of 3mm thick. The gap between the electrodes can be increased up to several millimeters, however, to ensure stable plasma operation the gap width was limited to 2mm. Plasma discharges can be generated at variable frequency comprised between 1 and 100kHz, and a dissipated power varying between 0.5 and 5W/cm^2. Various gasses can be used to generate plasma, such as nitrogen, helium, argon, mixtures with oxygen, carbon dioxide, tetrafluoromethane,… However, nitrogen is preferred for its cost advantage.

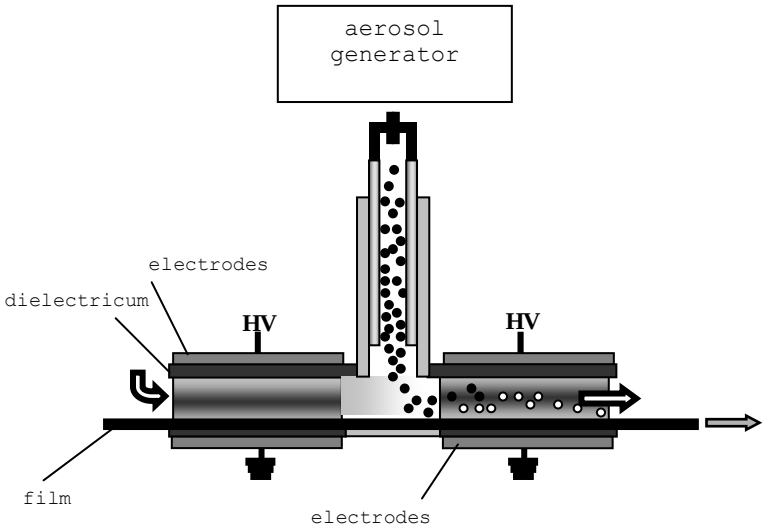

Scheme 1. DBD parallel plates configuration.

RESULTS & DISCUSSION

Adhesion enhancement of polymeric substrates

Plastics are usually more difficult to bond than other substrates. Even if some plastics are easy to bond (ABS, PS, …),on account of the low polarity and surface tension of certain plastics (ex. polyolefins), they can only be bonded after treatment to increase the surface energy. The use of atmospheric plasma technology may act at different levels; for example in the suppression of the need of a primer between the substrates and the adhesive, in enhancing the printability of a substrate, ...In order to tune the final surface properties, different functionalities have been introduced (hydroxyl, amino,…) using the following precursors: hydroxyethyl acrylate (HEA), acrylic acid, allylamine, acetic acid and ethyl acetate.

The surface wettability has been monitored with contact angle measurements carried out as a function of time using the acid-base model. Typical results (1month after plasma processing) are summarized for polypropylene (PP) in figure 1. Drastic and durable improvement of the substrate hydrophilicity is observed for all tested precursors. The most promising results in term of stable improved surface properties are obtained using ethyl acetate as precursor. Similar results have been obtained for polyethylene, polyamide, and poly(ethylene terephtalate).

The different precursors have been chosen for their ability to introduce particular functional group on the substrate surface. In order to characterize these functional groups, a labeling technique has been used, coupled with X-Ray Photoelectron Spectroscopy (XPS). In order to study the functional group concentration (OH, NH_x, C=O,..), a derivatization is applied introducing a fluorine group at the surface. The deposited coatings have been furthermore characterized by ATR-IR (an example is given in figure 2 using HEA as precursor). It is clear from these analyses that the starting precursors are completely “reorganized” during the plasma deposition process, where many reactions (such as fragmentation, recombination, polymerization,…) are taking place. A general trend for most precursors is the apparition of amide functions.

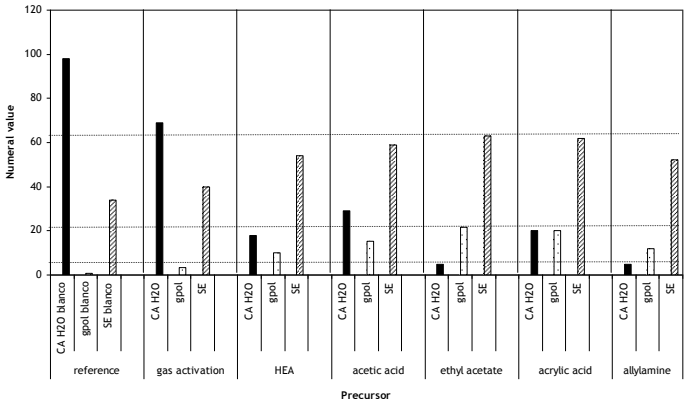

Figure 1. Summary of typical results for the contact angle with water (CA H_2O), the polar component ($\square_{pol}$), and the surface tension parameter (SE) for PP – 1month after plasma processing as a function of precursor chemistry

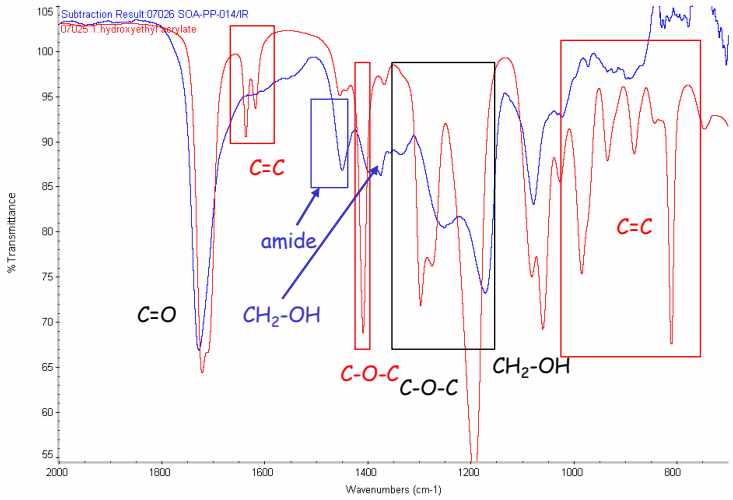

Figure 2. ATR-IR spectra of HEA monomer (a) and plasma polymerized HEA (b)

Release Coatings

In the pressure-sensitive technology, silicone coatings and waxes coatings are mainly used as non-polar release coating to ensure that adhesive tapes can be easily un-winded after production. A typical problem however, for these types of coatings is the presence of transfer and migration of the release coatings on all the surfaces they come in contact with. To minimize this problem, very thin coatings are applied, where high diluted silicone or waxes solutions in organic solvents are used, leading to heavy environmental and costs problems. The use of atmospheric plasma to synthesize thin release coatings could offer an interesting alternative.
Two types of chemistry have been used for this purpose, the first one – silicon free – based on apolar acrylates (such as ethyl-hexyl acrylate); the second one based on the plasma polymerization of hexamethyldisiloxane.

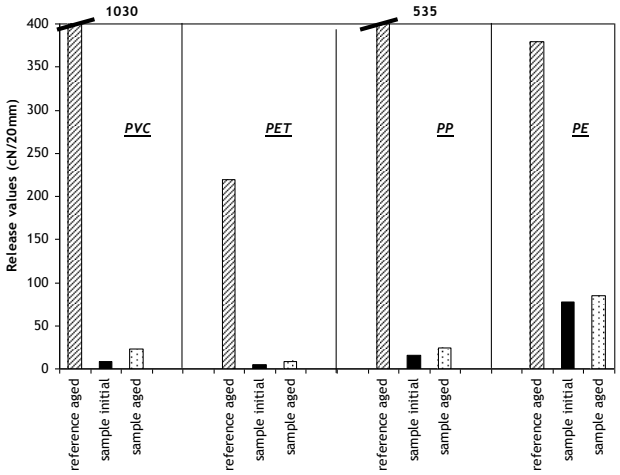

Figure 3. Release values for release coatings based on apolar acrylate for PVC, PET, PP and PE – initial and after complex ageing (1 week at 60°C)

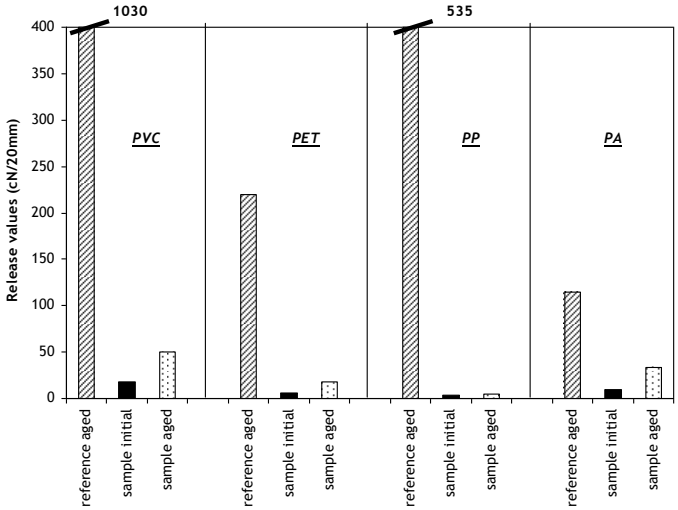

Figure 4. Release values for release coatings based on HMDSO for PVC, PET, PP and PA – initial and after complex ageing (1 week at 60°C)

The observed results are summarized in figures 3 & 4, where the release properties (initial and after ageing) are presented for poly(vinyl chloride), poly(ethylene terephtalate), polypropylene, polyethylene and polyamide. In both cases, drastic improvements of the release properties have been demonstrated for all substrates, even after ageing.

CONCLUSIONS

The above study has demonstrated that atmospheric plasma technology offers an environmental friendly and cost competitive solution for the modification of the adhesion properties of different substrates. The surface tension properties maybe completely modified to allow an adhesion enhancement, finding many applications, from ink deposition to enhancement of adhesion with a glue, replacement of a primer,…. On the contrary, thin release coatings can be applied on various polymeric substrates, opening new possibilities in the world of pressure-sensitive adhesive tapes for instance.
By choosing the right chemistry, the surface properties may be tailored using atmospheric plasma to fulfil the requirements of a given application.

ACKNOWLEDGEMENTS

Nitto Europe is acknowledged for the co-development of the release coatings based on apolar acrylates in the framework of a collaboration.
The Fraunhofer-Institut für Angewandte Polymerforschung is aknowledged for the XPS-analyses and their interpretation.

REFERENCES

[1)] Y. Nakayama, T. Takahagi, F. Soeda, K. Hatada, S.Nagaoka, J. Suzuki, A. Ishitani. J. Polym. Sci., A Polym. Chem. 26 (1998) 559.
[2)] J. Friedrich, G. Kühn, R. Mix, W. Unger. Plasma Proc. Polym. 1 (2004) 28.

LCA comparative analysis of different technologies for functional coating in food applications

Benveniste G[1]., Perucca M.[1], Baldo G.L[2]

1 Environment Park-Clean NT Lab , via Livorno 60, 10144, Torino, Italia, gabriela.benveniste@enivpark.com, Telephone : +39 0112257214
2 Studio LCE, via Livorno 60, 10144, Torino, Italia

INTRODUCTION

The general scope of this study is to compare alternative functionalisation technologies for surface protection and to analyse how the origin and type of energy and input materials employed in each process affect the overall environmental burden evaluation. For this reason, the analysis includes an assessment of Chromium plating process comparable to the Physical Vapour Deposition (PVD) of ceramics coatings and SiOx deposition by Microwave (MW) plasma technology for the functional output of the product system, whereas characterized by different physical/chemical properties and different process performances with respect to the other innovative solutions. In addition, this report shows how the change in the energy mix input may influence the results previously found.

Technologies description

The main objective of this work is to calculate the energy and environmental burdens generated by ceramics PVD-, SiOx Plasma-. and Chromium electroplating- coating processes using different energy mixes. In detail, data, calculation procedure and results refer to:

- PVD Arc DC ion-plating equipment;
- SiOx deposition from plasma experimental process carried
- Chromium electroplating process performed by typical electroplating process

In particular for food processing applications the technical and quality specifications of coatings refer to the wear resistance and hardness overall efficiency of the cutting tool surfaces (e.g. Blades) as well as components employed for hitting and moving material to be processed (screws, hammers, …). The specific characteristics to be achieved are: toughness, wear resistance and barrier function of coatings to the migration of heavy metals in order to attain bio-compatibility (food has not to be contaminated by allergenic substances or compounds as per FDA approval requirements).
In general the first system under consideration, PVD, has the purpose of processing a wide variety of materials (ferrous, steel, aluminium and titanium alloys,..) in order to improve their resistance to wear, to corrosion and for decorative applications. This functionality is obtained by PVD of a thin single/multi-layer coating of nitrides, carbo-nitrides, carbides, sulphides, borides and oxides on the surface of the product (hereafter referred to as “substrate”). For this study it has been analysed PVD TiN and TiCN deposition.
The second system considered, Chromium electroplating process, is used extensively for decorative, engineering and electroforming purposes, with the objective to improve surface finish, corrosion resistance and wear resistance of the materials processed (commonly ferrous, zinc and copper alloys and some plastics as ABS).
The third system considered, plasma SiOx deposition, is used extensively with the objective to improve surface finish, corrosion resistance and wear resistance of the materials processed (commonly ferrous, zinc and copper alloys and some plastics as ABS). The variation of the SiOx coating thickness is in the range of 0.4 µm and 3.1 µm.
The equipment used for plasma SiOx and PVD deposition in this study are a lab scale devices, equivalent in terms of results to large scale systems; on the contrary, the electroplating technology taken into account in this study corresponds to an industrial scale system already available at large scale. These differences may cause that parameters as energy consumption may appear not comparables among the 3 technology. Nevertheless it is important for future development and optimisation of the plasma technology to find out which are the weak point to be improved to

achieve a competitive effective plasma non wet technology compared to already available electroplating processes.

System Boundaries, Functional Unit and other considerations

Due to the shape and quality variability of the products managed in the two processes analysed, it was decided to express the results in terms of 1 m^2 x 1 µm of coated surface for PVD and SiOx since this F.U represents the reference unit that gives the same performance of the treated surface. For Chromium electro-plating the reference unit is 1 m^2 x 3 µm, which is the unit that is equivalent in terms of performance for this treatment to the unit that has been used for the other two treatments. For all the processes, the same substrate ASTM A 295-98 52100 (UNI-100Cr6) was employed. The boundaries of the considered systems include all phases from raw material extraction to the production and coating of a generic product. Product life durability and end of life have not been taken into account in this analysis (Fig. 1)
Moreover, the analysis does not take into consideration:

- the production and the transport of the substrate materials;
- the production and the end-of-life of the plants (PVD and chromed plating);
- the end-of-life of the coated products.

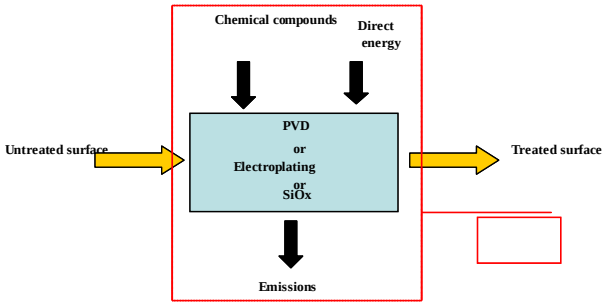

Figure 1. System boundaries

Life Cycle Inventory

The Inventory analysis provides a catalogue and quantification of the energy and material use as well as environmental releases associated with the processes included in the system boundaries.
Three different scenarios have been taken into account to determine how the origin of the energy may affect the environmental burden in the same process (Table 1)

Table 1. Summary of energy origin for each energy mix to produce 1MJ of electricity.

	Italy mix	***Europe mix***	***France mix***
Coal	12%	27%	7%
Oil	34%	8%	2%
Gas	34%	16%	1%
Hydro	10%	6%	7%
Nuclear	9%	39%	82%
Other	1%	2%	1%

Data and information used in LCA studies can be divided into two main categories, *primary data* and *secondary data*:

- *Primary data* are data collected directly from the plant and, therefore, guarantee an high level of accuracy.
- *Secondary data* are data obtained from databases, other previously carried out analysis or published reports. As far as the production of fuels, raw materials and transports in terms of energy, resources consumption and emissions to the environment are concerned, data come from the Boustead Model_V and refer to three different energy mixes: Italy, average Europe and France.

Results

The results of the LCA are split into the two following categories: Energy and resources results: energy, raw materials consumption and emissions and environmental results (natural resources consumption, air emissions, water emissions and solid wastes) all referred to the functional unit.
The values corresponding to the gross energy requirement for each process and for each energy mix are reported below (Table 2).

Table 2. Gross energy requirements for each technology (MJ/F.U)

TREATMENT	Indirect Energy	Direct Energy	Transport energy	Feedstock energy	Total Energy
PVD - TiCN Italy Mix	255	124	2	0	381
PVD - TiCN Europe Mix	248	124	2	1	375
PVD - TiCN France Mix	255	124	2	1	381
PVD- TiN Italy Mix	255	124	2	0	375
PVD- TiN Europe Mix	248	124	2	1	381
PVD- TiN France Mix	255	124	2	1	306
Cr^{VI} coating Italy mix	187.3	115	2.5	0.9	306
Cr^{VI} coating Europe mix	187.3	115	2.5	0.9	306
Cr^{VI} coating France mix	187.3	115	2.5	0.9	300
SiOx plasma- Italy mix	607	340	6	41	994
SiOx plasma- Europe mix	587	340	6	41	974
SiOx plasma-France mix	607	340	6	41	994

From the table 2, it can be noticed that plasma processes are more energy demanding than traditional electro-plating process (24 % more for PVD w.r.t. electroplating, SiOx-MW plasma 3 times more than electroplating) due to the fact of they use electricity as mainly energy source with an important indirect energy contribution (that is to say, the energy employed to produce the direct energy used in the process).

Regarding the demand of the main raw materials without taking into consideration the energy content (feedstock energy), table 3 shows the main values, referred only to the Europe mix for each technology.

Table 3. Average raw materials consumptions in mg/F.U

Raw material	TiCN/TiN coating	Cr coating	SiOx
S (elemental)	*2300*	*25077*	*700*
Cr	*0*	*81000*	*16*
O2	*21400*	*42500*	*45500*
Water (total) (l/F.U)	*5*	*8,5*	*51,1*

What is remarkable are the differences found among each technology considering the water emissions of main pollutants, expressed in figure 2 above all the values regarding the emission of Cr^{VI} ion, Zn and suspended solids as a by product of the plating technology.

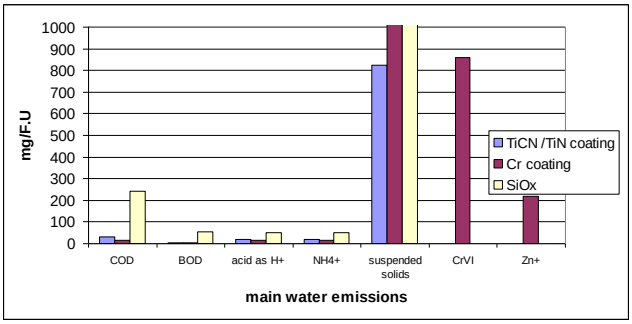

Figure 2. Main water emissions

According to ISO 14044, the general framework of the Assessment phase is composed of several mandatory elements that convert Inventory results into environmental indicators: Greenhouse effect (global warming -GWP); Acidification (AP), Photochemical oxidant formation (Photo-smog- POPC) and Eutrophication (EU) in Table 4.

Table 4. Classification and characterisation of total emissions (data referred to f.u.)

TREATMENT	GWP (kg CO2)	AP (g eq SO2)	POPC (g C2H4)	EU (g PO43-)
PVD - TiCN Italy Mix	23,53	276,79	32,75	8,76
PVD - TiCN Europe Mix	17,36	140,63	15,32	5,98
PVD - TiCN France Mix	4,19	38,88	7,45	1,71
PVD- TiN Italy Mix	23,39	245,47	32,38	8,71
PVD- TiN Europe Mix	17,22	139,32	14,95	5,93
PVD- TiN France Mix	4,05	37,6	7,08	1,66
Cr^{VI} Galvanic coating Italy mix	18.93	210.52	22.44	6.92
Cr^{VI} Galvanic coating Europe mix	14.38	110.13	9.59	4.86
Cr^{VI} Galvanic coating France mix	4.76	35.68	3.60	1.73
SiOx plasma- Italy mix	59,78	718,75	75,99	22,92
SiOx plasma- Europe mix	46,21	419,44	37,66	16,8
SiOx plasma-France mix	17,38	197,35	20,54	7,46

As shown in the previous table the energy mix affects the values of the GWP. For instance, concerning PVD process plant in France, where electricity energy is produced mainly by nuclear power plants, the variation on the GWP can be noticed in the figure 3 below. It is important to remark that the GWP_{100} indicator decrease of about 82 %.

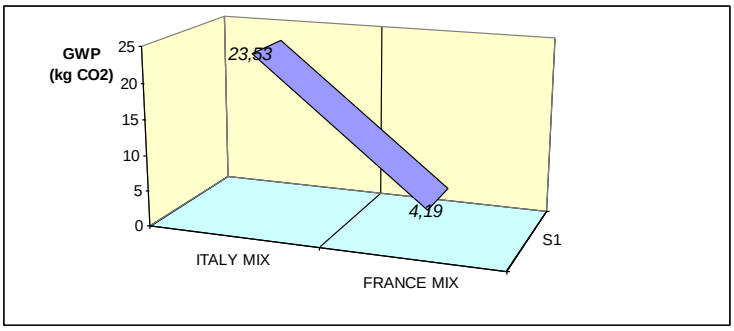

Figure 3. PVD: effect of the energy mix on the GWP_{100}

CONCLUSIONS

General considerations regarding the wealth of data provided prove that Chromium plating process determines a huge local or localised environmental burden, while PVD and plasma deposition of SiOx determine a greater environmental burden on global scale due to the higher energy consumption.
From an energy consumption point of view, the Cr coatings requires less process (direct) energy respect to the PVD/plasma processes This is especially relevant for the electricity consumption: the energy mix to produce electricity is therefore relevant to define the environmental burden of the two systems. Actually the environmental burden in terms of GWP is significantly different when applying different energy mixes. Dramatic differences can be noted taking into account the environmental parameters that have been listed before. Despite the higher use of electricity of the PVD and SiOx-MW plasma processes comparing to the plating process, this one has higher direct solid, air emission and generation of exhaust solution. This means that from a local environmental point of view, the PVD and SiOx-MW plasma processes avoid the direct emissions of metals (Cr, Zn and Cu in particular) but generate an indirect contribution from the electrical power plant.
Regarding the environmental burden generated by these processes in terms of GWP it is clear that the choice of different energy mix affects the results, and so the choice of a suitable and more

environmental friendly energy production (e.g. use of renewable energy sources) and transport systems represent the best option to reduce the global impact for greenhouse effect. For what pertaining the evaluation of SiOx plasma deposition process input data refinement should be considered as the processed data are referred to lab scale reactor, for actual technical implementation reasons. Further steps of the study will focus on the analysis of optimised plasma technologies, improving their energy consumption, in order to verify its effectiveness not only in terms of functionality of the treated surfaces, but also in terms of environmental and cost sustainability.

ACKNOWLEDGEMENTS

This study has been carried out within the FP6 European project ACTECO, and the collaboration of all the partners involved in.

REFERENCES

ANPA (2000), "*Banca dati italiana I-LCA*";
G.L. Baldo (2000), "*Life Cycle Assessment – Uno strumento di analisi energetica ed ambientale*", IPA Servizi Editore, Milano;
ISO 14040 (1997), "*Environmental Management – Life Cycle Assessment – Principle and framework";*
I. Amato, L. Montanaro (2000), "*Scienza e tecnologia dei materiali ceramici*" Vol. III, Edizioni Libreria Cortino, Torino;
MSR 1999:2, "*Requirements for Environmental Product Declarations, EPD*", Swedish Environmental Management Council, 27/03/2000.

Comparison between wet deposition and plasma deposition of silane coatings on metals for surface passivation

***I. De Graeve*[1], F. Brusciotti[1], A. Batan[2,3], M.Wenkin[4], F. Reniers[2], J.J. Pireaux[3], J.Vereecken[1], H. Terryn[1]**

1. Vrije Universiteit Brussel (VUB), Department of Metallurgy, Electrochemistry and Materials Science (META), Pleinlaan 2, 1050 Brussels, Belgium, idgraeve@vub.ac.be, tel 0032 2 6293482 fax 0032 2 629 3200;
2. Université Libre de Bruxelles (ULB), Faculty of Sciences - Analytical and Interfacial Chemistry, Brussels, Belgium;
3. Facultes Universitaires Notre-Dame de la Paix (FUNDP), LISE Laboratory, Namur, Belgium;
4. Coating Research Institute (CoRI), Limelette, Belgium

ABSTRACT
Silane coating is an environmentally sound multi-metal surface pretreatment for corrosion protection, hydration inhibition and adhesion promotion on metals. Silanes are hybrid organic-inorganic molecules. Films are mostly deposited from solutions. For pretreatment purposes the films are generally below 1 µm and are strongly bonded to the precleaned metal surface. Barrier properties can be created through thermal curing after wet film deposition. Using solvent free atmospheric and vacuum plasma deposition, very different layer morphologies are formed depending on the plasma conditions. The deposition of silanes using various wet and plasma deposition methods is investigated. The aim of this work is to determine if plasma deposition can result in innovative properties. Preliminary results of this new project will be presented. Films are characterized chemically and morphologically using various optical (ellipsometry and FTIR) and vacuum surface analytical methods (FEG-SEM and XPS).

INTRODUCTION
Silanes are mostly investigated as an alternative for the chromium-VI containing conversion treatments [1] for corrosion protection and adhesion promotion of metals. Silane coatings are environmentally sound, multi-metal [2-11] surface pre-treatments.
Silanes are hybrid molecules containing organic groups such as methoxy or ethoxy ones bound to silicon atoms. Additional functional groups, such as amines, epoxides or others, may be present to promote adhesion with covering organic coatings. Films are mostly deposited from solutions through dipcoating or rollcoating. In these wet deposition methods, addition of water to the silane molecules is required to hydrolyse the methoxy or ethoxy groups to form functional silanol groups i.e. $X\text{-}SiOCH_2CH_3 + H_2O \rightarrow \underline{X\text{-}SiOH} + CH_3CH_2OH$. Silanol groups are essential to form a covalent Si-O-metal bond at the metal/film interface [12] and for cross-linking in the bulk of the silane layer upon thermal curing. Cross-linking is due to the condensation of silanol groups i.e. $X\text{-}SiOH + HOSi\text{-}X \rightarrow X\text{-}SiOSi\text{-}X + H_2O$.
In the present work silane films will be deposited by different methods. Traditional wet deposition will be compared to atmospheric and vacuum plasma deposition where no solutions or solvents are required.

EXPERIMENTAL
For wet deposition (dipcoating and rollcoating), films were formed from water-based solutions of BTSE or bis-1,2-(triethoxysilyl)ethane, provided by Chemetall GmbH. BTSE is considered as a basic silane in various commercial silane mixtures for thin-film deposition. Concentrations range between 0.5 and 10 wt%. A selection of results is presented.
For atmospheric plasma deposition, films were deposited from a concentrated 98 wt% BTSE monomer solution. The apparatus consisted of a Surfx Technologies LLC, A-250D deposition system, operated at 250 W power of radio frequency 13.56 MHz. The deposition tool has a 5 cm^2 showerhead. The plasma was formed by feeding the argon into the system upstream of the electrodes at a flow rate of 30.0 l/min. The BTSE precursor was kept in a temperature controlled bath at 100 °C and was introduced into the plasma, downstream of the electrodes, by bubbling argon through the BTSE liquid. Samples were processed at deposition times ranging from 5 to 20 min at a distance of 0.5 cm downstream of the showerhead.

For vacuum plasma deposition, inductively coupled radio frequency glow discharge plasma deposition is used on mixtures of HMDSO or hexamethyldisiloxane with various levels of oxygen. The plasma chamber consisted of a grounded steel chamber with in the center a sample holder. The sample may be left at floating potential or grounded. The 13.56 MHz plasma source (ICP-P 200, JE PlasmaConsult GmbH, Germany) consisted of a four-antenna planar copper coil (Φ = 20 cm) which couples the RF energy through a dielectric window into the vacuum chamber. A home-made shower ring is located at 2 cm from the dielectric window of the antenna inside the plasma chamber.
The metal under investigation is 99.99 % aluminium sheet, electropolished and alkaline precleaned.

RESULTS AND DISCUSSION

Films formed by wet deposition

In figure 1 silane films deposited by rollcoating from water-based solutions of 0.5 and 5 wt% BTSE are shown in cross-section using FEG-scanning electron microscopy. For cross-sectional imaging purposes the coated aluminium samples were folded while submerged in liquid nitrogen; the liquid nitrogen results in the brittle fracture of the silane layer allowing when appropriately positioned in the vacuum chamber to observe the silane layer in cross-section.
The morphology of the water-based rollcoated BTSE layers is clearly depending on the solution concentration used, with a higher concentration resulting in a denser and more compact layer. For wet deposition (dip- or rollcoating) the BTSE film thickness is generally between 50 nm and 1 µm, depending on the concentration and application method used.

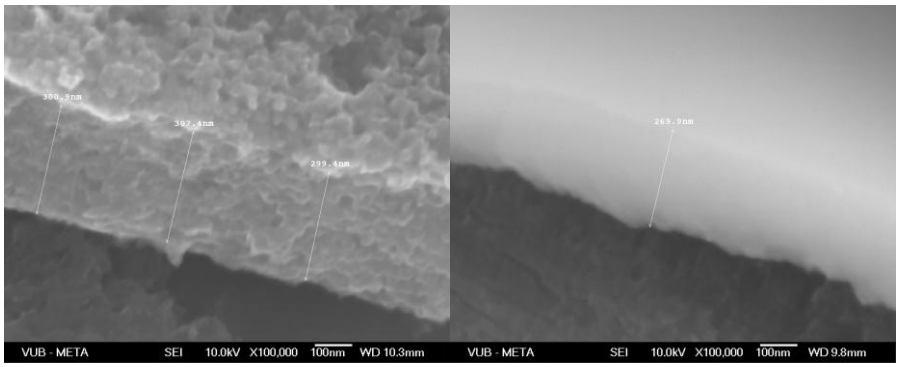

(a) *(b)*

Figure 1. FEG-SEM secondary electron images of (a) 0.5 wt% and (b) 2.5 wt% BTSE layers roll-coated on aluminium

In figure 2 the IR-SE absorption spectra (for two angles of incidence) show the typical IR absorption bands of a BTSE silane layer. The peaks are assigned in table 1.

Table 1. IR-SE absorption peak assignation for a BTSE film

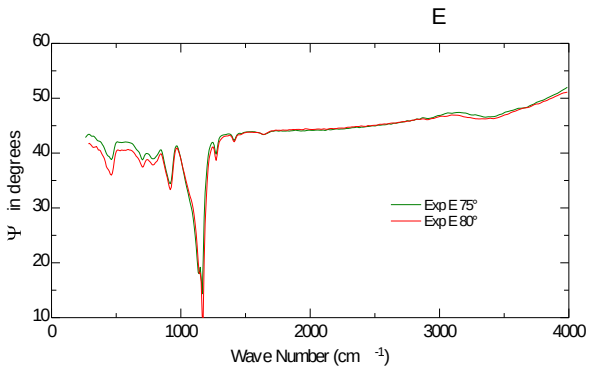

Figure 2. IR-SE absorption spectra (for 2 angles of incidence) of a 5 wt% BTSE silane layer

Peak position (cm^{-1})	***1.3 Assignment***
~ 700	-Si-CH_2-CH_2-Si-
~ 800	-Si-CH_2-CH_2-Si-
~ 920	-Si-O-H
~ 1050	-Si-O-Si-
~ 1150	-Si-O-C-
~ 1270	-Si-CH_2-CH_2-Si-
~ 1415	-O-CH_2-CH_3

Upon thermal curing of these layers the IR absorption signal of the Si-O-H bonds decreases and the one of the Si-O-Si bonds increases [13], indicating condensation reactions between silane molecules in the bulk of the layer, resulting in a cross-linked network. This network formation increases the barrier properties against hydration and corrosion of the substrate, as was observed using electrochemical impedance spectroscopy [13] (not shown).

Films formed by atmospheric plasma deposition

FTIR absorption spectra of plasma polymerized BTSE layers are shown in figure 3 as a function of deposition time and input power. Only three bands are present with peak positions at 1154 (Si-O-C), 912 (Si-O-C symmetric stretching) and 712 (C-H rocking) cm^{-1}. No significant shift is observed by varying the deposition time (figure 3a). By varying the input power (figure 3b) a small shift of these peaks is observed. This could be a consequence of the local environment of the Si–O groups which varies with the coating nature.

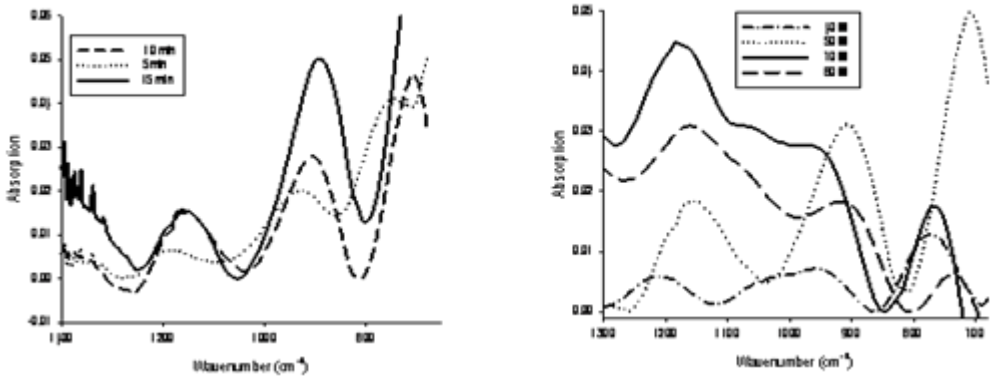

(a) *(b)*

Figure 3. IR spectra of plasma polymerized films deposited from BTSE monomer (a) Influence of the deposition time (atmospheric plasma, 50 W) and (b) Influence of the input power (atmospheric plasma, 10 min)

X-ray photoelectron spectroscopic analysis (XPS results not shown) reveals the presence of oxygen, carbon, aluminium and silicon at the surface. The presence of the aluminium signal suggests the deposition of only a very thin film (<10 nm). Other plasma conditions might result in thicker layers; this is being investigated in the ongoing project. With SEM (not shown) no particular film features are revealed.

Films formed by vacuum plasma deposition

The IR spectrum of a HMDSO plasma polymer is shown in figure 4. The bands are assigned in table 2. According to the literature the majority of these peaks were also observed in the polymer, which means a non-total decomposition of HMDSO into tiny fragments. The chemical composition of such films is often represented by the general formula SiO_xC_y:H.
The film shown in the spectrum of figure 5 was deposited under the presence of additional O_2. The addition of an oxygen content of 80% in the mixture results in a shift of the Si–O asymmetric stretching vibration. The spectrum of the plasma-polymerized coating obtained from a HMDSO/O_2: 20 %/ 80% mixture shows only a very weak band of the CH_3 vibration (1260 cm^{-1}) in Si–CH_3, and is characterized by the broadening of a band of the Si-O-Si vibration in the region 1000–1200 cm^{-1}.
One may conclude that in the case of pure HMDSO plasma, the deposited films consist of groups such as Si–O–Si, Si–O–C, Si–CH_3, CH_3. They can be considered as polymer-like coatings, comparable to the silane layers obtained by wet and atmospheric plasma deposition presented above. For the HMDSO/O_2:20%/80% mixture, the deposited coating is silica-like. It should be pointed out that if HMDSO is used for SiO_2 deposition, the O/Si ratio in the starting material is 0.5, which is only one quarter of that in SiO_2. Thus, in order to improve the oxygen balance, additional oxygen is necessary.

XPS was used to determine the relative amounts of O, C and Si at the polymer film surfaces (not shown). The results correlate with the FTIR results. There is a much lower C content in the polymer deposited under the influence of additional O_2. The relative proportion of the atoms at the polymer surface was found to be O/C/Si≈ 23.4/52.1/24.5 for pure HMDSO and ≈ 69/2/29 for an additional oxygen addition. If it can be supposed that the surface properties are representative of the bulk material, this means that Si-O-Si cross-links prevail in films that have grown in the presence of additional oxygen.

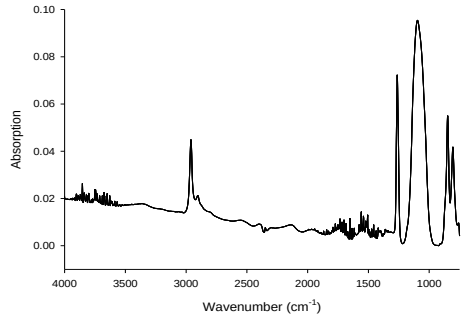

Figure 4. IR spectrum of plasma polymerized coating deposited from HMDSO (300 W, 300 mTorr, 10 min)

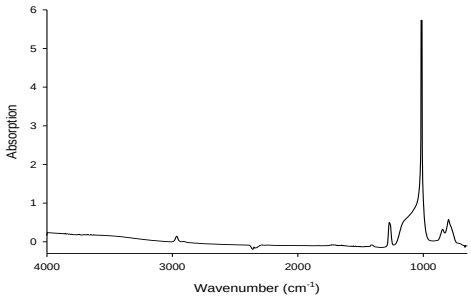

Figure 5. IR spectrum of plasma polymerized coatin deposited from 20% HMDSO/80% C (200 W, 300 mTorr, 10 min)

Table 2. Assignment of the absorption bands observed for the pp-HMDSO film

Peak position (cm^{-1})	**Assignment**
~ 2930	C-H symmetric and asymmetric stretching ($-CH_3$)
~ 1260	CH_3 symmetric bending ($-Si(CH_3)_X$)
~1100	Si-O/-Si-O-Si- stretching
800-795	$-Si(CH_3)_x$ stretching

CONCLUSIONS

The different deposition methods influence the type of silicon-based film that can be formed starting from a silane solution or precursor.
Using wet deposition, thin silane polymeric layers are formed with a uniform morphology depending in porosity on the solution concentration and deposition method used. The films can be cured to create barrier properties for corrosion protection.
Using atmospheric plasma, BTSE films can also be deposited, which was unknown until now. XPS and IR attest to the presence of Si-O bonds (siloxane).
For vacuum plasma deposition, SiO_X and SiO_XC_Y films are grown using HMDSO as a precursor. The films obtained from pure HMDSO plasma are polymeric; the surface film is rich in carbonated species. From the HMDSO/O_2 plasma, the deposited films are silica-like with only a low amount of carbon.

ACKNOWLEDGEMENTS

The project partners VUB, ULB, FUNDP and CoRI gratefully acknowledge the Belgian Science Policy for funding of the FOMOS project (P2/00/04) in the “Programme to stimulate knowledge transfer in areas of strategic importance”. www.belspo.be

REFERENCES

[1] R.W. Hinton, Metal Finishing 89 (1991) 55.
[2] M.A. Petrunin, A.P. Nazarov, Y.N. Mikhailovski, J. Electrochem. Soc. 143 (1996) 251.
[3] A.M. Beccaria, L. Chiarttini, Corros. Sci. 41 (1999) 885.
[4] W.J. van Ooij, D. Zhu, Corrosion 57(5) (2001) 413.
[5] A. Cabral, R.G. Duarte, M.F. Montemor, M.L. Zheludkevich, M.G.S. Ferreira, Corr.Sci. 47 (3) (2005) 869.
[6] A.M. Beccaria, C. Bertolotto, Electrochim. Acta 42 (1997) 1361.

[7] R. Tremont, H. De Jesus-Cardona, J. Garcia-Orozco, R.J. Castro, C.R. Cabrera, J. Appl. Electrochem. 30 (2000) 737.
[8] V. Subramanian, W.J. van Ooij, Corrosion 54 (1998) 204.
[9] W. Trabelsi, L. Dhouibi, E. Triki, M.G.S. Ferreira, M.F. Montemor, Surface & Coatings Techn. 192, 2-3 (2005) 284.
[10] W.J. van Ooij, A. Sabata, Surf. Interface Anal. 20 (1993) 475.
[11] F. Zucchi, G. Trabanelli, V. Grassi, A. Frignani, Proc. Eurocorr01, Associazione Italiana di Metallurgia (2001).
[12] E.P. Plueddemann, “Silane Coupling Agents”, 2nd ed., Plenum Press., New York, (1990).
[13] I. De Graeve, J. Vereecken, A. Franquet, T. Van Schaftinghen, H. Terryn, Progress in Organic Coatings 59 (2007) 224.

Implementing environmental friendly smart surfaces in steel sheet production.

De Strycker J., **Hörzenberger F.**

ArcelorMittal R&D Industry Gent, OCAS N.V., J. F. Kennedylaan 3, B-9060 Zelzate, Belgium, Joost.DeStrycker@arcelormittal.com, Telephone: + 32 9 345 12 40, Fax: + 32 9 345 12 04

ABSTRACT

For some decades hexavalent chromium compounds are known to be human carcinogens and have recently been addressed in legislations world-wide. To support these durable and environmental policies, ArcelorMittal introduced Cr(VI)-free post-galvanizing treatments on all its metallic coating lines in Western for more than three years and starts now production all over the world. New environmental friendly technologies were introduced. However, macro-, micro and nanoscopic analysis as well as depth and surface analysis of the layer were necessary to fully deploy these new technologies, creating a robust solution with optimum in-use and end-use properties comparable or even superior to the Cr(VI)-containing products. Some examples of the correlation between the macroscopic performance or galvanizing processing conditions and the micro and nanostructure of the treatments will be given. At several stages of the industrialization technology improvement was obtained by using the high-throughput (HTE) screening methodology, available at the Flanders Materials Centre (FLAMAC). The HTE-methodology proved to be very useful at early stages of the development and at the different optimization stages.

Hexavalent chromium was not the only hazardous compound which has been banned. Heavy metals like Pb, Cd, Hg, … and brominated organic compounds have also been eliminated. A general commitment towards environmental friendly products and green production technologies brought the development of the 'smart water' concept. In this concept the organic solvents were replaced by water. By introducing functional molecules and/or nano-sized particles different properties of the steel sheet like corrosion behavior, forming, … can be modified. The methodology and different examples will be elucidated. From this concept the development of ready-to-use semi-finished products was deduced. In this methodology different functions are added to the steel sheet surface, resulting in an easier production path of the finished product or even a lower amount of finishing steps. The eco-friendliness of the concept at different levels in the production process till the finished product will be shown. Finally the trend towards the complete elimination of any solvent, neither organic nor water, will be supported by examples for the protection of steel sheet and potential applications of new technologies like UV-EB curing, plasma treatments, … will be highlighted.

Medium pressure plasmas for surface modification.

***Morent R.*[1], De Geyter N.[1] and Leys C.[1]**

1 Research Unit Plasma Technology (RUPT), Department of Applied Physics, Faculty of Engineering, Ghent University , J. Plateaustraat 22, B-9000 Ghent, Belgium, rino.morent@ugent.be, Telephone: +32-(0)9-2644257, Fax: +32-(0)9-2644198

INTRODUCTION

Polymers are frequently used as films and foils for packaging, protective coatings and sealing applications, because of their superior bulk properties, such as transparency, a high strength-to-weight ratio, good thermal resistance,…. Despite these excellent characteristics, polymers are often unsuitable to use due to their low surface energies. Therefore, surface treatments are usually necessary to improve surface wetting and adhesion properties [1,2]. Chemical activation of the surfaces is the most utilized method, however, the ecological requirements force the industry to search for alternative environmentally benign methods. Recently, the application of cold plasmas to modify surface properties of polymers is experiencing rapid grow [2–9]. Plasma contains activated species, such as electrons, ions, radicals, photons,… which are able to initiate chemical and physical modifications at the polymer surface [5]. The advantage of this technique is that plasma treatment only changes the uppermost atomic layers of a material surface without modifying the bulk properties [10]. Moreover, it is a rapid and environmentally friendly process [11]. Atmospheric pressure plasmas [2,7,8,12–14] are predominantly studied, because the industry requires a plasma technology which can be integrated in a continuous production or finishing line. Therefore, vacuum and medium pressure technology is regarded as being non-competitive. However, plasma treatment at medium pressure (1-10 kPa) has some advantages over atmospheric pressure. A large plasma volume, available for surface treatment, can be easier created at medium pressure than at atmospheric pressure. This can result in a higher overall productivity at medium pressure. Furthermore, at medium pressure, the pumping equipment is relatively inexpensive. Until now, only little research [15-20] is done on medium pressure plasma treatment of textiles and polymers. Therefore, in this paper, the efficiency of a medium pressure and atmospheric pressure dielectric barrier discharge (DBD) is evaluated and some typical applications are given.

MEDIUM PRESSURE VERSUS ATMOSPHERIC PRESSURE

The differences in chemical and physical modifications between medium and atmospheric pressure plasma-treated PET films are studied in [20]. The plasma treatments were performed using a filamentary DBD operating in a helium/air mixture. The plasma treatment led to a significant decrease in water contact angle for both medium and atmospheric pressure plasma treatments. It was shown that the surface modification was quite homogeneous despites the filamentary character of the discharge. XPS measurements showed that the decrease in water contact angle was due to the incorporation of oxygen-containing functional groups (C–O and O–C=O) on the PET surfaces. At low energy densities, a medium pressure plasma treatment was more energy-efficient in incorporating oxygen on the surface than an atmospheric pressure plasma treatment. This effect was explained by the larger diameter of the microdischarges and the lower quenching of atomic oxygen at medium pressure. Results also showed that at energy densities higher than ±200 mJ/cm^2, no significant difference was found between medium and atmospheric pressure plasma treatments. AFM images of the medium and atmospheric pressure plasma-treated PET films showed that the water contact angle of the films could be decreased to a minimum without causing significant physical degradation of the surface. Thus, DBD treatments at medium and atmospheric pressure provide an efficient modification of the chemical surface properties without destroying the mechanical properties of the PET films. The ageing behaviour of the PET films was also studied after plasma treatment in the helium/air mixture at medium and atmospheric pressure. During the ageing process, the induced oxygen-containing groups re-orientated from the surface into the bulk of the material. In contrast to the plasma treatment behaviour, results showed that the operating pressure used during plasma treatment had no influence on the ageing behaviour of the plasma-treated PET films.

APPLICATIONS OF MEDIUM PRESSURE DISCHARGES

Surface activation of polymers

In [16-18], different polymers, like PET and PP (films and non-wovens), were modified by a DBD in air, helium and argon at medium pressure. The surface was analysed with XPS, contact angle or liquid absorptive capacity measurements and SEM. The films modified in air, helium and argon, showed a significant decrease in contact angle and the non-wovens showed a significant increase in liquid absorptive capacity, both due to the incorporation of oxygen-containing groups, such as C-O, O-C=O and C=O. It was shown that an air plasma is more efficient in incorporating oxygen functionalities than an argon plasma, which is more efficient than a helium plasma. SEM-pictures of the plasma-treated non-wovens revealed that the hydrophilicity of the polymers could be increased to a saturation value without causing physical degradation of the surface. The ageing behaviour of the plasma-treated samples after storage in air was also studied in detail. During the ageing process the induced oxygen-containing groups re-orientate into the bulk of the material. This ageing effect was the smallest for the argon-plasma treated polymer samples, followed by the helium-plasma treated samples, while the air-plasma treated samples showed the largest ageing effect.

Penetration of plasma into porous structures

Plasma treatment of textiles is becoming more and more popular as a surface modification technique. Plasma treatment changes the outermost layer of a material without interfering with the bulk properties. However, textiles are several millimetres thick and need to be treated homogeneously throughout the entire thickness. To control the penetration depth of the plasma effect, it is necessary to study the influence of operating parameters. In [15], three layers of a 100% polyester non-woven were treated in the medium pressure range (0.3–7 kPa) with a dielectric barrier discharge to study the influence of pressure and treatment time. Current and voltage waveforms and Lichtenberg figures were used to characterize the discharge. Process pressure proved to have an important effect on the penetration of the plasma through the textile layers. This was caused not only by the pressure dependence of diffusive transport of textile modifying particles but also by a different behaviour of the barrier discharge.

Adhesion enhancement of PDMS used for flexible and stretchable electronics

Currently, there is a strong tendency to replace rigid electronic assemblies by mechanically flexible and stretchable equivalents. This emerging technology can be applied for biomedical electronics, such as implantable devices and electronics on skin. In the first step of the production process of stretchable electronics, electronic interconnections and components are encapsulated into a thin layer of polydimethylsiloxane (PDMS). Afterwards, the electronic structures are completely embedded by placing another PDMS layer on top. It is very important that the metals inside the electronic circuit do not leak out in order to obtain a highly biocompatible system. Therefore, an excellent adhesion between the 2 PDMS layers is of great importance. However, PDMS has a very low surface energy, resulting in poor adhesion properties. In [19], PDMS films were plasma treated with a DBD operating in air at medium pressure. Contact angle and XPS measurements revealed that plasma treatment increased the hydrophilicity of the PDMS films due to the incorporation of silanol groups at the expense of methyl groups. T-peel tests showed that plasma treatment rapidly imparted adhesion enhancement, but only when both PDMS layers were plasma treated. Results also revealed that it is very important to bond the plasma-treated PDMS films immediately after treatment. In this case, an excellent adhesion was maintained several days after treatment. The ageing behaviour of the plasma-treated PDMS films were also studied in detail: contact angle measurements showed that the contact angle increased during storage in air and angle-resolved XPS revealed that this hydrophobic recovery was due to the migration of low molar mass PDMS species to the surface.

REFERENCES

[1] D.J. Upadhyay, N.Y. Cui, C.A. Anderson, N.M.D. Brown, Appl. Surf. Sci. 229 (2004) 352.
[2] M. Sira, D. Trunec, P. Stahel, V. Bursikova, Z. Navratil, J. Bursik, J. Phys., D, Appl. Phys. 38 (2005) 621.
[3] O. Kwon, S. Tang, S. Myung, N. Lu, H. Choi, Surf. Coat. Technol. 192 (2005) 1.

[4] N. Cui, N.M.D. Brown, Appl. Surf. Sci. 189 (2002) 31.
[5] R. Riccardi, R. Barni, E. Selli, G. Mazzone, M.R. Massafra, B. Marcandalli, G. Poletti, Appl. Surf. Sci. 211 (2003) 386.
[6] G. Borcia, C.A. Anderson, N.M.D. Brown, Appl. Surf. Sci. 225 (2004) 189.
[7] G. Borcia, C.A. Anderson, N.M.D. Brown, Plasma Sources Sci. Technol. 12 (2003) 335.
[8] M.J. Shenton, M.C. Lovell-Hoare, G.C. Stevens, J. Phys., D, Appl. Phys. 34 (2001) 2754.
[9] N. De Geyter, R. Morent, C. Leys, Surf. Coat. Technol. 201 (6) (2006) 2460.
[10] H.U. Poll, U. Schladitz, S. Schreiter, Surf. Coat. Technol. 142–144 (2001) 489.
[11] J. Yip, K. Chan, K.M. Sin, K.S. Lau, J. Mater. Process. Technol. 123 (2002) 5.
[12] F. Massines, G. Gouda, J. Phys., D, Appl. Phys. 31 (1998) 3411.
[13] D. Trunec, A. Brablec, J. Buchta, J. Phys., D, Appl. Phys. 34 (2001) 1697.
[14] T. Vatuna, J. Pichal, P. Spatenka, J. Koller, L. Aubrecht, A. Kolouch, Proc. 2nd International Workshop on Cold Atmospheric Pressure Plasmas: Sources and Applications (CAPPSA2005), Bruges - Belgium, (2005), p. 275.
[15] N. De Geyter, R. Morent, C. Leys, Plasma Sources Sci. Technol. 15 (2006) 78.
[16] N. De Geyter, R. Morent, C. Leys, L. Gengembre, E. Payen, Surf. Coat. Technol., 201, (2007) p. 7066.
[17] R. Morent, N. De Geyter, C. Leys, L. Gengembre, E. Payen, Surf. Coat. Technol., 201 (2007), p. 7847.
[18] R. Morent, N. De Geyter, C. Leys, L. Gengembre, E. Payen, Text. Res. J., 77, 471-488, 2007
[19] R. Morent, N. De Geyter, F. Axisa, N. De Smet, L. Gengembre, E. De Leersnyder, C. Leys, J. Vanfleteren, M. Rymarczyk-Machal, E. Schacht, E. Payen, Journal of Physics D: Applied Physics, 40 (23), 2007
[20] N. De Geyter, R. Morent, C. Leys, L. Gengembre, E. Payen, S. Van Vlierberghe, E. Schacht Surf. Coat. Technol., In press (2008) doi:10.1016/j.surfcoat.2007.11.001.

A comparative analysis of two industrial wet-coating processes and atmospheric plasma for metal passivation

Zimmermann F.[1], Benetto E.[1], Welfring J.[1], Bardon J.[2], Ruch D.[2]

1 Centre de Ressources des Technologies pour l'Environnement, francois.zimmermann@tudor.lu, Telephone : (+352) 54 55 80 645
2 Laboratoire des Technologies Industrielles, Centre de Recherche Public Henri Tudor, 66 rue de Luxembourg, 4002 Esch-sur-Alzette, Luxembourg

Since the prohibition of hexavalent chromium for corrosion protection coating, many chrome-free alternatives have been developed. Currently, most of the topcoat processes used for metal passivation are based on wet chemical techniques, which are expected to have a significant environmental impact. In order to comply with the stringent regulatory framework, the industrial decision-makers' strategy is to support sustainable production and competitiveness by focusing on a maximum of two or three topcoat processes. In parallel, researchers have continually attempted to develop improved coatings that can be implemented in industry. Among the most innovative coating, plasma polymerized coatings are now emerging and their technical performances are more and more competitive. Moreover, plasma techniques are often considered to be environmentally friendly solutions since there are solvent free.

The aim of this study is to compare the two main industrial wet-topcoats (Scenario 1: E-passivation and Scenario 2: Easyfilm) with a promising dry coating technique using atmospheric plasma (Scenario 3: ppHMDSO). The scenarios were defined in agreement with the surface finishing industrial partners. The comparison is based on economic, technical and environmental performance criteria. This comparison emphasizes that Scenario 1 is the least expensive coating process, its anti-corrosion resistance performs poorly, but is sufficient for most applications and its environmental impact is relatively low. Scenario 2 is more expensive but it offers very good resistance properties to corrosion. Its environmental impact is more significant, depending however on what impact categories are considered. Scenario 3, using atmospheric plasma, is the most expensive and the incurred costs are not competitive with other scenarios yet. Nevertheless, its anti-corrosion resistance is of high quality and continually improving. Scenario 3, unexpectedly, can have an important environmental impact depending on the coating quality required. It is shown that high environmental impacts and high costs are both linked with the same process steps. Thus optimization guidelines of this developing process in terms of price and environmental impact reduction will need to be defined. We conclude with recommendations directed towards atmospheric plasma topcoats developers.

INTRODUCTION

The topical restriction of toxic hexavalent chromium for large manufacturing activities gives rise to speculation finding suitable alternatives. In the surface finishing industry, passivation treatment by chromatation process is known as a cost-effective and functional process for metal passivation. A couple of valuable and emerging alternatives are being developed in academic and industrial research centres. Typically, industrials are more focused on the development of wet chrome-free processes, which are more and more eco-friendly as organic solvents are no longer used (e.g. E-passivation® or Easyfilm®) while research centre are more oriented toward innovative and dry processes, e.g. atmospheric plasma coating. Considering the worldwide production of coated steel sheets (more than 250 millions tons/years in Europe[6], US and Canada[7]), the identification of the best available techniques for anti-corrosion coating based on cost, technical and environmental performance criteria is crucial. Nevertheless, the evaluation of the criteria is not trivial mainly due to multicriteria aspects, overlaps of foreground and background processes and the relative lack of studies in literature for a comprehensive approach. This study aims to compare three relevant scenarios (E-passivation, Easyfilm and ppHMDSO), which can replace chromatation. The purpose

[6] European Steel Technology Platform, http://cordis.europa.eu/estep
[7] Metals Service Center Institute, http://www.ssci.org

of the comparison is to inform the industrial decision-makers about the performances of scenarios and provide recommendations for the sustainability of an atmospheric plasma development for coating.

APPROACH AND SCOPE

Definition of comparison criteria and functional unit

The comparison criteria include basic economic and technical evaluations, i.e., coating process costs and anti-corrosion resistances, and environmental impacts generated by the scenarios and evaluated using a Life Cycle Assessment (LCA) approach.
LCA approach allows one to compare scenarios fulfilling the same function(s) quantified by a functional unit. The main function considered in this study is the metal protection against corrosion. O*ne square meter of metal to coat*[8] is defined here as the functional unit.
It is supposed that:

- the function (protection against corrosion) is the same for all the scenarios, even if the protection provided by plasma topcoat may be significantly higher,
- the corrosion problem is not the responsible factor of the end-of-life materials.

These assumptions represent most of the situations. However, the LCA approach in this study does not take yet into account the "quality" of coating. These additional consideration might be useful when, for exemple, materials are exposed to a strong corrosive atmosphere. These aspects are under investigation and will be integrated within a comprehensive approach in the near future.

Scenarios

Data and information concerning the two industrial wet-coating scenarios (E-passivation and Easyfilm) were collected through a survey in two surface finishing facilities. The total production of steel sheet coating in both facilities is more than 74 millions m^2 (420 000 t/year). E-passivation and Easyfilm are already implemented at the industrial scale[9]. The third scenario, a dry-coating process using atmospheric plasma, is currently under research and in the development phase[10]. A few results from the survey concern the current development status and the (perceived) advantages/drawbacks of the three scenarios, summarized in **Fout! Verwijzingsbron niet gevonden.**.

Table 1: current status and perceived advantages/drawbacks of scenarios

Scenarios	S1 : E-passivation	S2: Easyfilm	S3: ppHMDSO
Status	Existing industrial process	Existing industrial process	Process in R&D
Perceived advantages	-Cost-effective - process easy to implement/operate	- very competitive coating quality - easy process	Innovative and environmentally sound alternative to wet chemical processes
Perceived drawbacks	-Not sustainable -Limited performance	Costly	Not implemented yet at industrial scale

Scenario S1: E-passivation is a water-based solution spread at the surface of metal by roll coaters. The coating deposition process is similar to the chromatation process, nevertheless, other metal-based compounds replace the chromium compounds. The substances contained in the E-passivation® preparation are mainly: zinc dihydrogénophosphate (10-25 %), manganese dihydrogénophosphate (2.5-10 %) and hexafluorotitanic acid (2.5-10 %). A post-treatment by air-

[8] In this study, the coated metal is galvanized steel (Aluzinc® galvanization layer from ArcelorMittal Dudelange)
[9] ARCELOR Dudelange plants (Ewald Giebel and Galvalange)
[10] Laboratoire des Technologies Industriels (LTI), Luxembourg, and Flemish institute for technological research (VITO), Belgium,
see for example : J. Bardon, J. Bour, H. Aubriet, D. Ruch, B. Verheyde, R. Dams, S. Paulussen, R. Rego, D. Vangeneugden, *Plasma Process. Polym.*, 2007, 4, S445

drying in heat furnace is required to increase the hardening and adherence of the coating. This scenario already exists in industry and currently represents about 15 % of the market share of galvanized steel coating in industry.

Scenario S2. Easyfilm is also a water-based solution spread at the surface of metal by roll coaters. The Easyfilm® preparation includes acrylic polymers dissolved in aqueous solution. The final coating solution requires an addition of ammonium zirconium carbonate as an additive (2 %)[11]. A post-treatment by air-drying in heat furnace is required to increase polymer crosslinking. This scenario represents about 40 % of the market share and it is more and more in demand by the customers.

Scenario S3. The plasma polymerized HMDSO (ppHMDSO) technique is completely different from the two previous scenarios. Water-based solutions are not required. The chemical precursor is HMDSO (hexamethyldisiloxane), a pure organic siloxane. HMDSO is atomized into a gas mixture (N_2/O_2) before entering the plasma zone. The plasma is generated between two high voltage electrodes. The steel sheet to be treated is the grounded lower electrode (**Fout! Verwijzingsbron niet gevonden.**).
The carrier gas mixture containing the precursor aerosol is injected into the plasma through a slit between the upper electrodes. Additional N_2 flows are injected through air knife systems to avoid contamination of the plasma zone by outside air and to create a laminar flow in the plasma zone. The precursor is broken down into plasma, then rearranged and deposited as a polymer. The coating step is carried out at atmospheric pressure and ambient temperature. An additional post-treatment step is a curing plasma treatment done under similar conditions as during the coating procedure, but without precursor injection.

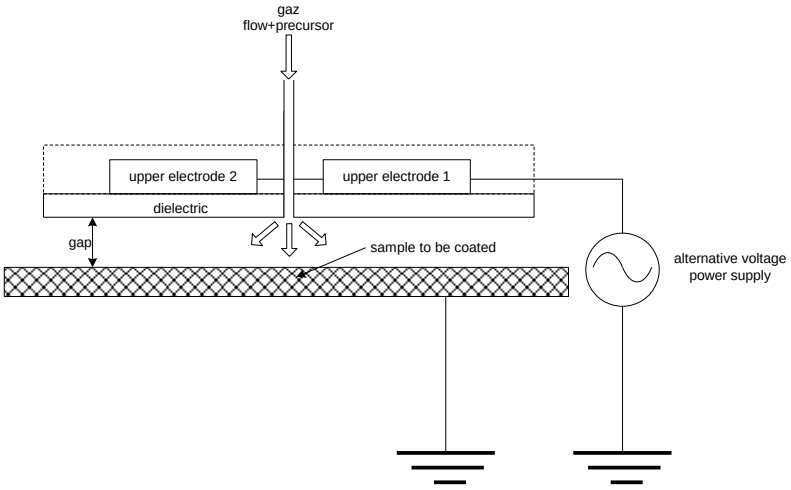

Figure 5. Schematic representation of the evaluated atmospheric plasma process

MULTICRITERIA COMPARISON

Economic comparison

The economic criterion is the coating process costs, including material and energy costs. Since detailed costs of existing scenarios are confidential, the comparison can only be qualitative (**Fout! Verwijzingsbron niet gevonden.**), based on the information gathered through the survey.

Table 2. Qualitative comparison of coating scenarios process costs

Scenarios	**S1 : E-passivation**	**S2: Easyfilm**	**S3: ppHMDSO**
Qualitative evaluation of	☺☺	☺	☹

[11] The production of ammonium zirconium carbonate has not been considered in LCA since no life cycle inventory data are publicly available so far

coating process costs			

ppHMDSO is by far the most expensive scenario at the current stage of development. The detailed ppHMDSO costs[12] are listed in table 3. The main cost is due to the high volume of carrier gases required by the atmospheric plasma process.

Table 3. Coating process costs of ppHMDSO scenario

	HMDSO raw material	**Gas flows (N_2 and O_2)**	**Electrical energy**	**Total cost**
Cost of ppHMDSO scenario	0.096 €/m^2	0.777 €/m^2	0.006 €/m^2	0.879 €/m^2

Technical comparison

The main technical aspects of scenarios are given in **Fout! Verwijzingsbron niet gevonden.**.

Table 4: Comparison of technical aspects of scenarios

Scenarios	**E-passivation**	**Easyfilm**	**ppHMDSO**
Coating quality/resistance*	😐	☺☺	☺☺
Properties of coating	Anticorrosion, painting adherence, autolubrication	Anticorrosion, painting adherence, autolubrication	Anticorrosion, other properties not tested yet
Current coating speed	180 m/min	180 m/min	4 m/min

* A quantitative evaluation of coating quality is under investigation and will be given in next stage

Environmental impacts comparison

Based on data collection and inventory, the three scenarios were evaluated through a standardized Life Cycle Assessment (LCA) approach. The lifecycle of the production of energy (e.g. electricity) and raw materials (e.g. HMDSO) used by the coating process was modeled and the environmental damages generated were evaluated using well-established methods[13, 6]. The environmental damages and impacts related to the waste and pollutant emissions from the coating process and end-of-life goods were also considered.
The main damage and impact results are shown in table 5[14].

Table 5: Extrapolation of environmental damages considering the industrial partners' annual production of steel sheets coated in a given scenario

Impact/Damage categories	**Environmental impacts (eq persons-year)**		
	E-passivation	**Easyfilm**	**ppHMDSO ***

[12] The price of HMDSO per mass unit was supplied by Dow Corning silicones (Discussion with Dow Corning by email, 17/04/07 - HMDSO referenced as 200 Fluid, 0.65 CST). The estimated price of gas flows was fixed following the agreed price between ArcelorMittal and Air Liquide. The price of electrical energy (kWh) is applied by SOTEL (electricity transport society in Luxemburg) for ArcelorMittal.
[13] ISO (International Organisation for Standardization). ISO 14040 Environmental management – Life cycle assessment – Principles and framework. ISO 14044 Environmental management – Life cycle assessment – Requirements and guidelines. 2006
[6] Frischknecht R., Jungbluth N., Althaus H.-J., Doka G., Heck T., Hellweg S., Hischier R., Nemecek T., Rebitzer G., Spielmann M. (2004) Overview and Methodology. ecoinvent report No. 1. Swiss Centre for Life Cycle Inventories, Dübendorf.
[7] Humbert S, Margni M, Jolliet O (2005). IMPACT 2002+: user guide. Draft for version 2.1. Lausanne: EPFL, p40
[14] A "person-year" represents the average impact in a specific category "caused" by a person during one year in Europe. In a first approximation, for human health, it also represents the average impact on a person during one year (e.g. an impact of 3 persons-year in ecosystem quality represents the average annual impact of 3 Europeans. This last interpretation is also valid for climate change and resources). It is calculated as the total yearly damage score due to emissions and extractions in Europe divided by the total European population[7]

Climate change	282	383	321 to 3851 *
Ecosystem quality	28	6	19 to 223 *
Human health	268	59	269 to 3229 *
Resources	328	454	459 to 5506 *

* The variation depends on the time to process the functional unit and the quality required for coating as quality is assumed to linearly increase with process time

The environmental impact contributions of the main ppHMDSO sub-processes are given in table 6.

Table 6: Environmental impact contributions of the main ppHMDSO sub-processes

Process parts	**N_2 feed**	**Electricity**	**CH_3Cl Production**	**Others**
Environmental impact contributions	73 - 82 %*	7 - 14 %*	5 - 16 %*	2 - 3 %*

* The percentages of contribution vary because they depend on what impact category is considered

CONCLUSIONS

The results of the comparative analysis suggest the following conclusions:

- As expected, the E-passivation topcoat is cost-effective and its anti-corrosion resistance is less performing but sufficient for many customers. However, contrasting with the perceived ideas, the environmental impacts caused by E-passivation scenario are relatively low and, if corrosion is not the responsible issue of the end-of-life products, it currently appears to be the most sustainable topcoat process regarding especially the climate change and the exhaustion of resources,.
- The Easyfilm topcoat is more expensive but it offers a very good resistance properties to corrosion. The Easyfilm scenario seems to have a relative low impact on the ecosystems quality and human health, and a quite significant influence on climate change and the exhaustion of resources. If corrosion appears to be a critical factor leading to waste generation, then the Easyfilm topcoat is advised.
- The ppHMDSO topcoat is the most expensive and not competitive yet compared to other topcoat scenarios. Though its anti-corrosion resistance is by now of high quality and is continually improving. Unfortunately, the environmental impacts caused by ppHMDSO can be relatively high and currently has very likely the highest impact in all studied categories. This is an unexpected result as ppHMDSO coating was expected to be an environmentally friendly technique. However the environmental impacts of ppHMDSO scenarios have a large range of variation depending on the quality required for coating. The impacts could then be widely minimized. In addition, the N_2 feed gas is responsible for 73 to 82 % of the environmental impacts and the gas flow nearly represents 90 % of the ppHMDSO process costs. The required electrical consumption to generate plasma and the CH_3Cl production processes, one of the main reagents required to produce HMDSO precursor, also contribute strongly to the environmental damages. Reducing cost and environmental impacts are strongly connected as important quantities of materials are involved. Moreover, the improvement potential of the plasma process is high and the process is being optimized under the frame of research projects.

To support the development, the competitiveness and the sustainability of atmospheric plasma for large-scale coating, we recommend the following research strategies:

- Further investigation should be lead allowing reasonable use of gas flow as a carrier gas and an inerting gas. Possible solutions might be a combination of the following; a gas feed composition closer to the air and a decrease of the gas flow required to carry the precursor and confine the plasma zone e.g. by confining plasma zone with physical barrier.
- A decrease of the electrical energy demand by decreasing the required number of coating and curing time, and/or by increasing the coating speed. (consequences on used gas and precursor quantities as well!)
- An improvement of polymerization and coating yields under plasma and a recycling/recovery of the exhausted gas/products e.g. by co-injecting polymerization catalysts with the precursor, setting up an air-knife suction mechanism, or recovering the unreacted HMDSO.

REFERENCES

European Steel Technology Platform, http://cordis.europa.eu/estep
Metals Service Center Institute, http://www.ssci.org
ARCELOR Dudelange plants (Ewald Giebel and Galvalange)
Laboratoire des Technologies Industriels (LTI), Luxembourg, and Flemish institute for technological research (VITO), Belgium,
see for example : J. Bardon, J. Bour, H. Aubriet, D. Ruch, B. Verheyde, R. Dams, S. Paulussen, R. Rego, D. Vangeneugden, *Plasma Process. Polym.,* 2007, 4, S445
ISO (International Organisation for Standardization). ISO 14040 Environmental management – Life cycle assessment – Principles and framework. ISO 14044 Environmental management – Life cycle assessment – Requirements and guidelines. 2006
Frischknecht R., Jungbluth N., Althaus H.-J., Doka G., Heck T., Hellweg S., Hischier R., Nemecek T., Rebitzer G., Spielmann M. (2004) Overview and Methodology. ecoinvent report No. 1. Swiss Centre for Life Cycle Inventories, Dübendorf.
Humbert S, Margni M, Jolliet O (2005). IMPACT 2002+: user guide. Draft for version 2.1. Lausanne: EPFL, p40

Theme 5: Controlling friction and preventing wear in industrial processing

All aspects of tribology are welcomed including experimental, modelling and theoretical work, as well as case studies. Papers dealing with practical problems and their solutions with respect to wear prevention and frictional effects on functionality and power gain of machines are especially welcome to promote the effective transfer of research results into industrial practice.

Effect of nanostructuring and metallic alloying on the tribological properties of WC-12Co coatings

***Basak A. K.*[1], Achanta S.[1], Celis J.-P.[1], Vardavoulias M.[2], Matteazzi P.[3]**

1 Katholieke Universiteit Leuven, Dept. MTM, B-3001 Leuven, Belgium,
Animesh.Basak@mtm.kuleuven.be, Tel.: +32 (0)16 321238, Fax: +32 (0)16 321991
2 PyroGenesis SA, Technological Park of Lavrion, 19500, Lavrion, Greece
3 MBN Nanomaterialia spa (www.mbn.it) and CSGI Via G. Bortolan 42 31050 Vascon di Carbonera (TV) Italy

ABSTRACT

Nanostructuring is an attractive way to improve certain material properties like toughness, strength, hardness etc. This research was initiated to find out the effect of nanostructuring on tribological properties of nanostructured cermet coatings deposited by HVOF process. The present study focuses on the tribological behaviour of nanostructured HVOF WC-12Co based cermet coatings tested under different contact conditions, namely reciprocating sliding, two-body abrasion, and three-body abrasion. The effect of alloying elements like Al and/or Cr to nanostructured WC-12Co coatings, on the tribological properties is the main interest. Friction and wear behaviour of such nanostructured WC-12Co based cermet coatings are compared to the ones of common engineering wear resistance materials and coatings (see Figures 1 and 2). This study showed that the effect of nanostructuring on the increase of wear resistance is more pronounced than on the reduction of friction. The addition of Al addition as alloying element increases the wear resistance of nanostructured WC-12Co coatings by a factor of two, where as Cr addition decreases it by a factor of one and half. An in-depth investigation of nanostructured WC-12Co-2Al coatings by TEM was carried out to clarify the role of aluminium addition on the wear resistance.

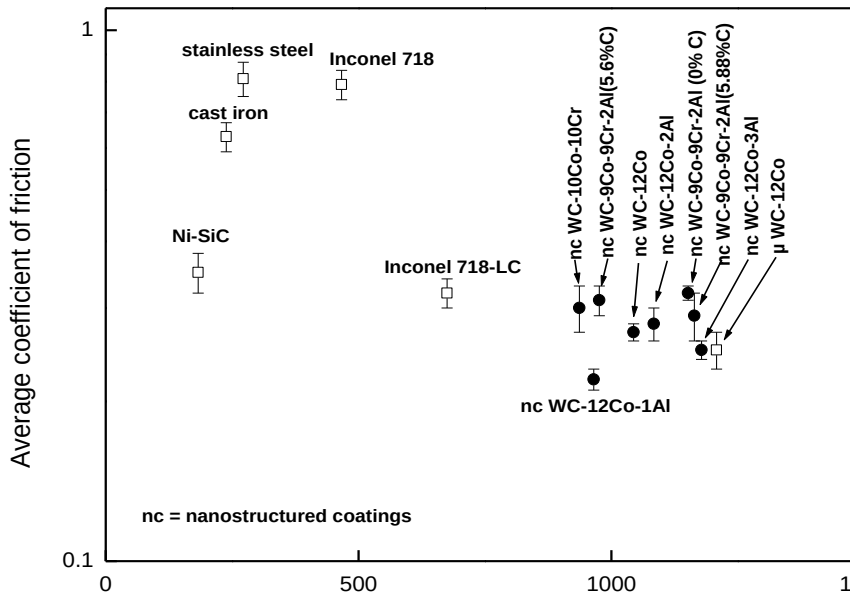

Figure 1: Comparison of HVOF sprayed nanostructured WC-Co coatings with reference coatings and materials in terms of friction sliding against corundum performed at 5 N normal force, 500 µm peak-to- peak displacement amplitude, 5 Hz frequency, 10,000 cycles. Fretting tests were done in ambient air of 23° C and 50% RH.

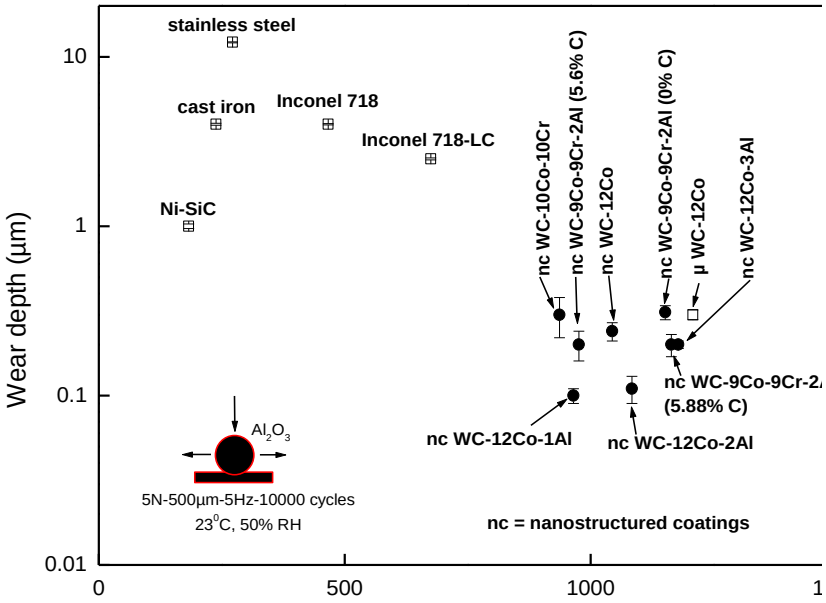

Figure 2: Comparison of HVOF sprayed nanostructured WC-Co coatings with reference coatings and materials in terms of wear depth after sliding against corundum performed at 5 N normal force, 500 µm peak-to- peak displacement amplitude, 5 Hz frequency, 10,000 cycles. Fretting tests were done in ambient air of 23° C and 50% RH.

ACKNOWLEDGEMENTS

This work was done in the framework of an European GROWTH 2003–2006 project Nanospraying (contract G5RDCT-
2002-00862). A. K. Basak acknowledges Katholieke Universiteit Leuven for providing a fellowship.

Progress in development of the Al eutectic alloys for preventing wear at elevated temperatures

Milman Yu.[1], Grinkevych K.[1], Korzhova N.[1], Podrezov Yu.[1], Barabash O.[2] and Legkaya T.[2]

1 Frantsevich Institute for Problems of Materials Science, National Ukrainian Academy of Sciences, 03142, 3, Krzhyzhanovsky St., Kyiv, Ukraine
2 Kurdyumov Institute for Metal Physics, National Ukrainian Academy of Sciences, 03680, 36, Acad. Vernadsky St, Kyiv, Ukraine

INTRODUCTION

Cast aluminum alloys are prominent candidates to be increasingly used for future cars. The development of these alloys began at the middle of the XX-th century and a great number of various cast alloys has been developed [1]. Most spread are complexly doped alloys on the base of the eutectic of the binary Al-Si system alloying with Mg, Cu, Zn, Fe, Ni, Mn and Ti. Nowadays the development of these alloys continues and is realized in different ways: the improvement of their chemical and phase compositions; development of casting technologies of those alloys, and others. It is worth noting that one of the essential difficultly removable drawbacks of modern cast alloys concerns their chemical and phase compositions. The matter is in that the increase in the number and amount of alloying elements is inevitably accompanied by a decrease in the melting temperature of alloys. However, there exists a solution of these problems which seem to be unsolvable, prima facie.
This solution is based on the change of the basic binary system by a ternary system containing a quasibinary eutectic [2, 3]. This will ensure a higher melting temperature of developed alloys and its conservation on a high level on the introduction of alloying elements and will lead to a damping of the diffusion-dependent processes on high temperatures of the operation. Such an eutectic should be formed by Al and an intermetallic phase which must be more refractory and more thermodynamically stable as compared with Si phase.
The analysis of the available ternary phase diagrams of Al with different elements showed that the ternary Al-Mg-Si system and its quasibinary section α-Al-Mg_2Si can be such a base system most completely satisfying the above-presented requirements. For example, the melting temperature of the quasibinary eutectic of this section is 597 °C, which is greater than the melting temperature of the binary eutectic system Al-Si (577 °C). This paper gives a progress of developments in the use of new eutectic aluminum alloys to reduce wear and friction.

Experimental details

For carrying out of researches alloys of ternary Al-Si-Mg system with a different volume part of eutectic which are located on quasibinary section, and also alloyed eutectic the laboratory ingots have been produced in the air in a resistance furnace in Al_2O_3 crucibles (below ASM alloys). For comparison commercial 356.0 and 390.0 alloys were subjected to the tests. The alloys were studied by the methods of light microscopy, thermal analysis and scanning electron microscopy. The short-term tests in tension were carried out in the temperature interval of 20-400 °C by the conventional method including the heating of a sample without load for 0.5 h at a testing temperature with the subsequent loading up to the fracture. The rate of tension was 10^{-3} sec^{-1}. The tests were performed on cylindrical samples.
The quasistatic and dynamic tribology tests were carried out by the tribocomplex CATC by the ball-on-plate test with reciprocating sliding movement of the indenter was an 8 mm in diameter at ambient and elevated temperature. The sphere indenter was made from Si_3N_4 ceramic. The sliding velocity was 0.013 m/s, the load on the indenter was 22 N, a lubricant of motor oil TNK SAE15W40 was used. The tests in the quasistatic mode were carried out at constant load. The tests in the dynamic mode were carried out imposing an alternating component of the load with the amplitude equal to 10 % of that for the static mode and with the frequency of 25 Hz. The duration of each test was 30 minutes. The results of experiments within restricted temperature range (20 °C - 300 °C) are denoted by the subscripts “s” and “d” for the static and dynamic modes, respectively. During the

motion of the indenter some material is displaced from the contact zone, and lateral pile-ups of material form on both sides of the friction track. The transverse profiles of the friction tracks for areas under investigation were determined using a profilometer. The friction force F was registered by measuring the displacement of an elastic circular element rigidly connected with the specimen. All the tribological characteristics represent the average of three experiments. The error in determining of wear profiles depend on the vertical and horizontal magnifications of the profilometer and did not exceed 1 %.

Results and discussion

Early after both the thermodynamic calculations and the complex experimental study of phase equilibrium and structures of alloys, a fragment of the melting diagram in the Al-corner of the ternary Al-Mg-Si system with a high accuracy was constructed [2] and the region of concentrations, in which the univariant eutectic alloys (α-Al+Mg_2Si) exist are determined.
In the given work the dependences of wear and frictional force of the alloys of a quasibinary section on the volume part of a strengthening phase have been established (Fig. 1).

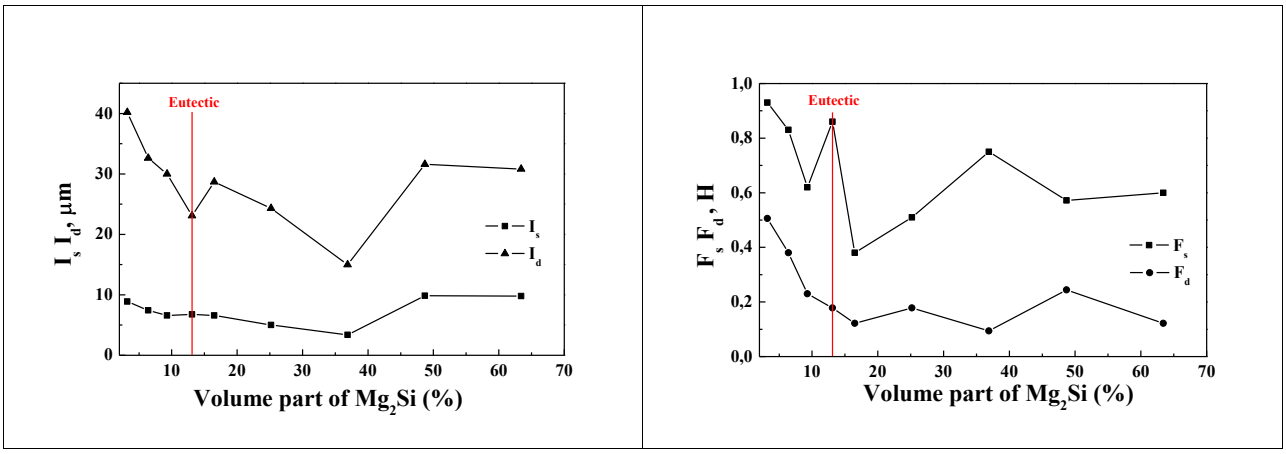

Figure 1. Linear wear and frictional force of alloys which are situated on the quasibinary (α-Al+Mg_2Si) section of the ternary Al-Mg-Si system at static (I_s, F_s) and dynamic (I_d, F_d) loading.

These dependences reveal a nonmonotonic character: minimum values of the wear at static loading are attained in the hypereutectic region for the alloy with 36.9 vol. % of Mg_2Si. It is possible to explain it by change of the mechanism of wear process: in structure of hypereutectic alloys the large precipitations of a brittle phase are present (Fig. 2).
For all alloys under study, we observed the effect of the intensification of wear in the dynamical mode of a loading. On the curve of the wear rate I_d, two minima are observed: at the volume part of Mg_2Si equal to 13.1 % (eutectic alloy) and 36.9 % (hypereutectic alloy). The analysis of the obtained results allows us to conclude that, in order to get the good wear resistance, one should choose an alloy close to the eutectic one as the base alloy (wear rate of hypereutectic alloys at 36.9 % still less, but this alloys have low plasticity). In view of the above-presented discussion, we chose the hypoeutectic (α-Al+Mg_2Si) alloy of quasibinary section as a baseline one.

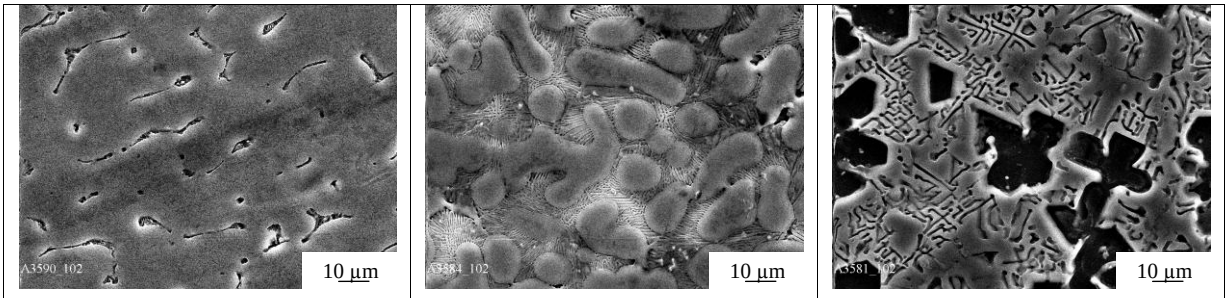

hypoeutectic alloy (3.16 vol. % Mg_2Si)	hypoeutectic alloy (9.25 vol. % Mg_2Si)	hypereutectic alloy (36.94 vol. % Mg_2Si)

Figure 2: The typical structures of alloys of quasibinary (α-Al+Mg_2Si) section of the ternary Al-Mg-Si system, SEM.

It is known, that wear-resistant materials are, as a rule, complexly doped alloys with a complicated composition. To get a high level of the physical and mechanical properties at room and elevated temperatures, the baseline eutectic alloy was doped with a complex metals, whose introduction ensures the realization of the solid-solution and dispersive strengthening mechanisms. On the one hand, such a system conserves a high melting temperature of base alloys. On the other hand, it must ensure the efficient strengthening at elevated temperatures. The possible concentration of each element of the alloy and their relative concentrations were determined.
The comparison of the temperature dependence of the mechanical properties of ASM alloys with those of the known commercial cast 356.0 alloy indicates their advantage in the whole temperature interval under study (Fig. 3). These strength characteristics are much superior to those of hypoeutectic Al-Si alloy in the «dangerous interval» (260 °C) for piston. Moreover, this advantage over other cast alloys of Al enhances with increase in the testing duration.

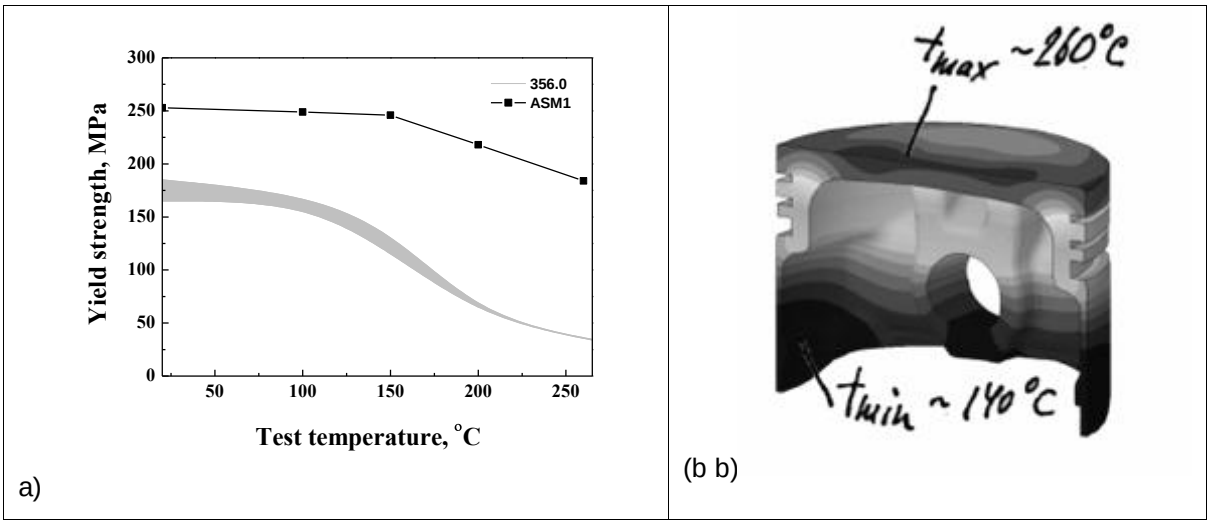

Figure 3. Comparison of the temperature dependence (a) of the mechanical properties of (α-Al+Mg_2Si) eutectic alloyASM1 with those of the known commercial cast alloy 356.0 [4] and the piston temperature fields (b) "AVTRAMAT"©*[5].*

Alloying elements influence on the friction processes considerably and raise the wear resistance of ASM alloys (Table 1).

Table 1: Results of tribotechnical tests for cast aluminum alloys.

Alloy	Quasistationary regime		Dynamical regime	
	I_S (μm)	F_S (H)	I_S (μm)	F_S (H)
ASM alloys				
ASM 1 (baseline alloy)	6.298		15.58	
ASM 2 (Me^{III} Me^{IV})	6.322		16.097	
ASM 3 ($Me^{III}Me^{IV}$B Mn)	2.99		8.39	
ASM 4 (Me^{III} Me^{IV} Fe Ni)	6.322	1.240	14.08	0.255
ASM 5 (Me^{III} Me^{IV} Cr Mn)	4.711	1.208	7.846	0.168
ASM 6 (Me^{III} Me^{IV} Cu Ni)	3.612	1.005	8.445	0.174
Commercial cast alloys				
356.0	2.204	0.8963	15.34	0.192
390.0	1.557	0.786	1.989	0.115

Actually the wear of ASM alloys is less than of alloy 356.0 at dynamic loading. However the 390.0 alloy has the best characteristics of wear resistance at room temperature.
What properties ASM alloys have at the increased temperatures? The established better wear resistance of complexly doped alloy ASM as compared with the alloy 356.0 was confirmed also in the tests at enhanced temperatures (Fig. 4). Moreover on raising temperature, the wear resistance of alloyed ASM alloys is the same as 390.0 alloy at dynamic loading, and same one is the less at static loading

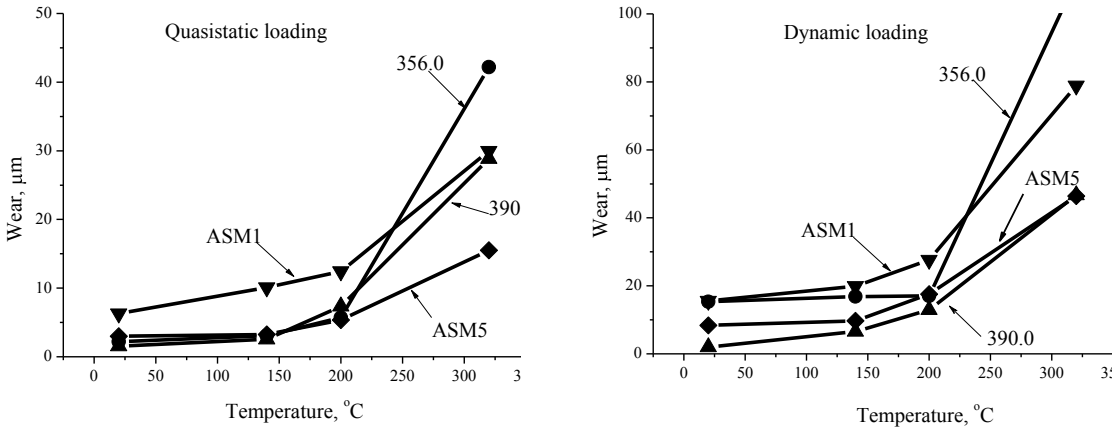

Figure 4: The wear vs temperature under quasistatic and dynamic loading.

The wear resistance is an integral characteristic of alloys. Up to now, there appear the works which relate the wear resistance to the hardness and the ultimate strength. It is assumed that the higher these parameters, the higher the wear resistance. It is obvious that one should not relate the wear resistance to average mechanical properties of the bulk of an alloy by simple empiric relations. One should relate it to the properties of structural components and their resistance to the fracture under various specific local loads. On such an approach, we account the multiple interrelations between the structure and properties of alloys and the factors of external actions. The process of wearing is characterized by the interaction of surfaces which leads to the formation of the certain fields of stresses in the surface layers, plastic deformations, and temperatures, structural transformations, and the accumulation of defects in the structure. The ability of alloys to resist to the wear is considered as a structurally sensitive characteristic especially under dynamic loading. The analysis of the literature and our studies [6-8] indicate that two main ways of the synthesis of wear-resistant alloys are possible:

- creation of materials with a structure capable to attract the energy introduced from outside and to dissipate it by means of reversible phase and structural transformations;
- creation of materials with a relatively thermostable structure.

As cast wear-resistant materials, it is expedient to apply the alloys with heterogeneous structure. In this case, the wear resistance is significantly affected by the structure of a metal matrix and the amount and the nature of a strengthening phase. In the first approximation, such alloys can be considered as natural composites.
The great possibilities to increase the wear resistance of separate details are opened by the development of special technological methods aimed at the improvement of the quality of ingots and their structure. A temperature of the pouring, cooling rate, design features of mold influence the process of crystallization and the formation of a structural state of an alloy on the various surfaces of a cast detail.
In view of the performed studies, we conclude that the new cast alloys with high thermal stability and high wear resistance can be successfully used for the substitution of available hypoeutectic alloys of the binary system Al-Si for application in automotive industry.

CONCLUSIONS

1. The new conception that is based on the using the ternary phase diagram Al-Mg-Si that have quasibinary eutectic type cross sections between the aluminum solid solution and the intermetallic phases (α-Al-Mg_2Si) was proposed.
2. The peculiarities of a structure**,** tribology parameters of the new alloys ensure their high wear resistance and high heat resistance, which are important for the operation of piston grooves, piston bosses, and piston skirt.
3. It was shown that the cast (α-Al-Mg_2Si) alloys of Al-Mg-Si ternary system with a unique complex of physical, mechanical and tribology properties can be successfully used for the substitution of conventional Al-Si hypoeutectic alloys.

REFERENCES

1. Franklin Bronze & Alloy Company; www.franklinbronze.com.
2. O.M. Barabash, O.V. Sulgenko, T.N. Legkaya and N.P. Korzhova. Experimental Analysis and Thermodynamic Calculation of the Structural Regularities in the Fusion Diagram of the System of Alloys Al-Mg-Si. J.Phase Equilibria, Vol. 22, No. 1 (2001) 5.
3. O.M. Barabash, Yu.V. Milman, N.P Korzhova, T.N. Legkaya, and Yu.N. Podrezov. Design of New Cast Aluminium Materials using Properties of Monovariant Eutectic Transformation L⇆α-Al+Mg_2Si. Materials Science Forum, Vol. 396-402, Part 2 (2002) 729.
4. Aluminum and Aluminum Alloys. ASM International Materials Park, USA, 1993.
5. "AVTRAMAT" www.avtramat.com
6. D.K. Dwivedi. Sliding temperature and wear behaviour of cast Al–Si base alloy. Materials. Science and Engineering A, Vol. 19, No. 8 (2003) 1091.
7. I.M. Hutchings, A.T. Alpas, S. Wilson. Wear of Aluminum-based Composites. Compr. Compos. Mater., 3 (2000) 501.
8. M. Elmadagli, T. Perry, A.T. Alpas. A parametric study of the relationship between microstructure and wear resistance of Al-Si alloys. Wear 262 (2007) 79.
9. K. Grinkevych, Some postulates of the structural dynamic concept of the tribo-system and its practical implementation. Friction and Wear, Vol.24, No.3 (2003) 344.

Product embedded surface sensors integrated under wear resistant coatings

Lars Pleth Nielsen[1], Helena Ronkainen[2], Tommy Schonberg and Magnus Svensson[3], Niels Peter Østbø[4]

1 Danish Technological Institute, Denmark
2 VTT Technical Research Centre of Finland, Finland
3 Acreo, Sweden
4 SINTEF ICT, Norway

ABSTRACT

The results of the research work carried out in the transNordic COSMOS project (**Co**mponents and **S**mart Machines with **M**icroNan**o** Surface Embedded **S**ensors) will be given. The project has successfully merged clean room based sensor design with wearresistant hard coatings fabricate a temperature sensor on a steel substrate.
The best result was obtained for a multilayer coating system such as: (i) an Atomic Layer Deposition of Al2O3 followed by Dual Magnetron Deposition of Al2O3, or (ii) several layers of Diamond Like Carbon (Ta:DLC), or (iii) a multilayer system composed of several layers of Al2O3/Cr2O3. The sensor adhesion was observed to be increased significantly by treating the substrate with oxygen implantation.
The temperature sensor was buried under DiamondLike Carbon (DLC) revealing promising properties for a range of industrial applications.
The COSMOS project was funded by Nordic Innovation centre (NICE) and the participating research organizations.

Low-friction coatings on elastomers

M. Rombouts, A. Vanhulsel, B. Verheyde, W. Engelen and D. Havermans

Vlaamse Instelling voor Technologisch Onderzoek (VITO), Boeretang 200, 2400 Mol, Belgium, Marleen.Rombouts@vito.be, Telephone: +32 14 33 57 45, Fax: +32 14 32 11 86

INTRODUCTION

An important driving factor for new developments in the field of tribology are environmental considerations concerning the effects of grease and lubricants. Sliding and sealing systems with elastomer moving components generally require the use of lubrication due to the high dry sliding friction of elastomers. The subject of this study is the application of different coatings on elastomers with the aim to reduce or eliminate lubrication. Altering the tribological performance by surface treatment has the advantage that the material can be tailored in terms of tribological properties while its bulk properties are not significantly affected. The surface treatments involved in this study are laser cladding for the production of thick polymer (composite) coatings and atmospheric plasma treatment for the production of thin coatings. The effect of the coatings on the friction coefficient against bearing steel was evaluated by pin-on-disc tribotesting.

RESULTS AND DISCUSSION

Laser cladding

The used substrate material is thermoplastic polyurethane (TPU). Powder mixtures based on commercially available polyamide 11 powder are used as feedstock for the coating process. The effect of solid lubricants like MoS_2 and PTFE is studied. In addition, TPU coatings with incorporation of MoS_2 are produced by laser cladding. The roughness value R_z of the coatings is 15-30 µm, which is one order of magnitude larger than of the TPU substrate and the thickness is about 100 µm. The coatings are characterized by the presence of spherical gas inclusions, which are caused by thermal degradation.

The friction coefficient during ball-on-disc tribotesting is presented in **Fout! Verwijzingsbron niet gevonden.**. The PA 11 and PA 11 + 9% MoS2 coatings have a similar friction characteristic. The coatings both reduce the friction of TPU with 50%. The PA 11 + 15% PTFE coating clearly yields the largest reduction in friction. A stable friction coefficient of about 0.2 is obtained.

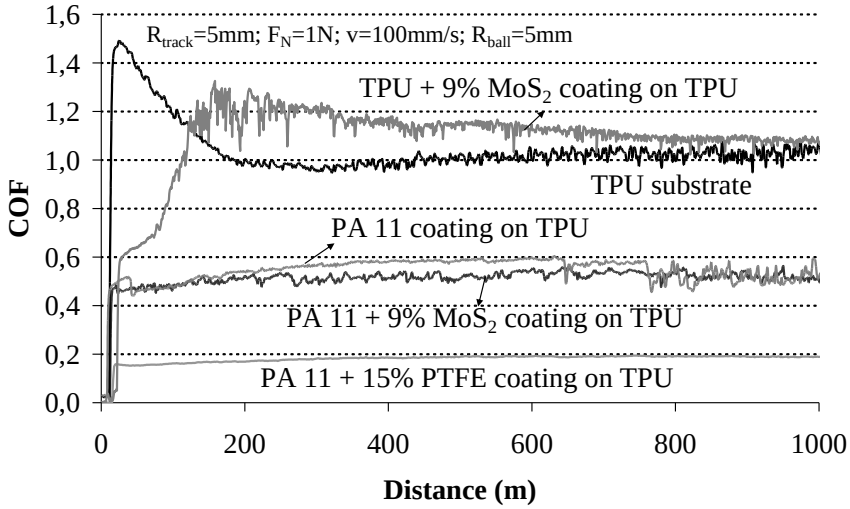

Figure 6. Friction coefficient during ball-on-disc tribotesting of untreated and laser cladded TPU.

Atmospheric plasma treatment

Two types of plasma coatings have been deposited on HNBR substrate: GLYMO and APEO. Both coatings have low roughness values, and they do not alter the roughness of the uncoated substrate material. Directly after coating deposition cracks are visible on the surface of the coatings.
After a running-in period of some hundreds of meter, a decrease of 55% in the friction coefficient is found for the GLYMO coating compared to the untreated HNBR (see **Fout! Verwijzingsbron niet gevonden.**). Applying an APEO-coating on the elastomer substrate resulted in even lower friction values (decrease with 80%).
Although the GLYMO coating was partially removed from the substrate material due to a lacking adhesion of the coating to the substrate material, the friction level remained stable for the full duration of the tribotest.

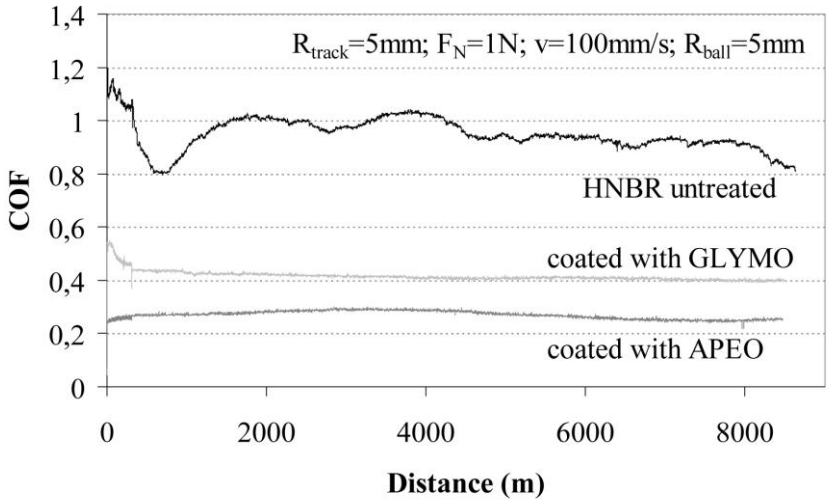

Figure 7. Friction coefficient during ball-on-disc tribotesting of untreated and atmospheric plasma treated HNBR.

CONCLUSIONS

Surface treatment of elastomers by laser cladding and atmospheric pressure plasma coating has been performed. The results of tribological testing of these treated samples are very promising as a significant reduction of the coefficient of friction against steel is demonstrated.

ACKNOWLEDGEMENTS

The Author(s) wish to acknowledge the support of the Partners of the Kristal project and in particular Merkel Freudenberg and Macpuarsa, and the European Commission for their support in the integrated project “Knowledge-based Radical Innovation Surfacing for Tribology and Advanced Lubrication” (EU Project Reference NMP3-CT-2005-515837).’

A novel form of hard hydrogenated amorphous carbon for tribologic applications

R. Groenen[2], S.V. Singh[1], T. Zaharia[1], M. Creatore[1], K. Van Hege[2] and M.C.M. van de Sanden[1]

[1] Eindhoven University of Technology, Department of Applied Physics, P.O. Box 513, 5600 MB Eindhoven, The Netherlands, s.v.singh@tue.nl, Telephone: 31 40 247 5617, Fax: 31 40 245 6442
[2] NV Bekaert SA, Dept. of Advanced Coating Technologies, Bekaertstraat 2, 8550 Zwevegem, Belgium

INTRODUCTION

A novel form of amorphous hydrogenated carbon deposited using an expanding thermal remote Ar/C_2H_2 plasma is reported. The plasma is generated in a cascaded arc at subatmospheric pressure in argon. The discharge expands into a low pressure (remote) chamber where acetylene is introduced downstream by means of an injection ring. The downstream plasma is characterised by a low electron temperature which leads to ion driven chemistry and negligible physical effects like ion bombardment (< 2 eV) on the substrate. Furthermore, no external bias has been applied, discarding any possibility of high energy ion bombardment. The carbon films are deposited by a PECVD (plasma enhanced chemical vapour deposition) process at growth rates exceeding 15 nm/s.

EXPERIMENTAL RESULTS

The material properties are studied with respect to a range of argon to acetylene gas flow ratios. Distinct from previous works [15, 16], relatively low argon to acetylene gas flow ratio has been used in this study. Infrared transmission shows a reduced concentration of CH stretching and that endgroups (sp^2 - CH_2 and sp^3 – CH_3) are absent from these films. Other characteristics of the films include a relatively low optical band gap, low hydrogen content (< 25%) and a high refractive index. Nanoindentation measurements revealed hardness to be in excess of 16 GPa.

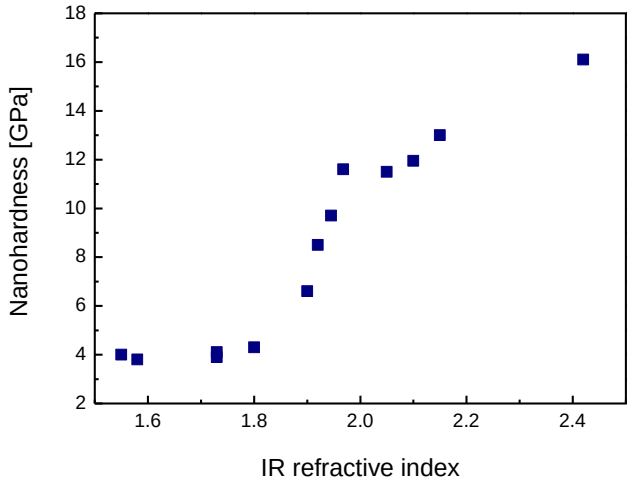

Figure 8. Nanohardness against IR refractive index for amorphous hydrogenated carbon films deposited under various plasma conditions

[15] Gielen, J.W.A.M, van de Sanden, M.C.M., Kleuskens, P.R.M. Schram, D.C. 1996. Quality improvement of plasma-beam-deposited amorphous hydrogenated carbon with higher growth rate. Plasma Sources Sci. Technol. 5: 492-498.
[16] Benedikt, J., Woen, R.V., van Mensfoort, S.L.M., Perina, V., Hong, J., van de Sanden, M.C.M. 2003. Plasma chemistry during the deposition of a-C:H films and its influence of films properties. Diamond and Related Materials 12: 90-97.

The hydrogen content extracted from IR spectra using absorption coefficient of Tanaka et al. [17] indicates a substantial decrease in bonded hydrogen concentration. From Threshold Ionization Mass Spectrometry we have clear indications that the atomic hydrogen to C_3H_x radical flux is paramount in understanding the deposition process and is key in the formation of this novel carbon based material [18].

Further characterizations by means of Raman spectroscopy, spectroscopic ellipsometry (SE) and Rutherford back scattering (RBS) indicate that the carbon and hydrogen atoms are well cross-linked in a graphite-like hydrogenated structure making these films suitable candidates for tribologic applications.

The film properties are presented in view of the specific plasma chemistry taking place in the expanding thermal plasma.

CONCLUSIONS

Amorphous hydrogenated carbon films have been deposited at high rates using an expanding thermal plasma technique. The extensive characterization of these films revealed promising mechanical and optical properties, making them suitable candidates for tribologic applications.

[17] Tanaka, M., Iwata, Y., Fujimoto, F., Komaki, K., Kobayashi, K., Yamashita, H., Haba., M.1990. Determination of the infrared proportionality coefficient of the CH_n stretching mode for a-C:H and a-SiC:H films using ERD methods. Nucl. Instr. Meth. Phys. Res. B45: 223-226.

[18] Benedikt, J., Schram, D.C., van de Sanden, M.C.M. 2005. Detailed TIMS Study of Ar/C_2H_2 Expanding Thermal Plasma: Identification of a-C:H Film Growth Precursors. J. Phys. Chem. A, 109: 10153-10167.

Corrosion-wear studies on PVD coatings for aeronautical applications.

R. Bayón, A.Igartua, G. Mendoza, X. Fernández, I. Ciarsolo, U. Ruiz de Gopegui[1],

1 Fundación TEKNIKER (www.Tekniker.es), Avda. Otaola, 20, 20600 Eibar, Spain. Telf. +34 943206744. rbayon@tekniker.es

One of the greatest environmental problems in the aeronautic world is the current replacement of chromium VI and cadmium, present in numerous processes including anodizing and hard chromium plating as well as mastic or paint type ingredients used in the aeronautic, military and space industries.

One alternative for the substitution of these materials on steel substrates is the application of PVD coatings. PVD coatings can increase the lifetime and steel substrate service quality, due to enhanced tribological and corrosion resistance properties.

In this work, corrosion and wear behaviour of PVD coated nickel based alloy has been investigated by means of electrochemical measurements such as electrochemical impedance spectroscopy and dynamic polarizations because they are powerful analysis tools which can provide a wide information about the effect of the coating structure (pores and defects) on the corrosion processes that take place when the material is in contact with an aggressive environment.

INTRODUCTION

Inconel belongs to the family of austenitic nickel-based superalloys. This alloy possesses several interesting properties like high resistance to oxidation and corrosion and high strength over a wide range of temperatures. That makes it particularly attractive in a great number of applications such as gas turbine blades, seals, combustors, turbocharger rotors and seals, high temperature fasteners and heat exchanger tubing. Particularly, strengthened INCO 738 superalloy is extensively used in hot sections of aero-engines and power generation turbines due to its excellent elevated temperature strength and hot corrosion resistance.

Functional hard chromium coating is a process usually employed in the manufacturing and maintenance operations of aircraft, vehicles and ships, both in military and civil sectors. Hard chromium is used to produce a high wear-resistant coating but the plating bath used in the process contains hexavalent chromium, which has bad health and environmental effects. In the last years, alternative technologies have been developed for replacement electrodeposited chromium. The most commonly alternatives are physical vapour deposition (PVD), chemical and plasma-assisted chemical vapour deposition (CVD, PACVD) and thermal spraying.

The tribological properties and high temperature corrosion resistance of CrN-PVD coatings on substrates of INCO 738 have been studied previously for military applications. These studies showed an improvement in wear characteristics, corrosion resistance, and rolling contact fatigue behaviour of INCO 738 with CrN and TiN coatings deposited by magnetron sputtering.

In this work, CrN and multilayer TiN/CrN -PVD coating is proposed as alternative to chromium coating on Inconel substrate. Corrosion and wear properties will be compared to consolidate this type of clean coatings as an effective alternative in aeronautical applications.

Materials characterization

CrN monolayer, TiN/CrN multilayer and hard Cr coatings were deposited on superalloy INCO 718 substrates. CrN and TiN/CrN coatings were deposited by PVD (Physical Vapour Deposition) method. The chemical composition of substrate (Inconel 718) is showed in Table 1

Table 1. Inconel chemical composition

element	C	Mn	Si	Cr	Ni	Fe	Co	Al	Ti	Mo	V	Cu	Nb
%	0.05	0.26	0.05	18.50	bal.	17	-	0.47	1.15	3.11	0.03	0.04	5

Samples surfaces were carefully characterized before and after corrosion and tribocorrosion studies. Before corrosion and tribocorrosion tests, Vickers hardness measurements, adhesion tests, roughness and thickness measurements were performed. After tests, SEM, EDS, confocal and optical microscopy techniques were applied on surfaces in order to understand the combined corrosion-wear degradation processes suffered.

Experimental

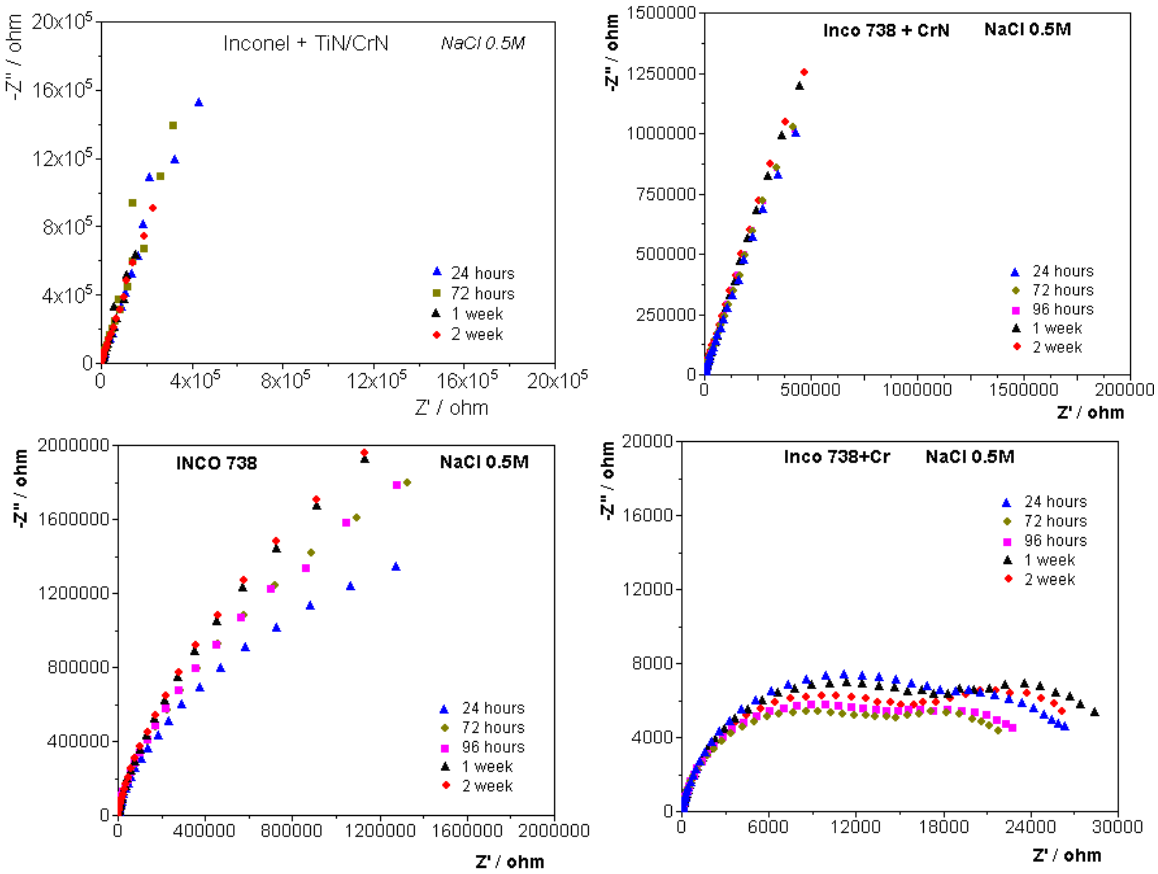

Figure 1. Nyquist diagrams of surfaces studied in NaCl 0.5M for different immersion times

Corrosion and corrosion-wear tests were carried out at room temperature under aerated conditions. The solution used to simulate an aggressive environment was NaCl 0.5M. The electrochemical techniques employed to characterize these materials were electrochemical impedance spectroscopy and cyclic polarizations. Impedance spectroscopy diagrams and potentiodynamic curves were registered with an Autolab PGSTAT30/FRA2 system (Eco Chemie).

The electrochemical measurements were carried out in a conventional cell of three electrodes where the reference one was Ag/AgCl (0.207 V vs SHE), the counter one was a stainless steel piece and the working electrode the sample under study.

For perform corrosion-wear measurements simultaneously a tribometer adapted for this type of measurements was selected with ball on disk configuration. As counterbody we have employed silicon nitride balls of 4mm of diameter. The applied load was set at 10N and the rotating speed 25 rpm. Potential and coefficient of friction were measured simultaneously before, during and after the sliding test. Impedance spectroscopy was registered before and after the mechanical interactions in order to compare the evolution of the surfaces state due to the wear effects.

Analyzing experimental results obtained in corrosion tests (Figure 1), it is possible to observe an improvement of the PVD coatings properties with time.

When corrosion and wear test are performed simultaneously, is possible to evaluate the surfaces degradation as consequence of wear and the corrosive media. Electrochemical parameters such as potential and current can be related with friction coefficient in order to establish synergic relationships of the global process. In all surfaces tested, the break down of the passive layer as consequence of the mechanical load (Figure 2) is the common effect observed but the kinetic of this process differs in each surface.

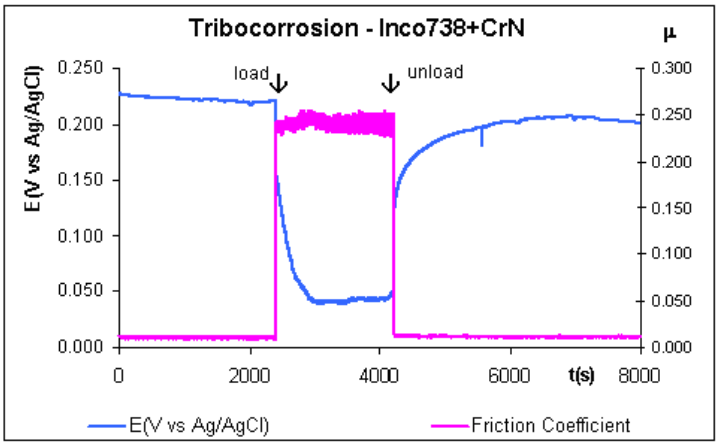

Figure 2. CrN coating wear track after tribocorrosion tests

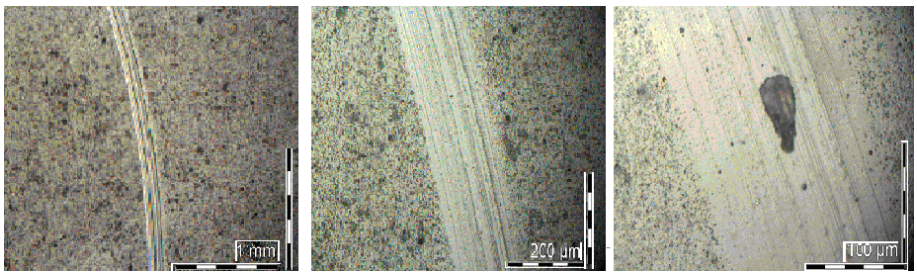

Figure 3. CrN coating wear track after tribocorrosion tests

The exhaustive surface analysis after test (Figure 3) will allow us to determine the quality of the alternative coatings proposed for hard chromium replacement

CONCLUSIONS

Under corrosion and wear conditions, PVD coatings improve substrate properties as well as hard chromium properties. PVD-TiN/CrN multilayer layers show especially good wear resistance in the corrosive media tested under the specific mechanical conditions applied. Differences between tribocorrosion behaviour of both PVD coatings are minimal, so these types of layers could be in certain situations, an acceptable clean alternative to electroless chromium.

ACKNOWLEDGEMENTS

The authors would like to acknowledge to the Spanish Minister Of Science and Technology for the financial of the national project RAMPE, as well as the partners involved, AERNNOVA
ITP, SENER, INTA, GUTMAR and CESA.

REFERENCES

M. C. Chaturvedi, O. A. Ojo and N. L. Richards. Azojomo “Diffusion Brazing of Cast Inconel 738 Superalloy”.Journal of materials online, 2005.
J.A. Picas, A, Forn, G, Matthaus “HVOF coatings as an alternative to hard chrome for piston and valves”. Wear 261 (2006) 477-484
B. Navinsek, P. Panjan, I. Milosev. “PVD coatings as an environmentally clean alternative to electroplating and electroless processes”. Surface and coatings Technology 116-119 (1999), 476-487
F. Rastegar, D. E. Richardson. “Alternative to chrome: HVOF cermet coatings for high horse power diesel engines”. Surface and coatings technology, 90 (1997) 156-163
A. Skopp, N. Kelling, M. Woydt, L. M. Berger. “Thermally sprayed titanium suboxide coatings for piston ring/ cylinder liners under mixed lubrication and dry-running conditions”. Wear (2006).
E. Broszeit, C. Friedrich, G. Berg. “Deposition, properties and applications of PVD CrxN coatings”. Surface and coatings technology 115 (1999) 9-16.
Beatty, J.H. ; Huang, P.J. ; Fountzoulas, C.G. ; Kelly, J.V. “Tribological evaluation of magnetron-sputtered coating for military applications”. Technical report 1999
J. Ross Macdonald. Impedance Spectroscopy. Wiley, 2005
F. Mansfeld, M. W. Kendig, E. M. Meyer, G. Lindberg. “A computer analysis of electrochemical impedance data” Corrosion science 9 , 1983
C. Liu, Q. Bi, A. Matthews. “EIS comparison on corrosion performance of PVD TiN and CrN coated mild steel in 0.5N NaCl aqueous solution”. Corrosion science, 43, 2001
J.-P. Celis, P. Ponthiaux, F. Wenger. “Tribo-corrosion of materials: Interplay between chemical, electrochemical, and mechanical reactivity of surfaces”. Wear, 261, 2006
V. Vignal, N. Mary, P. Ponthiaux, F. Wenger. “Influence of the friction on the local mechanical and electrochemical behaviour of duplex stainless steel”. Wear, 261, 2006.
S. Kaciulis, A. Mezzi, G. Montesperelli, F. Lamastra, M. Rapone, F. Casadei, T. Valente, G. Gusmano. “ Multi-technique study of corrosion resistant CrN/Cr/CrN and CrN:C coatings”. Surfaces and coatings technology, 201, 2006.
J. Creuss, H. Idrissi, H. Mazille,F. Sanchette, P. Jacquot. “Improvement of the corrosion resistance of CrN coated steel by an interlayer”. Surface and coatings technology, 107, 1998

Steps to efficient laboratory simulation of wear and lubrication issues in industrial components

Satish Achanta*, *Dirk Drees
Falex Tribology N.V., Wingepark 23B, Rotselaar B3110, Belgium

ABSTRACT

Industrial components are often evaluated in different modes for example through field tests, bench tests, component bench tests, model tests, and finally lab scale tests. Each of these simulations gives useful information concerning the performance of a component with a certain degree of accuracy. Three important parameters namely degree of extrapolation, cost, and testing time could be used to express the versatility of each simulation process [1]. A schematic representation of different simulation tests with respect to these parameters is shown in Fig. 1.

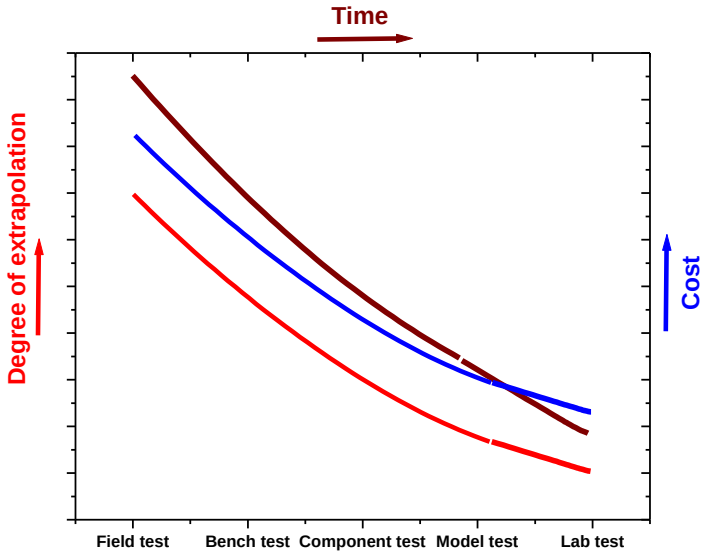

Fig. 1. Schematic representation of information gathered from different simulation tests

Fig. 1 indicates that field test is the best simulation one could opt to have a good degree of extrapolation for an industrial component. However, the cost and time scales involved are so high that not many tests can be simulated to evaluate a range of components. Among all the simulation tests laboratory scale testing is ideal method to screen a range of components because of low price and small time scale. However, a major downside of lab scale tests is its poor degree of extrapolation. In this paper it is shown as how this low degree of extrapolation of test results could be improved through smart selection and modification of test parameters is shown and obtained results were compared with field observations.

Case study on lubricant additives [2]

A major requirement for refrigeration oils is that they provide effective lubrication for compressor bearings. Especially automotive air conditioning compressors have to work under hard conditions. Bearing loads vary and can be extremely high; in addition to this the oil film is often disturbed by refrigerant “flooding” or can be disrupted by vaporization of dissolved refrigerant. For proper bearing design viscosity data of lubricating oil with dissolved refrigerant is essential.

After the phase out of chlorinated HCFC refrigerants due to international regulations with respect to the protection of the ozone layer, now there is a tendency to use again natural refrigerants like ammonia and hydrocarbons. Also carbon dioxide (R 744) can be seen as one of the most interesting

alternative working fluid for different applications. First prototype systems for automotive air conditioning and heat pumps show increased efficiency in comparison to the state of the art systems using refrigerant R-134a. While the working fluid in conventional systems is in the subcritical state, CO_2 is sub and- supercritical with respect to pressure and temperature. Experiences based on experimental and practical tests show lubricant behaviour to be one of the key issues in these systems, as the right choice of lubricant must also be considered to be part of the system construction.

The applications of future transcritical CO_2 systems will require special synthetic lubricants due to the high pressure and the resulting high bearing loads. Therefore, lubrication properties need to be measured and compared to achieve high system performance and reliability. Experimental solubility data of different synthetic lubricants show extremely high dilution of the oil by dissolved CO_2 significantly reduces the viscosity of the pure lubricant. POE type oils show good miscibility, while PAG are less miscible with CO_2. First tests with CO_2 indicate different friction characteristics but do not confirm a drastic negative effect of CO_2 on lubricity. Wear test results obtained with Falex Pin & Vee Block saturated with CO_2 at room temperature and atmospheric pressure (gaseous CO_2 was continuously bubbled through the lubricant sample during a five-hour test period). Ranking of four ISO VG 220 synthetic base stock lubricants from best to worst based on the results of those Falex tests is : PAG > POE > PAO >> AB. While it might be expected that higher solubility (more CO_2 dissolved in the lubricant at a given temperature) would result in lower viscosity at that temperature, the experimental data did not confirm this expectation. This led to the conclusion that further tribological research at higher CO_2 pressures and more practical conditions is needed to develop an effective lubricant. Clearly, the Pin&Vee Block and Almen-Wieland methods with bubbling of CO_2 gas are not sufficient and do not predict field experience correctly. After all, a method that does not correlate with field behaviour has no use. The difficulty of predicting the field behaviour of newly developed products led to the definition of another simulation method, which is presented in this paper.

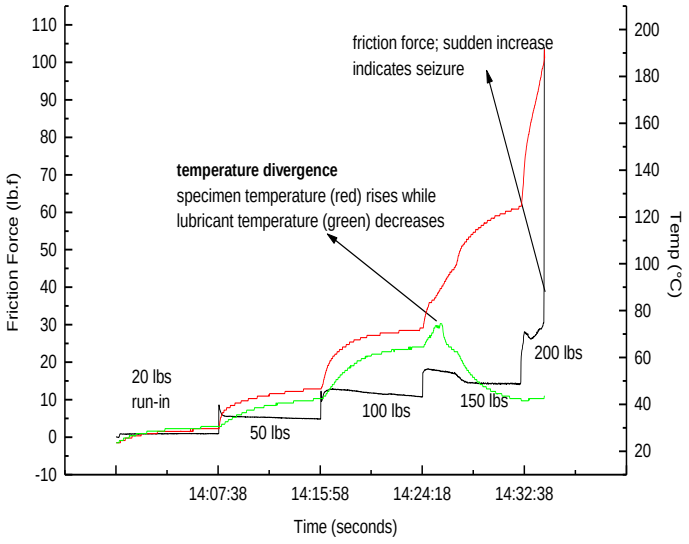

Fig. 2 : On-line friction force in the extreme pressure Block-on-ring test, steel block. Immediate increase in friction force when lubricant film breaks down

REFERENCES

1. Tribological testing – test selection with the Tribological Aspect Number, presentation at the 13th International Colloquium Tribology, Esslingen January 15-17, 2002.
2. D.Drees, J.Fahl, J.Hinrichs, Effects of CO_2 on the lubricating properties of esters and glycols, 13th International Colloquium Tribology, Esslingen January 15-17, 2002

Evaluation of surface treatments for high pressure die casting dies.

***W. Lauwerens*[1], R. Kastelein[2], P. Cosemans[1] and P. Theunissen[3]**

1 Sirris, Materials Engineering, Wetenschapspark 3, 3590 Diepenbeek, Belgium,
walter.lauwerens@sirris.be, Telephone: +32 11 260856, Fax: +32 11 260859
2 Sirris, Materials Engineering, Technologiepark 915, 9052 Zwijnaarde, Belgium
3 Flanders' DRIVE, Oude Diestersebaan 133, 3920 Lommel, Belgium

INTRODUCTION

High pressure die casting of aluminium and zinc castings are a much used industrial process for the production of high quality parts in series of hundred thousands up to several millions. In view of the increasing demand in the automotive sector for light weight components, the potential for aluminium components is still growing. However, due to the interaction with the molten metal, the dies and die inserts such as core pins are subjected to several types of wear. The steel surface is attacked by the liquid metal and corrodes by dissolving or by forming brittle phases such as Fe-aluminides. Solidified aluminium can built up on the surface, a phenomenon that is often referred to as 'soldering'. In addition the die surfaces are subjected to large thermal shocks, leading eventually to thermal fatigue and the formation of cracks in the surface, a phenomenon usually called 'heat checking'.
To prevent wear and prolong the life time of dies and core pins, surface treatments such as nitriding or ceramic PVD or CVD coatings can be applied [1]. We report here on the results of a project in which several surface treatments have been evaluated in laboratory tests and field tests regarding their performance in high pressure die casting.

SURFACE TREATMENTS AND LABORATORY TESTS

The overview of the selected surface treatments is given in table 1. Also indicated is the thickness and roughness after the treatment.

Table 1. Overview of selected surface treatments.

Treatment	Technology	Roughness (R_a, µm)	Thickness
QPQ	Salt bath nitriding + oxidizing	0.39	25 µm
TiN	PVD ion plating	0.22	3 µm
CrN	PVD ion plating	0.22	5 µm
CrAlN	PVD arc evaporation	0.19	2 µm
TiAlN	PVD arc evaporation	0.31	2 µm
CVD-TiN	Thermal CVD + polishing	0.08	8 µm
CVD-W	Thermal CVD	0.60	10
Reference	uncoated	0.18	/

The substrates used in the tests were made from hot working steel (DIN 1.2343) and a substrate with blank surface was used as reference. The substrates had a ground surface finish as is common for the industrial dies.
To evaluate the wettability of a surface to a liquid metal, the method of the so-called sessile drop was used, as illustrated in Figure 1 (see also [2]). In this method a drop of the liquid metal is positioned on the flat, horizontal surface of the substrate. The substrate is placed in a protecting, slightly reducing atmosphere and kept at high temperature (700 °C for Al, 425 °C for Zn). After an equilibration time which was always 30 minutes, a photograph of the drop was taken. From the image the contact angle was measured as an indication for the wettability.
A second laboratory test was set up to evaluate the force needed to remove core pins from a casting. A tapered pin, resembling a core pin, with a specific surface treatment, was placed in a crucible and liquid aluminium was poured into the crucible. After cooling down, the pin was pulled out in a tension testing machine. The maximum pulling force, which is attained just before the release, was noted and is an inverse measure for the ease-of-release.

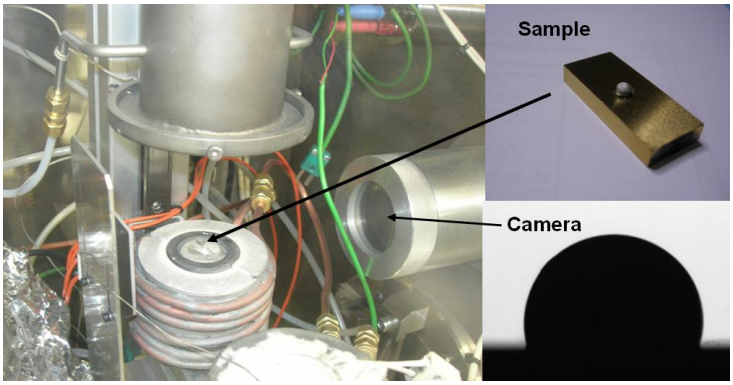

Figure 1. Experimental details of the sessile drop test.

The surface treatment or coating has to protect the substrate from corrosive attack from the liquid aluminium. To examine the interaction of liquid aluminium with the surface and to evaluate the barrier function of the coating, samples were cut through the (solidified) aluminium drop after the sessile drop measurement and the cross section was investigated with an electron microscope.

RESULTS AND COMPARISON WITH FIELD TESTS

In Figure 2 the results of the sessile drop measurements are presented, both for aluminium and zinc. For aluminium the highest contact angles, and hence the lowest wettability is realised by the QPQ treatment and to a slightly less degree by the PVD CrAlN and TiAlN coatings. In case of Zinc, the highest non-wettability is noticed for the CVD-W coating, immediately followed by the TiAlN and CrAlN coatings.

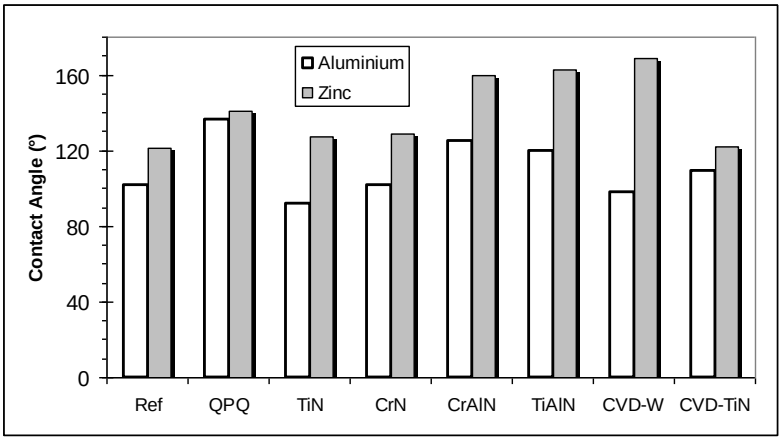

Figure 2. Contact angle measurement results.

It was found that the release forces measured in the pulling test, showed a clear correlation with the surface roughness of the coatings. This is understandable since the liquid metal shrinks around the pin when solidifying and cooling. The asperities in case of high roughness will mechanically anchor the pin. No correlation between release forces and contact angles were observed, although a visual ranking based on the amount of adhered aluminium on the pin after pulling out, corresponded indeed to the wettability as measured by the contact angle.

The examinations of the cross sections of Al drops revealed that both CVD coatings formed an excellent barrier against corrosive attack. This is illustrated in Figure 3(b) for the CVD-TiN coating. Also in case of the QPQ treatment the substrate did not show signs of corrosive wear. The arc evaporated CrAlN and TiAlN coatings on the other hand, as can be seen from Figure 3(a), show a more limited protection of the substrate. This is not only due to the small thickness of these coatings (only 2 to 3 µm), but also to specific defects such as pinholes and small metal droplets through which liquid aluminium can react with the substrate.

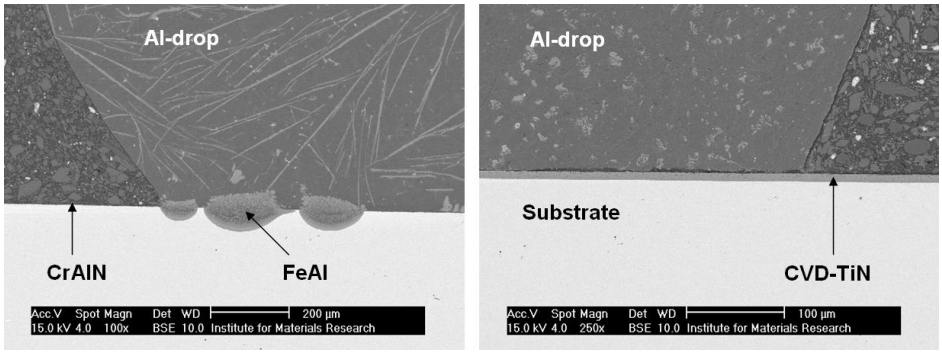

(a) (b)

Figure 3. Cros sections of tool steel substrate with CrAlN coating (a) and CVD-TiN coating (b) after the sessile drop test.

The above findings were compared with results from field testing and were used to select coatings. In a high volume aluminium casting application non-coated core pins have a maximal lifetime of 16.000 shots. Core pins coated with CrAlN showed a significant longer lifetime (36.000 to 43.000 to date). Wear investigation of the coated pins revealed the typical features as seen in Fig.3(a). Based on Fig.3 it can be expected that other coatings can prolong the lifetime further. In the production of a power-coupler (aluminium), the removal of the large core pin often led to the rupture of the casting. Two tests were set up. In the first the polished CVD-TiN coating was used, in the second a polished CVD-W coating was used. In neither of the tests, failure due to rupture of the casting has been observed till now. In another aluminium die casting application, four sliding die inserts were used The problem here was soldering of aluminium on the functional surface. A first coating, namely PVD CrN, was tried, but this did not result in an obvious improvement. Based on the data of the contact angle measurements (Fig.2), QPQ was selected to treat the inserts. Adhesion of aluminium is much reduced now.

CONCLUSIONS

In this work the performance of different surface treatments in dedicated laboratory tests and in high pressure die casting field tests was evaluated. It was found that the wettability behaviour as measured by the sessile drop test can indeed be used to select a suitable surface treatment to reduce adhesion of aluminium (soldering) on industrial dies. The lifetime of core pins is considerably increased by applying a coating, but when treating core pins surface roughness is important and decisive when high release forces are the problem. The examination of a cross section of the drop-substrate interface after the sessile drop test, is relevant for evaluating the corrosion protective properties of a coating or surface treatment.

ACKNOWLEDGEMENTS

The authors gratefully acknowledge the collaboration with the industrial partners in this project, in particularly, P. D'Haeyer from Pedeo, C. Quaak from MGG Antwerpen, J. Vits from Hayes Lemmerz Belgium, and M. Gilles and A. Schoofs from Umicore RDI/Nyrstar.
Dr. L. Bordignon from the Centre for Research in Metallurgy (CRM, Liège) is acknowledged for carrying out the sessile drop wettability measurements.
This work was financially supported by IWT, the Institute for the Promotion of Innovation by Science and Technology in Flanders.

REFERENCES

[1] S. Gulizia, M.Z. Jahedi, E.D. Doyle 2001. Performance evaluation of PVD coatings for high pressure die casting. Surface and Coatings Technology 140, 200-205.

[2] J. Lin, S. Carrera, A.O. Kunrath, D. Zhong, S. Myers, B. Mishra, P. Ried, J.J. Moore 2006. Design methodology for optimize die coatings: The case for aluminum pressure die-casting. Surface and Coatings Technology 201, 2930-2941.

Evaluating self-lubricating materials for large scale bearings functioning under seawater conditions

Van Autrève S.[1], Ost W.[1], Van Wittenberghe J.[1] and De Baets P.[1]
1 Ghent University, Department of Mechanical Construction and Production, St.-Pietersnieuwstraat 41, 9000 Gent, Belgium,
Stijn.VanAutreve@ugent.be, Telephone: +32 9 264 32 98, Fax: +32 9 264 32 95

INTRODUCTION

Large scale journal bearings are extensively used in marine applications. Moreover, a large part of them operate in seawater where no external lubrication (grease, oil) is possible or desired (the seawater itself works as a lubricant). Furthermore, these underwater journal bearings have to work under slow reciprocating motion of the journal and high loads whereby no hydrodynamic lubrication can be developed.
To deal with this lubrication problem self-lubricating materials are increasingly used providing additional benefits as low cost, cleanliness and low maintenance. Traditional materials are bronze sintered with solid lubricant and bronze with holes in the surface filled with a solid lubricant (pockets), but nowadays more and more fibre (glass, carbon, polyester) reinforced polymer bearings are used, due to their resistance to corrosion and the fact that they are less sensitive to edge stresses resulting from misalignment of the bearing.
Despite the fact that conventional tribotesting prefers small-scale tests due to cost- or time-efficiency and flexible handling of test samples, large scale test setups are still necessary. This is because extrapolation of small scale test often results in important errors and many effects are scale dependent (pocket distribution, misalignment, e.g.). In the present study a new test apparatus has been developed in order to investigate the tribological properties of selflubricating materials which are used in large scale journal bearings functioning under seawater conditions, reciprocating motion and heavy loading. In the following sections, the test-rig and test conditions are elaborated together with a methodology to calculate the coefficient of friction (COF). Preliminary *'dry'* (no seawater) tests have been conducted on a composite material (with high normal pressures, low friction values and very good wear/abrasion/corrosion resistance as most important properties), more commonly known as Multiglide T814, in order to validate the experimental results with the theoretical predictions.

TEST RIG

General working principle

A schematic overview of the test rig is given in Figure 1. The test bearing (1) is fixed in a bushing (2) by means of a back-up ring (15). A lever arm (7) connects the bushing to a load-cell (8). These five components are all stationary and are not driven in any way during the conducted tests.
As the test bearing has to run under seawater conditions (the test results reported in this paper are *'dry'* test results) flanges are fitted at the sides of the bushing to create an internal reservoir which is filled with seawater that circulates during the conducted tests in a closed water circuit by a pump.
A counter face (14) is attached on the main shaft (3) which follows the reciprocating movement of the centre trunnion hydraulic cylinder (5) through a lever arm (6) and slides against the stationary test bearing. The trunnion pins of the hydraulic cylinder are carried by needle roller bearings, allowing the cylinder to pivot, following the motion of the lever arm while the actuator's displacement is changing. The main shaft is carried by two self-aligning double row spherical roller bearings which are each part of a stationary support (4), fixed to the ground.
The radial load on the test bearing is applied by a vertical hydraulic actuator (9) via a load transmission trolley (11) and is measured with a load-cell (10). A spherical pressure plate (13) allows small misalignments of the vertical hydraulic actuator and ensures that the load is transmitted in the radial direction to the bushing. To pull the trolley back up a threaded flange (12) is screwed on the load-cell threads and bolted to the trolley. The vertical actuator is connected to a stationary supporting frame. Limit switches are placed around the cylinder of the vertical actuator to ensure its vertical alignment.

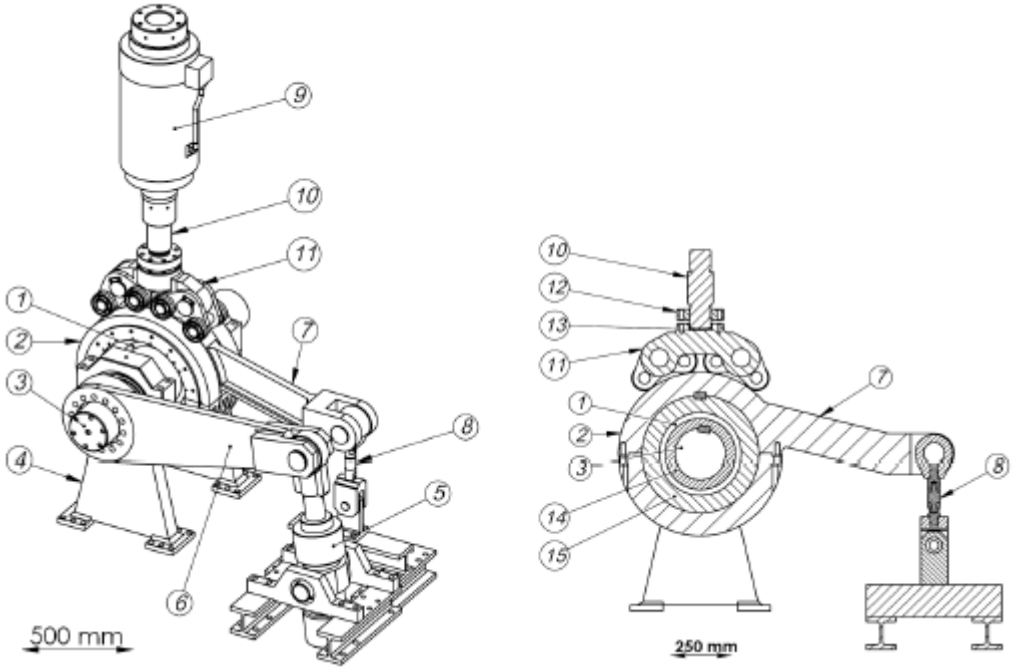

Figure 1. Schematic overview of the test rig (left: general view, right: section view).

The main characteristics of the test rig are given in Table 1.

	Characteristic values
Test bearing (1)	Inner diameter: 300 mm
	Width: 50 – 300 mm
Bushing (2)	Inner diameter: 500 mm
Counter face (14)	Outer diameter: 300 mm
Drive piston (5)	Max oscillation amplitude: ± 10°
	Max oscillation frequency: 1 Hz
	Pushing capacity: 323 kN
	Pulling capacity: 190 kN
Lever arm drive piston (6)	Length: 1100 mm
	Max transferable torque: 93 kNm
Vertical hydraulic actuator (9)	Max radial load: 1350 kN

Table 1. Main characteristics of the test rig, numbers between parentheses as in Fig. 1.

Measured signals

The test-rig is fully servo controlled. All measuring signals (summarized in Table 2) are registered continuously and logged by means of a computer with data-acquisition card.

Measured quantity	*Sensor*	*Capacity*
Friction force on bushing (1)	Load-cell (8)	*50 kN (low loads), 100 kN*
Vertical and horizontal bushing displacement	2 LVDT sensors	+/- 5 mm
Displacement of the drive piston	Internal magnetostrictive sensor of trunnion hydraulic cylinder (5)	+/- 100 mm
Temperature change of counter face (14)	Thermocouple inserted in counter face	-40°C to 100°C
Radial load on bushing	Load-cell (10)	1500 kN
Displacement of vertical piston	Internal magnetostrictive sensor of vertical actuator (9)	+/- 50 mm

Table 2, Measured signals and sensors, numbers between parentheses as in Fig. 1.

Test conditions

The displacement of the drive piston follows a triangular waveform with amplitude 5 mm. The normal pressure and speed of the drive piston are held constant during the experiment. An overview of the main test conditions used for the test material discussed in this paper is given in Table 3.

Test conditions		*Test material*
Normal load (F_p in Fig. 2)	100 kN (compression)	Filament wound composite material with matrix deposition consisting of polyester fibres (strength), phenol (binding) and PTFE (internal lubrication).
Constant velocity bearing	10 mm/s	
Sliding stroke at bearing diameter	10 mm	
Bearing size	∅300 mm x 120 mm	
Wear sleeve material	Steel S355	
Temperature bearing	– 17° C	

Table 3, Materials and test conditions.

Calculation of the COF

A section view of the test-rig with the forces occurring during working conditions is given in Figure 2. The shaft follows a predefined oscillating movement during which it rotates around its own centre line over a certain angle j (not shown in Fig. 2) and makes contact (we assume a line contact for the calculations) with the bearing (rolling and sliding).

Between q = -a and a the shaft purely rolls against the bearing, without slipping. The angle q represents the angular displacement of the contact line between shaft and bearing with respect to the vertical position. The bearing will shift position (horizontal and vertical displacement) relative to the stationary shaft. When the angle position a or -a (which corresponds with a shaft rotation of ja or j-a) is reached slip occurs over a certain slip length, resulting in wear. The angle position q will then remain fixed while the shaft keeps rotating around its own centre line over an angle |j| > |ja| or |j-a|. This behavior was verified by preliminary tests; small rotations of the shaft were taken up by rolling while only larger shaft rotations caused sliding of the shaft versus the bushing.

The measured forces FP and FL can not be directly used to determine the COF, but with the aid of Figure 2 together with the force balance and the torque balance around the centre line of the bearing the COF can be calculated as follows:

$$\mu = \frac{F_F}{F_N} = \tan\alpha = \frac{1}{\sqrt{\frac{1}{\sin^2\alpha} - 1}} \quad , \quad \sin\alpha = \frac{R_L F_L}{R_B F_P + F_L}.$$

Rb (0.15 m) and RL (1 m) are known geometrical quantities. Positive values for a correspond to a clockwise shift of thecontact line, while negative values correspond to a counter-clockwise shift of the contact line.

The above derived equation for the coefficient of friction is only valid in the case of sliding. The shaft rotation j that can be taken up by rolling depends on the bearing play, the shaft radius and the coefficient of friction of the material combination. The larger the ratio of bearing play versus shaft radius, and the larger the coefficient of friction, the more shaft rotation can be taken up by rolling.

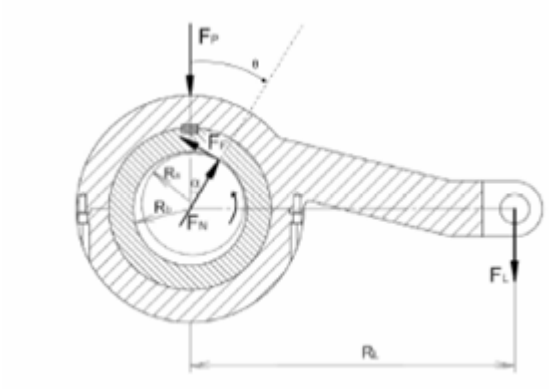

FL: force in the load-cell (8)
FP: normal load
RL: horizontal distance between the points of action of FP and FL
Rb: bearing radius
Rs: shaft radius
q: angular displacement of the contact line between bearing and counter face
a: transition point from rolling to sliding
FF: tangential reaction force component
FN: normal reaction force component

Figure 2, Schematic representation of the acting forces (counter-clockwise shaft rotation).

Elastic deformation of the bearing material under load has to be taken into account in order to quantify the relative position of the bearing which can be calculated out of the measured bearing play (no load) and the angle a.

DRY TEST RESULTS AND DISCUSSION

Figure 3 shows the measured values of the displacement of the piston (saw tooth curve), force on the load arm (FL) and horizontal displacement of the bearing, together with the calculated friction force FF, normal force FN and horizontal displacement of the bearing (for a measured unloaded bearing play of 1.1 mm). As can be observed in Figure 3.b the measured total bearing play differs from the theoretical predicted value due to the elastic deformation under load. The latter can be corrected by taking into account the measured additional bearing play under load.

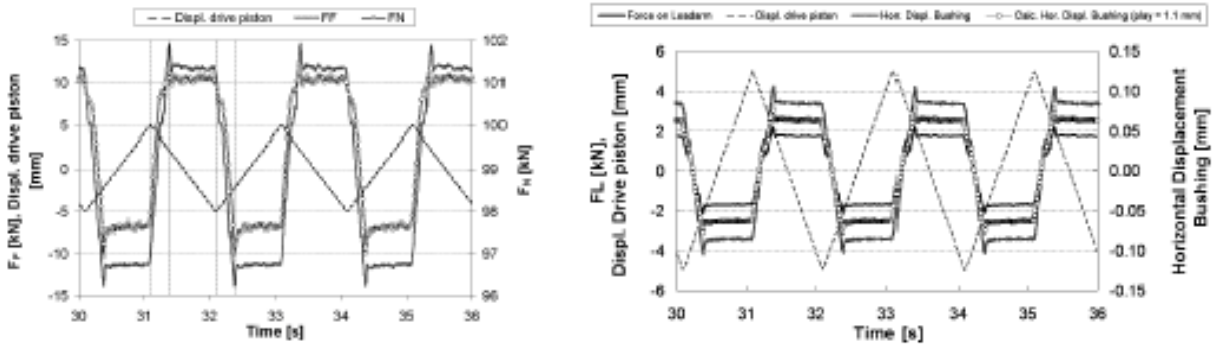

(a) **(b)**

Figure 3, (a) Displacement of the drive piston, friction force FF and normal force FN , (b) displacement of the drive piston, FL and horizontal displacement of the bearing (measured and calculated).

Figure 4.a gives an example of a friction-displacement characteristic (wherein the arrows indicate the time evolution of the cycles) used to calculate the static and dynamic COF. Because of the build up of the saw tooth displacement of the piston at the beginning of the test, the friction-displacement characteristic starts with a smaller cycle and then evolutes to cycles with a shaft rotation amplitude of almost 0.26°. Figure 4.b shows the calculated COF and displacement of the drive piston versus time. At the moment the rotation of the shaft reverses the calculated value of the COF drops to a low value (rolling instead of sliding).

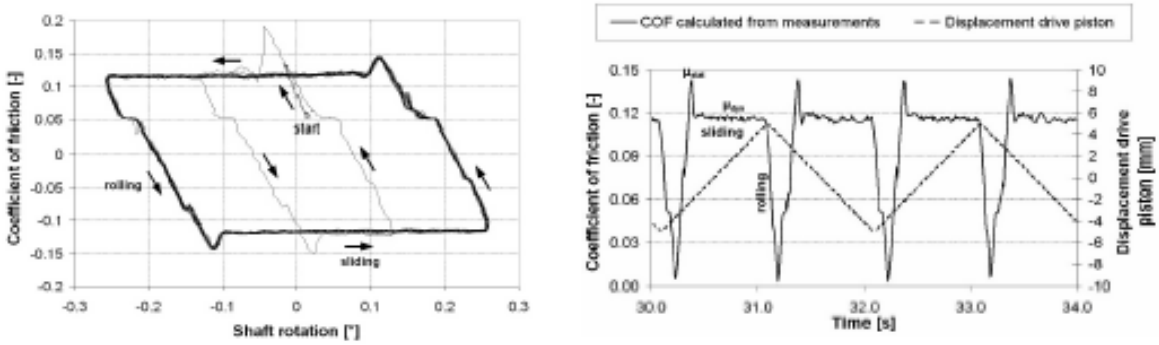

(a) **(b)**

Figure 4, (a) COF versus shaft rotation, (b) calculated COF and displacement of drive piston versus time.

From both figures a static COF (μstat) of approximately 0.14 and a dynamic COF (μdyn) of approximately 0.12 can be observed.

CONCLUSIONS

- Preliminary tests have been successfully conducted on a new developed large scale test apparatus for the evaluation of self-lubricating journal bearing materials functioning in seawater.
- From the measured values of FP and FL the coefficient of friction can be calculated in a simple and straightforward way.
- The calculated *'dry'* coefficients of friction for the used material in this paper are, taking the test conditions into account, in good agreement with values found in literature.

- Elastic deformation of the bearing influences the dynamical behavior of the test-rig and must therefore be taken into account.

ACKNOWLEDGEMENTS
The authors gratefully acknowledge *Kühne Industrie* for providing the test material.

REFERENCES
Stachowiak, G.W. 2005. Wear: Materials, Mechanisms and Practice. Wiley.
Fusaro, R.L. 1990. Self-lubricating polymer composites and polymer transfer film lubrication for space applications.
Trib. Int., 23: 105 – 21.
Samyn, P. 2004. Large-scale tests on friction and wear of engineering polymers for material selection in highly loaded
sliding systems. Materials & Design, 27: 535-555.

Oxygen activity measurement in cast iron as a method to improve ecological features of engines.

Mampaey F.

Sirris, Technologiepark 915, 9052 Ghent-Zwijnaarde, Belgium, frans.mampaey@sirris.be, Telephone: (32) 9 264 57 01, Fax: (32) 9 264 58 48.

INTRODUCTION

During the last decades, European legislation (Euro 0-V) has pushed manufacturers of cars and trucks to improve the performance of engines. However, further improvement of engines is limited because the present day engine materials, aluminium alloys and lamellar graphite cast iron, have reached their mechanical limits. In the family of cast iron alloys, compacted graphite cast iron offers a possibility to substantially increase mechanical properties. Unfortunately, the production window of compacted graphite cast iron is extremely narrow. As a result, only few engines using this material are produced today. These engines produce less toxic exhaust gases and are more energy efficient. A new sensor [HEN], which became available only very recently, can measure very low oxygen activities in cast iron. Research carried out at Sirris by the present author in cooperation with the sensor manufacturer, indicates that this device could be used during production of compacted graphite cast iron. Indeed, the sensor determines the activity within 12 seconds. The present contribution will discuss in more detail the problems and research results.

ENGINE ISSUES

Future engines will be characterized by an increase of the specific performance (Downsizing) and by a higher peak combustion pressure for diesel engines [Pischinger 2003]. The primary goals are

- a reduction of the exhaust emissions (NOX, hydrocarbon, CO, particulate matter),
- less fuel consumption,
- a better performance and
- to improve comfort.

Downsizing can reduce the fuel consumption of a high middle class car by about 25 percent. The European car manufacturers (ACEA, [EurActiv 2002]) agreed to reduce the CO_2 emissions from 180g/km (2002) to 140g/km in 2008. Three options exist to realize this goal: less weight, better fuel economy and a raise of the diesel engine share. The first two objectives can be influenced by cast engines. The specific mass of a Diesel engine has decreased from about 2,5 kg/kW (1990) to about 1,30 kg/kW in 2002. Today, Diesel engines are cast in lamellar graphite. Cast iron is also the first choice for petrol engines with average combustion pressure up to 20 bar; the other engine blocks are produced in aluminium alloys. The idea that aluminium would replace cast iron for the major part of all engines has not become true. Aluminium engines have lower weight for cylinder volumes above 2 l. On the other hand, cylinder heads are generally produced in aluminium alloys. Weight reduction was the driving force to substitute cast iron for aluminium. In 2006, about the same number of engine blocks in cast iron and aluminium were produced in Europe.

An improvement of the fuel economy requires higher peak pressures during combustion [Weiss 2002]. Increasing the peak pressure with 10 bar raises the specific performance of the engine with 6,7 kW/l (engine cylinder capacity). Additionally, higher peak pressures also diminish the harmful components in the exhaust gases. This is illustrated in Figure 1 which shows the peak pressure in conjunction with the European standards for the case of heavy trucks. At present, a max pressure up to 180 bar is possible in series production of cars.

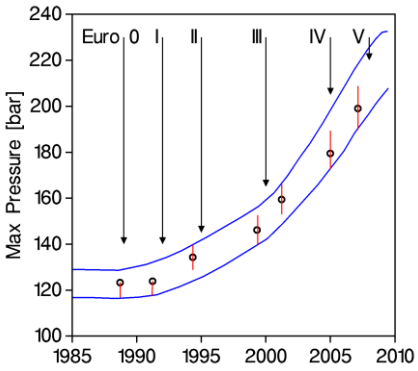

Figure 1. In order to meet the European exhaust standards (Euro 0-V on top), the combustion pressure in trucks must be raised to 200 bar [Vollrath 2003].

Unfortunately, the current aluminium alloys and lamellar graphite cast iron — the present day two materials used to manufacture engines — have reached their mechanical limits. For example, in series production, the limit for aluminium alloys is 160 bar [Weiss 2002]. With higher combustion pressure, also the internal cylinder temperature goes up from 200°C to 260°C [Röhrig 2003]. The present day aluminium alloys considerably loose strength above 200°C. Even for cylinder heads, which are now produced in aluminium alloys, temperatures above 230°C become critical with respect to the fatigue strength. Cast iron room temperature mechanical properties remain the same up to 400°C.

COMPACTED GRAPHITE CAST IRON

As opposed to lamellar graphite cast iron, which has a tensile strength of 250 MPa, compacted graphite cast iron easily withstands 400 MPa. Because of the higher strength, the wall thickness of the engine may be reduced, giving 15 percent less mass. The improved properties of compacted graphite cast iron result from a change in the graphite shape within the iron. Because lamellae are thin and long, the strength of the iron matrix drops substantially from about 800 – 1000 MPa in a graphite free matrix to 150 – 250 MPa in lamellar graphite cast iron. Additionally, this material does not present a measurable elongation. One of the favourable features is the high thermal conductivity which is needed in engines to remove the heat from the combustion chamber through the cylinder wall. In the forties of the previous century, it was found that the addition of a strong deoxidizer to the melt (Mg or Ce) resulted in the presence of spheroidal graphite. This graphite structure raises strength (400 – 700 MPa) and elongation (20%) considerably. Unfortunately, thermal conductivity also drops and thin walls are less easily cast. Ductile iron, is now produced in large quantities world wide (21 M tons in 2006 as compared to 42 M ton lamellar iron and 12 M ton Al castings). Soon after the invention of ductile iron, one noticed that in case of insufficient magnesium addition, an intermediate graphite structure resulted. Here, graphite appears as vermicular particles. Figure 2 shows the different types of graphite in cast iron. However, because the material could not be produced in a controlled and reproducible way, it remained a research curiosity.

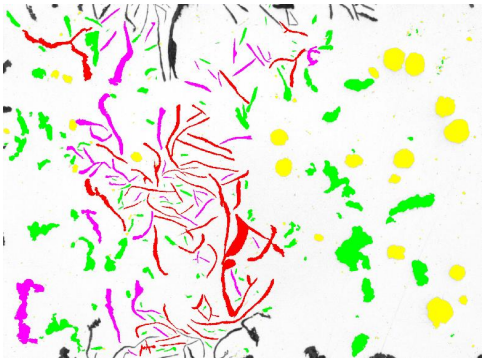

Figure 2.Different graphite forms in cast iron: lamellar (red), spheroidal (yellow) and compacted (magenta). Graphite particles touching the edge are not analysed.

Later, it was found that the addition of titanium could enlarge the production window to some extent [Evans 1976]. Unfortunately, titanium combines to carbo - nitrides which are extremely hard. As engines require a lot of high speed machining, the titanium route was excluded for series production. However, legislation and the need for better fuel efficiency, pushed the manufactures to start producing engines in compacted graphite cast iron. Examples are Audi 3,3lV8, BMW 3,9lV8, DaimlerCrysler OM501 LAR [Steller 2003] and Ford-PSA 2,7lV-6. Today, the only possible production control is based on thermal analysis. However, the analysis requires about three minutes which is long in production circumstances. Mampaey [2007] examined the possibility of acoustic resonance analysis. While this method is very suited to control castings after production, the research showed that examination during production is difficult and time consuming too.

2 OXYGEN ACTIVITY MEASUREMENT

As mentioned above, the transition of graphite lamellae to spheroids occurs by adding magnesium to a melt. The magnesium combines with oxygen and sulphur. As long as sufficient magnesium is available (about 0.040%) ductile iron is produced. Because the boiling temperature of magnesium is 1107°C and the melt temperature is much higher (1450°C), magnesium continuously evaporates from the melt. Putting too much magnesium in the melt is harmful. Compacted graphite cast iron appears in a very small production window (for example Mg range of 0,05%). However, this small window is not constant and additionally varies. The reason is the fact that total magnesium is measured as the sum of free (active) magnesium and magnesium oxide and sulphide compounds. An alternative is the measurement of the activity of oxygen. Oxygen activity measurements are quite common in steel. Here, oxygen activities are 5 ppm or higher. However, in ductile iron melts oxygen activities are much lower, about 0,1 ppm, and pose more technological problems to sensor producers. Only very recently, an improved version of a sensor became available. At first, the sensor was examined for the case of ductile iron [Mampaey 2008].

In case of ductile iron, a close relation exists between oxygen activity and various mechanical properties. At about 0,1 ppm, the iron has optimal properties, the highest strength in combination with maximal elongation. The research also examined the nodularity, which represents the percentage of well shaped spheroidal graphite particles (i.e. approximating the circular shape). Too much magnesium, giving oxygen activities below 0,1 ppm, decreases nodularity. On the other hand when magnesium becomes too low, graphite spheroids gradually change to vermicular graphite particles. For the first time, the graphite transition in ductile iron could be examined using the oxygen activity sensor during production itself, and not afterwards by examination of graphite structures in castings.

Encouraged by the results obtained for ductile iron, Sirris and Heraeus Electro-Nite started with a specific research for compacted graphite cast iron. Here, a melt is monitored when it passes through the production window. In order to take full advantage of the high thermal conductivity of the graphite phase, the standard for compacted graphite specifies a maximum of 20 percent of spheroidal graphite. Indeed, the vermicular graphite particles which appear during microscopic examination (a two dimensional plane) as single particles, in fact represent a three dimensional connected structure.

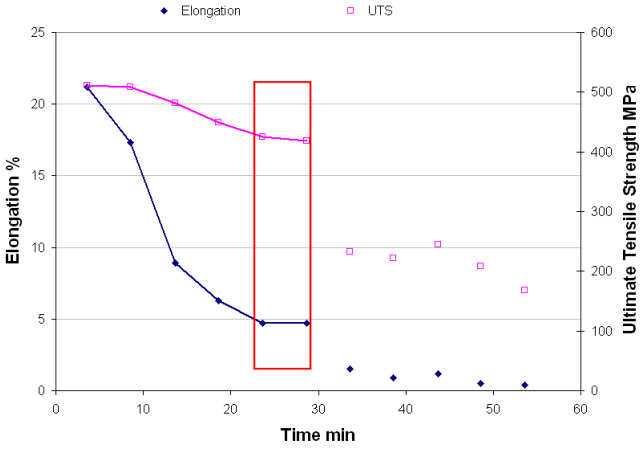

Figure 3.The transition from compacted graphite (within the red rectangle) to lamellar graphite (right of the rectangle) is accompanied by a sudden drop in strength and elongation. Spheroidal graphite appears far left from the rectangle.

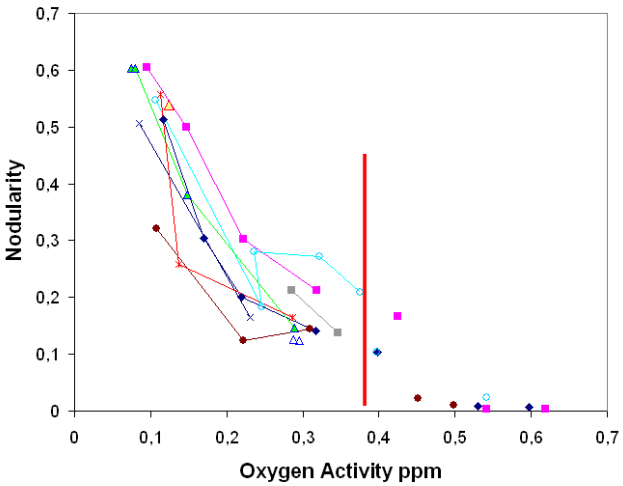

Figure 4.Compacted graphite always occurs below a well defined oxygen activity (left of the red line).

Figure 3 shows experimental results during the fading of magnesium from the melt. The Figure illustrates a major problem when magnesium becomes too low (or equivalently, oxygen activity too high). Once only traces of lamellar graphite occur, the strength and the elongation of the iron suddenly drop to unacceptably low values. With such low mechanical properties, the engine would crash immediately. Because of these severe limitations, engine manufactures tolerate 30 percent nodularity, which widens the production window somewhat at the other side.

The time is not a suitable parameter to determine the production window; in fact, oxygen activity is needed to define optimal production conditions. Figure 4 shows how nodularity decreases when oxygen activity goes up. The Figure indicates the existence of a critical oxygen activity (0,35 ppm), above which graphite lamellae appear. Below this value, a variable fraction of vermicular particles occurs. The fact that no single curve seems to be present, has probably to do with sulphur, the other element which controls the graphite structure. Despite the fact that ductile iron has been invented for more than 50 years, a generally accepted and detailed explanation for the formation of the different graphite types during solidification, is not available today.

CONCLUSIONS

A new commercial sensor opens perspectives for easier production control of compacted graphite cast iron. If successful, production of compacted graphite cast iron engines in large series could be stimulated. Considering the large numbers of cars and trucks, even a small increase of this type of engines would have a tremendous positive effect on the environment.

ACKNOWLEDGEMENTS

The author acknowledges the financial support of IWT for various research projects in the past concerning compacted graphite cast iron(e.g. convention VIS/CO/30926/WTCM). The author also acknowledges Heraeus Electro-Nite for permitting to release research results obtained in cooperation with this company.

REFERENCES

EurActiv 2002 :http://www.euractiv.com/en/environment/commission-pushes-co2-reductions-car-industry/article-113634

Evans, E.R. , Lalich, M.J. 1976. Compacted Graphite Cast Irons and Their Production by a Single Alloy Addition, AFS Transactions, 84:215-220.

HEN, Heraeus Electro-Nite Celox-Foundry, CF 10100692.

Mampaey, F. 2007. Acoustic Resonance Analysis for Examining the Graphite Shape in Cast Iron, AFS Transactions, 115, paper no. 07-129.

Mampaey, F., Habets, D., Seutens, F. and Plessers, J. 2008. The use of oxygen activity measurement to determine optimal properties of ductile iron during production, accepted for publication in International Foundry Research / Giessereiforschung.

Pischinger, S., Ecker, H.-J. 2003. Zukünnftige Motoren – Anforderungen an Werkstoffe und Gießtechnik, Gesserei 90: no. 5, 63-69.

Röhrig, K., 2003. Gießtechnik im Motorenbau – Anforderungen der Automobilindustrie, Giesserei-Praxis, no. 5, 191-197, no. 6, 255-262.

Steller, I., 2003. Das neue VDG-Merkblatt W 50 Gußeisen mit Vermiculargraphit, konstruieren + giessen, 28, no. 2, 22-24.

Vollrath, K. 2003. Motorguss – Werden die Werkstoffkarten neu gemischt? konstruieren+giessen 28: no. 2, 25-27.

Weiss, G., Kaiser, R.W. 2002. Hochleistungsmotoren nur mit Gusseisen! Giesserei-Rundschau 49, 70-71.

Theme 6: Looking at materials at the nano scale

The development of nanomaterials for various fields of applications triggers the need for different characterization techniques able to investigate extremely small volumes and with high spatial resolution. Tools designed for surface analysis, scanning probe techniques, AES, TOF-SIMS and electron beams are only a few examples of possible characterization techniques. Papers, describing useful characterization techniques of nanostructured materials are welcomed.

Constitutional transcription of nucleobase self-assembly codes in functional hybrid materials

Mihail Barboiu
Institut Européen des Membranes, Adaptative Supramolecular Nanosystems Group, IEM/UMII, Place Eugene Bataillon, CC047, F-34095 Montpellier, France. E-mail: mihai.barboiu@iemm.univ-montp2.fr

Many research groups have demonstrated that the functional self-organization can be readily transcribed into hybrid nanostructures by using the sol-gel process. [1] Accordingly, we have reported synthetic routes for preparing self-organized ion-channels systems which have been "frozen" in a polymeric matrix, as a straightforward approach for the design of a novel class of solid hybrid nanomembranes. [2]

Nucleobases oligomerization [3] can be an advantageous choice to reinforce the controlled communication between interconnected "*dynamic supramolecular*" and "*fixing siloxane*" systems. Moreover, the different interconverting outputs that nucleobases may form by oligomerization define a dynamic polyfunctional diversity which may be "extracted selectively" by sol-gel polymerization in solid state, under the intrinsic stability of the system.

In this context, alkoxysilane nucleobases form in solution different types of hydrogen bonded aggregates which can be expressed in the solid state as discrete higher oligomers. After the sol-gel process, the constitutional preference for compact geometries in hybrid materials is most likely dictated by hydrophobic interactions and Hoogsteen H-bonding self-assembly.

The G-quadruplex with a chiral twisted supramolecular architecture represents a nice example of a dynamic supramolecular system, when guanine and guanosine molecules are used. [6] We have recently reported a new way to transcribe the supramolecular chirality of G-quadruplex at the nanometric and micrometric scale. Figure 1 represents the first picture of the *dynamic* G-quadruplex transcribed at the nanometric level; it unlocks the door to the new materials world paralleling that of biology.

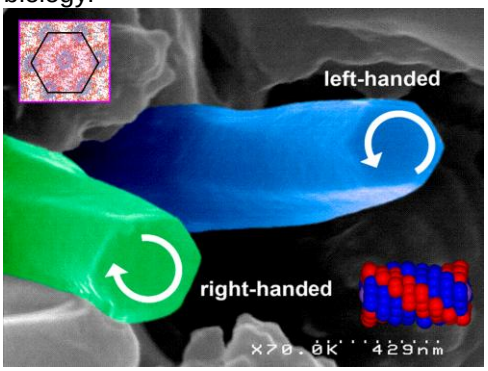

Figure 1. SEM image of the twisted hexagonal nanorods resulted by sol-gel transcription of the chiral G-quadruplex in the hybrid material.

ACKNOWLEDGEMENTS

This work, conducted as part of the award “Dynamic Adaptative Materials for Separation and Sensing Microsystems” made under the European Heads of Research Councils and European Science Foundation EURYI (European Young Investigator) Awards scheme in 2004, was supported by funds from the Participating Organisations of EURYI and the EC Sixth Framework Programme. **See *www.esf.org/euryi***

REFERENCES

1. C. Arnal-Hérault, M. Barboiu, A. Pasc, M. Michau, P. Perriat, A. van der Lee, Constitutional Self-Organization of Adenine-Uracil-derived Hybrid Materials, *Chem. Eur.J.* **2007**, *13,* 6792-6800.
2. C. Arnal-Herault, A. Pasc-Banu, M. Barboiu M. Michau, A. van der Lee, Amplification and transcription of the dynamic supramolecular chirality of the G-quadruplex, *Angew. Chem. Int. Ed*. **2007**, *46*, 4268-4272. in press. (**Cover Communications Picture, June 2007**)
3. C. Arnal-Herault, A. Pasc-Banu, M. Michau, D.Cot, E. Petit, M. Barboiu Functional G-Quartet Macroscopic Membrane Films, Angew. Chem. **2007**, 119, 8561-8565; Angew. Chem. Int. Ed. **2007**, 46, 8409-8413.
4. M. Barboiu, Constitutional transcription of nucléobases self-assembly codes, Wiley Encyclopedia of Chemical Biology, **2007**, DOI: 10.1002/978047004876.wecb527.

The self-assembly and reactivity of porphyrin molecules at copper/electrolyte interfaces: a potentiodynamic electrochemical scanning tunneling microscopy study

N.T.M. Hai[1,2], S. Furukawa[1,3], K. Wandelt[2], P. Broekmann[2] and S. De Feyter[1]

1Department of Chemistry, Division of Molecular and Nanomaterials, Laboratory of Photochemistry and Spectroscopy, and Institute of Nanoscale Physics and Chemistry, Katholieke Universiteit Leuven (KULeuven), Celestijnenlaan 200 F, B-3001 Leuven, Belgium, (Email: minhhai.nguyenthi@chem.kuleuven.be, Steven.DeFeyter@chem.kuleuven.be) Tel. 016/327608, Fax. 016/327990)
2Institute for Physical and Theoretical Chemistry, University of Bonn, Wegeler Str. 12, D-53115 Bonn Germany
3 ERATO Kitagawa Integrated Pores Project, Japan Science and Technology Agency (JST), Kyoto Research Park Bldg 3, Shimogyo-ku, Kyoto 600-8813, Japan

The self-assembly of a free base porphyrin (Meso-Tetra (N-methyl-4-pyridyl) porphyrin (H_2TMPyP)) (Figure 1a) was investigated on the chloride-precovered Cu(100) surface by means of a potentiodynamic Electrochemical Scanning Tunneling Microscope (EC-STM).[1] The result shows that the negatively charged chloride modified Cu(100) surface is an excellent template for the adsorption of positively charged porphyrin cations from aqueous solution. At potential -150< E < +200 mV vs. RHE, the electro-reduced porphyrin species ($[H_4TMPyP(-II)]^{4+}$) adsorb spontaneously on Cu(100)/Cl and form a self-assembled monolayer as shown in Figure 1b. Molecules lie flat on the Cu(100)/Cl substrate with a p($\sqrt{17} \times \sqrt{17}$)R14^o - commensurate lattice related to the ($\sqrt{2} \times \sqrt{2}$)Cl structure. In the anodic potential regime, i.e. E > +250 mV, the copper dissolution is promoted in the presence of porphyrin such that the copper material is removed preferentially at the step edges of both upper and lower terraces. The lack of the copper redeposition and the porphyrin reduction current features (Figure 1c) in the cyclic voltammogram in the presence of porphyrin reveals that the dissolved copper species (Cu^{2+}) incorporate directly into the free base porphyrin, forming Cu-porphyrin. The result was confirmed by UV-Vis spectroscopy.

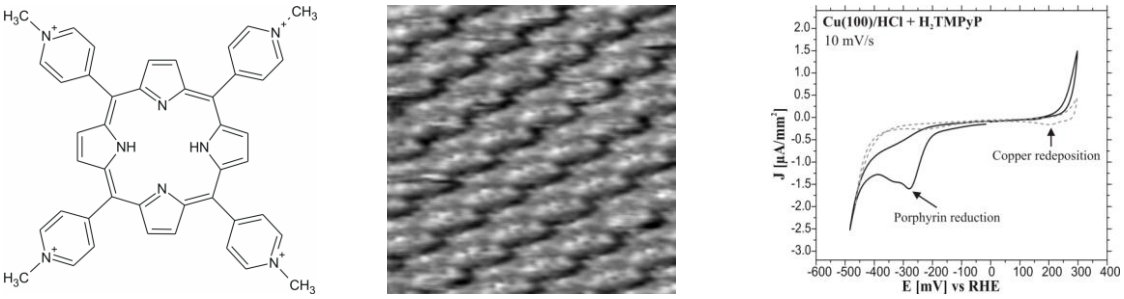

Figure 1. a) Cation Meso-Tetra(N-Methyl-4-pyridyl)porphine ($H_2TMPyP]^{4+}$) b) Self-assembly of H_2TMPyP on chloride modified Cu(100), 7.8 nm × 7.8 nm, I_t = 0.38 nA, U_b = 256 mV, E = -100 mV vs RHE; c) Cyclic voltammograms of Cu(100) in pure 10 mM HCl (grey dashed curve) and in 10 mM HCl + 1 mM $[H_2TMPyP]^{4+}$ (black solid curve).

REFERENCES

1. Safarowsky C. et al., Angew. Chem. Int. Ed., 2004, **43** (10): p. 1291-1294.
2. Klymchenko, A. et al., Nano Letters, 2007, **7** (3): p. 791-795.

Two-Dimensional Surface-Confined Nanoporous Molecular Networks at the Solid-liquid Interface

Shengbin Lei[‡], Kazukuni Tahara[†], Xinliang Feng[$], Frans C. De Schryver[‡], Klaus Müllen[$], Yoshito Tobe[†], Steven De Feyter[‡]*

1 [‡]*Department of Chemistry, Division of Molecular and Nanomaterials, Laboratory of Photochemistry and Spectroscopy, and Institute of Nanoscale Physics and Chemistry, Katholieke Universiteit Leuven (KULeuven), Celestijnenlaan 200 F, B-3001 Leuven, Belgium, shengbin.lei@chem.kuleuven.be, telphone: 32 16 327608*
2 [†]*Division of Frontier Materials Science, Graduate School of Engineering Science, Osaka University, Toyonaka, Osaka 560-8531, Japan*
3 [$] *Max Planck Institute for Polymer Research, Ackermannweg 10, 55128 Mainz, Germany*

Surface-confined two-dimensional (2D) molecular networks, especially those with void spaces, so-called “2D porous networks”, attract a lot of interest. The porous networks are typically sustained via hydrogen bonds, metal-ligand coordination or even van der Waals interactions. These 2D porous networks are used as hosts to immobilize functional units as guest molecules in a repetitive and spatially ordered arrangement. Alkoxylated hexadehydrotribenzo[12]annulene (DBA) derivatives are ideal building blocks concerning this topic. In this work 2D porous networks with tunable cavity size has been constructed at the liquid-solid interface following two different strategies: concentration control and guest induced transformation. At high concentration, in the absence of appropriate guest molecules, DBA derivatives with short alkoxy chains form two-dimensional (2D) porous honeycomb type patterns while those with long alkoxy chains form predominantly dense-packed linear type patterns. However, by lowering the concentration well-ordered honeycomb networks could be successfully constructed up to a diameter of 5.4 nm. As a second strategy, addition of proper guest molecules such as nanographene molecules could convert the guest-free dense-packed linear type patterns into guest-containing 2D porous honeycomb type patterns, even at high concentration. For the DBA derivative with the longest alkoxy chains ($OC_{20}H_{41}$), up to a maximum of six nanographene molecules can be hosted in the same cavity. The host matrix changes its structure in order to accommodate the adsorption of the guest clusters. This flexibility arises from the weak intermolecular interactions between interdigitating alkoxy chains holding the honeycomb structure together. Diverse dynamic processes have been observed both at the level of the host matrix and the co-adsorbed guest molecules.

REFERENCES

1. Lei, S; Tahara, K.; De Schryver, F. C.; Van der Auweraer, M.; Tobe, Y.; De Feyter, S. *Angew.Chem. Int. Ed.* **2008**, in press.
2. Tahara, K.; Furukawa, S.; Uji-i, H.; Uchino, T.; Ichikawa, T.; Zhang, J.; Mamdouh, W.; Sonoda, M.; De Schryver, F. C.; De Feyter, S.; Tobe, Y. *J. Am. Chem.Soc.* **2006**, *128*, 16613.

Atomic scale elemental analysis with Cs-corrected STEM

T. Oikawa[1], ***E. Okunishi*** [2] ***and S. Kuypers***[3]

1 JEOL(Europe) SAS, Espace Claude Monet, 1 Allée de Giverny, 78209 Croissy-sur-Seine, France
2 JEOL Ltd., 1-2, Musashino 3-chome, Akishima, Tokyo 196-8558, Japan
3 JEOL(Europe) B.V., Planet II, Gebouw B, Leuvensesteenweg 542, B-1930 ZAVENTEN, Belgium

INTRODUCTION

Recently, scanning transmission electron microscopy (STEM) has made huge progress owing to a stable field emission gun (FEG) (Honda, T. et al., 1994), sophisticated lens designing technologies (Tsuno, K., 1999), and spherical aberration corrected (Cs-corrected) lens systems (Haider, M., 1998). In this paper, we report ultra high-resolution (atomic scale) elemental analysis - using Cs-corrected STEM - of different technological materials.

EXPERIMENT

The instrument used in this experiment was the JEM-2100F (200 kV FEG TEM/STEM) equipped with a Cs-corrector for the probe forming lens. Figure 1 shows the appearance of the instrument with analytical attachments, such as STEM detectors, an EDS detector and an electron energy-loss spectrometer (EELS). The specimen under investigation was an Al-Cu-Mg-Ag alloy containing omega-phase precipitates.

Figure 1. Appearance of the JEM-2100F (200 kV FE-TEM/STEM) equipped with Cs-corrector for the probe forming lens.

RESULTS

Figure 2(a) shows a high-resolution high angle annular dark-field (HAADF) image of an omega-phase precipitate. Figure 2(b) shows elemental mapping of Al, Cu and Ag, superimposed on a magnified image from (a). The elemental mappings were reconstructed from data series of EELS spectrum images for corresponding energies. Figure 2(c) shows the intensity distribution along the horizontal direction for each element, as well as the intensity distribution in the HAADF image. The elemental mappings allow identifying differences in composition between the different atom layers. There is strong evidence for the segregation of Ag to the boundaries of the precipitate.

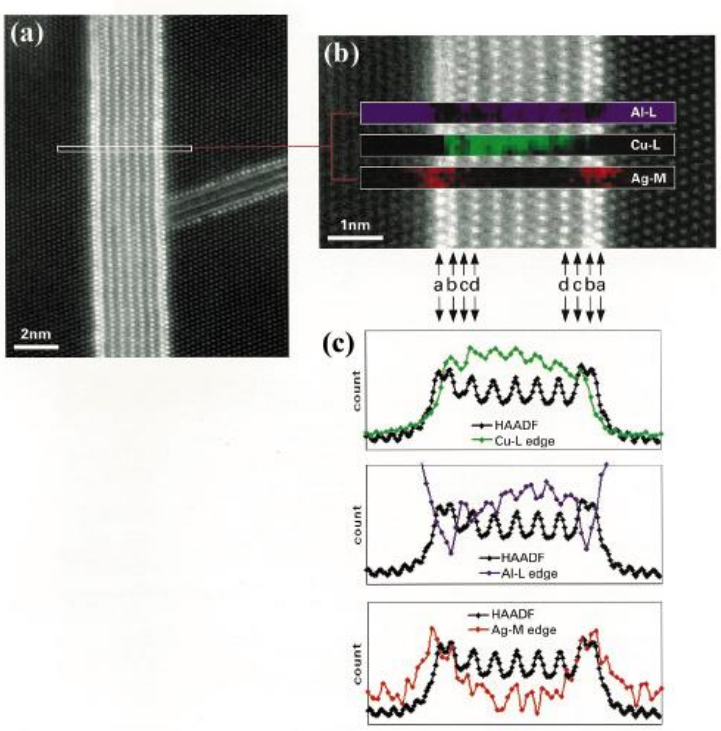

Figure 2(a) HAADF image of omega-phase precipitate in Al alloy. (b) EELS-mapping images superimposed on enlarged HAADF Image. (c) Intensity distributions of HAADF and EELS-mapping images.

CONCLUSIONS

State-of-the-art Cs-corrected STEM can achieve elemental mapping on the atomic scale. Atomic scale resolution EELS-maps of omega-phase in Al-Cu-Mg-Ag were reconstructed from a data series obtained by the spectrum imaging method. Ag was shown to segregate to the boundaries of the precipitate.

ACKNOWLEDGEMENTS

The specimen used in this experiment was provided by Professor K. Hone of the National Institute for Materials Science in Japan.

REFERENCES

Honda, T. et al., 1994. Field emission ultrahigh-resolution analytical electron microscope, Ultramicroscopy, 54, 132-144.

Tsuno, K. 1999. Optical design of electron microscope lenses and energy filters. J. Electron microscopy, 48, 801 -820.

Haider, M. et al., 1998. Electron microscopy image enhanced, Nature, 392, 768.

Growth mechanism of graphene layers deposited by microwave plasma enhanced CVD

Vitchev R.G.[1], Malesevic A.[1,2], Vanhulsel A.[1], Kemps R.[1], Mertens M.[1], Van Haesendonck C.[2] and R. Persoons[1]

1 VITO Materials, Flemish Institute for Technological Research, Boeretang 200, B-2400 Mol, Belgium
roumen.vitchev@vito.be, Telephone: (+32) 14-335747, Fax: (+32) 14-321186
2 Laboratory of Solid-State Physics and Magnetism, K.U. Leuven, Celestijnenlaan 200D, B-3001 Leuven, Belgium

ABSTRACT

Graphene has recently attracted considerable attention as a potential material for nanoelectronic devices. A promising method of its mass production is microwave plasma enhanced chemical vapour deposition (MW PECVD). This technique is known for the synthesis of carbon nanotubes and has recently been optimized to produce high quality crystalline freestanding graphene flakes. However, the growth mechanism of PECVD synthesized graphene is not well understood. The aim of this work was to investigate the growth process of graphene deposited by MW PECVD with different parameters (power, gas mixture/pressure, deposition time, etc.) on several substrates (quartz, silicon, platinum). The resulting thin films were characterized by X-ray diffraction (XRD), scanning electron microscopy (SEM), Raman spectroscopy and X-ray photoelectron spectroscopy (XPS). Three stages of film growth on silicon were identified by XPS: formation of a carbide layer on the substrate, deposition of a carbon amorphous layer and finally formation of a graphene layer. This growth mechanism appears to be substrate dependent since no intermediate carbide layer was formed on both quartz and platinum surfaces. Further, because of the good matching between the crystal lattices of platinum and carbon, no amorphous carbon layer was detected on platinum substrates either. The high quality of the synthesized graphene flakes was confirmed by SEM, XRD and Raman spectroscopy studies.